MICROWAVE REMOTE SENSING OF SOIL WATER CONTENT

Remote Sensing Laboratory
RSL Technical Report 264-6

Josef Cihlar
Fawwaz T. Ulaby

August, 1975

Supported by:

NATIONAL AERONAUTICS AND SPACE ADMINISTRATION
Lyndon B. Johnson Space Center
Houston, Texas 77058

CONTRACT NAS 9-14052

THE UNIVERSITY OF KANSAS CENTER FOR RESEARCH, INC.
2291 Irving Hill Drive—Campus West Lawrence, Kansas 66045

TABLE OF CONTENTS

TABLE OF CONTENTS (CONTINUED)

ACKNOWLEDGEMENTS

The authors would like to express their appreciation and thanks to the following individuals:

- Professor W. L. Powers (Department of Agronomy, Kansas State University) for his advice regarding the tensiometric method of soil water content measurement;
- Drs. R. D. Jackson and S. B. Idso (U. S. Water Conservations Laboratory) for providing experimental data necessary for parts of this study;
- Professor K. F. Casey (Department of Electrical Engineering, Kansas State University) for performing reflection coefficient calculations;
- Dr. W. J. Burke (N.R.C., Johnson Spacecraft Center) for supplying a programmed version of his brightness temperature model; and
- Mr. A. Wichman for providing an experimental site for soil water regime study.

ABSTRACT

Water in the soil is one of the key environmental parameters. With increasing attempts to understand and to manage the environment, the demand for an accurate, timely, and location-specific soil water content information can be expected to grow. Two types of techniques appear potentially capable of providing such information, namely water balance and remote sensing methods. In this study, the attention was focused on the microwave remote sensing method, and in particular on bare soil temperature and moisture regimes and their impact on the microwave technique. A layered water balance model was developed for determining soil water contents and their changes in the upper zone (top 30 cm of soil), while soil moisture regime characteristics at greater depths and those near the surface during the diurnal cycle were studied using experimental measurements. Soil temperature and its variations due to several parameters were investigated by means of a simulation model. Using the two models, moisture and temperature profiles of a hypothetical soil located at mid-latitudes were generated, analyzed, and subsequently used for computing microwave soil parameters at three frequencies (1.4 GHz, 4.0 GHz, 10.0 GHz) for a clear-sky summer day. The results suggest that (i) soil moisture in the top 30 cm can be predicted on a daily basis for 1-cm depth increments within approximately 0.02 cm^3/cm^3, (ii) soil temperature presents no problem in microwave remote sensing of soil moisture provided that surface soil temperature can be measured with infrared radiometers from the same platform, and (iii) surface layer domination exists, i.e., remotely measured microwave response of a bare soil is determined primarily by the moisture at and near the surface unless appreciable air-soil discontinuities (in terms of wavelength) exist within the soil. In conclusion, an algorithm is proposed which combines the water balance and microwave methods to monitor profile soil water content changes over large areas. Finally, a summary of passive and active microwave measurements of soil moisture is presented.

LIST OF FIGURES

LIST OF FIGURES (CONTINUED)

LIST OF FIGURES (CONTINUED)

LIST OF FIGURES (CONTINUED)

LIST OF FIGURES (CONTINUED)

LIST OF TABLES

LIST OF TABLES (CONTINUED)

CHAPTER 1.

INTRODUCTION AND PROBLEM STATEMENT

1.1 INTRODUCTION

Soil water, due to its presence near the earth's surface, plays a fundamental role in mass and energy exchange processes at the lithosphere/atmosphere interface and in the ecosystem's functioning. Its importance has long been recognized and is presently topical in such diverse scientific disciplines as hydrology, ecology, plant physiology, meteorology, climatology, geomorphology, hydrogeology, pedology, etc. Hydrology and agriculture are concerned primarily with those features of soil water which affect man. The physical geographer's interest in soil water stems from the important function surface waters have in differentially shaping the earth's topography, the latter occurring mainly due to spatial variations of water availability. In a recently proposed unifying concept of physical geography (Carter et al., 1972), soil water was considered a basic component of the interface environment. Because of its indispensability for survival and a prosperous livelihood, soil water also affects various phenomena in the domain of cultural geography.

A necessary requirement in dealing with many aspects of water in the soil is some means of measuring the amounts present over large areas. The numerous methods developed for estimating soil water content may be divided into two groups based on how the moisture value is obtained.

1.1.1 Direct Methods

In the direct approach, water content of a soil segment at a given time is determined by directly examining the segment at that time. Thus discrete moisture values are provided, although in some cases continuous recording is possible. The following direct methods are used most often.

Gravimetric Method

The segment is physically removed, and its water content is determined by separating the sample into dry soil material and water components, respectively. The method is destructive, i.e., the soil segment is destroyed during this procedure and thus repeated determinations are not possible.

Resistance Method

The resistance to electric current flow decreases with increasing moisture content along the path of the current. This decrease can be measured and through calibration related to water contents. Blocks made of porous materials such as gypsum or nylon (Bover, 1956) are inserted into the soil segment to be measured. The method is non-destructive.

Tensiometric Method

Due to the forces of cohesion and adhesion existing between water molecules or between water molecules and soil particles, a force inversely related to the amount of water present must be exerted to remove the water out of the soil segment. The magnitude of this force (tension) can be determined by measuring the force applied by the soil on a pool of free water across a permeable membrane. The measured force can then be related to soil water contents through calibration curves for a given soil. This approach yields repeated measurements of a soil segment once the tensiometer is installed; it is not applicable, however, for tensions higher than about 0.85 atmosphere (Taylor and Ashcroft, 1972).

Psychrometric Method

Relative vapor pressure of soil water depends on the difference in water potential that results from changes in matric, osmotic, and pressure potentials. Although the vapor pressure range is relatively small for water contents in the plant growth range (Taylor and Ashcroft, 1972), accurate measurements can be made provided that the ambient temperature effect on the vapor pressure is taken into account. For example, Rawlins and Dalton (1967) developed a field psychrometer that can measure soil water potentials with a precision of $\pm$ 50 joules/kg in soils where ambient temperature changes less than 4°C.

Scattering Methods

When high energy neutrons collide with atomic particles of approximately the same size, they are rapidly slowed down by successive collisions until they attain the same velocity as particles with which they collide. Since the hydrogen atom is most effective in slowing down fast neutrons, the number of slow neutrons will be proportional to the amount of water present. The slow neutron count may be obtained by means of a detector inserted into the soil segment, and water content within the segment can be determined from a calibration curve. This approach is called the neutron method (Bell, 1973).

Another way of estimating water content nondestructively is by measuring attenuation of gamma rays as they pass through the soil segment. This method is most useful for laboratory work since it requires that the source and detector be placed on opposite sides of the segment (Gardner and Calissendorff, 1967). However, the technique has also been applied in the field (Ryhiner and Pankow, 1969; Reginato and Jackson, 1971).

The direct methods supply relatively accurate data about the soil in close proximity to the sensor, or in the case of the gravimetric method, about the sample taken; however, their applications are limited by the cost of instrument installation and operation.

1.1.2 Indirect Methods

Since they do not require physical contact with the soil, indirect methods represent the only realistic means of determining soil water content over large areas. There are two basically different indirect methods, namely water balance and remote sensing. The estimates by remote sensing are discrete in time while the water balance approach can in principle be used on a continuous basis.

Water Balance Method

Rather than by direct measurement, water content is determined as a residual after all inputs (precipitation, irrigation) and outputs (runoff, drainage below the terminal depth, evaporation, transpiration) have been accounted for. While most techniques in this category yield water content for the entire soil column, some models (e.g., Baier and Robertson, 1966) subdivide the column into several zones. Water balance models have proven useful and reasonably accurate (Baier, 1967). More successful applications are hindered by the necessity for areal extrapolation of point measurements which is intrinsic to the method.

Remote Sensing Methods

Remote sensing of soil moisture is based on the change in electromagnetic properties of the soil resulting from an addition of water. The changes and their potential usefulness for soil moisture estimations have been studied in the visible, thermal infrared, and microwave parts of the electromagnetic spectrum.

(i) The Photographic Method - The proportion of incident visible radiation that is reflected from soil particles decreases with increasing thickness of water film around the particles. This is a result of several phenomena (Planet, 1970), the most

important one being multiple reflection at the air/water interface. Successful utilization of this effect is hampered by the interference of soil color and soil drying patterns (Winkler, 1966; Cooper and Smith, 1966), negligible subsurface penetration of the visible radiation, atmospheric interference, etc.; consequently, only qualitative estimates of the surface moisture content have been made by this approach to date.

(ii) The Infrared Method - The flux density of radiation emitted by the soil in the thermal infrared region is proportional to the fourth power of soil temperature. Inasmuch as water has an important effect on soil thermal properties, soils with various moisture contents may sometimes be delineated on thermal imagery (Hunter, 1969), especially if sequential coverage is available. Interference of atmospheric and other variables also influencing the radiation recorded by an infrared sensor represents an important drawback with regard to obtaining quantitative moisture estimates. The depth of penetration is very small for thermal infrared radiation but some response to subsurface moisture exists, mainly due to the diffusivity variations with changing moisture content (Myers and Heilman, 1969; Blanchard et al., 1974; Idso et al., 1975).

(iii) The Microwave Method - The basis of the microwave method of soil water content determination is the difference in dielectric constant of dry soil and of water. While the real part of the relative dielectric constant of dry soil is less than 5, that of water can be higher than 80 at low microwave frequencies. Consequently, the dielectric constant of moist soil will increase compared to that of dry soil; the increase should be in some proportion to the amount of water present. Figure 1 shows real and imaginary parts of the relative dielectric constant of loam as a function of volumetric water content measured at three frequencies. It is apparent that the dielectric constant increases with increasing moisture content. However, the imaginary part responds differently to frequency change than the real part (Figure 1). These differences become important in interpreting microwave signals in terms of soil moisture (Ulaby et al., 1974).

For a homogeneous soil with a smooth surface the amount of reflected microwave energy is given by the power reflection coefficient ρ (Cihlar and Ulaby, 1974). Figure 2 demonstrates that the reflection increases with increasing moisture in the soil. Although the data cover a wide range of frequencies and soil textures, no systematic trend of the power reflection coefficient with frequency or texture is apparent. If the soil is in addition in thermodynamic equilibrium with its environment, then emissivity ϵ is equal to $1 - \rho$; this parameter is indicated on the second vertical axis in Figure 2. Moisture content change from 0.0 cm^3/cm^3 to 0.45 cm^3/cm^3 can be seen to cause emissivity (and power reflection coefficient) change of 0.4.

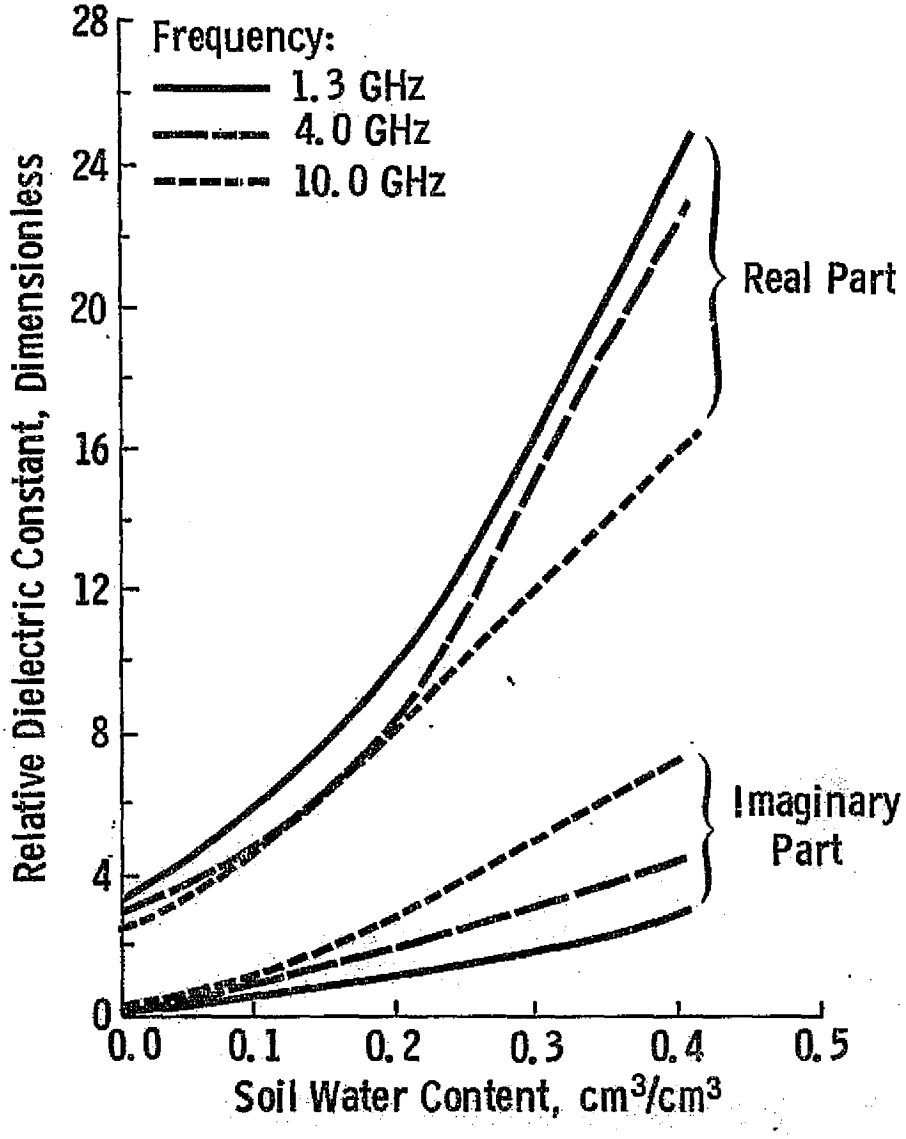

Figure 1. Relative dielectric constant of loam as a function of moisture content. After Cihlar and Ulaby (1974).

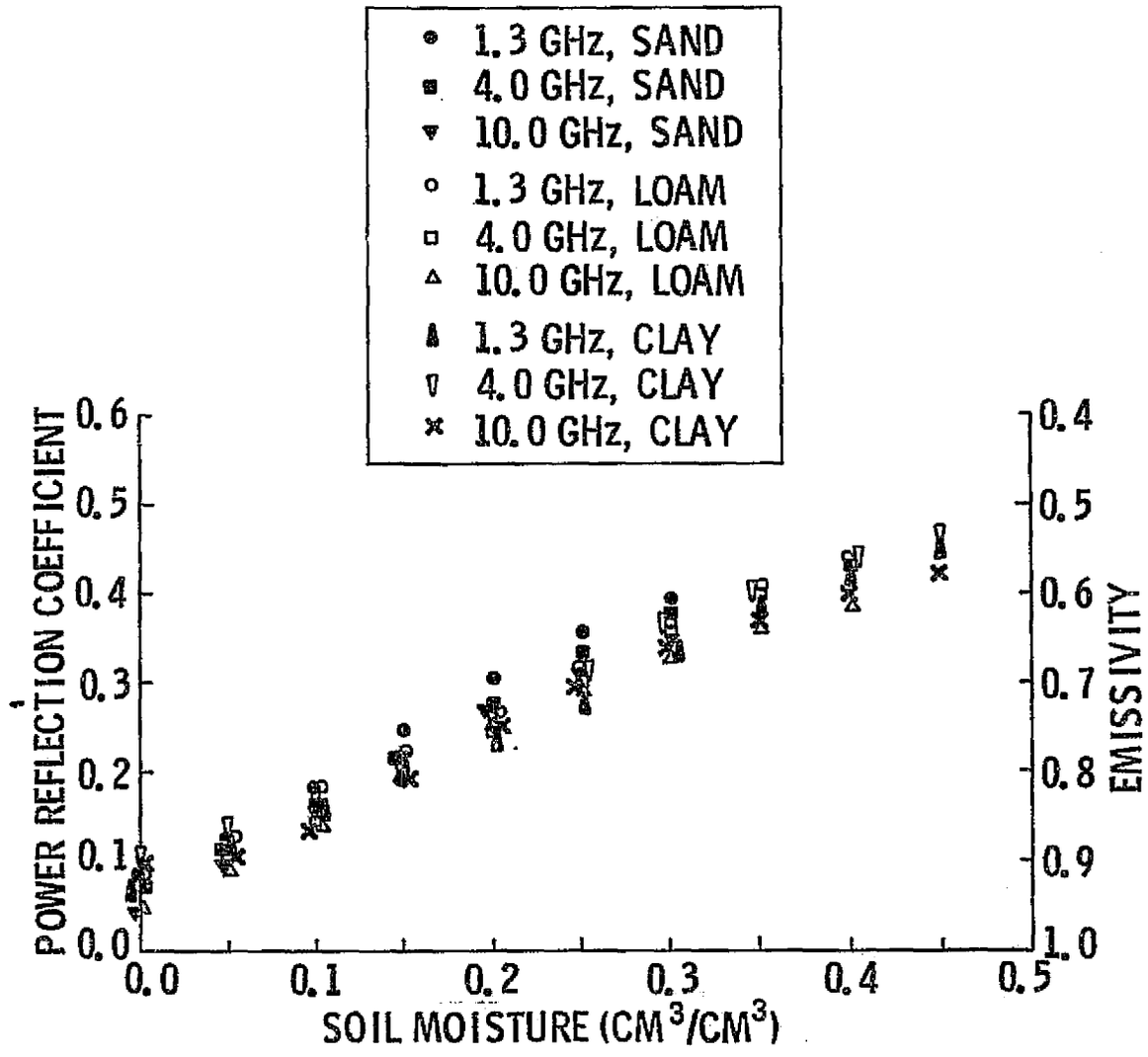

Figure 2. Power reflection coefficient and emissivity as a function of moisture content, frequency, and soil type. From Cihlar and Ulaby (1974).

The two above parameters, ρ and ϵ, are directly related to the outputs of microwave sensors. For example, the scattering coefficient σ^o measured by radar at nadir over a smooth surface is given by (Peake, 1959)

$$\sigma^o = 4\pi\rho \quad . \tag{1}$$

Similarly, radiometric temperature T_{ap} is proportional to emissivity:

$$T_{ap} = \epsilon T_p + (1 - \epsilon) T_s \quad . \tag{2}$$

T_p is physical soil temperature, and T_s is microwave radiation emitted by the upper hemisphere and reflected by the surface in the direction of the radiometer. Atmospheric attenuation effects were neglected in Equation (1) and (2).

Under natural conditions, soil surfaces are generally not smooth; Equation (1) must therefore be modified to account for surface scattering. Secondly, the soil profile is usually not homogeneous because of variations in moisture content, soil texture, bulk density, etc.; subsurface reflection and scattering may therefore occur, thus affecting the signal magnitude measured by the sensor. Thirdly, since the measured signal can consist of contributions from the surface as well as subsurface, it follows that the vertical distribution of soil moisture (due to reflection coefficient ρ and emissivity ϵ) and soil temperature (due to both radiometric temperature T_{ap} and temperature dependence of the dielectric constant of water) can become important. Fourthly, the maximum depth at which moisture can be measured from satellite altitudes appears limited to the upper part of the soil profile (see Chapter 4). Consequently, if moisture information about deeper layers is also needed, the microwave method must be supplemented with another technique.

1.2 PROBLEM STATEMENT

Due to limitations of photographic remote sensing techniques, the only potentially useful methods of large-scale soil moisture determinations are water balance and microwave and infrared remote sensing techniques.

Studies of the microwave method of soil moisture determination conducted so far centered primarily on experimentally documenting the response of microwave sensors to soil moisture, and, more recently, on developing models which would allow prediction of soil moisture content from microwave signal measurements; a list of previous studies has been compiled by Cihlar and Ulaby (1974). The above discussion suggests, however, that an understanding of problems involved in the microwave apporach to soil moisture content determination as well as the development of an operationally efficient algorithm for an extraction of moisture information from the microwave data will not be completely successful unless consideration is also given to moisture and temperature regimes of the soil. It is in this direction that the present study was undertaken, its objective being to establish a basis for incorporating soil moisture and temperature regimes into the microwave method of soil water content determination. The study was limited to bare soil where the microwave method appears more accurate. In addition, studies of moisture and temperature regimes of a vegetated soil require an approach different from that for bare soil. Consideration of both bare and vegetated soil would be beyond the scope of a project of this type. Furthermore, the ground water level is assumed to be sufficiently deep so that it does not affect moisture flow within the soil profile.

Moisture and temperature regimes have been the subject of research in numerous countries, by many investigators, and for a number of years. Rather than attempting to encompass all the various aspects that have been dealt with in the past by the investigators involved, the approach taken here was (i) determining specific parts of these regimes which are of importance to the microwave method, and (ii) attempting to provide answers through research based on relevant data collected either for this study or by other investigators. The following specific problems were identified:

(i) Vertical moisture changes near the surface of a bare soil and the possibility of accurately predicting them by means of a mathematical model. Such a model could be used as a counterpart or complement of the microwave method in a large-area moisture estimation scheme.

(ii) Diurnal variation of soil moisture near the surface. Since the microwave method is time-specific, large diurnal changes in moisture could cause error in predicting the actual water content for a given location.

(iii) Vertical and temporal moisture changes at greater depths in the soil and the extent to which they are related to near surface moisture fluctuations. If such a relationship exists, subsurface moisture might be predicted without necessitating its direct measurements.

(iv) "Mean maximum" bare soil temperature variations to be expected at mid-latitudes as a result of varying surface slope and aspect, time of day, soil moisture content, and soil depth. Knowledge of these values may facilitate estimating errors to be expected in moisture determination by the microwave method due to soil temperature, as well as ways of minimizing these errors.

(v) Brightness temperature and power reflection coefficient changes of a bare soil in which both temperature and moisture vary diurnally. This step combines some of the above results in terms of the microwave method.

(vi) An algorithm for soil water content monitoring over large areas.

The specific problems outlined above also suggest convenient subdivisions for presenting the results. Chapter 2 deals with soil moisture regime (problems (i) through (iii)). Chapter 3 describes results of soil temperature simulations, while the combined effect of moisture and temperature as it is reflected in the brightness temperature and the large area moisture estimation scheme are discussed in Chapter 4. A limited discussion of power reflection coefficient changes is also included in Chapter 4. Chapter 5 presents a review of experimental investigations using active and passive microwave sensors to determine soil moisture content.

CHAPTER 2.

SOIL MOISTURE REGIME

2.1 ALTERNATIVE APPROACHES TO STUDYING SOIL MOISTURE REGIME

Various aspects of soil moisture regime have been studied in several disciplines for a number of years. Most investigations of bare soils were made by soil physicists, although meteorologists and hydrologists also contributed to an understanding of soil water behavior, particularly under field conditions. Studies of soil moisture may be classified as atomistic vs. holistic, field vs. laboratory, and empirical vs. theoretical, among others. This discussion is approached with the assumption that in a large-area determination of soil moisture, only the holistic, field, and empirical or semi-empirical concepts are of interest at this stage. The preference for a holistic approach is determined by the fact that soil water is a part of a dynamic system and is therefore affected by many, often interacting, parameters. The other choices (field and empirical) will be briefly commented upon before a review of pertinent literature is given.

Laboratory experiments, although valuable for explaining the mechanisms involved in soil water behavior, are usually too simplified compared to the field situation. Assumptions commonly made include isothermal conditions, uniform profile, nonradiative regime, constant evaporation rate, etc. It should be noted, however, that some of these studies gave rise to simplified theoretical models of soil water which will be discussed later.

Theoretical equations can, in principle, accurately describe soil water status. Because of the dynamism of soil water, it has been argued (Nielsen et al., 1967) that only numerical, as opposed to analytical, methods are of potential practical usefulness. Either technique involves parameters which must be evaluated for a given soil before the theoretical models can be used; these parameters may vary with distance, time, and soil condition (Nielsen et al., 1973). In addition, solution of the differential equation of water flow requires knowledge of the boundary condition which, especially for a wet or moist soil, is a function of atmospheric conditions. Due to these characteristics, theoretical models appear to have little usefulness for predicting field moisture changes

at the present. Other models, developed after simplifying assumptions were made, have been shown to yield soil moisture estimates which agreed with experimental measurements (Black et al., 1969). Some authors (Gardner, 1973; Gardner and Gardner, 1969) have demonstrated that the simplified solutions can be used to predict total evaporation for a homogeneous soil. However, the practicality of these methods under field conditions is yet to be established.

Apart from direct measurements, almost all traditional methods of soil water content determination under field conditions are based on a budgeting approach. The basic relationship involved in determining change in storage S is

$$\frac{dS}{dt} = I(t) - O(t) \tag{3}$$

where I(t)and O(t) refer to all inputs and outputs in the soil at time t. Equation (3) may be applied to a system of any size provided that I(t)and O(t) can be determined. For a three dimensional body of bare soil the boundaries of which extend above the surface, Equation (3) can be written in the following form for a period Δt:

$$\Delta S \doteq P + I + F_i - F_o - AE, \tag{4}$$

where

S = change in soil water storage;
P = precipitation and dew during Δt;
I = irrigation during Δt;
AE = actual evaporation during Δt.

Assuming subsurface lateral homogeneity, the inflow F_i and outflow F_o have surface horizontal (F_{ih}, F_{oh}) and subsurface vertical (F_{iv}, F_{ov}) components. Usually runoff R and drainage D are defined respectively as

$$R = F_{oh} - F_{ih}, \tag{5a}$$

$$\text{and} \quad D = F_{ov} - F_{iv}. \tag{5b}$$

If one assumes horizontal uniformity (R = 0), Equation (4) can be written as

$$\Delta S = P + I - AE - D. \tag{6}$$

The amount of water held in the soil at the time $(t + \Delta t)$ can then be computed as

$$S(t + \Delta t) = S(t) + \Delta S$$

$$= S(t) + P + I - AE - D. \qquad (7)$$

Individual components of Equation (7) can be determined in various ways.

Initial Water Storage

Initial water storage S(t) is determined by direct sampling or assumed to have a certain value, for example after snowmelt. If the computation is performed for a sufficiently long time prior to the time interval of interest, the choice of S(t) becomes insignificant.

Precipitation

Precipitation amounts are measured by rain gauges and extrapolated into areas between gauges to obtain "areal" rainfall. However, there is considerable uncertainty associated with this extrapolation. A measure of this uncertainty can be obtained from dense raingauge networks. Figure 3 shows the ratio of maximum average areal rainfall in an area to the average maximum point rainfall over the area plotted vs. the area size. Data for 30 minutes, 1 hour, and 24 hours duration were measured at networks located throughout the United States, while curves for 3 and 6 hours were interpolated. It is apparent that as the area size increases and duration of a storm rainfall decreases, the differences between point and areal rainfall become more pronounced. For example, in a 110 sq. mi. area, a 30 minute rainfall may be 1.67 times higher at some point than the average rainfall over the area (Figure 3). The location of maximum rainfall is believed to be random (U.S. Department of Commerce, 1958). Hershfield (1969) concluded from dense networks data collected in various parts of the U. S. that in general, the standard deviation of point rainfall increases with an increasing rainfall amount; that is, the coefficient of variability remains relatively constant as the area size increases. Extreme variations of storm totals, actually observed at 20 dense networks and during storms 30 minutes to 39 hours in duration, are shown in Figure 4 by an enveloping line as a function of the shortest

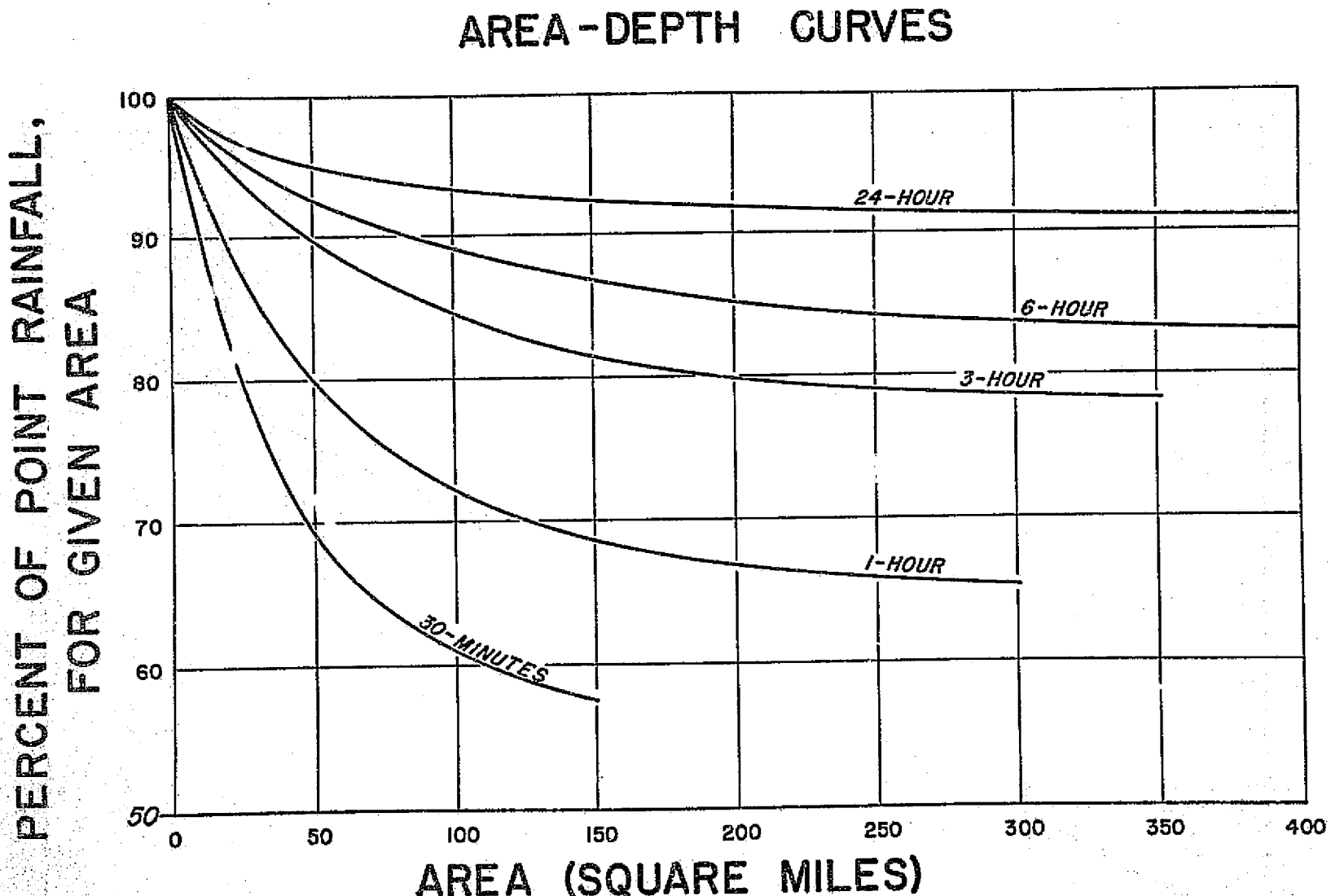

Figure 3. Variability of rainfall as a function of area and rainfall duration. From U.S. Department of Commerce (1958).

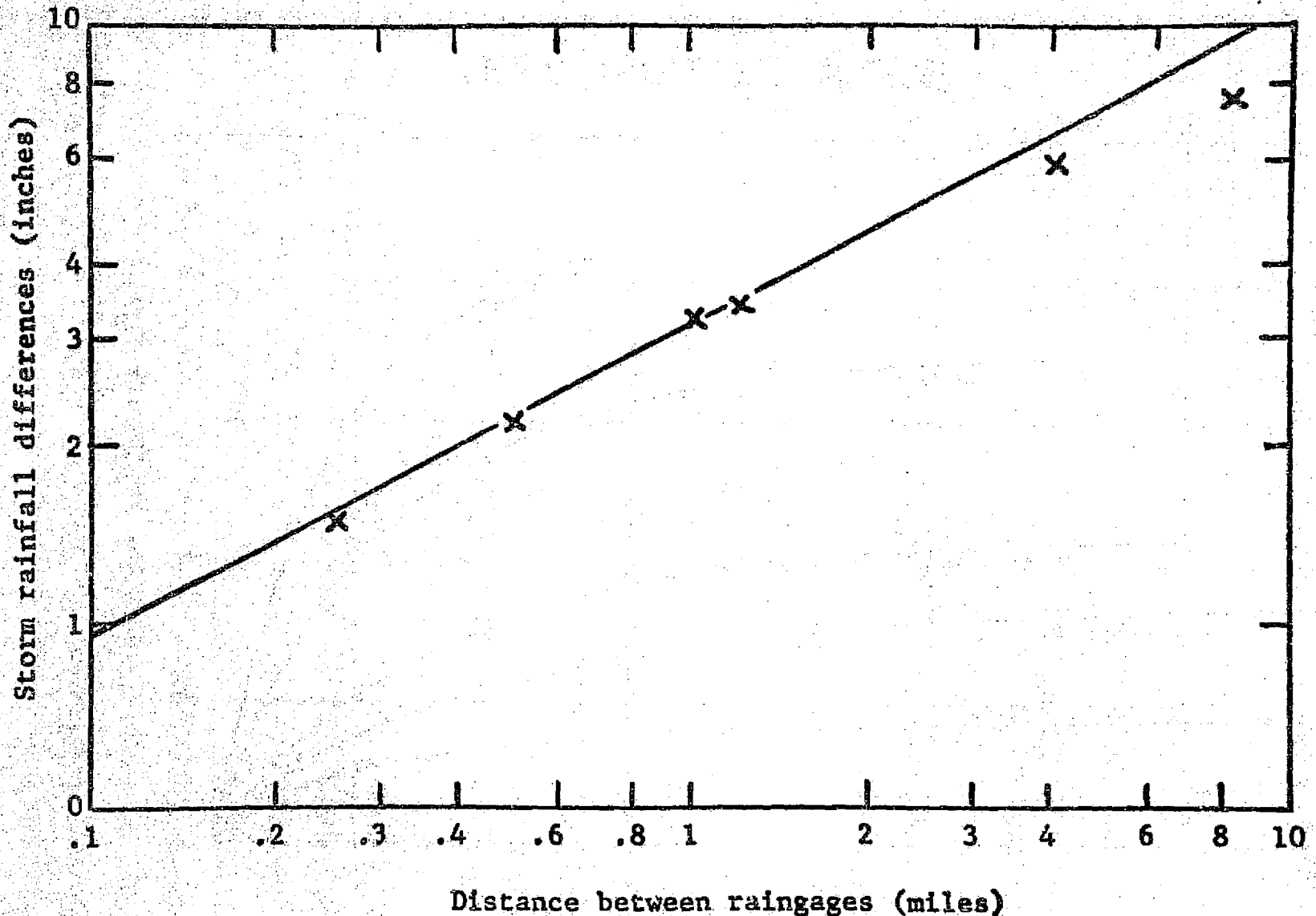

Figure 4. Storm rainfall differences as a function of distance between raingauges. From Hershfield (1969).

distances between raingauges. Since these data were based on a relatively small sample, a larger search using denser networks would provide measurements to raise the enveloping line (Hershfield, 1969); nevertheless, Figure 4 suggests that the rainfall could differ by 2.54 cm over a distance of 0.16 km.

From the above data it is evident that precipitation can be a source of considerable uncertainty in using the water balance approach for soil moisture content estimation. Various methods have been developed for estimating areal rainfall from limited raingauge measurements (e.g., Hutchinson and Walley, 1972; Chidley and Keys, 1970), but the predictions given by these models are limited by the input data.

Irrigation

In contrast to precipitation, irrigation amounts are usually well known. The areal distribution is also more uniform although, depending on the method of application, differences in the amount of water added to various parts of a field can occur.

Evaporation

Three conditions must be satisfied before evaporation from bare soil can occur. First, water must be available at or sufficiently near the soil surface. Secondly, latent heat must be available at the same sites. Thirdly, a positive water vapor pressure gradient must exist between the soil surface and the air above it.

The evaporation from an initially wet bare soil occurs in three stages (Penman, 1941; Philip, 1957; Philip, 1967). The first stage is characterized by a high evaporation rate with the maximum evaporative water loss limited by atmospheric condi The second stage is initiated when soil water cannot be transmitted fast enough to t evaporation sites. Here evaporation rate decreases, surface dries rapidly, and wat transfer in vapor form becomes important. The third stage is typified by a low, relatively constant evaporation rate controlled by forces of adsorption at the liquid-solid interfaces (Lemon, 1956). Idso et al. (1974) demonstrated the existence of these three stages under field conditions. They showed that the third stage is initiated at the surface water content that corresponds to a retention of two molecular layers around surface soil particles. The transitions between stages 1, 2 and 2, 3 could be identified on the basis of albedo measurements.

The above discussion indicates that bare soil evaporation is either primarily atmosphere-limited or primarily soil-limited. Accordingly, the process has been studied extensively by both meteorologists and soil scientists, among others. Numerous approaches with various degrees of empiricism and with more emphasis on some portion of the evaporative process than on others have been developed. Nunn et al. (1970) summarized four mass transport formulas, twelve aerodynamic formulas, an eddy correlation method, an energy balance method, and five empirical methods for computing evaporation. Equations of Baier and Robertson (1965), Christiansen (1968), and Eagleman (1967) should be added to the last group. These formulas require various inputs, but in general, the more complex ones are more accurate and can be applied to shorter time periods. The simplest formulas have been developed for a period of one month, although their use for one day intervals can give satisfactory results (McGuinness and Bordne, 1972; Eagleman, 1971).

The soil-limited evaporation stages have been dealt with at various levels ranging from theoretical to empirical. Many of the theoretical studies are of limited interest here because they do not yield a practical method for evaporation determination in the field. Two recent studies warrant mentioning, however. Black et al. (1969) predicted cumulative evaporation from a Plainfield sand to within 0.3 cm of water for a period of 3 months. The prediction was based on an analytical solution of the flow equation. Gardner (1974) used fractional water loss vs. square root of time curve as the basis for predicting evaporation from a fallow field soil. It should be noted that in both studies, the necessary relationships were derived experimentally for the same soil, i.e., the "training" and "testing" sets overlapped; thus the predictive capability of these techniques for other soils has not been fully demonstrated. The studies did show, however, that simplified theoretical relations can be used successfully under field conditions.

On the more empirical side, the most common approach to studying the soil-limited evaporation stages have been attempts to determine the relationship between the actual (AE) and the potential (PE) evaporation. Various relationships have been derived from studies of evaporation or evapotranspiration (Baier, 1967; Selirio, 1969). Selirio (1969) argued that the type D-relationship (exponential decrease of AE when soil moisture is reduced to a certain level), presented by Lemon (1956), Philip (1957), Holmes and Robertson (1960) and others, is valid for both bare and vegetated surfaces. Selirio and Brown (1971) obtained close correspondence between bare soil moisture measured and calculated using the type D-curve. On the basis of data from five different lysimeter

studies, Priestley and Taylor (1972) plotted the AE/PE ratio against the accumulated actual evaporation minus precipitation difference. They concluded that the AE/PE ratio equals unity until the accumulated difference reaches some critical value and then decreases linearly; the critical value was 0.2 cm in one bare soil case. According to Baier (1969), the AE/PE relationship depends on the moisture characteristics of the soil.

Drainage

Soil water in excess of that which can be retained for extended periods of time drains out of the soil profile. Its amount can be determined directly by measuring moisture content changes in the profile when evaporation is prevented (Wilcox, 1959; Ogata and Richards, 1957; Hillel, 1971; etc.). Alternatively, the drainage amounts can be estimated from water flow theory using experimentally measured hydraulic gradient (Stone et al., 1973). However, without direct measurements or some knowledge of soil profile characteristics, drainage estimates become difficult. Consequently, when computing moisture storage in the subsoil, it is often assumed that water in excess of a storage capacity of the soil profile drains into deeper layers.

Various water balance studies have been made, for both bare and vegetated conditions. The studies involve Equation (7) and differ primarily in the way in which individual components are determined. Black et al. (1969) based the estimates on soil water flow theory and on empirical determination of the parameters needed. Quashu (1969) computed moisture depletion from soil initially at field capacity by an exponential decay relation in which a "depletion coefficient" was an experimentally evaluated lumped parameter; this coefficient expressed a combined effect of climatic, biotic, and soil variables. Eagleman (1971) calculated AE from a formula involving powers of PE and of moisture ratio (ratio of available water to the maximum available water in the soil profile). Baier and Robertson (1966), Selirio and Brown (1971), and Vanderlip and Brown (1974) used layered models, in which water balance is computed separately for a number of layers within the soil profile. In general, these studies demonstrated that water content within the soil profile can be monitored using the water balance method, but the accuracy achieved varied with the complexity of the model and the input parameters used. For application to larger areas, rainfall variability presents a major problem. In addition, runoff enters as an important factor on sloping surfaces.

It should be noted that hydrologic models of watersheds (Holton et al., 1974; Smith and Lumb, 1967) are also water balance models. Some of these models use Antecedent Precipitation Index as the measure of soil moisture deficiency; its value is determined as

$$API(t) = API(t-1)\,K + P(t), \qquad (8)$$

where API(t) = value of API for day t.

K = recession factor.

As stated in section 1.2, three specific soil moisture problems were pursued in this study.

(i) Development and testing of a layered water balance model for predicting bare soil moisture changes in the upper portion of the soil profile. Layered models are preferrable to models which regard the entire soil profile as one layer because they allow prediction of the temporal moisture changes as a function of depth; moisture varies with depth in both bare and vegetated soil. However, existing layered water balance models do not have sufficient depth resolution. For example, the bare soil model of Baier et al. (1972) consisted of three layers, and that of Selirio and Brown (1971) of four layers. In addition, layered models require depth-dependent coefficients as an input, and these coefficients are not readily available.

(ii) Diurnal variation of soil moisture near the soil surface. Since the time increment for which moisture changes are predicted by water balance models is one day or more, diurnal water content variations would not be accounted for by this technique. Therefore, from the viewpoint of real-time measurements, the magnitude of the diurnal soil moisture changes under various conditions becomes important.

(iii) Vertical and temporal moisture changes at greater depths ("subsurface") and the extent to which they are related to near-surface moisture fluctuations. This problem refers to the possibility of estimating subsurface moisture without necessitating its direct measurement.

2.2 NEAR-SURFACE MOISTURE REGIME

2.2.1 Layered Water Balance Model

2.2.1.1 Development

Development of a layered water balance model involves (i) specifying methods for computing inputs (precipitation, drainage) and losses (evaporation,

drainage) into individual layers, and (ii) combining these into a model. Since evaporation is the main depletion mechanism near the surface, its determination is crucial for constructing an accurate model; therefore, it will be dealt with first.

2.2.1.1.1 Evaporation - Several methods for computing evaporation have been described in section 2.1. Because of its simplicity, the approach based on AE/PE ratio as a function of soil moisture was adopted here. If the soil profile consists of n layers, the amount of water lost by evaporation from a soil layer j on day i, AE_{ij}, can be calculated as (Baier et al., 1972)

$$AE_{ij} = k_j C_{ij} PE_i \quad , \tag{9}$$

where C_{ij} = coefficient accounting for those soil characteristics in the j^{th} layer which affect evaporation loss;

PE_i = potential evaporation on day i;

k_j = depth coefficient for the j^{th} layer.

The total amount lost from n layers, AE_i, is equal to

$$AE_i = PE_i \sum_{j=1}^{n} k_j C_{ij} \quad . \tag{10}$$

If moisture content is sufficiently high, $AE_i = PE_i$ (section 2.1), and $C_{ij} = 1$ (Baier et al., 1972). Therefore,

$$\sum_{j=1}^{n} k_j = 1. \tag{11}$$

Equation (11) shows that coefficients k_j distribute the total evaporated amount AE_i to individual layers within the profile. The values of k_j can thus be determined directly from Equation (9) when $C_{ij} = 1$. When actual evaporation falls below potential evaporation, C_{ij} becomes less than one and its value will be a function of soil drying characteristics (Section 2.1).

In order to use Equation (9), one must obtain estimates of k_j and of C_{ij}. As noted before, k_j values published in the literature (Baier et al., 1972; Selirio and Brown, 1971; Vanderlip and Brown, 1974) do not provide the spatial refinement needed. It therefore became necessary to obtain new k_j estimates with adequate depth resolution. Since this method of AE_i computation is essentially empirical, the new estimates must be derived from accurate measurements in order for Equation (9) to yield adequate results.

In the course of an experiment dealing with near surface water fluxes in a bare soil, researchers at the U.S.Water Conservation Laboratory in Phoenix, Arizona, acquired a set of detailed measurements of soil moisture. These included volumetric soil water contents m_j for seven depth increments (0-1 cm, 1-2 cm, 2-3 cm, 3-4 cm, 4-5 cm, 5-7 cm, and 7-9 cm) at 20 minute intervals for a number of days, and total actual evaporation AE_i (see Appendix B for their experimental procedure). Jackson (1973) presented daily values of moisture for a 37-day experiment conducted in March and April of 1971; the same data were provided for the present study in tabular form*. Since these values were computed from individual measurements between 0000 (midnight) and 2400 for any given day, the averages were considered representative of conditions at 1200* hours. Values of AE_{ij} were computed as the difference between m_j for adjacent days, and corresponding m_j was determined as the average of m_j's for adjacent days. Pan evaporation measurements were obtained from the University of Arizona Citrus Experimental Station (latitude 33°23'N, longitude 111°58'W for the same time period. Under the conditions of the evaporation experiment (Appendix B), the potential evaporation (PE) could be expected to occur at the levels close to pan evaporation because of the large thermal advection. This was also confirmed by the ratios of actual and pan evaporation which were close to 1.0 for the first three days in the March, 1971, experiment. Consequently, the measured pan evaporation values were considered equal to potential evaporation (PE) for all data collected at the U. S. Water Conservation Laboratory. Since the PE values were recorded at 0800 hrs., the measured PE values were partitioned for the 1200 to 1200 periods. Consequently, sets of m_{ij}, AE_i, AE_{ij}, and PE_i data were available for an evaporation period of 37 days.

*Courtesy of Dr. R. D. Jackson, U. S. Water Conservation Laboratory, Phoenix, Ariz.

To determine values of k_j, ratios AE_{ij}/PE_i were plotted against the corresponding m_{ij}'s for each of the seven layers between 0 and 9 cm. Data points from a July, 1970, experiment were plotted in Figure 5 and others for comparison only; it should be stressed that the March, 1971, data alone were used in deriving k_j and X coefficients. Figure 5 shows the AE_{ij}/PE_i ratios for depth 0-1 cm: at the highest moisture content, the value is approximately 0.13. In this fashion, preliminary estimates of k_j were obtained for depths 0 to 9 cm. These estimates were preliminary because even for the highest moisture content for which data were available, AE_i was less than PE_i, their ratio being 0.90. For this reason, a second k_j set was obtained after dividing the preliminary estimates by 0.90.

In the computations described so far, no account was taken of the layers below 9 cm from which evaporation also occurs. The total thickness of the evaporation zone in bare soil is not constant but depends on soil water diffusivity, moisture gradients, evaporation demand, etc. Data from the same experiment indicated that the plane of zero water flux varied between 15 and 35 cm (Jackson et al., 1973). Laboratory and field experimental data have been presented which show that the bulk of evaporated water originates in the 0-15 cm to 0-70 cm layer (Benoit and Kirkham, 1963; Keen, 1922; Fritton et al., 1970; Hanks and Gardner, 1965; Willis and Bond, 1971). In this study, a constant thickness of 30 cm was chosen; this also corresponds to an upper moisture zone thickness in some hydrological models (e.g., Smith and Lumb, 1967). Since no detailed measurements were available for the layers between 9 and 30 cm depth, it was assumed that k_j values decrease linearly in that region. These extrapolated values, together with the experimentally derived values, are shown in Figure 6 and Table 1.

Given k_j's from Table 1, values of C_{ij} (Equation (9)) can be computed for all measured moisture contents; for any day i and layer j,

$$C_{ij} = \frac{AE_{ij}}{k_j\, PE_i} . \qquad (12)$$

C_{ij} will thus decrease from unity when $AE_i = PE_i$ to zero when $AE_i = 0$. Figure 7 and 8 show C_{ij} values calculated for data from several experiments (all on Adelanto loam) at two depths, 0-1 cm and 2-3 cm. The values of C_{ij} remained constant to some value of moisture content and then sharply decreased; this suggests that the exponential decay relation between C_{ij} and m_j (type D-curve, section 2.1) holds for these data. There are two noteworthy regularities, however. First, the critical moisture content below

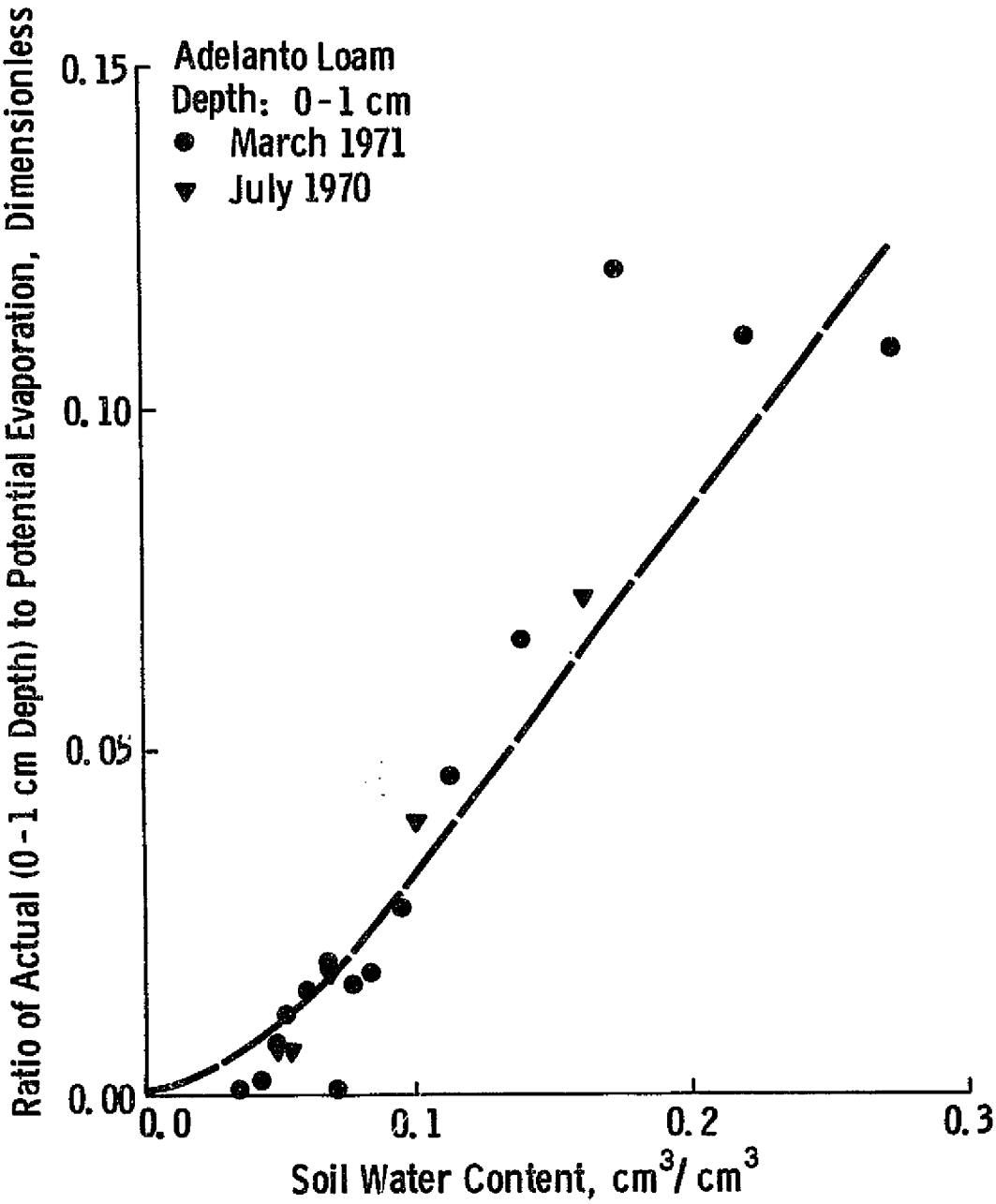

Figure 5. Relationship between the ratio of actual (depth 0-1 cm) and potential evaporation and soil water content.

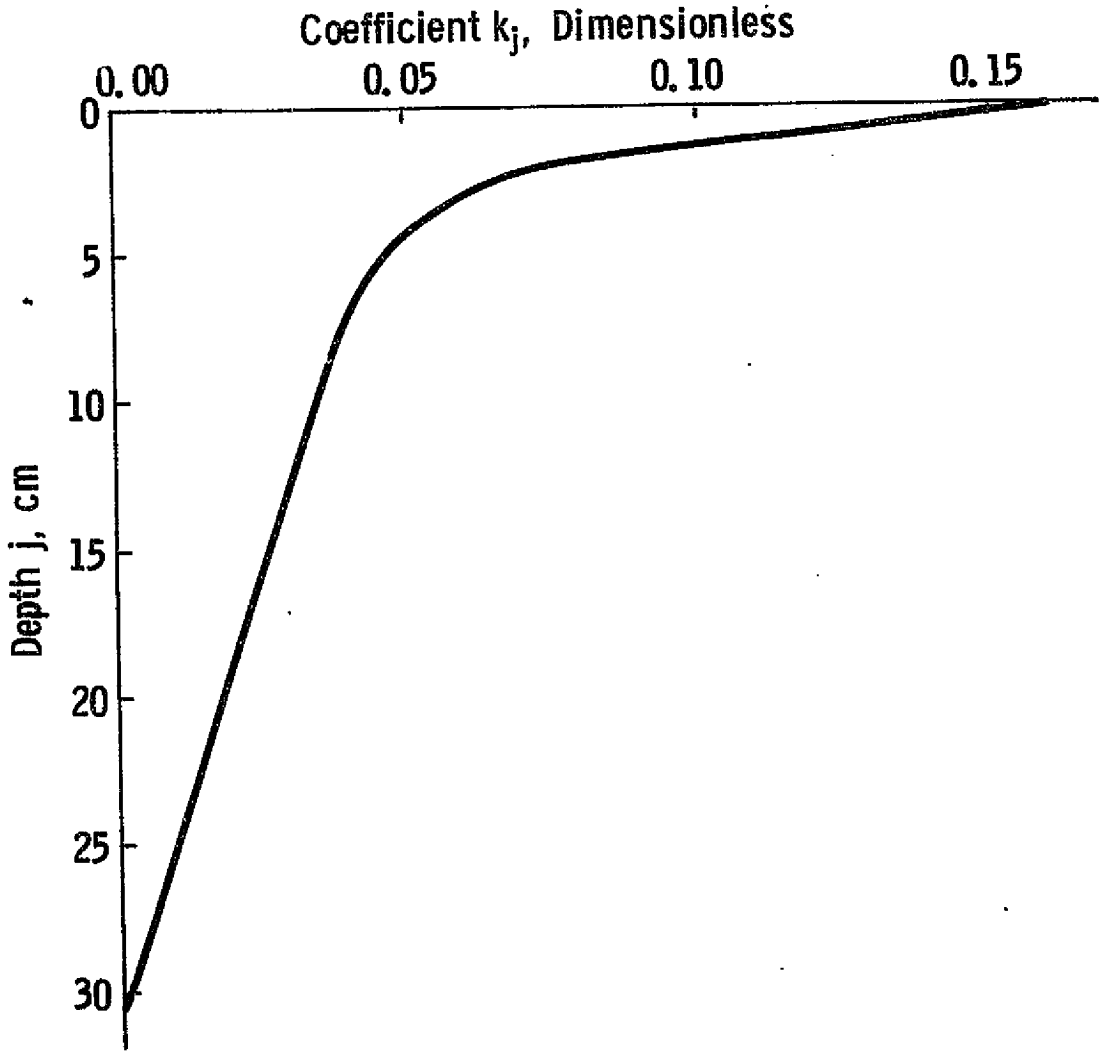

Figure 6. Coefficient k as a function of depth.

Table 1. Depth coefficients k_j for the layered water balance model.

Depth j (cm)	Coefficient k_j (dimensionless)	Depth j (cm)	Coefficient k_j (dimensionless)	Depth j (cm)	Coefficient k_j (dimensionless)
0-1	0.148	10-11	0.035	20-21	0.018
1-2	0.094	11-12	0.033	21-22	0.016
2-3	0.069	12-13	0.032	22-23	0.015
3-4	0.060	13-14	0.030	23-24	0.013
4-5	0.051	14-15	0.028	24-25	0.011
5-6	0.047	15-16	0.026	25-26	0.009
6-7	0.042	16-17	0.025	26-27	0.008
7-8	0.039	17-18	0.023	27-28	0.006
8-9	0.038	18-19	0.021	28-29	0.004
9-10	0.037	19-20	0.020	29-30	0.002

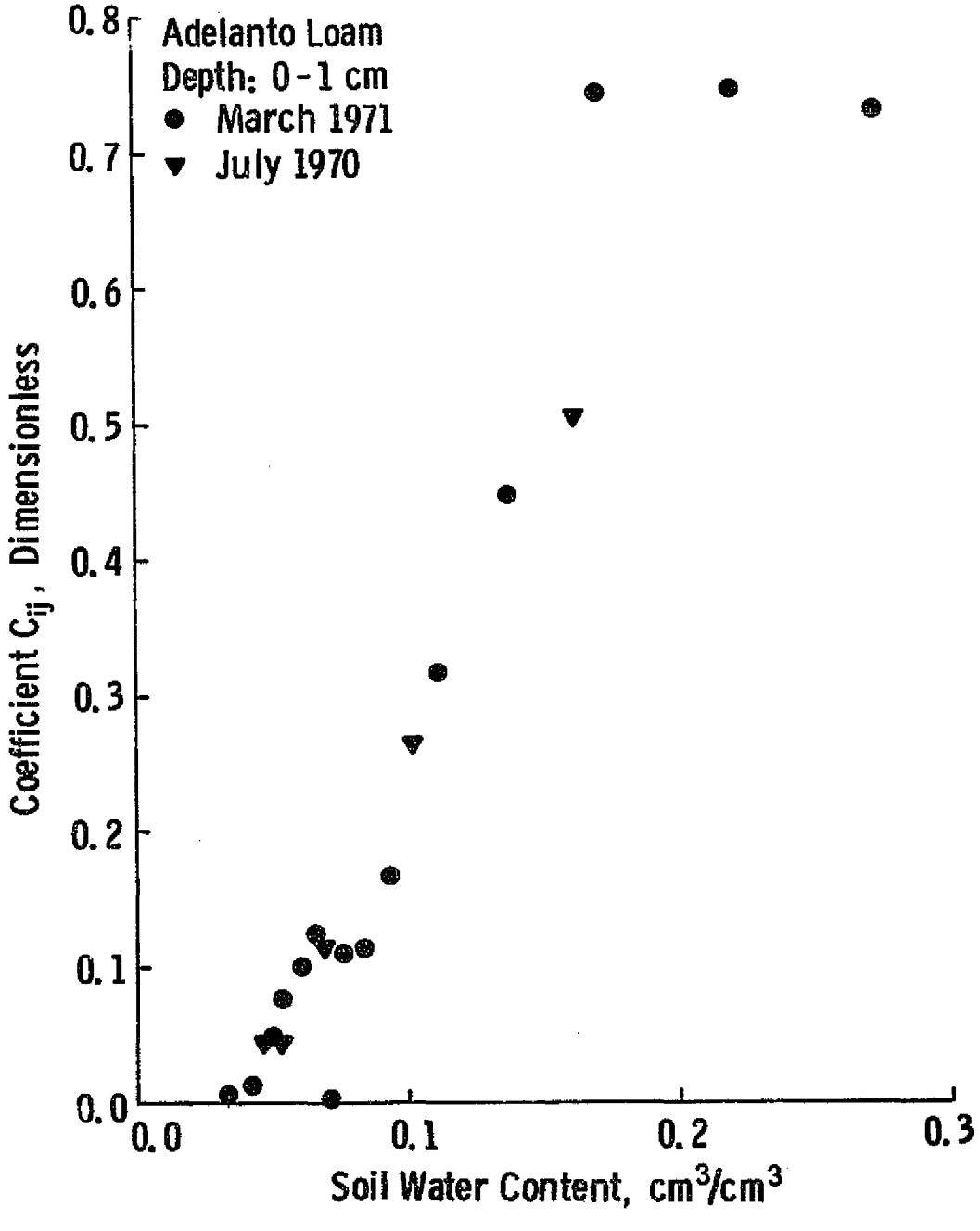

Figure 7. Coefficient C_{ij} as a function of soil water content (depth 0-1 cm).

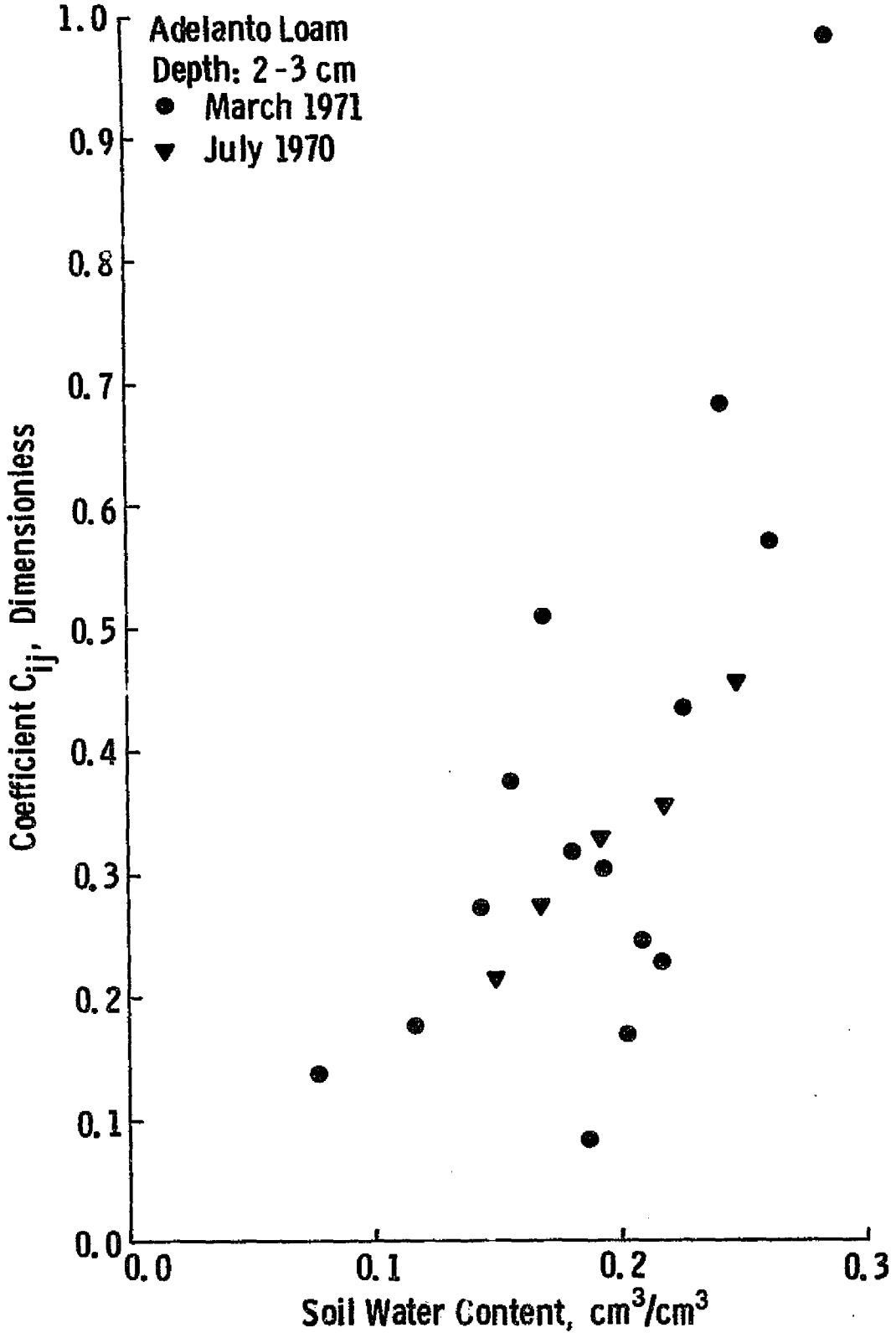

Figure 8. Coefficient C_{ij} as a function of soil water content (depth 2-3 cm).

which C_{ij} decreased to less than one, is lower near the surface than at greater depths. Secondly, the decrease of C_{ij} becomes more rapid as the depth increases (Figure 7 and 8).

The exponential decay relationship may be expressed as

$$C_{ij} = 1 \qquad \text{if } m_{ij} \geq 0.95\, SC_j \tag{13a}$$

$$= X^{\frac{m_{ij} - 0.95SC_j}{SC_j}} \qquad \text{otherwise.} \tag{13b}$$

where SC_j = storage capacity of the j^{th} layer. Selirio (1969) used X = 127.42. Equation (13b) represents a family of curves, however, which differ primarily in the rates of decay. Attempts to calculate X from the experimental data were not successful because of the large scatter of data points (Figure 7 and 8). Therefore, values of X were derived by trial and error so as to represent the scatter of C_{ij} points for each layer. It may be noted that Equation (13b) can also be written as

$$C_{ij} = \exp\left(\alpha \frac{m_{ij} - 0.95SC_j}{SC_j}\right), \tag{14}$$

$$\alpha = \ln X.$$

Values of X and α for 30 layers 1-cm thick are given in Table 2. Values for depths greater than 9 cm were extrapolated on the basis that as X increases by a factor of 2, so does the thickness of the soil layer to which this X value applies.

2.2.1.1.2 Distribution of Precipitation - The technique used to distribute precipitation to various layers was identical to that of Baier et al (1972). As water infiltrates below the surface, each layer is saturated to its storage capacity before water drains through it into the next layer; water remaining after saturating the deepest layer was considered as drained out of the profile and did not enter any computations.

Table 2. Values of X and α as a function of depth for the layered water balance model.

Depth (cm)	X (dimensionless)	α (dimensionless)
0-1	20.	2.9957
1-3	80.	4.3820
4-5	400.	5.9915
5-9	800.	6.6846
9-17	1600.	7.3778
17-30	3200.	8.0709

2.2.1.1.3 Model - A flowchart for the water balance model is shown in Figure 9. The actual computation of soil moisture change for a given day i consisted of three steps:

(i) Assignment of depth coefficients k_j to each layer j. For a sufficiently moist soil, k_j's were equal to those in Table 1. If the near-surface layers dried out below a "critical water content" (CRWC), k_j values were shifted down one layer for each "dry" layer. This modification was based on the observation that after moisture content of the 0-1 cm layer decreased below approximately 0.06 to 0.08 cm^3/cm^3, moisture loss from the 1-2 cm layer increased. According to Jackson (1973), moisture content of 0.06 cm^3/cm^3 for Adelanto loam corresponds to approximately two molecular layers, and that of 0.08 cm^3/cm^3 is equivalent to a tension of 200 bars. In the following sections, CRWC was assumed equal to 0.08 cm^3/cm^3 for loam and silt loam, and 0.10 cm^3/cm^3 for clay loam.

(ii) Computation of actual evaporation AE_{ij} and total evaporation AE_i for NL layers. This computation followed Equations (9) and (13). Values of AE_{ij} were set equal to 0.0 if m_{ij} was less than 0.03 cm^3/cm^3.

(iii) Distribution of precipitation measured for day i was carried out as previously explained (section 2.2.1.1.2; Figure 9) with one modification: the deepest layers reached by the rainfall were not recharged completely so that a more realistic moisture gradient with depth could be obtained.

2.2.1.2 Testing

The water balance model described in previous sections was tested on four sets of data (Table 3). The first set (TS1) was used to derive values of k_j and C_{ij}. The second set (TS2) was obtained in an experiment carried out in July, 1970, which was otherwise similar to the March, 1971, experiment (Appendix B). The third (TS3) and the fourth (TS4) testing sets were obtained during measurements of radar backscatter from bare soils near Eudora, Kansas; data for the 1973 season (TS3) were presented by Cihlar (1973). For these comparisons (Tables 5 though 8) predicted values were averaged so as to coincide with the depth increments sampled in various testing sets. The follow-

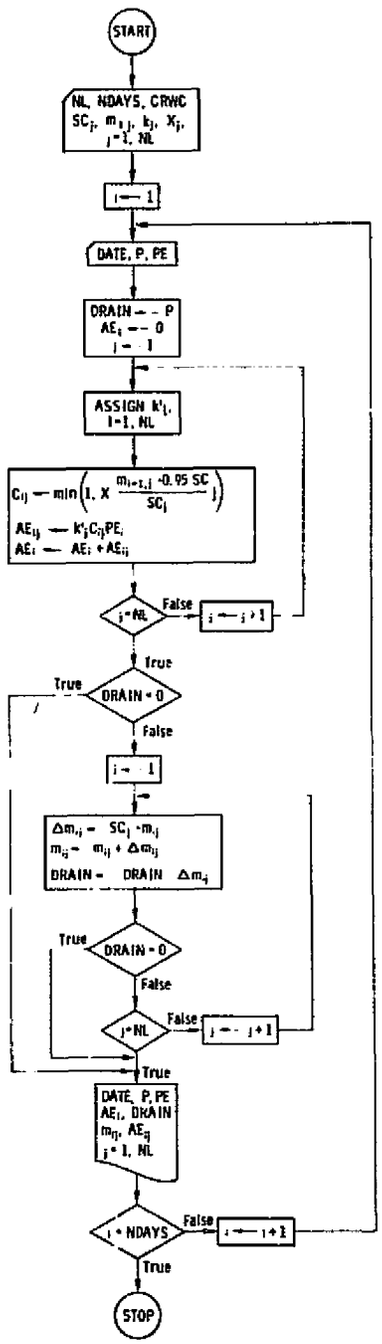

Figure 9. Flowchart of the layered water balance model.

Table 3. Parameters of four data sets (TS1 through TS4) used to test the layered water balance model.

Data Set No.	Location and Soil	Date		Number of Days		Depth Increments sampled (cm)	Potential Evaporation		
		From	To	Total	When Soil Samples Taken		Source	Statistics (cm) Mean	Statistics (cm) Standard Deviation
1	Phoenix, Az. Adelanto loam	3/6/71	4/8/71	33	15	0-1, 1-2, 2-3, 3-4, 4-5, 5-7, 7-9	Pan evaporation*	0.526	0.069
2	Phoenix, Az. Adelanto loam	7/12/70	7/17/70	6	6	as above	Pan evaporation*	1.077	0.063
3	Eudora, Ks. Eudora silt loam	7/25/73	9/5/73	43	8	0-1, 1-2, 2-5, 5-9, 9-15, 15-25, 25-35	Computed*	0.560	0.104
4	Eudora, Ks. Pawnee clay loam	8/25/72	9/15/72	28	3	0-2, 2-5, 5-9, 9-15	Computed*	0.445	0.095

*See text for explanations.

ing data sources were employed to calculate potential evaporation for TS3 and TS4. Temperatures, relative humidities, wind speed, and rainfall were either measured at the experimental site or computed from linear regression equations developed on the basis of on-site measurements (dependent variable) and of the University of Kansas meteorological station measurements (independent variable) for the overlapping periods. Estimates of percent sunshine were obtained by averaging values reported by the U. S. Weather Bureau Airport Stations in Topeka and Kansas City, respectively. Values of daylight duration and total radiation outside the atmosphere were taken from List (1951). Using these data, potential evaporation values were computed by methods of Penman (1948), Baier and Robertson (1965), Christiansen (1968), Eagleman (1967), and Thornthwaite (1948); however, only results obtained from the Penman equation were used in the water balance calculations.

Figure 10 shows computed and measured (TS1) moisture contents for three layers (0-1 cm, 3-4 cm, 7-9 cm). The predicted values were in good agreement with measured values, especially for the period 4 to 16 days after irrigation. For the remaining two measurements (23 and 37 days after irrigation), soil at greater depths dried out faster than the model predicted. This suggests that the "sinking" of k_j values for lower moisture contents did not raise AE_{ij} values sufficiently. It is possible that the CRWC value should also increase with depth, thus allowing for faster "sinking" of k_j coefficients. The difference between computed and measured values was worst at the depth of 3-4 cm as indicated in Table 4. These data show that 23 days after irrigation, prediction was satisfactory for all depths except the 3-4 cm layer, while its accuracy decreased for the adjacent layers during the subsequent period.

Table 5 gives a statistical description of the correspondence between measured and computed values for TS1; all pairs of values are plotted in Figure 11. The good predictive capability of the model is indicated by the high correlation coefficient (≥ 0.959 for individual layers) and low standard error of estimate (≤ 0.0111 for individual layers). An interesting and repeatedly occurring feature of the predicted moisture contents was that the slope of regression lines for individual depths was less than unity; that is, the model overestimated actual evaporation for a moist soil but underestimated it when the soil became dry. This is probably again related to k_j values although the slope was also below unity for the surface layer in two of the four testing sets (TS1, TS3; see Table 5,7).

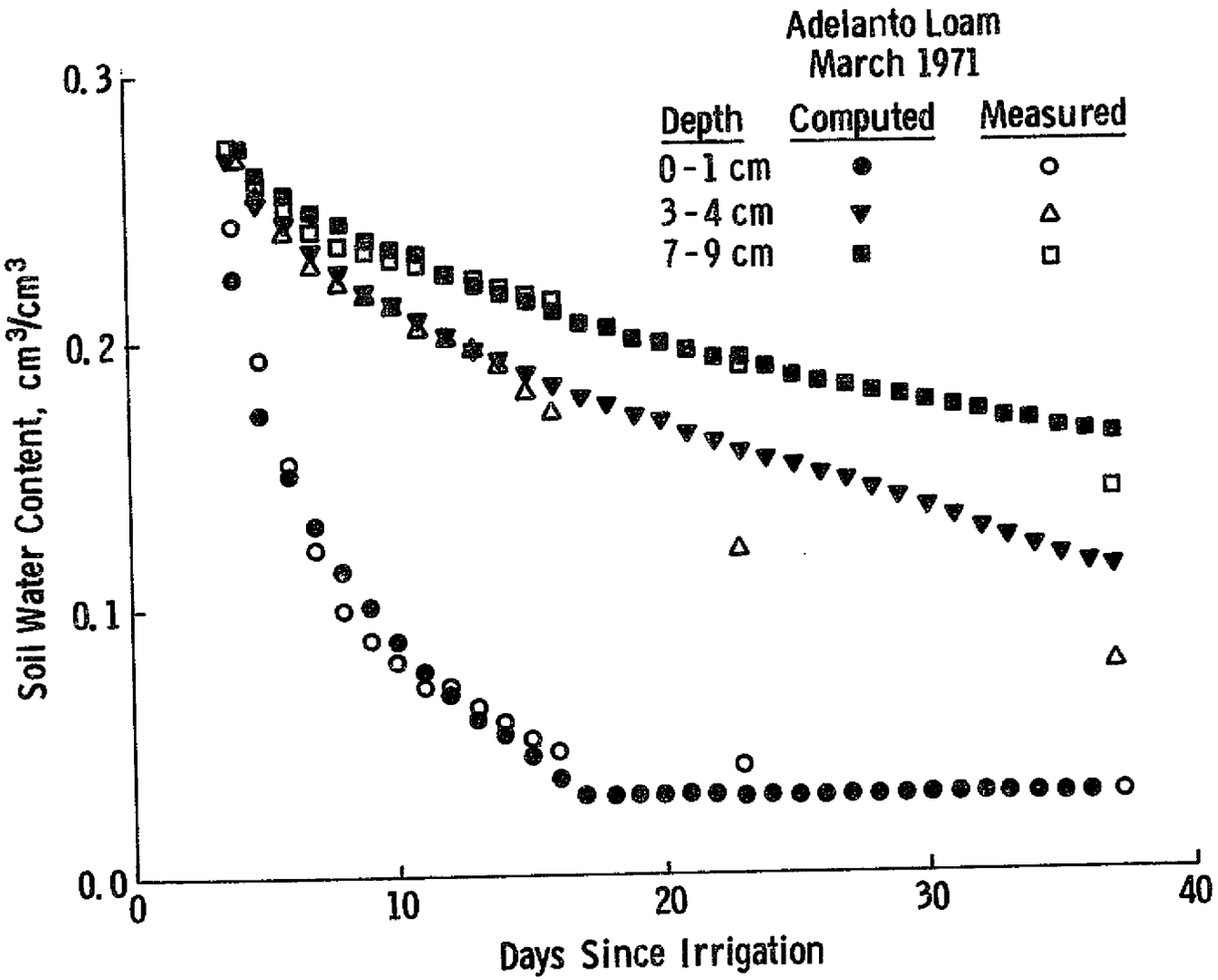

Figure 10. Comparison of computed and measured soil water contents for three depths as a function of time.

Table 4. Differences between computed and measured soil water contents at 16, 23, and 37 days after irrigation, data set TS1.

Day Since Irrigation	Difference between computed and measured moisture content for depth increment (cm^3/cm^3).						
	0-1	1-2	2-3	3-4	4-5	5-7	7-9
16	-0.010	+0.008	+0.010	+0.011	0.000	0.000	-0.003
23	-0.011	0.000	+0.013	+0.038	+0.022	+0.011	+0.001
37	0.000	-0.015	-0.009	+0.036	+0.036	+0.037	+0.021

Table 5. Statistics for the layered water balance model performance, data set TS1.

Depth	Mean		Slope	Intercept	Correlation Coefficient	Standard Error of Estimate
	Measured	Computed				
0-1	0.094	0.092	0.936	0.004	0.984	0.0107
1-2	0.148	0.142	0.887	0.010	0.986	0.0073
2-3	0.183	0.184	0.914	0.017	0.975	0.0054
3-4	0.199	0.208	0.717	0.065	0.959	0.0073
4-5	0.208	0.214	0.774	0.052	0.959	0.0080
5-7	0.217	0.223	0.782	0.054	0.965	0.0073
7-9	0.224	0.228	0.892	0.028	0.976	0.0061
all data	0.182	0.186	0.940	0.015	0.976	0.0135

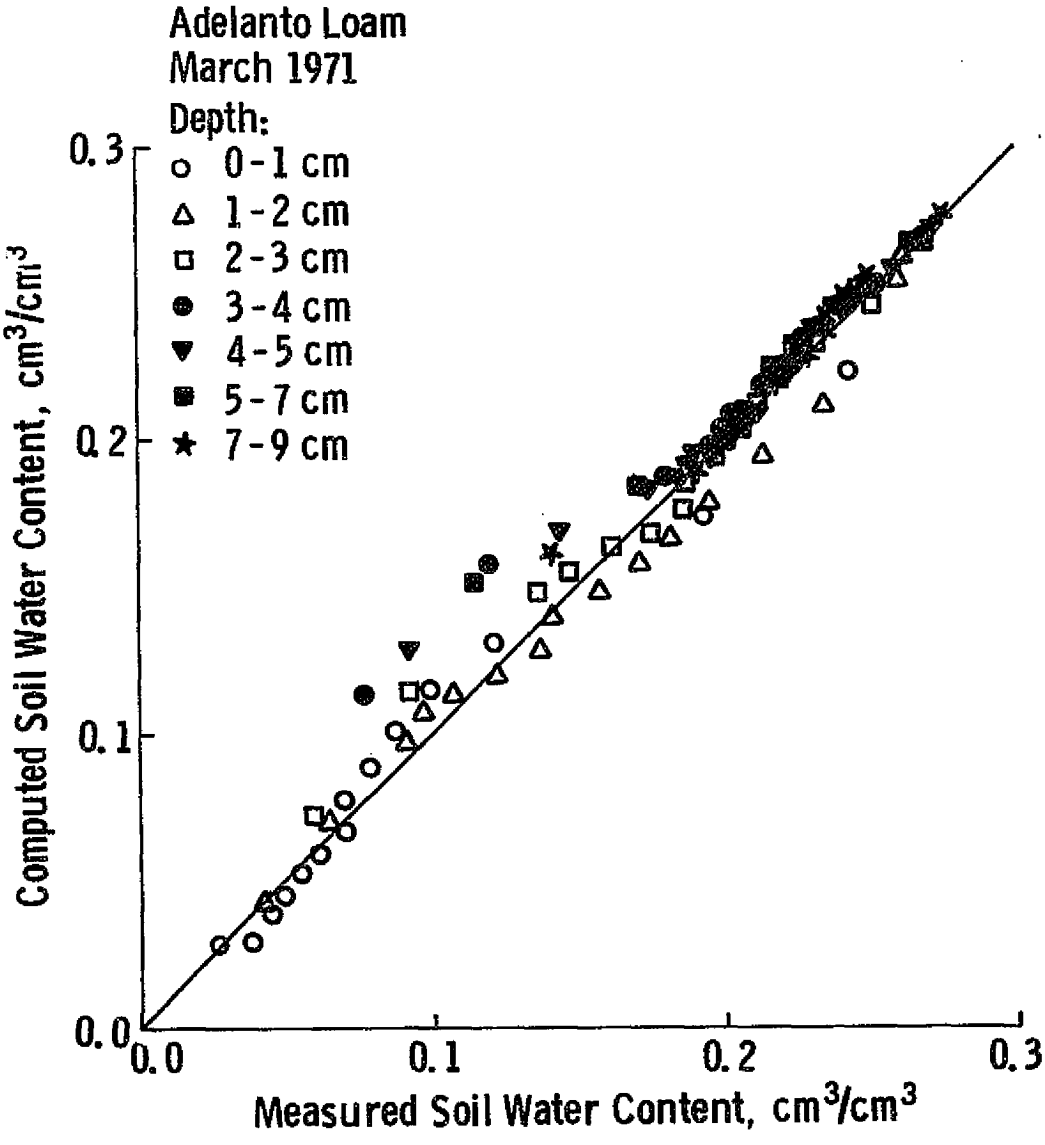

Figure 11. Comparison of computed and measured soil water contents. Data Set TS1.

The correspondence between moisture values for Adelanto loam collected in July, 1970 (Jackson, 1973) and predicted values is shown in Figure 12. Except during two days for the 1-2 cm layer, the pairs of values agreed closely. Since the measurements were made only for the initial evaporation period, the accuracy of prediction was excellent in terms of both correlation and standard error (Table 6).

Both TS1 and TS2 were related to the model derivation, so that a close correspondence between computed and measured moistures may not be surprising. Indeed, a cursory examination of the statistics for individual depths of TS3 (Table 7) reveals substantial decrease in accuracy. However, measured moisture values used for the statistical comparison with computed values were means of one or more samples, and the individual samples exhibited considerable variations around the means. The sampled mean values were plotted against the computed ones in Figure 13. In addition, error bars were placed on the extreme measured values when more than one sample were taken. If cases with only one sample are ignored and assuming for the remaining points that the actual soil moisture could be anywhere within the error bars, then the maximum difference between computed and measured values is less than 0.035 cm^3/cm^3 for all (50) points, less than 0.025 cm^3/cm^3 for 92% of all points, and less than 0.020 cm^3/cm^3 for 84% of all points. In other words, although the correspondence between measured and computed values was worse than for TS1 and TS2, it was nevertheless rather close. This conclusion is further supported by comparing the computed values for depths of 10 cm and 25 cm with values measured tensiometrically (these data are discussed in section 2.4, and the experimental procedure used in their acquisition is described in Appendix B). For the period between 8/5/73 and 11/3/73, the absolute difference between computed and measured values was generally less than 0.020 cm^3/cm^3.

Comparison between computed and measured moisture contents for TS4 yielded similar results: the intial scatter of points around the 1:1 line was reduced to less than 0.01 cm^3/cm^3 when the error bars were taken into consideration (Figure 14). Each data point in TS4 was a mean of two samples. The occasionally large difference between their moisture contents was attributed by Ulaby (1974) to the presence of a ditch which facilitated drainage of one site only. In addition, heterogeneity of the soil infiltration rates could be involved as the differences were greatest following a large rainfall. A statistical analysis of the predictive accuracy for TS4 (Table 8) shows good agreement between measured and computed values. It should be noted that for both TS3 and TS4, the statistics (Table 7,8) are based on the mean measured values only; obviously, the parameters would change somewhat if the error bars were taken into consideration.

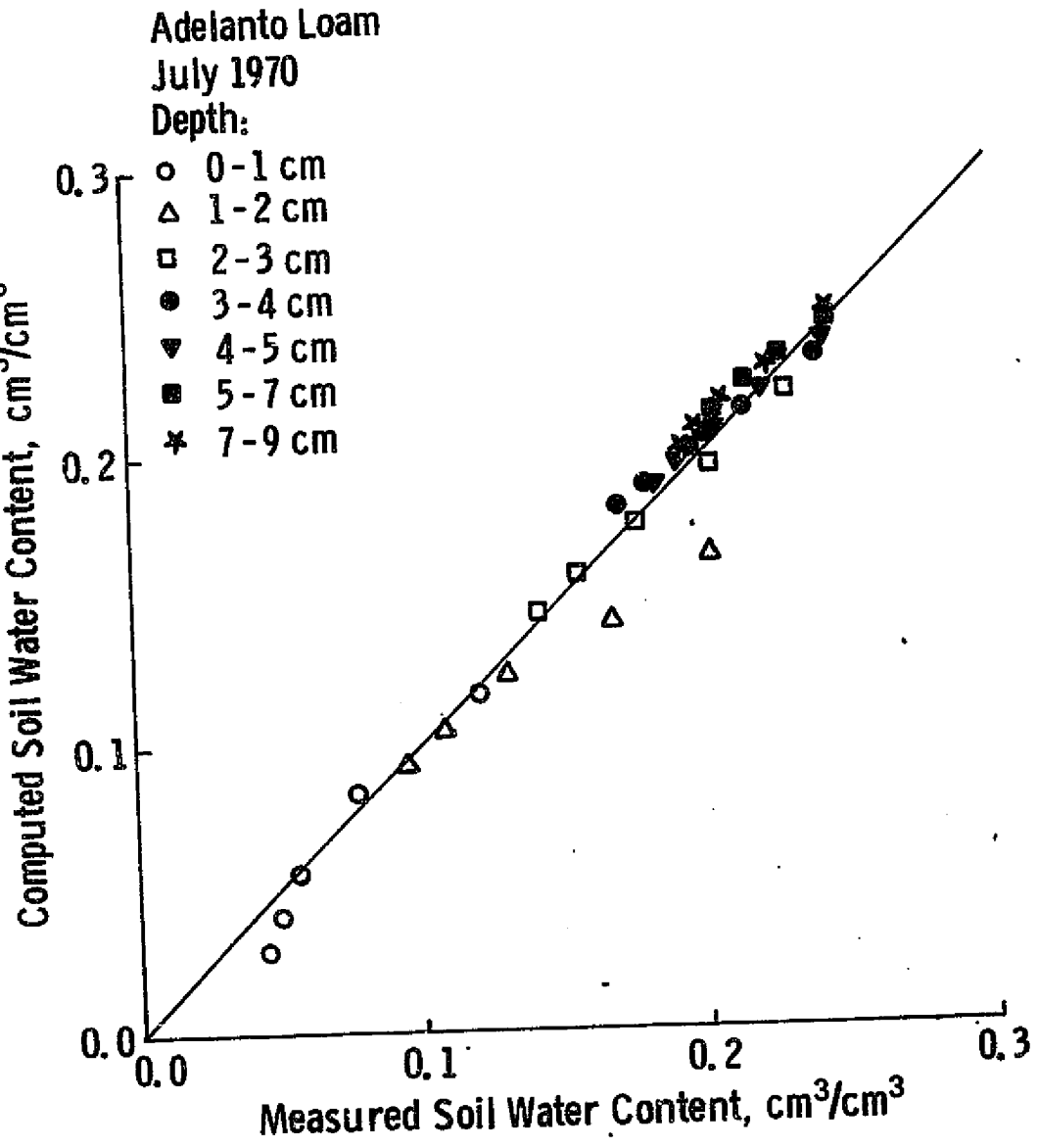

Figure 12. Comparison of computed and measured soil water contents. Data set TS2.

Table 6. Statistics for the layered water balance model performance, data set TS2.

Depth	Mean		Slope	Intercept	Correlation Coefficient	Standard Error of Estimate
	Measured	Computed				
0-1	0.071	0.065	1.131	-0.016	0.974	0.0093
1-2	0.141	0.125	0.635	0.036	0.994	0.0035
2-3	0.183	0.179	0.839	0.026	0.999	0.0012
3-4	0.201	0.204	0.755	0.052	1.000	0.0007
4-5	0.208	0.210	0.853	0.033	0.998	0.0016
5-7	0.214	0.220	0.859	0.037	0.995	0.0021
7-9	0.219	0.226	0.897	0.030	0.997	0.0015
All Data	0.177	0.176	1.043	-0.009	0.985	0.0105

Table 7. Statistics for the layered water balance model performance, data set TS3.

Depth	Mean		Slope	Intercept	Correlation Coefficient	Standard Error of Estimate
	Measured	Computed				
0-1	0.187	0.174	0.941	-0.002	0.975	0.0213
1-2	0.201	0.197	1.080	-0.020	0.905	0.0319
2-5	0.222	0.245	1.441	-0.076	0.947	0.0199
5-9	0.234	0.252	0.881	0.046	0.664	0.0303
9-15	0.264	0.257	0.670	0.080	0.467	0.0322
15-25	0.301	0.283	0.334	0.182	0.286	0.0243
25-35(30)	0.312	0.293	0.463	0.149	0.533	0.0090
All Data	0.246	0.243	0.913	0.018	0.900	0.0282

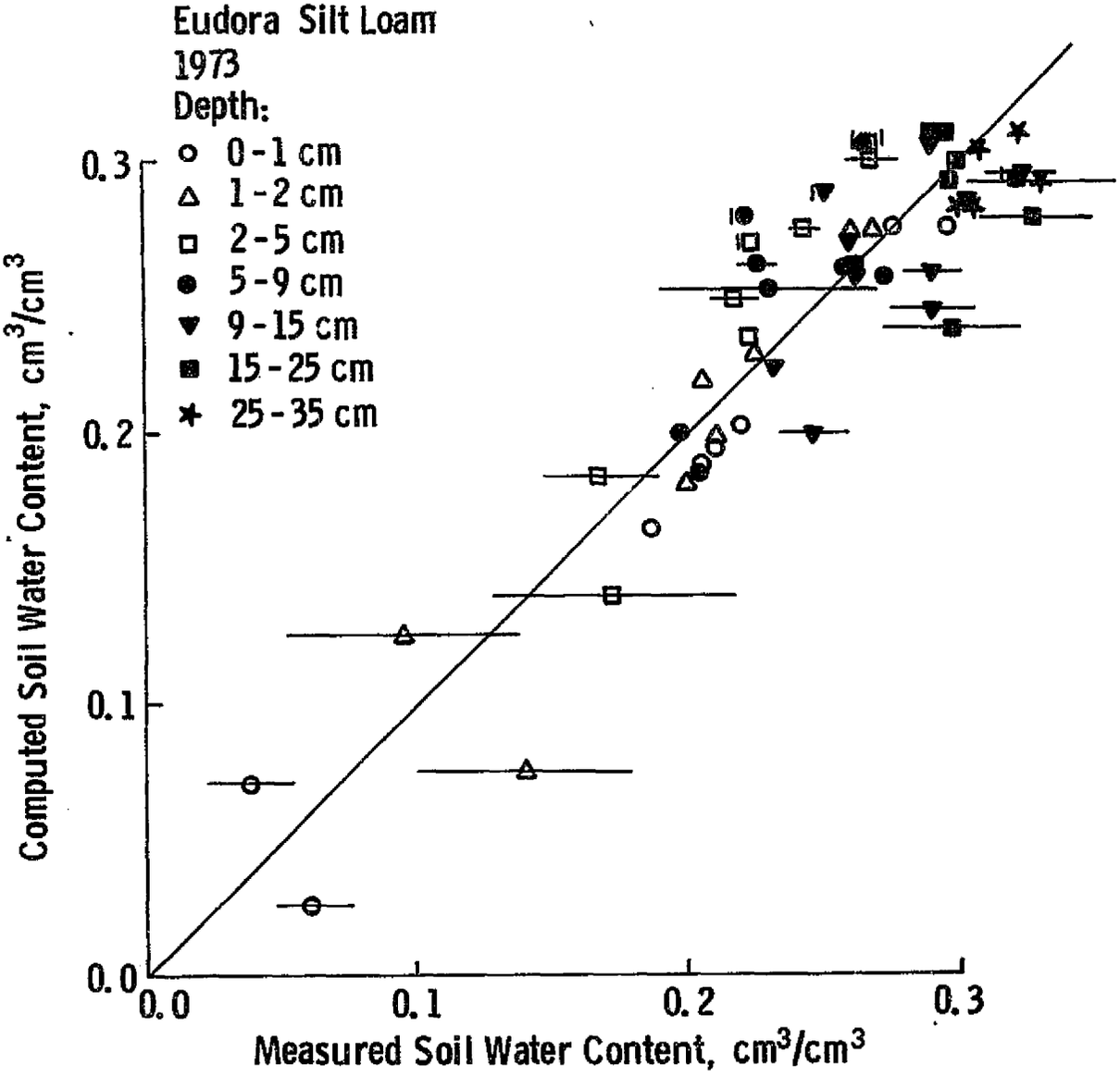

Figure 13. Comparison of computed and measured soil water contents. Data set TS3. Horizontal bars designate standard deviation, vertical bars indicate that only one sample was taken.

Table 8. Statistics for the layered water balance model performance, data set TS4.

Depth	Mean		Slope	Intercept	Correlation Coefficient	Standard Error of Estimate
	Measured	Computed				
0-2	0.290	0.262	1.042	-0.040	0.998	0.0056
2-5	0.331	0.327	0.672	0.105	0.955	0.0166
5-9	0.359	0.354	0.762	0.081	0.868	0.0293
9-15	0.393	0.383	0.565	0.161	0.794	0.0351
All Data	0.333	0.318	0.996	-0.013	0.947	0.0224

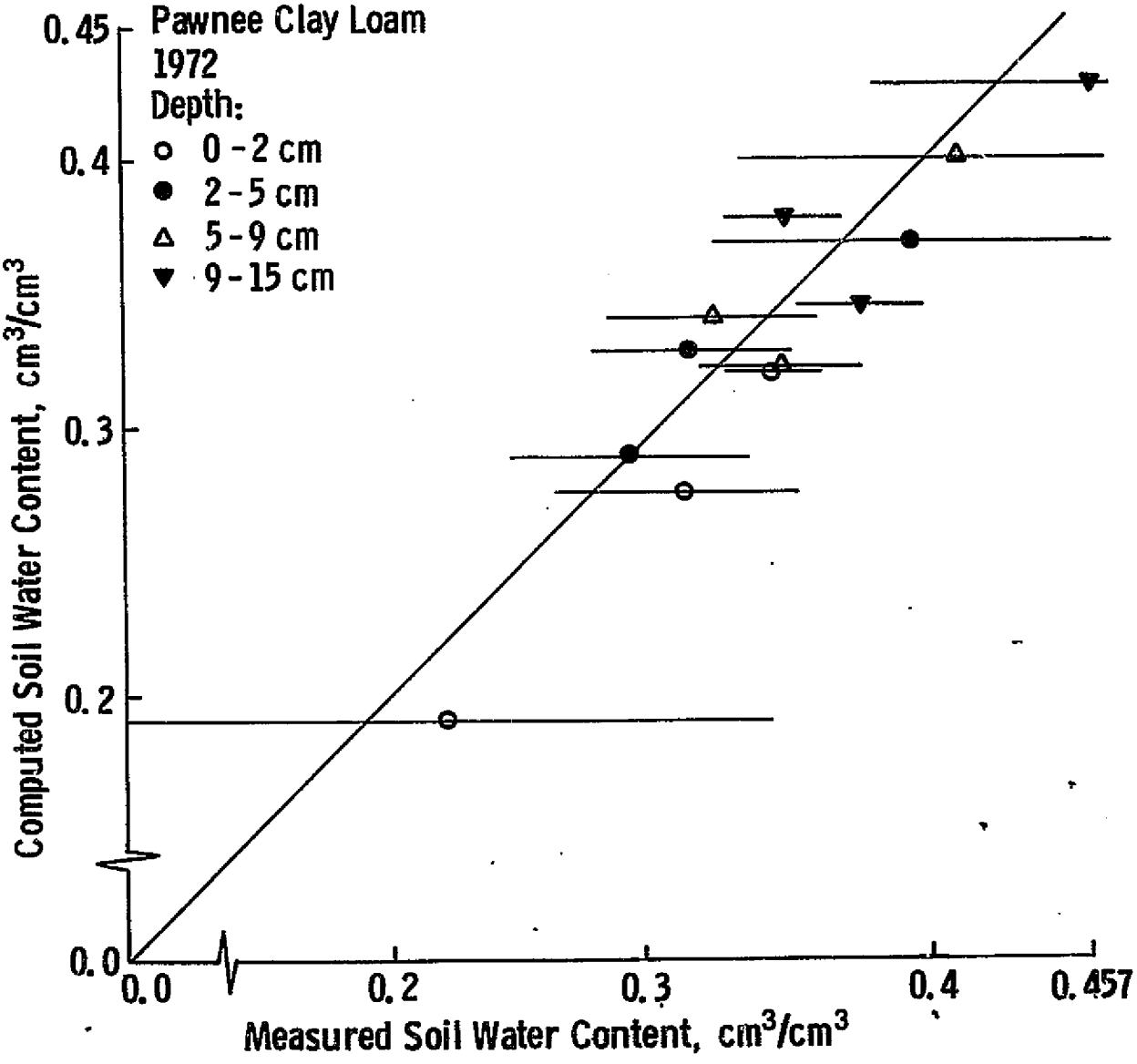

Figure 14. Comparison of computed and measured soil water contents. Data set TS4. Horizontal bars designate standard deviation.

The above results indicate that soil moisture in the 0 to 30 cm zone may be predicted for 1-cm depth increments within 0.02 cm^3/cm^3. Precipitation, daily potential evaporation, soil storage capacity, and initial soil moisture contents are required as input. Two remarks concerning the storage capacities are in order. First, the appropriate value of storage capacity appears to correspond to a tension of approximately 0.09 bars. The moisture values used for TS1, TS2 and TS3 (Table 9) represent a tension of 0.09 bars, according to moisture characteristics given by Jackson (1973) and those obtained by measurements (Appendix B). The storage capacity initially used for Pawnee clay loam (TS4) was the field capacity value for a clay loam given by Salter and Williams (1965), multiplied by empirically determined bulk density (Ulaby et al., 1974). The predicted values were too low, however; the results given in Table 8 were obtained only after the above storage capacities were multiplied by 1.10. The low tension values cannot be explained by the necessity to provide storage space for precipitated water during the first two days after rain because no water was added in TS1 and TS2. Although these results are consistent, further testing with data from widely different conditions should be made before a final value of storage capacity suitable for this model is accepted. It is also conceivable that the storage capacity varies within a moisture tension range similarly as the field capacity. Secondly, the storage capacity for the top 2 cm was 0.9 that of what it would be if the layers were located deeper below the surface. This adjustment, derived from Jackson's (1973) data, was due to the observation that for the top two layers, AE_{ij} values were high even several days after irrigation when their moisture content was much below the field capacity (Figure 5). The close correspondence between computed and measured moisture values for these layers (Table 5 through 8) suggest that the trend of higher evaporation rates from near-surface layers was real; it may be due to the evaporative demand of the atmosphere which is most effective at the surface.

Although the water balance model was constructed for 24-hour time increments, it was of interest to determine the accuracy with which hourly soil moisture changes could be predicted. If the model performs well for hourly time intervals, it could be used to simulate diurnal changes of soil moisture. Results described in this paragraph have actually been computed using the soil temperature simulation model (Chapter 3), which included the water balance model for computing hourly profile moisture changes; they are presented here to provide a more comprehensive picture of the model's

Table 9. Storage capacities for the four testing data sets.

Depth (cm)	Storage Capacity (cm^3/cm^3)		
	TS1, TS2	TS3	TS4
0-1	0.270	0.275	0.320
1-2	0.270	0.275	0.320
2-3	0.315	0.305	0.356
3-4	0.315	0.305	0.366
4-5	0.315	0.305	0.378
5-6	0.315	0.305	0.387
6-7	0.315	0.305	0.396
7-8	0.315	0.305	0.405
8-9	0.315	0.305	0.417

Depth (cm)	Storage Capacity (cm^3/cm^3)	
	TS3	TS4
9-10	0.305	0.423
10-11	0.305	0.426
11-12	0.306	0.428
12-13	0.306	0.428
13-14	0.307	0.428
14-15	0.307	0.428
15-16	0.308	0.428
16-17	0.310	0.426
17-18	0.312	0.423
18-19	0.315	0.420
19-20	0.320	0.416
20-21	0.323	0.410
21-22	0.326	0.408
22-23	0.329	0.405
23-24	0.332	0.403
24-25	0.335	0.403
25-26	0.338	0.406
26-27	0.341	0.408
27-28	0.344	0.410
28-29	0.347	0.413
29-30	0.350	0.417

performance. The computed hourly soil water contents for Adelanto loam were compared with values measured on 9/20/73 (high moisture) and 10/2/73 (low moisture content); the measured data are described in Sections 3.1 and B.2. In the water balance model, potential evaporation was calculated as LE/L, where LE is given in Appendix A and L is the latent heat of vaporization. Diurnal moisture content changes at two depths are shown in Figure 15. These results indicate that the layered evaporation model predicted moisture losses rather well even for small time periods. Since the evaporation model did not compute soil water movement, the recharge during the night could not be predicted. It should be noted that the evaporation process was simplified in that water was assumed to evaporate directly from a given depth rather than to flow to the evaporation sites which may be confined to a narrow zone in the soil (Hillel, 1971).

It should be noted that the values of k_j and C_{ij} (Table 1, Equation 13) were developed and the performance of the water balance model was tested primarily for high potential evaporation values. The last two columns of Table 3 show that data set TS1, which served as the basis for developing k_j's and C_{ij}'s, had approximately the same evaporation levels as TS3 and somewhat higher than TS4. Since k_j and C_{ij} coefficients have been derived empirically, their validity for other potential evaporation levels should not be assumed without appropriate testing. The excellent prediction of water contents for TS4 where potential evaporation was almost twice as much as for TS1 suggests that the k_j's and C_{ij}'s derived here may be valid when potential evaporation exceeds 0.5 cm/day. When the atmospheric evaporative demand is low, however, less water would be lost from the soil, and consequently even lower rates of water flow (associated with lower moisture contents for a given soil) would entirely satisfy the evaporative demand. Thus, at low potential evaporation values, one would expect that the critical storage capacity fraction would decrease from the 0.95 used in Equation 13. Secondly, the low rates of water loss might lead to a slower decrease of k_j values with depth and consequently to a more uniform profile soil moisture distribution. These hypotheses should be tested to determine whether modifications of the layered water balance model for low potential evaporation levels are necessary. From the point of view of water loss to the atmosphere, however, high evaporation conditions (where the present model appears to perform satisfactorily) are of greater importance.

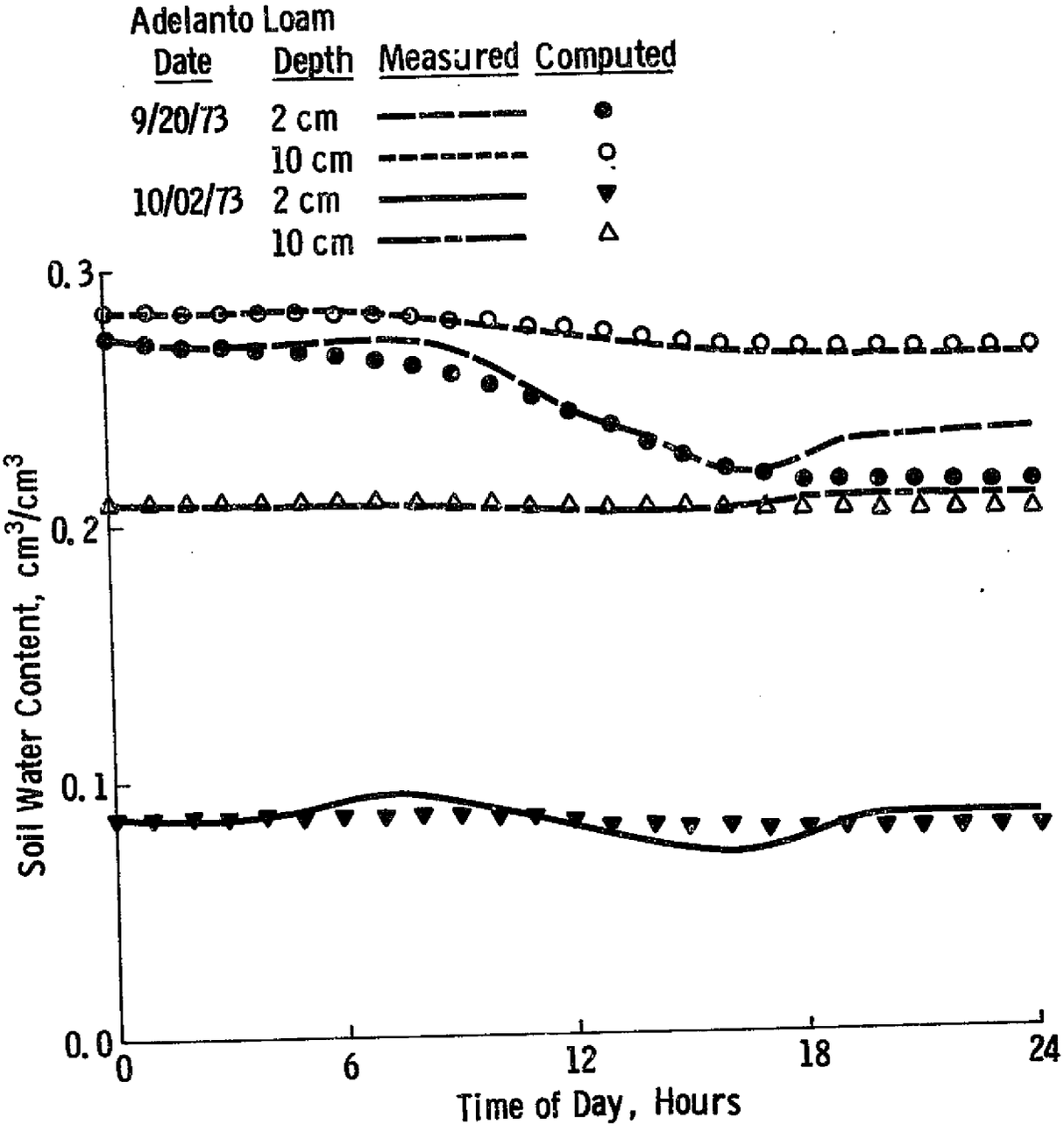

Figure 15. Comparison of computed and measured soil water contents for wet and dry soils, calculated using the layered water balance model.

2.2.2 Diurnal Soil Moisture Variations

Changes in soil water content dealt with in the previous sections were average changes that occurred over a period of 24 hours. In this case, diurnal fluctuations of soil temperature may be ignored in computing evaporation (Gardner and Gardner, 1969) because of the periodicity of temperature variations. In reality, however, soil moisture may change considerably during the diurnal cycle, mainly near the surface where the temperature gradients are at maximum.

Field studies of diurnal moisture variations have been rather limited, in part due to the difficulties involved in accurately determining small moisture changes over short time periods. In fact, only two studies have been reported in the literature, namely by Rose (1968 a,b) and by Jackson (1973) and Jackson et al. (1973, 1974). Data collected during the latter series of experiments form the basis for the following discussion; the experimental procedure is briefly described in Appendix B. These data have been analyzed by Jackson and his co-workers in terms of water flux; here we are primarily interested in absolute moisture levels.

Figure 16 shows hourly moisture content changes at three depths of wet soil over a 24 hour period. Water content remained unchanged until sunrise and then began to decrease rapidly. The moisture loss started earlier and proceeded at a faster rate at locations closer to the surface. Jackson et al. (1973) attributed the rapid surface drying during morning hours to bidirectional movement of water: soil water from the surface to about 1 cm moved upward, while that below 1 cm moved downward. In the late afternoon, moisture recharge from deeper layers exceeded evaporative loss and the water content increased again, although it did not reach the morning level. Thus there was a net loss in all three layers shown in Figure 16; this net loss was approximated by the layered evaporation model (section 2.2.1). As the soil dried out, the amplitude of diurnal moisture changes was dampened (Figure 17) and the net loss at any depth during 24 hours decreased; as before, the amplitude was at maximum near the surface. Furthermore, the recharge of the near surface layer continued until sunrise.

Data in Figure 16 and 17 represent relatively simple patterns of moisture change: moisture is highest before dawn, then decreases until late afternoon, and subsequently increases again until it levels off at some pre-dawn value. In general, however, these changes are not so regular, especially at greater depths. Figure 18 shows diurnal water content changes at five different days for a drying Adelanto loam. It is apparent that the above described pattern holds well for the top 1 cm layer during the entire

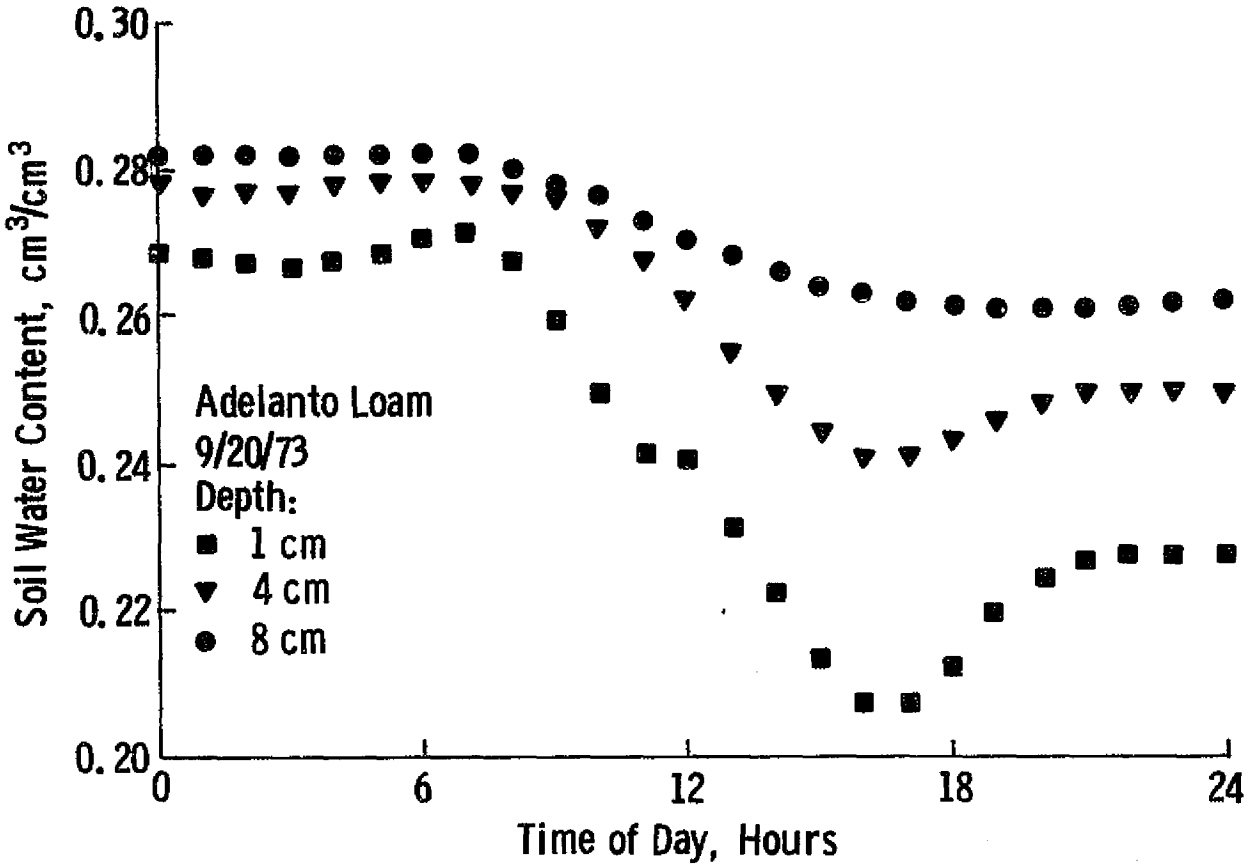

Figure 16. Diurnal soil water content changes, wet soil.

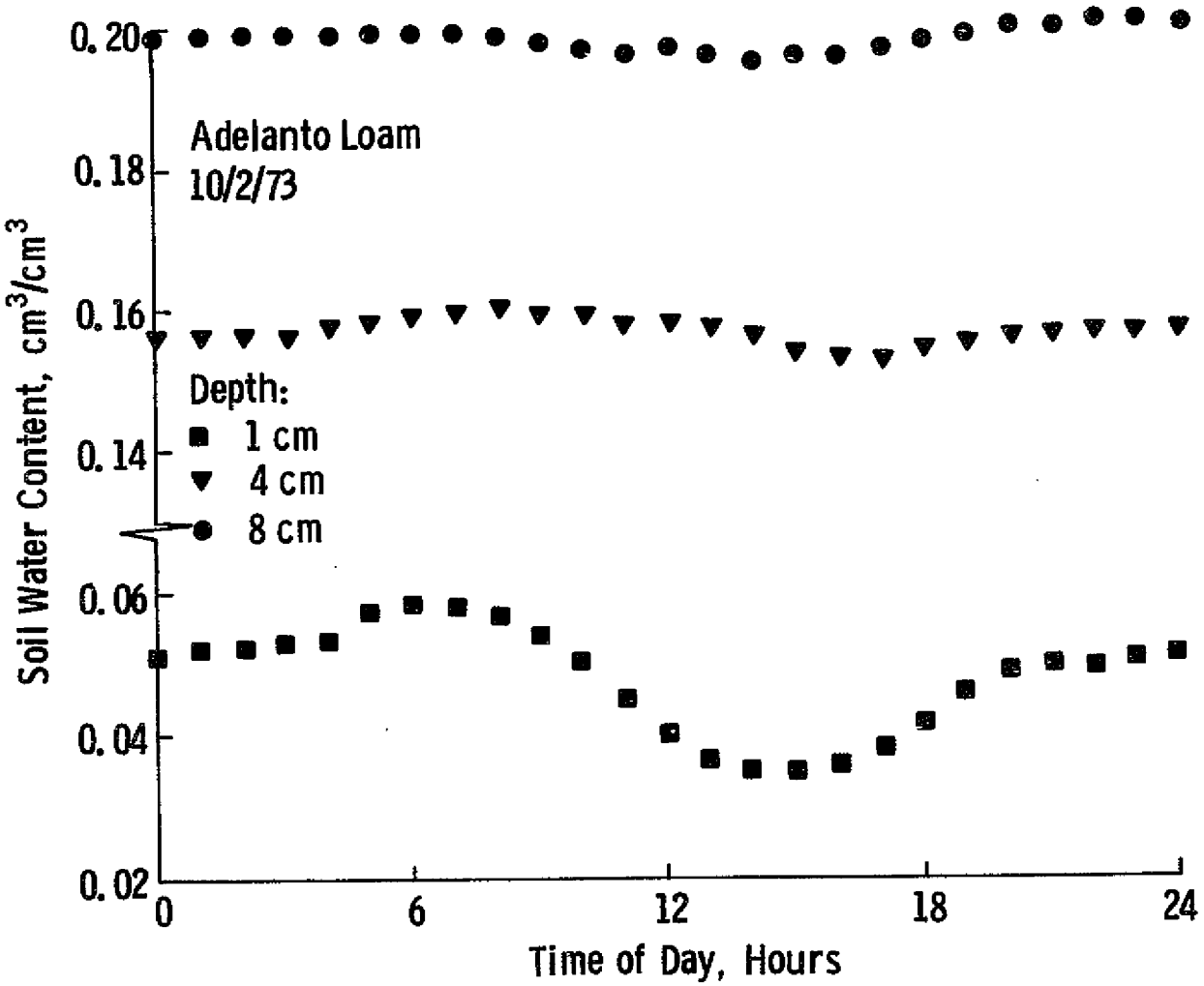

Figure 17. Diurnal soil water content changes, dry soil.

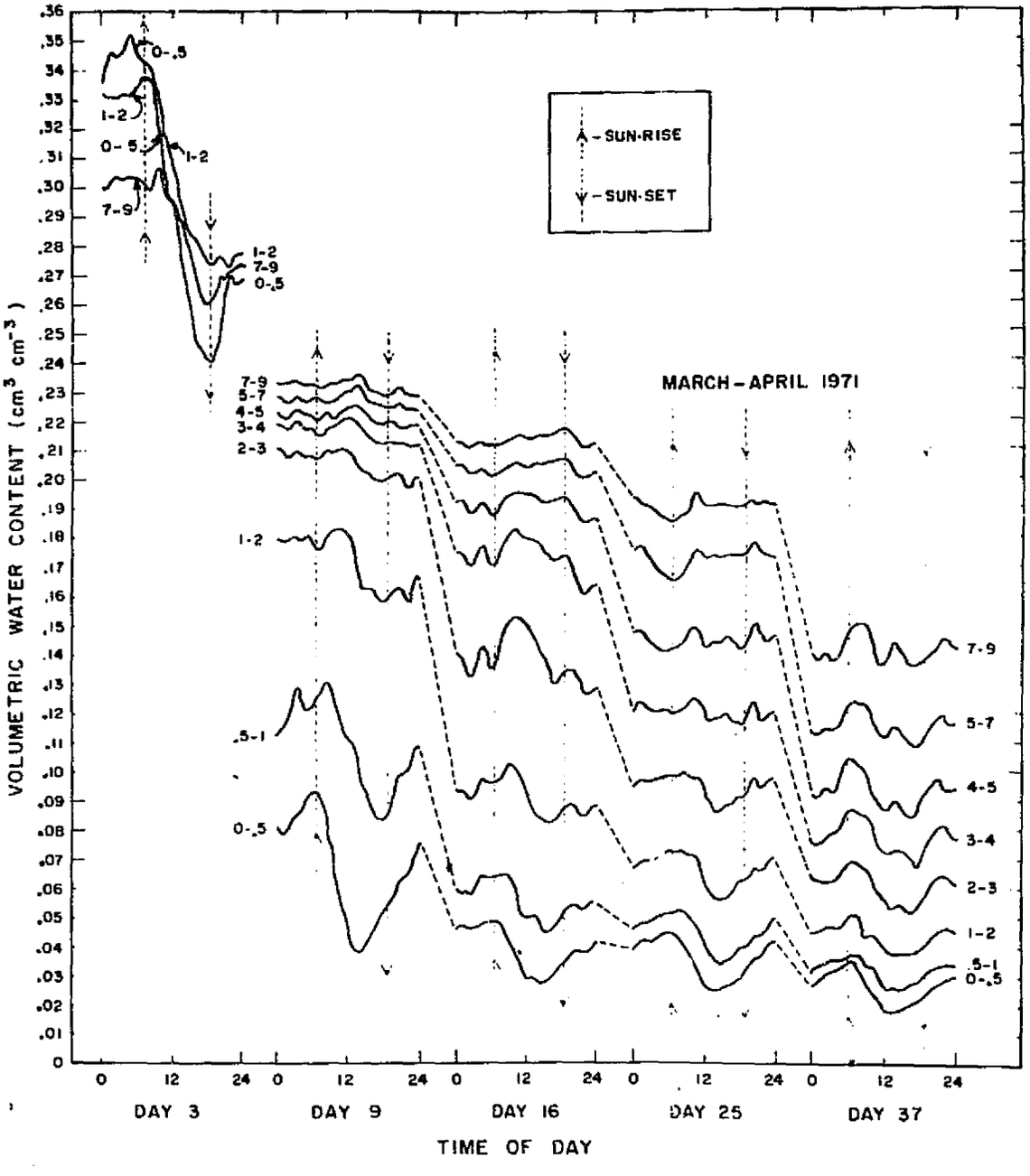

Figure 18. Diurnal soil water content changes for several depths at 3, 9, 16, 23, and 37 days after irrigation. From Jackson (1973).

period of measurements. For the greater depths, the main pattern of moisture changes is poorly defined, partly due to the presence of higher frequency perturbations superimposed on the moisture vs. time curves. When the moisture content at a given depth decreased below approximately 0.120 cm^3/cm^3, however, the regular pattern observed in Figure 16 and 17 emerged, and the perturbations became minor (Figure 18); this condition was reached prior to day 16 (depth 1-2 cm), day 25 (2-3 cm), and day 37 (5-7 cm), respectively.

The above results indi'e that the total moisture exchange (summed absolute values of moisture gains and losses) generally exceeds the effective moisture loss, i.e, the difference between final (2400 hours) and initial (0000) moisture content; the second quantity is equivalent to actual evaporation AE_{ij} (section 2.2.1). In Figure 19, pairs of total moisture exchange and effective loss points for Adelanto loam are plotted against the average daily moisture content; the values were determined from measurements collected during seven days in two experiments (March, 1971; September, 1973). Total exchange was calculated for four time periods: midnight to sunrise, sunrise to noon, noon to sunset, and sunset to midnight. Both effective loss and total exchange were divided by the actual evaporation AE_i to remove the effect of varying evaporative demand of the atmosphere. At high moisture contents, total exchange was only slightly greater than the effective loss. As the moisture content decreased, effective loss decreased to zero while the total exchange increased to more than half of the actual evaporation AE_i. When the effective loss for near surface layers is zero, the total exchange should equal unity. This is not the case in Figure 19 because the 24-hour period was subdivided into only four increments for which the total exchange was determined; thus the total exchange values should actually be higher than shown in Figure 19. The negative loss values (i.e., moisture increase over a 24-hour period) were measured on day 16 (3 values) and day 37 (1 value); they could be real or due to errors in reading off moisture contents from Figure 18, as very small quantities of water were involved.

Figures 16 through 19 show that the diurnal change in moisture can be considerable depending on the depth and mean moisture level at that depth. To obtain some idea about the ranges of values involved, the average daily moisture was plotted against the maximum and the minimum moisture contents during that day at a given depth (Figure 20). These data were taken from the same sources as those for Figure 19 and thus represent reasonably extreme conditions in terms of a large atmospheric evaporative demand. They may therefore serve as an indication of an upper limit of diurnal moisture fluctuations

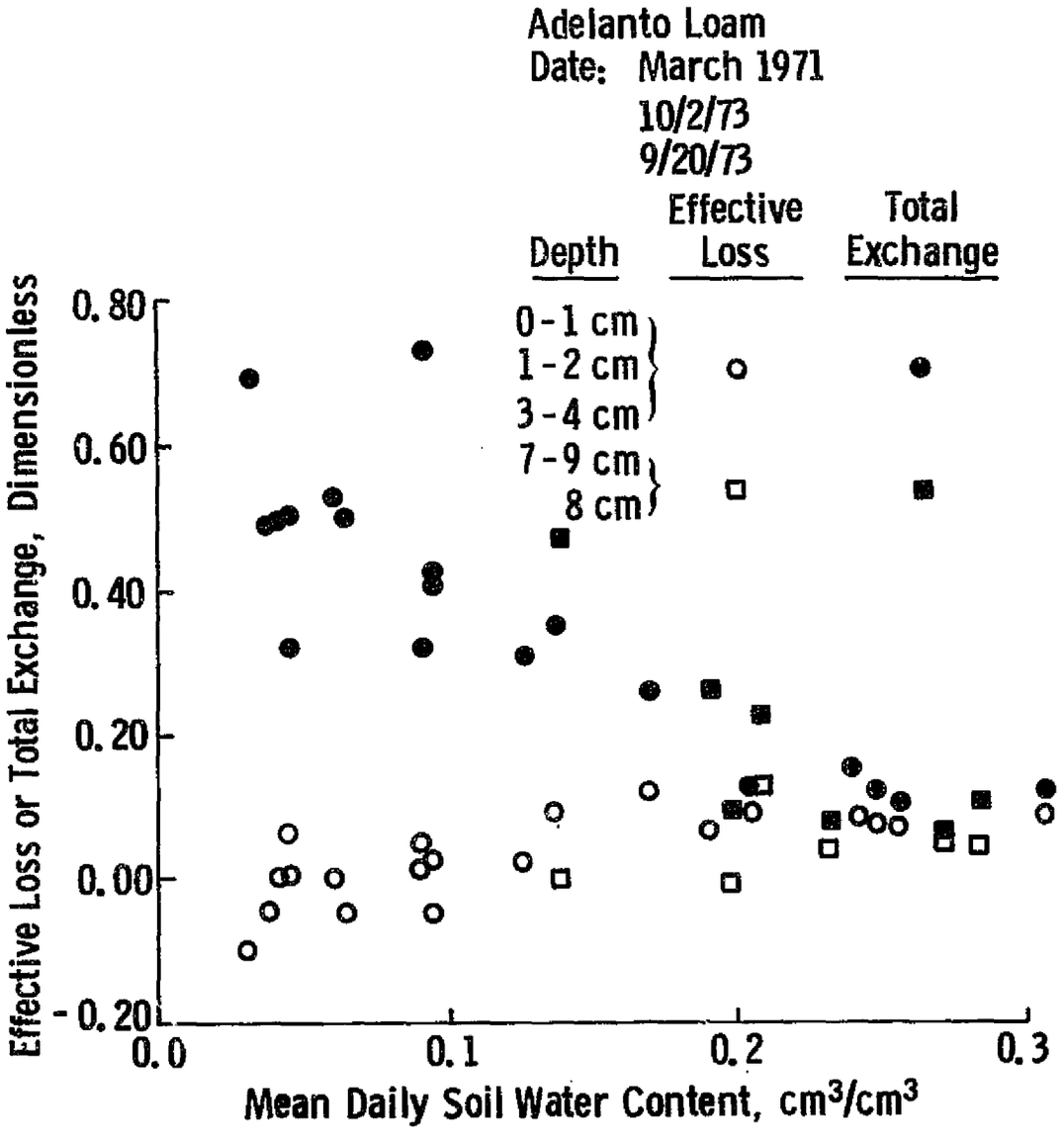

Figure 19. Diurnal effective loss and total exchange of soil water as functions of mean daily soil water content.

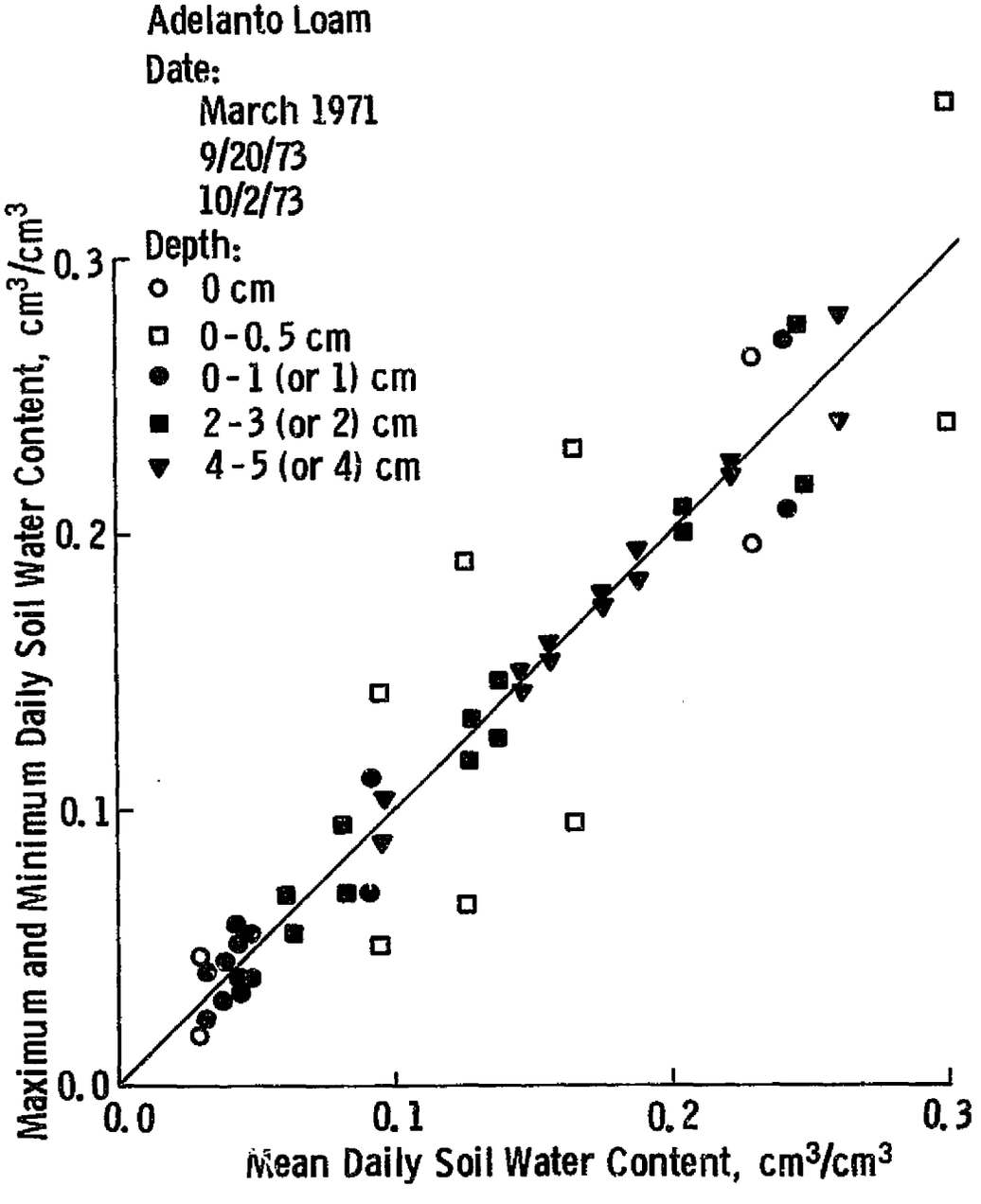

Figure 20. Maximum and minimum daily soil water content versus the mean daily water content at several depths.

near the surface of a bare soil. The variation was large for depths smaller than 1 cm but decreased rapidly at greater depths; for the 0-0.5 cm layer, the range was as high as 0.135 cm^3/cm^3. Daily moisture ranges for the same data are plotted in Figure 21. Except for one anomalously low value (0 cm; 9/20/73), the trend was consistent: maximum range of moistures was observed at or near the surface; (ii) with decreasing soil moisture, the range decreased faster at greater depths than at the surface; and (iii) the range became small for depths greater than 4 cm. Typical maximum values of the diurnal moisture range appeared to be 0.125 cm^3/cm^3 for 0-0.5 cm, 0.06 cm^3/cm^3 for 0-1 cm, and 0.02 cm^3/cm^3 for a depth of 4 to 5 cm.

2.3 SUBSURFACE MOISTURE REGIME

The layered water balance model developed and tested in section 2.2.1 accounted for soil moisture changes in the top 30 cm only. There were several reasons for this restriction. First, it was assumed that the dynamics of the moisture regime of a bare soil is greatly attenuated at depths greater than 30 cm. Secondly, soil water present near the surface has a more direct effect on microwave radiation as well as on the exchange processes between atmosphere and soil, both mass (e.g., infiltration, evaporation) and energy (latent heat). Thirdly, the depth-of-penetration limitations of microwave sensors render the upper part of the soil profile most suitable for microwave remote sensing. Nevertheless, there are activities in which moisture content of the deeper layers is of importance; examples are crop production and ground water recharge. For such purposes, a method of soil moisture determination over large areas would be expected to yield information about water content status of deeper layers, in addition to those for the upper portion of the soil profile.

The purpose of this section is twofold: (i) to determine whether substantial differences in soil moisture dynamics exist between 0-30 cm layer (hereafter "upper zone") and the layer below 30 cm ("lower zone"), thereby justifying their separation in the previous sections; (ii) to examine the main features of the subsurface moisture regime and establish a relation between moisture regimes of the two zones which could serve for estimation of moisture content of the subsurface zone without direct sampling.

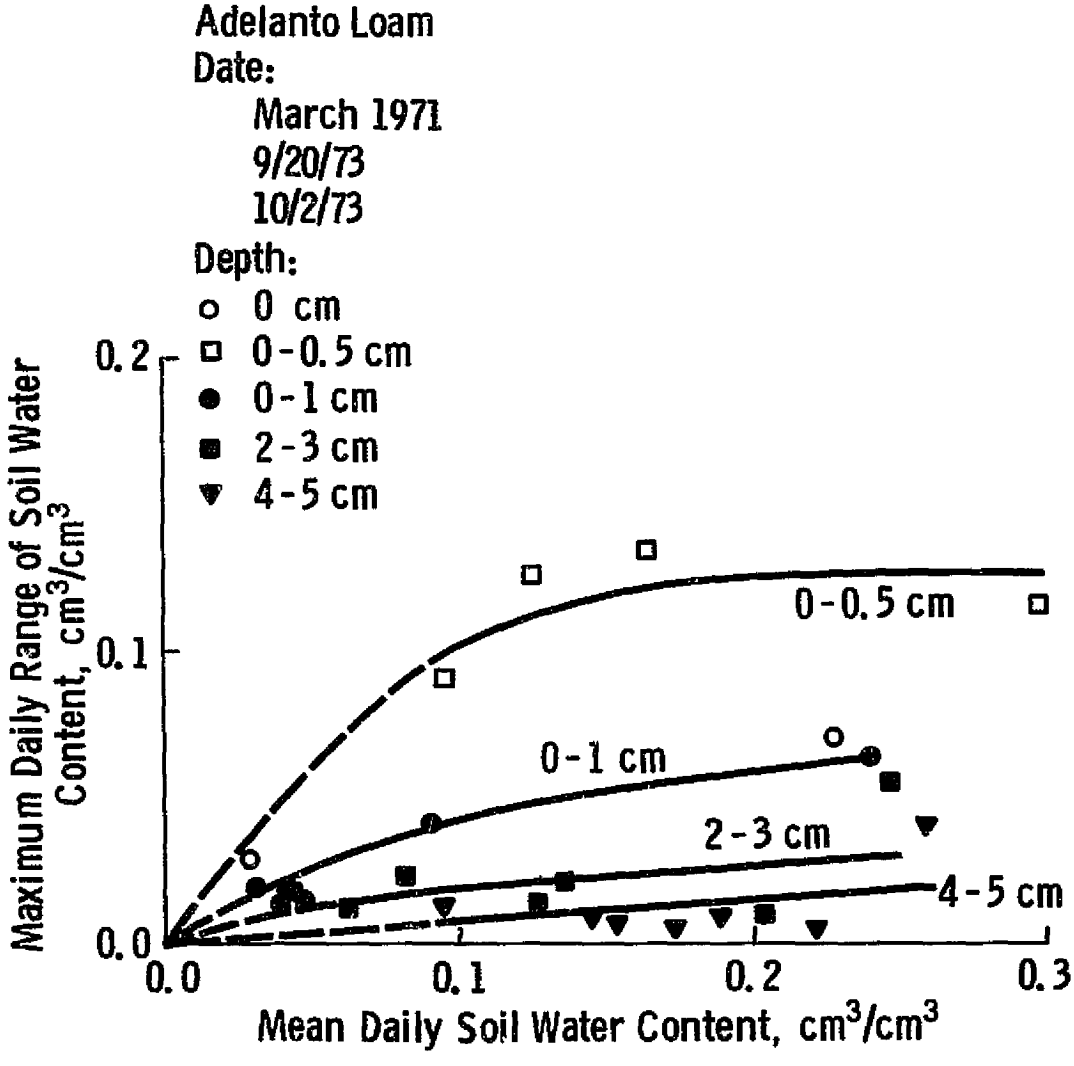

Figure 21. Maximum daily soil water content range versus the mean daily soil water content at several depths.

The following discussion is based primarily on field soil water content measurements. The experiment during which the data were collected is described in Appendix B. The data represent one soil only, Eudora silt loam. While two complete sets of tensiometers (S1 and S2) were installed in this soil, the data were not averaged because it was found that small differences existed between S1 and S2 which could obscure subtle trends otherwise observable in both sets. Figure 22 shows the relationship between moisture contents simultaneously determined by the gravimetric and tensiometric methods. From the total of 32 measurements, 16 were within 0.01 cm^3/cm^3 from the 1:1 line, 11 within 0.02 cm^3/cm^3, and 5 within 0.03 cm^3/cm^3. Since most of the gravimetric measurements include some uncertainty (the upper zone data have been discussed in section 2.2.1.2), the correspondence between the two methods of measurements can be considered satisfactory. More importantly, the tensiometrically acquired moisture measurements appear to have accurately responded to small changes in profile moisture conditions (refer to Figure 28).

2.3.1 Soil Moisture Profile Dynamics

Changes in soil moisture content occur as a result of flow, and flow in the soil is proportional to hydraulic conductivity and potential gradient according to Equation (15) for one-dimensional flow

$$\frac{\delta \theta(z,t)}{\delta t} = \frac{d}{dz}\left(K(\Phi)\ \frac{d\Phi}{dz}\right) + \frac{dK(\Phi)}{dz}, \qquad (15)$$

where θ = moisture content, in cm^3/cm^3;

$K(\Phi)$ = hydraulic conductivity, in $cm^3/cm^2/min$;

Φ = pressure head, in cm;

z = distance from the reference level, in cm;

t = time in minutes.

Since the potential gradient $d\Phi/dz$ is determined primarily by the differences in matric suction, changes of tensiometric values (which are a measure of matric suction) may be used as an indicator of the potential of soil moisture to change. Figure 23 shows the highest (8/30/73) and lowest (9/27/73) values of moisture tension recorded during the period of measurements. The highest values were recorded after two weeks practically without rain during which the potential evaporation averaged 0.566 cm/day. The

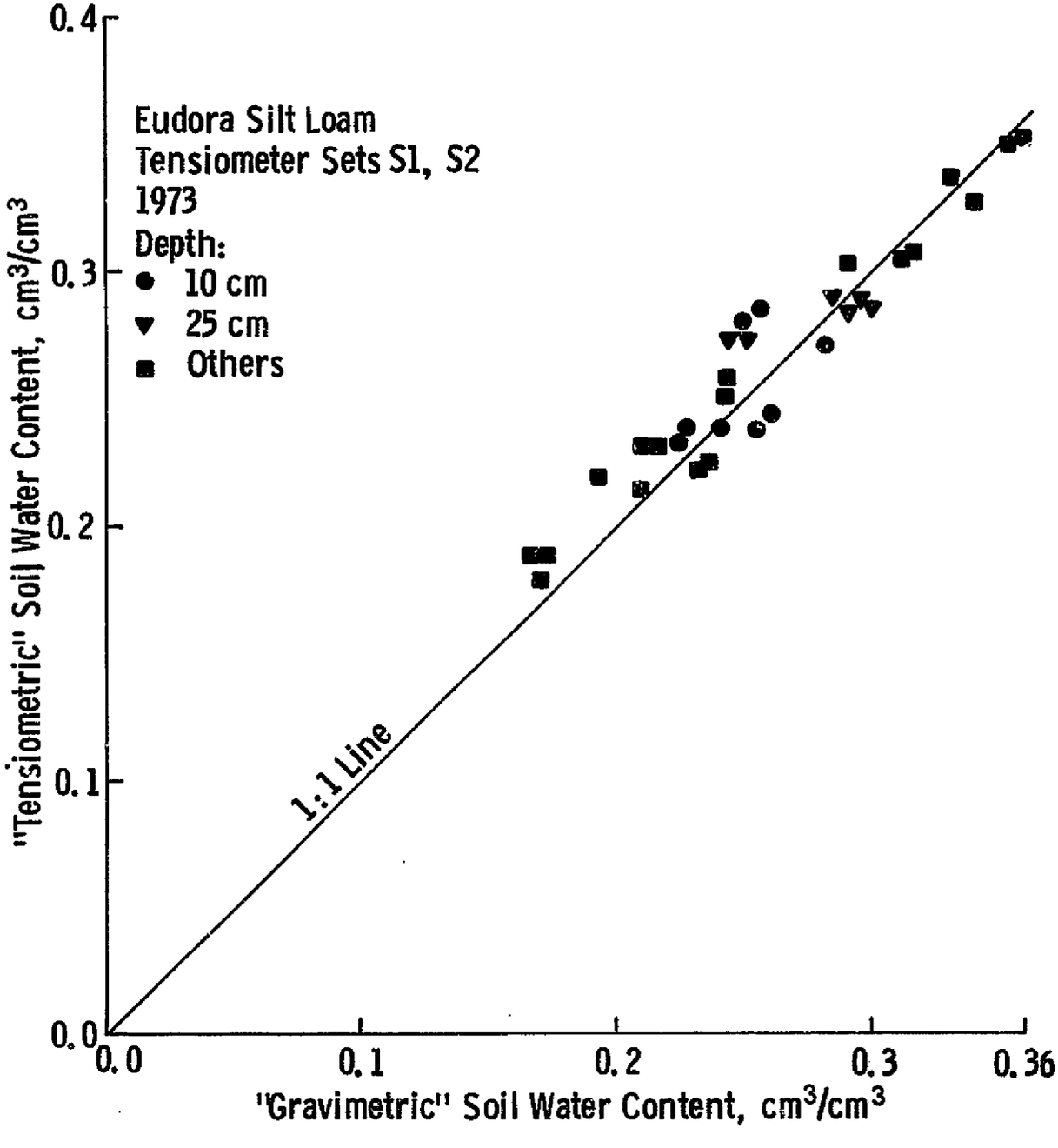

Figure 22. Relationship between soil moistures determined by gravimetric and tensiometric methods.

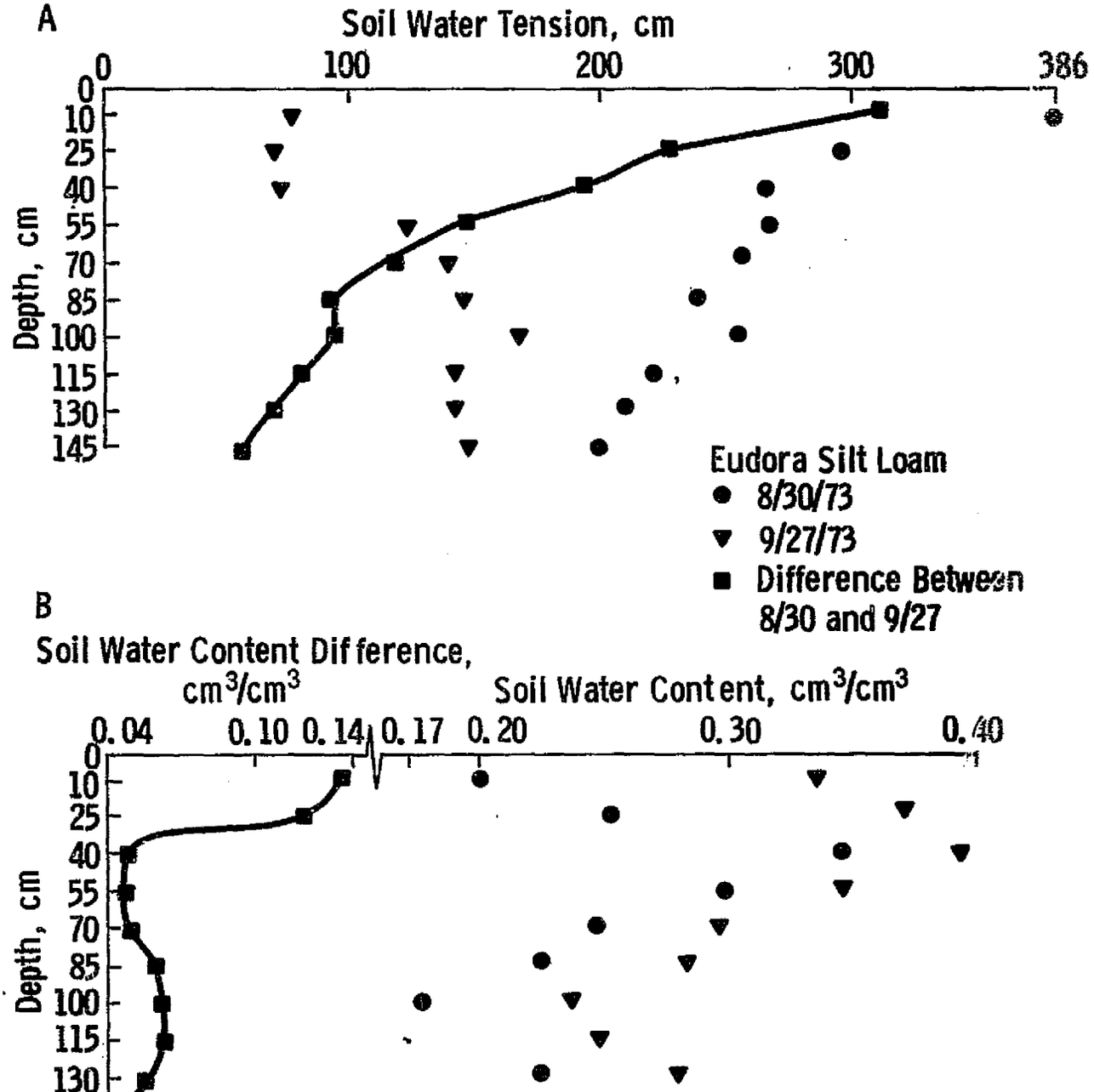

Figure 23. A. Maximum, minimum, and range of soil water tensions measured during the experimental period.
B. Soil water contents corresponding to the tensions in A.

lowest values were measured after five days of precipitation with a total rainfall of 17.27 cm (Figure 24). For the dry condition, tension was 386 cm at the depth of 10 cm, but decreased rapidly to 40 cm and more slowly at greater depths. Following the large rainfalls, tensions were low between 10 cm and 40 cm, and then increased slowly. The reason for increase in moisture tension at 100 cm depth is not clear, especially because it occurred consistently throughout the period of measurements. Differences between the maximum and the minimum recorded tensions are plotted as the third curve in Figure 23A. The range of tensions encountered during the experiment decreased monotonically with depth, although changes in slopes of the difference curve can be noted at 25 cm and 85 cm.

Moisture content change in time is a function of both potential gradient (and therefore moisture tension differences) and hydraulic conductivity. The hydraulic conductivity dependence explains why the tension difference curve (Figure 23A) changed gradually with depth while the moisture difference curve (Figure 23B) decreased abruptly between 25 and 40 cm. The plowed layer consisted of loosely packed coarse silt loam with a bulk density increasing with depth from 1.15 g/cm^3 to 1.37 g/cm^3, while the layer between 40 cm and 55 cm had finer texture (Figure 25) and higher bulk density (1.47 g/cm^3 to 1.37 g/cm^3). These differences, probably due to either management practices or local depositional pattern of the floodplain sediments, may have been the cause of different conductivity values. Hydraulic conductivity data are not available here; however, the differences in hydraulic properties are also reflected in moisture characteristic curves which are shown (Figure 25) for depths of 10 cm, 25 cm, 40 cm, and 55 cm. For the 10 and 25 cm curves, a small change in moisture tension between 100 cm and 400 cm results in a large change of soil moisture content; the same tension change will cause a much smaller moisture shift at 40 or 55 cm. The above considerations suggest that while tension gradients similar to those in Figure 23A may develop in more than one soil in a given area (due to their partial response to atmospheric evaporative demand), moisture contents in these soils can be quite different. The same is true for different depths in one profile. For example, tension values on 9/27/73 were identical at 40 cm and 55 cm (Figure 23A) but the moisture content at 40 cm was 0.047 cm^3/cm^3 higher than that at 55 cm (Figure 23B). Similarly, whereas the moisture tension decreased almost uniformly with depth below 55 cm, moisture contents decreased until 100 cm depth and then increased. In other words, moisture profiles in the soil may be expected to be nonuniform, particularly when the soil heterogeneity existing under natural conditions is taken into consideration.

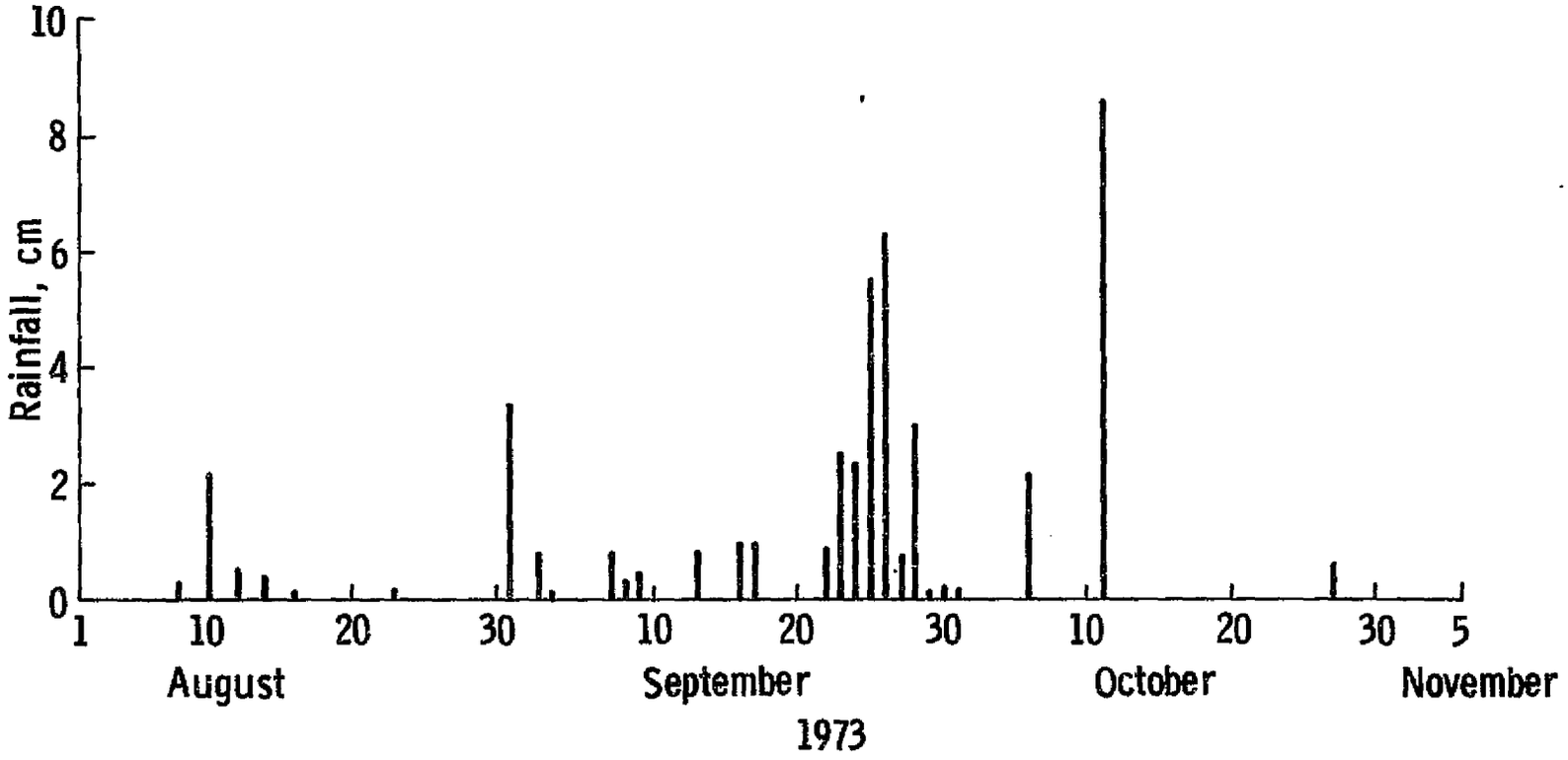

Figure 24. Precipitation history for the Eudora site and the experimental period, 1973.

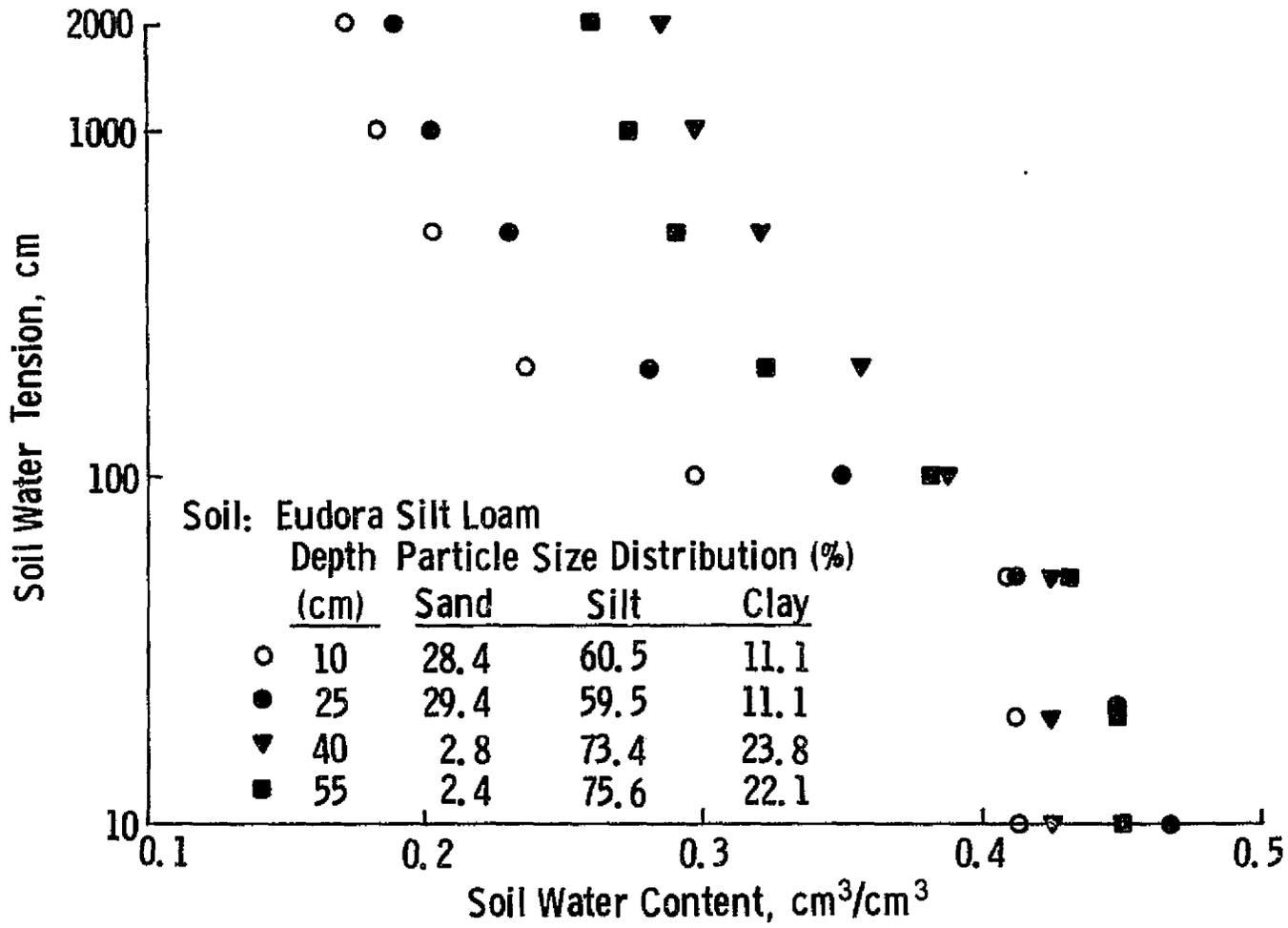

Figure 25. Moisture characteristic of Eudora silt loam at four depths.

A further illustration of the differences in moisture dynamics between the upper and lower zone is given in Figure 26 which shows the total amount of water in the 0-32.5 cm layer and 32.5-152.5 cm layer as a function of time. The values were computed from measured moisture contents and the constant layer thickness of 15 cm; moisture content near the surface was estimated from the moisture gradient between 10 and 25 cm. The upper zone was depleted faster during rainless periods (e.g., 8/12/73 to 8/30/73) than the lower zone. However, larger fluctuations in the upper zone water storage were caused by rainfall as is evident by comparing the two curves (Figure 26) for the period between 8/31/73 and 9/22/73. During this period, the generally low rainfall amounts (Figure 24) did not infiltrate into the lower zone. The maximum range of water storage in the upper zone during the 8/12/73 to 9/22/73 period was 2.085 cm which represented about 25% of the mean storage value; equivalent figures for the lower zone are 0.960 cm and 3%.

From data presented in Figure 23 and 26 it is evident that soil moisture in the upper zone changed more often and reached more extreme values than that in the lower zone; in addition, a sharp break in intensity of these changes occurred between 25 and 40 cm below the surface. Precipitation amounts were identified as one reason. Figure 27 shows the depth of penetration as a function of the precipitation amount; the least square second-order polynomial curve indicates that a daily rainfall of 1.27 cm or less would not penetrate below 30 cm. During the 106-day long experimental period, 33 days with precipitation above 0.0254 cm were recorded in Lawrence, Kansas, with a total of 48.92 cm; this yields an average daily rainfall of 1.48 cm, and a corresponding depth of penetration of 34.8 cm. Consequently, even during this unusually wet period the precipitation amounts were not large enough, on the average, to significantly affect moisture contents in the lower zone.

The second reason behind differences in soil moisture dynamics is evaporative loss of water to the atmosphere. The sharp break in the moisture difference curve (Figure 23B) indicates that the evaporation loss was small at the depth of 40 cm. A further approximation of the lower zone contribution to actual evaporation was obtained by the following procedure based on the water balance technique:

(i) calculation, for a rainless period 8/14/73 through 8/30/73, of daily drainage out of the soil profile (i.e., below the lower zone) from Equation (6);

(ii) calculation of total daily loss of water from the lower zone (32.5 cm to 152.5 cm) only.

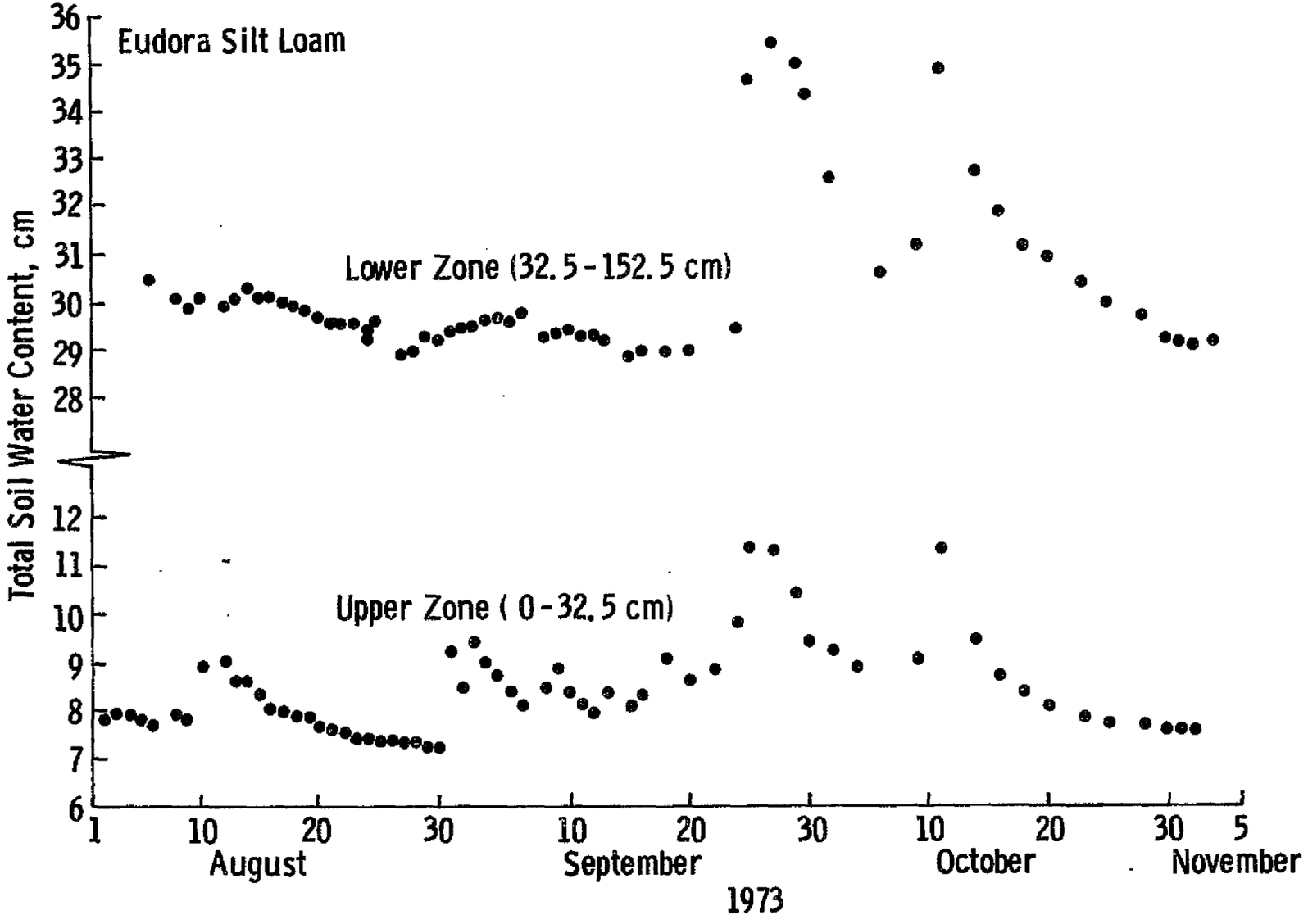

Figure 26. Total water content in the upper and lower zones as a function of time.

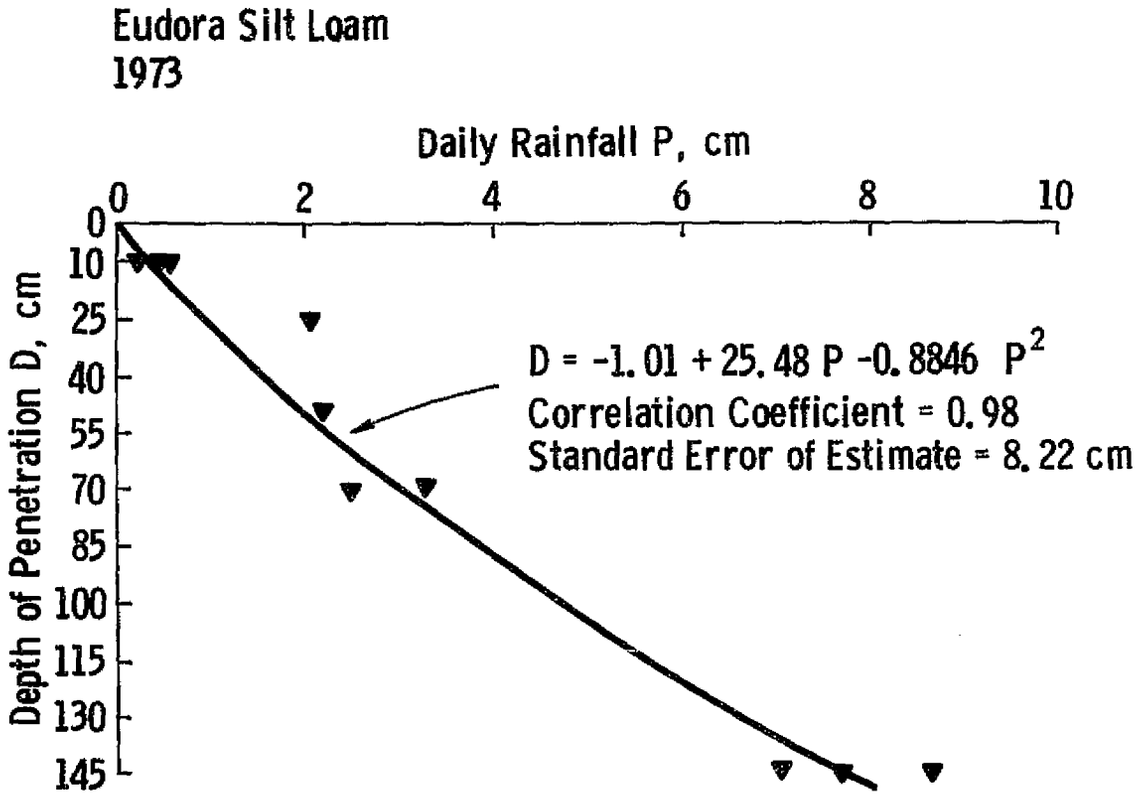

Figure 27. Depth of rainfall penetration as a function of the rainfall amount.

Results of (i) and (ii) are plotted for corresponding days in Figure 28. If the evaporation contribution from the lower zone were zero, the points should fall on the 1:1 line. However, most of the points are located above the line, suggesting that some water from the lower zone moved toward the surface and was lost through evaporation; the scatter of points precluded a reliable estimation of the proportion of actual evaporation. It should be noted that some points are not shown on Figure 28 because their coordinates were too large for the scale shown.

It may be argued that the small evaporation contribution from the lower zone was caused by the fine-textured layer at depths 40-55 cm which restricted water movement. However, Jackson's (1973) data also show that for the first 16 days (March, 1971) and 7 days (July, 1970) after irrigation with 10 cm of water, an average of 55% of evaporated water originated in the top 9 cm of the Adelanto loam (deep, fairly uniform soil). Furthermore, layers with reduced capability to conduct water are common in agricultural fields (Baver et al., 1972). Trouse and Baver (1965) found that almost every agricultural implement created compacted layers under moist conditions which decrease the rate of water movement through the soil. Consequently, the conclusions arrived at for Eudora silt loam appear valid for a wider class of soils.

2.3.2 Moisture Changes in the Lower Zone

Since evaporation loss from the lower zone is relatively small, the only components which enter the water balance equation (Equation (7)) for the lower zone, in addition to initial water storage, are precipitation which infiltrates through the upper zone, and drainage which escapes below the terminal depth of the soil profile. Precipitation is the main source of variations of the moisture status in the lower zone; consequently, the depth-time changes in soil water content following rainfall were of main interest here.

During a rainless period, moisture losses in the lower zone occur but are small; these losses are mainly due to drainage below the terminal depth. Figure 29 shows three moisture profiles for an almost rainless period between 8/20/73 and 8/30/73. Moisture decrease at depths below 40 cm was less than 0.01 cm^3/cm^3 for this 11-day period, while the upper zone was loosing water continuously. Precipitation on 8/31/73 (3.27 cm) and 9/2/73 (0.78 cm) raised moisture content up to a 40-cm depth by

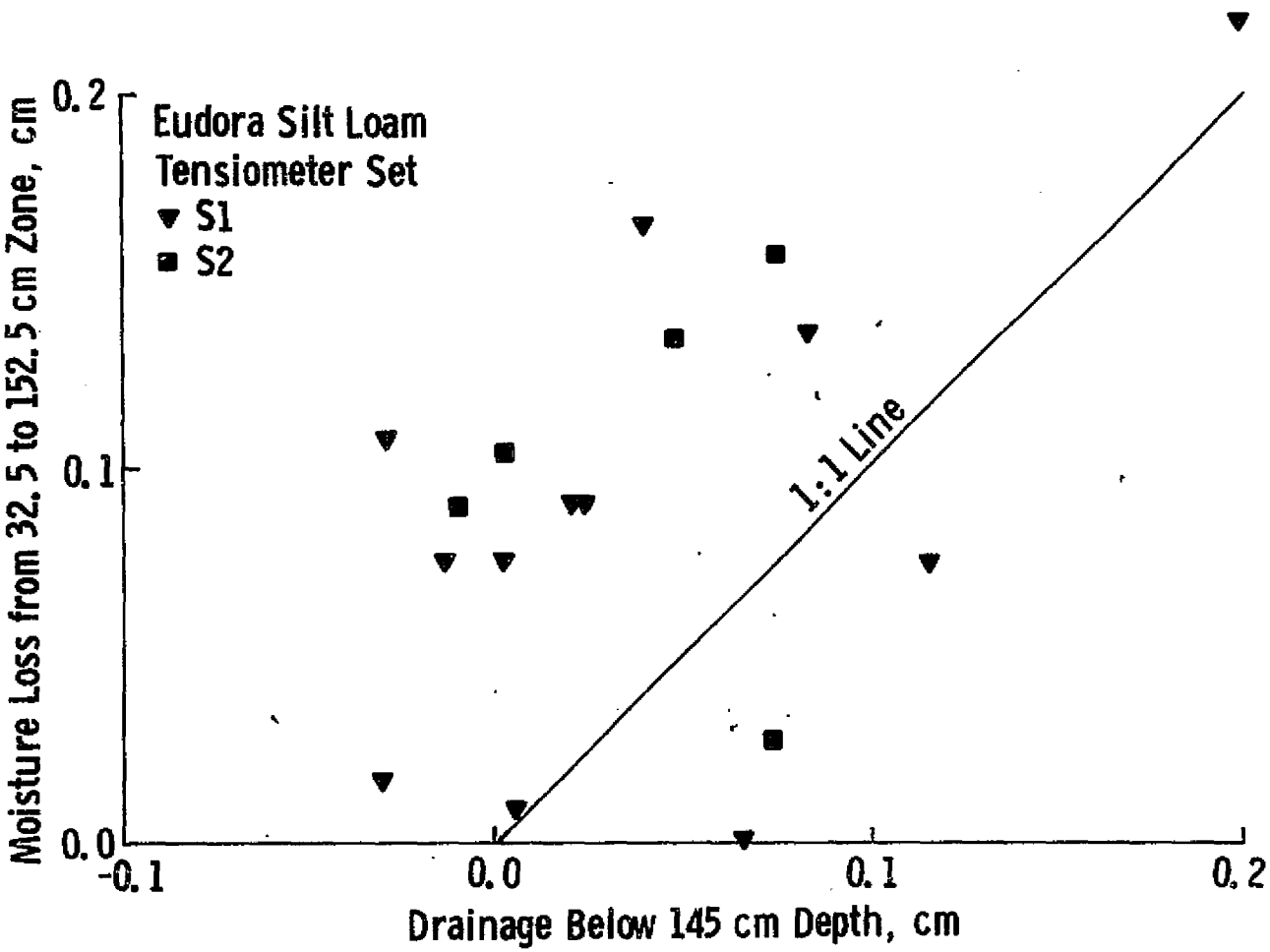

Figure 28. Lower zone contribution to the actual evaporation.

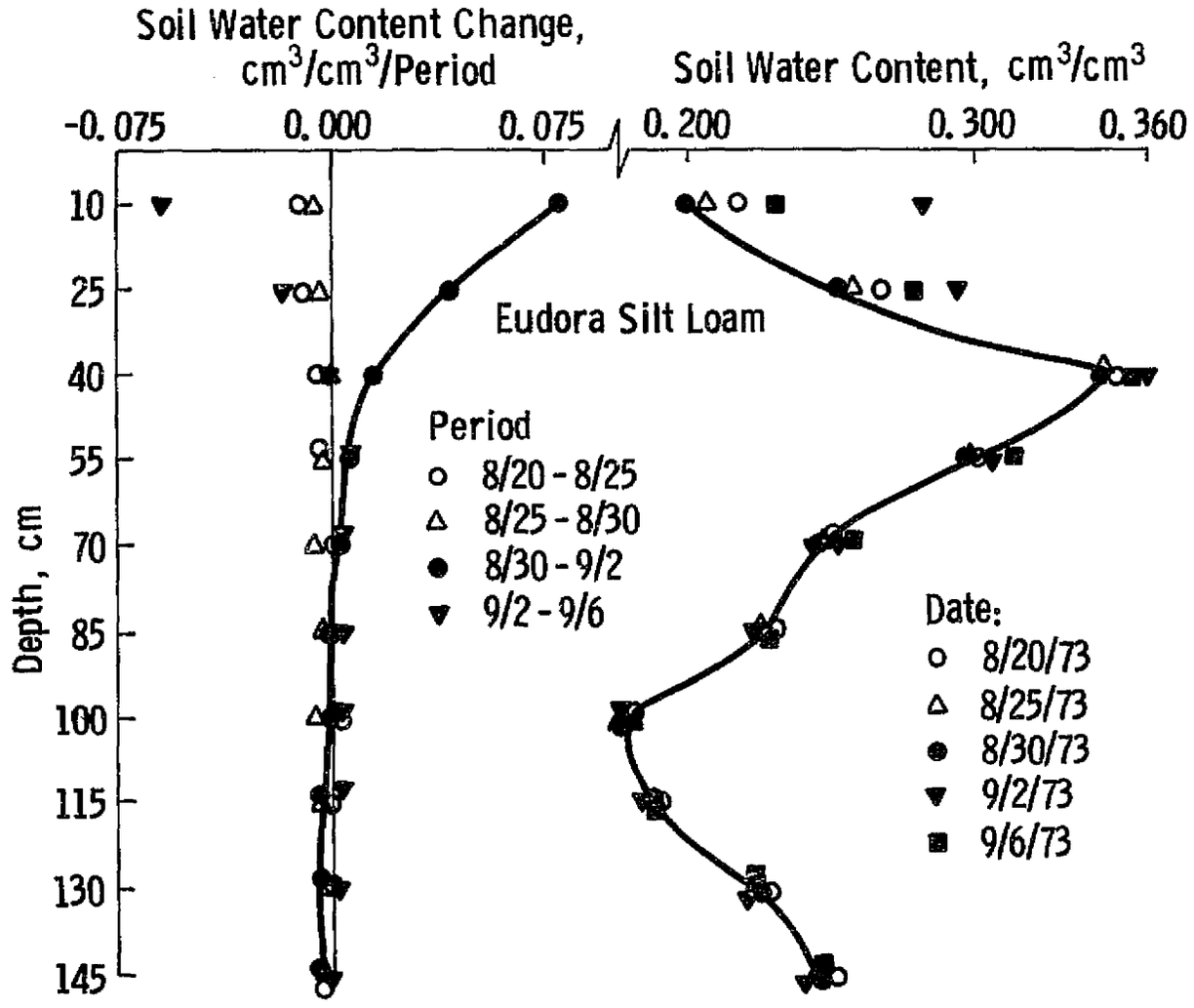

Figure 29. Soil water content (right-hand side) and soil water content changes (left-hand side) before and after rainfalls of 3.27 cm (8/31/73) and 0.78 cm (9/2/73).

9/2/73 but lower depths remained unchanged. Between 9/2/73 and 9/6/73, moisture decreased rapidly above 25 cm, slowly between 25 and 40 cm, and increased somewhat at greater depths as a result of water redistribution from the upper layers; this increase was largest at 55 cm and smaller below, but it did not exceed 0.010 cm^3/cm^3. The left part of Figure 29 shows moisture changes at individual depths between the dates mentioned. It is apparent that most of the moisture dynamics was confined to the upper zone and a few days after the rainfall.

Whereas the small rainfall reached only to a depth of 40 cm, a large precipitation on 10/11/73 (8.61 cm) penetrated through and increased moisture at all depths (Figure 30). However, more than half of this newly acquired moisture was lost through drainage during the next three days (left part of Figure 30). On 10/20/73, lower zone moistures were at the levels of 10/6/73, i.e., prior to the large precipitation. The rate of moisture decrease further declined as is apparent from curves for the periods 10/16 to 10/20 and 10/20 to 10/31. On 10/31/73, the amount of water in the lower zone reached a level typical for prolonged rainless periods (Figure29).

These results thus suggest that after the lower zone moisture content was increased through precipitation, water was rapidly redistributed to greater depths or lost out of the profile; the process was most intense after the addition of water and less so as the time progressed. Furthermore, the moisture contents tended to assymptotically approach a relatively stable vertical distribution in the profile; once this condition was reached, the lower zone moisture changed only slowly.

Richards et al. (1956) conducted an experiment on Pachappa sandy loam the results of which support the above conclusions. They measured moisture content changes in the 0 to 50 cm layer for 60 days after an initial irrigation by 45 cm of water. Curves in Figure 31 were generated from equations derived by Richards et al. (1956). The curves show that moisture loss was greatest near the surface (due to evaporation) and shortly after irrigation but decreased exponentially with time. After 20 days, the loss at depths greater than 30 cm was less than 0.0015 $cm^3/cm^3/day$. The exponential decay type-relationship for moisture loss due to drainage was also confirmed by Wilcox (1959) and Ogata and Richards (1957); evaporation was excluded in these studies.

The conclusions regarding rapid redistribution rate and establishment of an assymptotical vertical moisture distribution are valid only if sufficient amount of water is available initially and provided that water movement in the soil is not

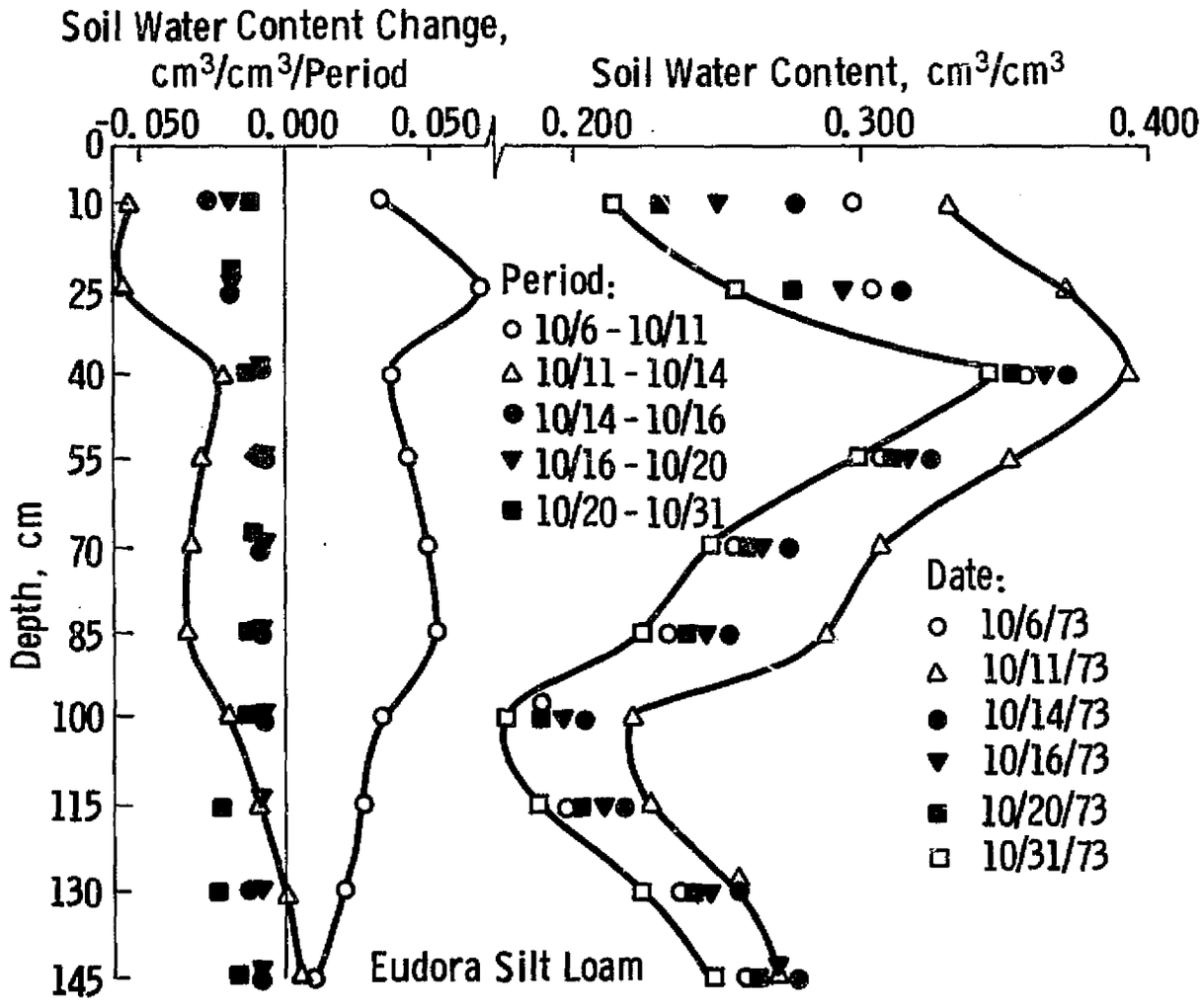

Figure 30. Soil water content (right-hand side) and soil water content changes (left-hand side) before and after a rainfall of 8.61 cm (10/11/73).

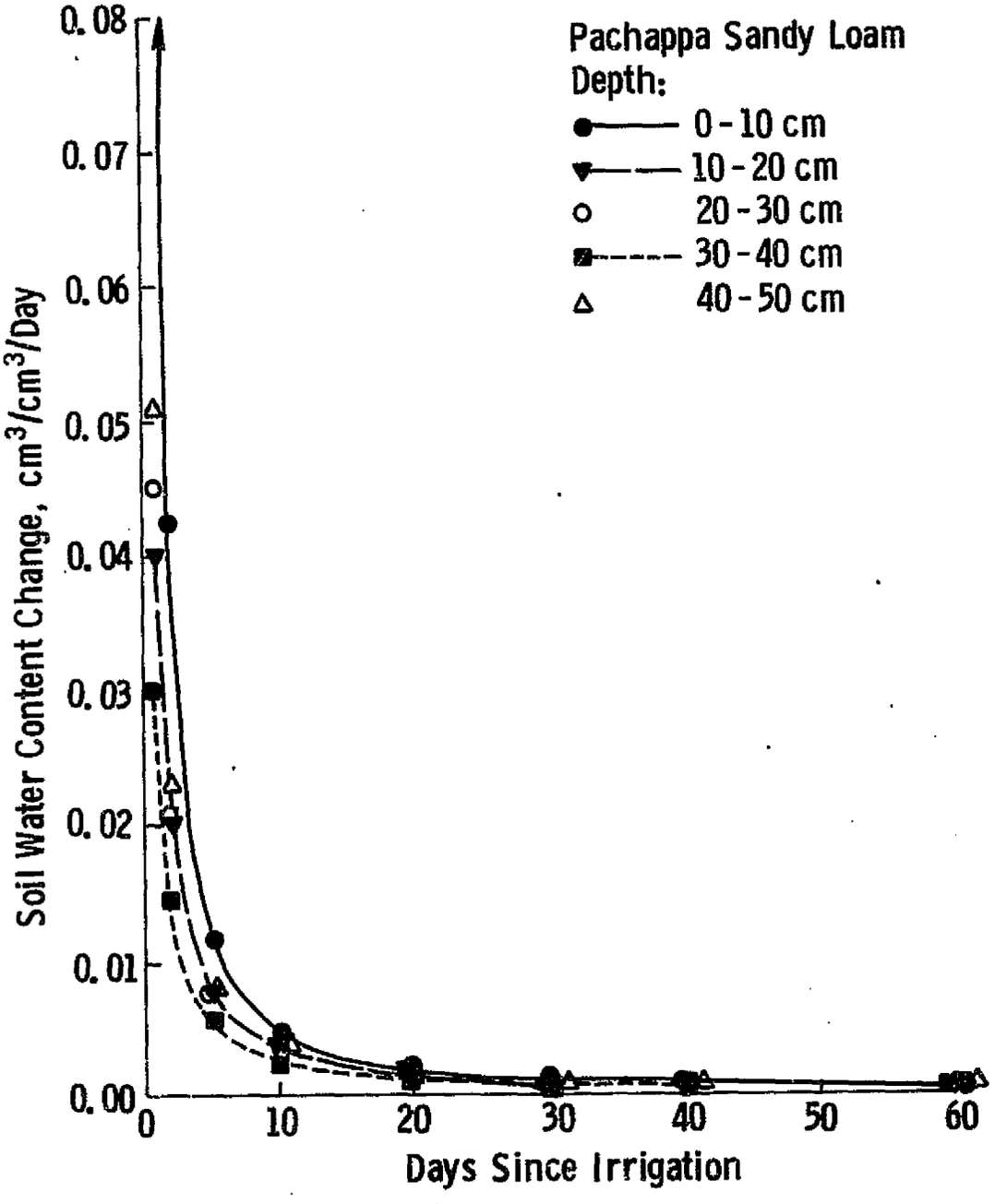

Figure 31. Soil water content change as a function of depth and time. Based on the data of Richards et al. (1956).

appreciably inhibited. In that case, soil releases all water which it cannot retain. However, in many situations, soil is capable of retaining more water than is available. An example is water depletion by plants. Figure 32 presents average monthly soil moisture storage for four geographic locations (Mather, 1964) computed according to the climatic water balance technique of Thornthwaite and Mather (1957); the computations assumed soil moisture storage of 30 cm. At three of the four locations, the soil water is not replenished during the entire year. If water were supplied here, it would not be completely released as drainage until the soil storage capacity is replenished. In one case (Topeka), the moisture storage is full for four months and in this period the conclusions reached previously would apply. Secondly, the data referred to in this section were measured in soil profiles with apparently high hydraulic conductivity which facilitated rapid movement of water. The rate of response to precipitation would be slower in the case of soils with low conductivities, e.g. clays. These considerations are important because they place restrictions on the algorithms that might be designed to estimate the actual moisture storage of the lower zone.

Station	Latitude	Longitude	Elevation (m)	Years of Record
○ Topeka	39° 04' N	95° 38' W	267	1905-60
● Austin	30° 18' N	97° 42' W	187	1905-60
▼ Bismarck	46° 46'N	100° 45' W	503	1905-60
■ Phoenix	33° 26' N	112° 01' W	338	1905-60

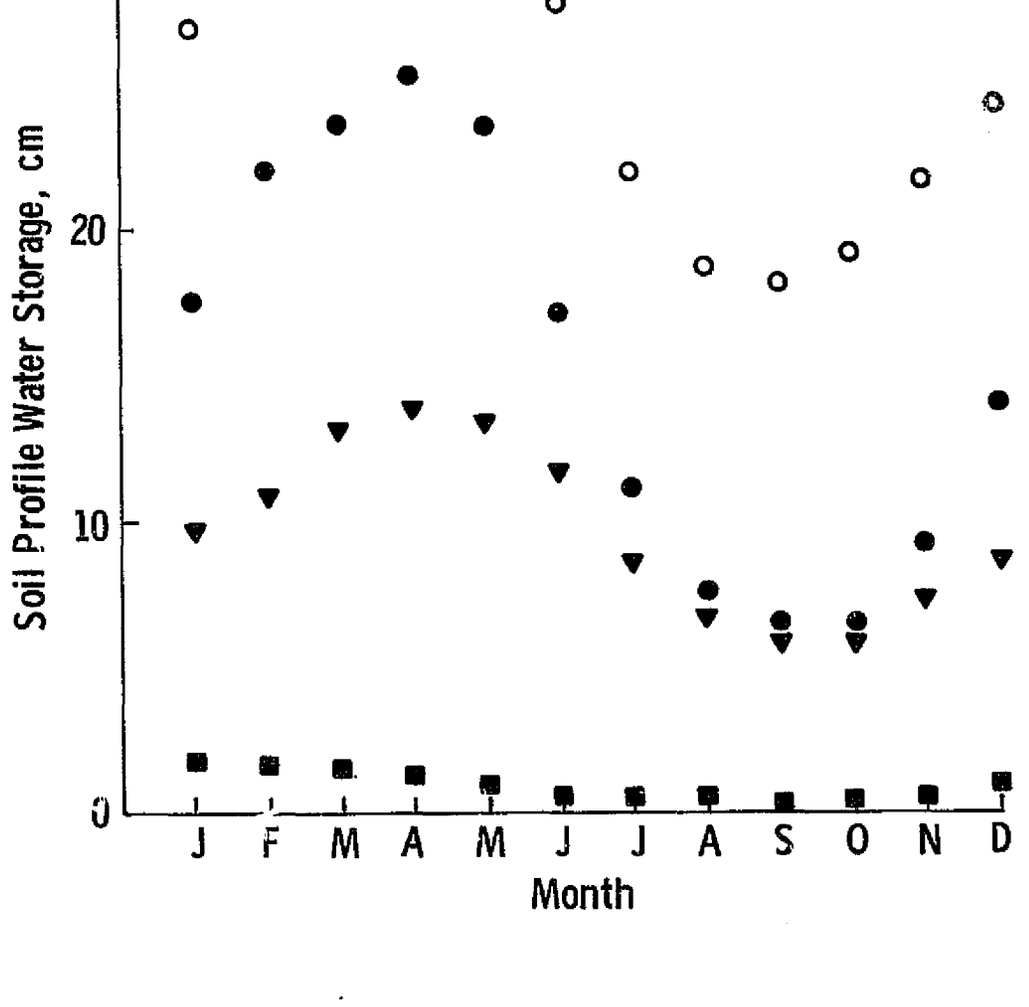

Figure 32. Mean monthly soil profile water storage at four locations. From Thorntwaite and Mather (1964).

CHAPTER 3.

SOIL TEMPERATURE REGIME

Temperature of a bare soil is a result of interactions of numerous variables, both external and internal to the soil profile. Because of its importance to mass and energy exchange near the earth's surface, soil temperature and its changes with these variables have been studied extensively by soil physicists, meteorologists, climatologists, civil engineers, and others. For example, Willis (1964) listed 1,152 references dealing with soil temperature. More recently, attempts have been made to combine the various kinds of information into simulation models. If the established concepts are correct, computed temperatures should agree with the measured ones. Once the validity of a model is established, the model may be used to predict the effect of changing various parameters, environmental conditions, etc., whereas it would be very difficult to collect equivalent data experimentally.

Soil temperature changes with time are described by the diffusion equation, and the analytical approach to soil temperature modeling has been based on simplified solutions of this equation. Several examples of this type were given by van Wijk (1963), van Wijk and de Vries (1963), and van Wijk and Derksen (1963). These solutions hold for cases in which soil is homogeneous and boundary conditions can be described analytically. Under natural conditions, however, soil thermal properties vary with depth and the upper boundary condition (surface temperature) changes may deviate from an analytical function. For these reasons, numerical modeling has been attempted as computers became available; its advantage is that the two above restrictions are no longer necessary.

Numerical models involving soil temperature have been employed by soil physicists (Wierenga et al., 1969; Wierenga and de Wit, 1970; Hanks et al., 1971; Westcot and Wierenga, 1974), and meteorologists or climatologists (Effimova and Tsitsenko, 1963; Myrup, 1969; Outcalt, 1972; Foster, 1972; Foster and Fye, 1973; Dyer, 1974). The former studies are of limited interest here because they use a measured upper boundary condition, usually 1 cm or so below the surface. In contrast, the latter models compute surface soil temperature and then use it as a boundary condition for the heat wave propagation below the surface. Most of the above meteorological models compute surface temperature from the energy balance equation; differences exist in the assumptions made and input parameters.

To determine the magnitudes of bare soil temperature fluctuations under various conditions, a numerical model of soil temperature was prepared (Appendix A); it followed, in its general features, the model developed by W. D. Sellers and described by Foster (1972).

3.1 SOIL TEMPERATURE MODEL AND ITS PERFORMANCE

The energy balance equation for the soil surface can be written as

$$R_N = H + LE + G. \tag{16}$$

R_N is net radiation and consists of absorbed solar (shortwave) radiation and absorbed longwave atmospheric emission minus thermal infrared radiation emitted by the soil surface. H and LE are sensible and latent heat terms, and G is soil heat flux. All terms in Equation (16) can be positive or negative. If the aerodynamic concept is used to compute H and LE, an analytical solution of the diffusion equation to compute G, and semiempirical equations to calculate the components of R_N, soil surface temperature T_s can be found using Equation (17):

$$T_s = T_a + \frac{S_a - C_2 - C_5 - C_7}{C_1 + C_3 + C_4 + C_6}, \tag{17}$$

where

$$C_1 = 4 \epsilon \sigma T_a^4,$$

$$C_2 = \epsilon (1 - kn) (0.165 - 0.000769\ RH),$$

$$C_3 = \frac{\rho C_p D}{R T_a},$$

$$C_4 = \frac{0.38688\ L^2\ D\ a\ e_{sa}}{R^2\ T_a^3},$$

$$C_5 = \frac{0.622\ L\ D\ a\ (e_{sa} - e_z)}{R T_a},$$

$$C_6 = 0.7071\ (\lambda C \omega)^{1/2}\ (1 + 1/\omega),$$

$$C_7 = 0.7071\ (\lambda C \omega)^{1/2}\ \left(T_a - \overline{T}_s + \frac{T_a - T_{s1}}{\omega}\right),$$

and:

S_a = absorbed solar radiation, in ly/min;

T_a = air temperature, in °C;

σ = Stefan-Boltzman constant, $\sigma = 8.17 * 10^{-11}$ ly/min /°K^4;

ϵ = infrared emissivity of the soil, dimensionless;

n = cloud cover in tenths, dimensionless;

k = parameter varying with cloud type, given by Sellers (1965, p. 58);

p = air pressure, in mb;

C_p = specific heat of air, in cal/g/°K;

D = transfer coefficient, in cm/min;

R = gas constant, R = 2870.4 mbcm^3/ °K/g;

L = latent heat of vaporization, in cal/g;

a = AE/PE ratio, dimensionless;

e_{sa} = saturation vapor pressure at T_a, in mb;

e_z = actual vapor pressure at the height of wind speed measurements; in mb;

ω = angular frequency, in radians per time increment of soil temperature calculation;

C = soil heat capacity, in cal/cm^3/°C;

λ = soil thermal conductivity, in cal/cm/sec/°C;

$\bar{T}_s$ = average day soil surface temperature, in °C;

T_{s1} = soil surface temperature for the previous time increment, in °C.

The derivation of Equation (17) is given in Appendix A.

Assuming horizontal uniformity and heat transfer by conduction, the temperature change with time t at depth z, T(z,t), is described by

$$\frac{\delta T(z,t)}{\delta t} = \frac{d}{dz}\left(D'(z) \frac{\delta T(z,t)}{\delta z} \right), \qquad (18)$$

where D'(z) = apparent thermal diffusivity in cm^2/min. The computer program incorporating Equation (17) and the finite difference form of Equation (18) is also described in Appendix A.

Before the model can be used to simulate soil temperature variations under various conditions, its performance must be tested to ascertain its correspondence to reality. Two sets of profile soil temperatures measured over a 24 hour period* were used

*Courtesy of Dr. S. B. Idso, U. S. Water Conservation Laboratory, Phoenix, Arizona.

for this purpose; the experimental procedure used for their acquisition is described in Appendix B. Table 10 gives values of bulk density, field capacity, initial moisture content and soil temperature for both sets; it should be noted that bulk densities below 10 cm and soil moisture below 30 cm were assumed as no direct measurements were available. Field capacity was taken as moisture content at 110 cm tension (Jackson, 1973), and the value for 0-2 cm was reduced by 0.9 (see Section 2.2.1). Additional variables for both test runs are listed in Table 11.

The correspondence between computed and measured soil temperatures for the 9/20/73 set (wet soil) is shown in Figure 33 and 34. Calculated surface temperatures followed the measured values fairly closely, although a systematic shift occurred: the computed surface temperatures increased and decreased more slowly than the measured ones (Figure 33). The difference was greatest at 1600 hours (3.5°C) but decreased to small values during night hours. The diurnal variation of computed and measured temperatures at 5 cm, 10 cm, and 20 cm (Figure 34) also indicates reasonable predictive accuracy of the model. At all depths, however, the predicted diurnal temperature amplitude was greater than the measured one.

Comparison of computed and measured soil temperatures for dry soil (10/02/73) revealed similar results (Figures 33, 35). Surface temperature was predicted accurately until the maximum value at 1300 hours, but it decreased more slowly than measured temperatures between 1300 and 2000. Subsurface predicted temperatures also followed the measured values until approximately 1300, after which the difference between the two increased.

Results shown in Figures 33 through 35 suggest that the accuracy of soil temperature prediction differed somewhat for surface and subsurface temperatures. The lag in surface temperatures of the wet soil (Figure 33) during the morning hours could be due to the latent heat; this possibility is enhanced by the differences being negligible for the dry soil case (Figure 33). Similarly, an error in predicting the latent heat term could be responsible for the lag of computed surface temperatures in the afternoon; note that on 10/02/73 for example, the moisture loss proceeded faster than the model predicted, thereby leaving less heat for warming the soil (depth 2 cm, time 1300 hours to 1800 hours, Figure 15). In general, however, surface soil temperatures were predicted with good accuracy as the above mentioned differences were not large. In the case of subsurface temperatures, diurnal temperature amplitude was consistently larger, indicating that the computed heat conduction into the soil was too high. The apparent thermal diffusivity employed in computing temperature changes from Equation (18) was determined using thermal conductivity calculated from de Vries' (1963) model, and a

Table 10. Bulk density, field capacity, initial soil moisture, and initial soil temperature profiles for two soil temperature data sets used for a soil temperature simulation model testing.

Depth (cm)	9/20/73 & 10/02/73		9/20/73			10/02/73	
	Bulk density (g/cm^3)	Field capacity (cm^3/cm^3)	Moisture (cm^3/cm^3)	Temperature* (°C)	Temperature** (°C)	Moisture (cm^3/cm^3)	Temperature (°C)
2	1.43	0.275	0.275	21.3	20.2	0.087	21.8
4	1.49	0.305	0.279	22.7	21.4	0.156	23.9
6	1.50	0.305	0.281	23.8	22.6	0.186	24.8
8	1.51	0.305	0.282	24.6	23.6	0.199	25.7
10	1.52	0.305	0.284	25.4	24.6	0.208	26.3
12	1.52	0.305	0.286	26.0	25.4	0.213	26.9
14	1.52	0.305	0.286	26.6	26.1	0.219	27.4
16	1.52	0.305	0.286	27.0	26.7	0.222	27.8
18	1.52	0.305	0.287	27.4	27.2	0.223	28.0
20	1.52	0.305	0.286	27.8	27.6	0.225	28.2
22	1.52	0.305	0.284	28.1	27.9	0.230	28.3
24	1.52	0.305	0.281	28.4	28.2	0.233	28.3
26	1.52	0.305	0.277	28.6	28.4	0.236	28.3
28	1.52	0.305	0.271	28.7	28.6	0.239	28.1
30	1.52	0.305	0.264	28.8	28.7	0.240	28.2
32	1.52	0.305	0.258	28.9	28.8	0.240	28.1
34	1.52	0.305	0.255	29.0	28.9	0.240	28.1
36	1.52	0.305	0.251	29.1	29.0	0.240	28.0
38	1.52	0.305	0.245	29.3	29.1	0.240	28.0
40	1.52	0.305	0.240	29.3	29.2	0.240	28.0
42	1.52	0.305	0.234	29.5	29.3	0.240	27.9
44	1.52	0.305	0.228	29.6	29.4	0.240	27.9

Table 10. (Continued) Bulk density, field capacity, initial soil moisture, and initial soil temperature profiles for two soil temperature data sets used for a soil temperature simulation model testing.

Depth (cm)	9/20/73 & 10/02/73		9/20/73			10/02/73	
	Bulk density (g/cm^3)	Field capacity (cm^3/cm^3)	Moisture (cm^3/cm^3)	Temperature* (°C)	Temperature** (°C)	Moisture (cm^3/cm^3)	Temperature (°C)
46	1.52	0.305	0.223	29.7	29.5	0.240	27.9
48	1.52	0.305	0.220	29.9	29.6	0.240	27.9
50	1.52	0.305	0.220	30.0	29.8	0.240	27.9
52	1.52	0.305	0.220	30.1	29.9	0.240	27.9
54	1.52	0.305	0.220	30.2	30.1	0.240	27.9
56	1.52	0.305	0.220	30.3	30.2	0.240	28.0
58	1.52	0.305	0.220	30.5	30.4	0.240	28.0
60	1.52	0.305	0.220	30.6	30.6	0.240	28.1
62	1.52	0.305	0.220	30.7	30.7	0.240	28.1
64	1.52	0.305	0.220	30.8	30.9	0.240	28.1
66	1.52	0.305	0.220	30.9	31.1	0.240	28.1
68	1.52	0.305	0.220	31.0	31.3	0.240	28.1
70	1.52	0.305	0.220	31.1	31.5	0.240	28.1

Note:

*Measured vales.

**Values computed by starting with a constant soil temperature with depth, and then computing successive iterations until the temperatures at depth 0 cm and 70 cm at 2400 hrs. differed by less than 0.1°C for two adjacent diurnal runs.

Table 11. Operational parameters for the soil temperature simulation model.

Parameter	Data Set			
	9/20/73	10/2/73	Hypothetical	
			HMP*	LMP*
PERL	10 min.	10 min.	10 min.	10 min.
DT	2.5 min.	2.5 min.	2.5 min.	2.5 min.
Number of layers	35	35	35	35
Anemometer height	60 cm	60 cm	240 cm	240 cm
Roughness length	0.003 cm	0.003 cm	0.5 cm	0.5 cm
Previous day average surface temperature	27°C	25°C	26.2°C	28.6°C
Previous hour surface temperature	21°C	18°C		
Emissivity of the soil	0.90	0.90	0.90	0.90

*HMP (LMP) = high (low) moisture content profile

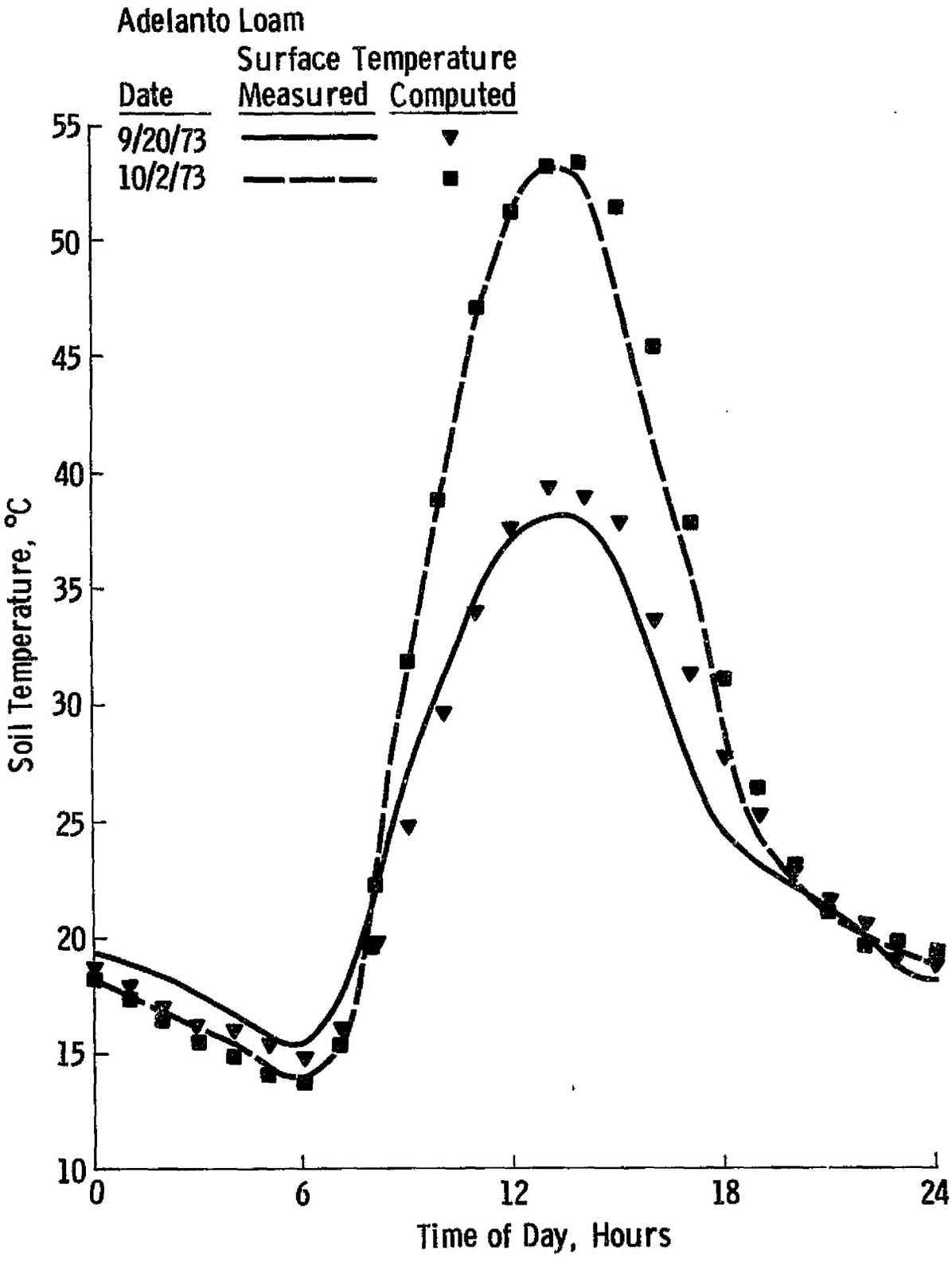

Figure 33. Comparison of computed and measured surface soil temperatures for dry and wet soil.

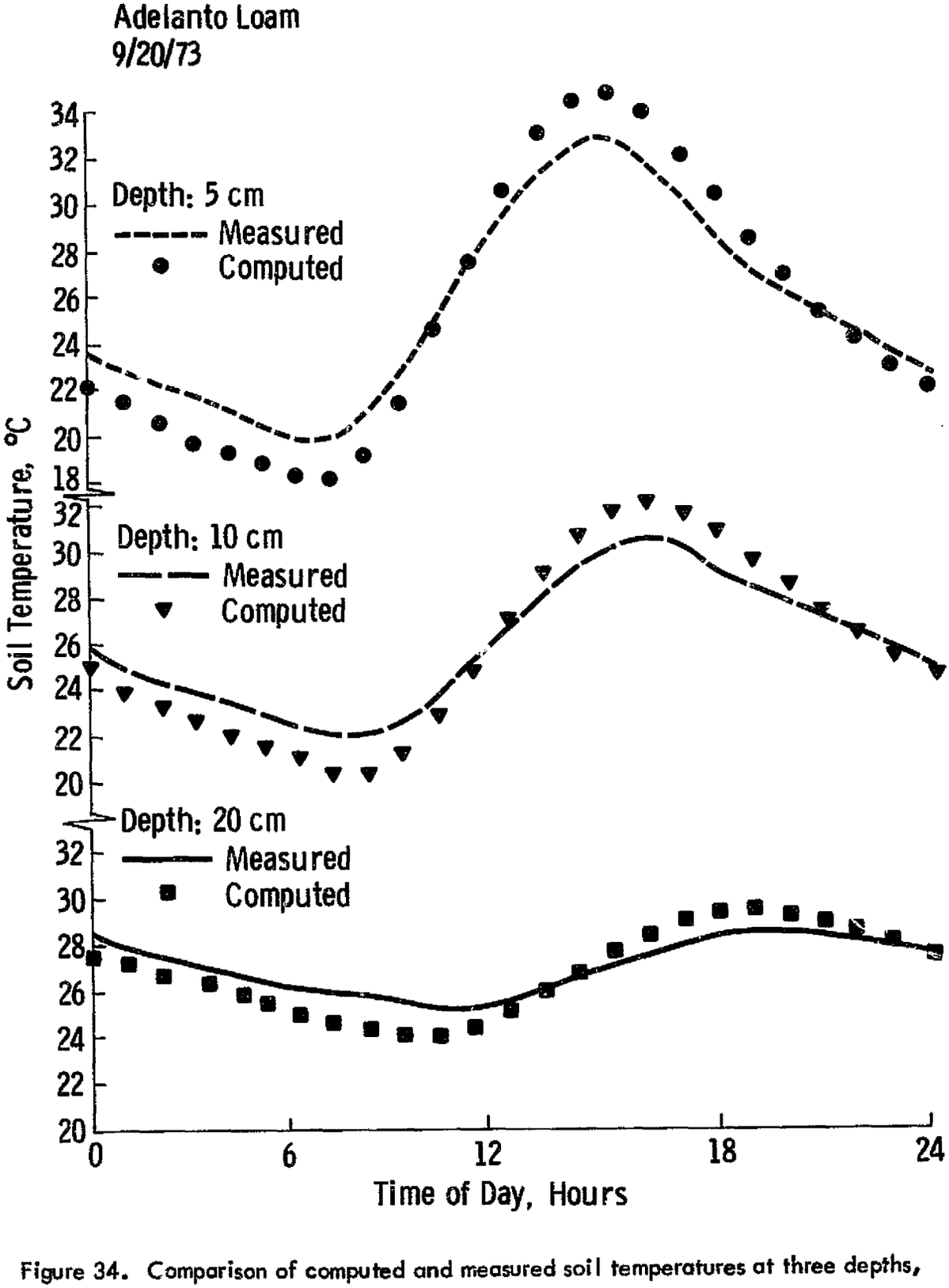

Figure 34. Comparison of computed and measured soil temperatures at three depths, wet soil.

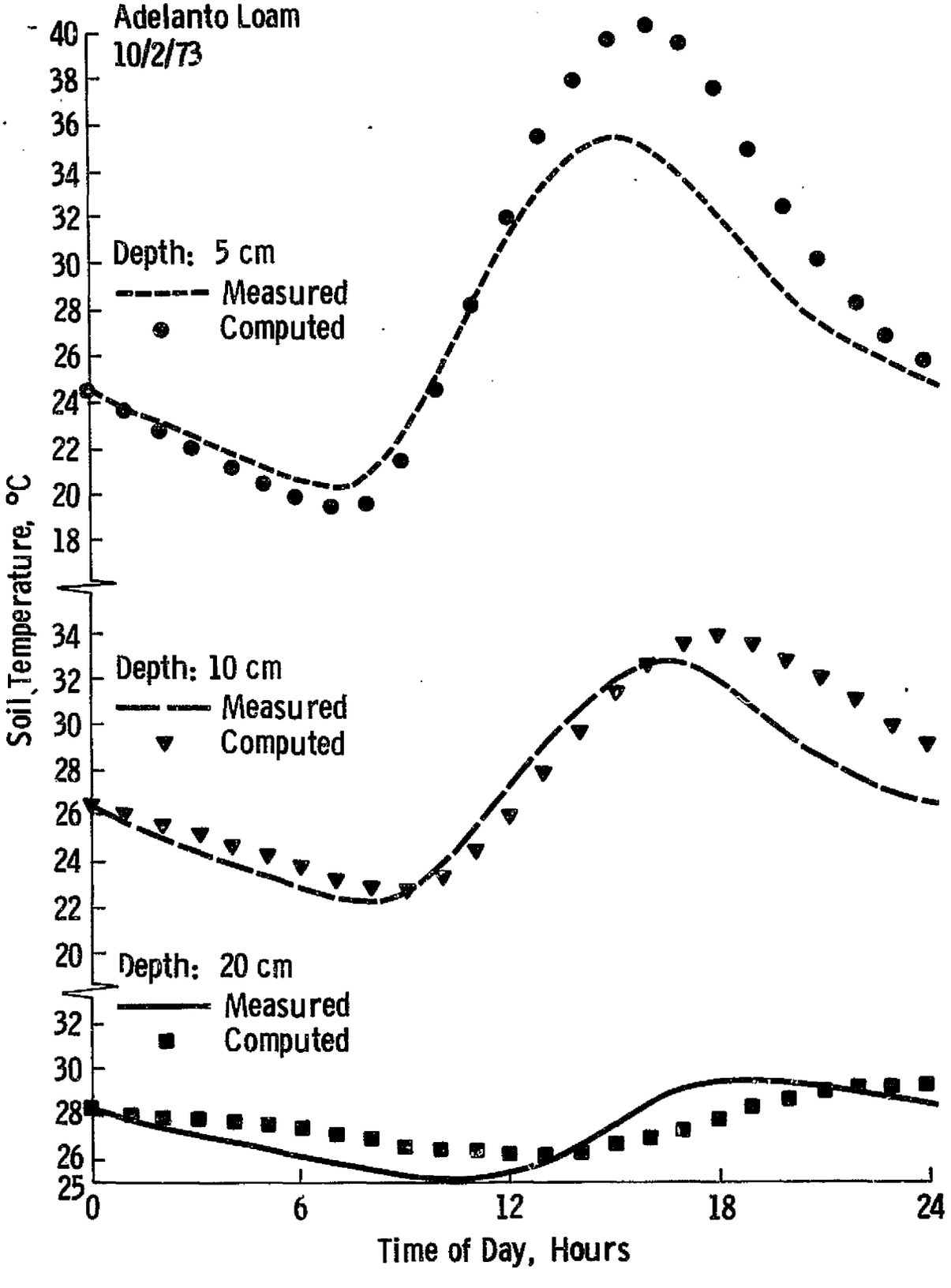

Figure 35. Comparison of computed and measured soil temperatures at three depths, dry soil.

simple formula was used for estimating heat capacity (see Appendix A). Both of these methods have previously been found to yield satisfactory results (Hanks et al., 1971; Wierenga et al., 1969; de Vries, 1963). The thermal diffusivities generated in this manner for the dry soil case ranged from 0.353 cm^2/min. at 2 cm depth to 0.410 cm^2/min at 10 cm. Considering the relatively high bulk densities of Adelanto loam (Table 10), these values are consistent with those determined by Wierenga et al. (1969) as well as those used by Hanks et al. (1971) for similar conditions. To estimate what the diffusivity should be in order for the computed temperatures to follow the measured ones, an "effective" thermal diffusivity α was computed from the dry soil data using an amplitude equation (Wierenga et al., 1969):

$$\alpha = 0.002182 \left(\frac{z_2 - z_1}{\ln (A_1/A_2)} \right)^2 \qquad (19)$$

where A_1 (A_2) is the amplitude of the diurnal temperature wave at depth z_1(z_2). The following results were obtained:

z_1 (cm)	0	1	2	3	4	5	10	0	0
z_2 (cm)	1	2	3	4	5	10	20	5	10
A_1 (°C)	39.5	29.1	23.2	19.3	17.1	15.2	10.5	39.5	39.5
α(cm^2/min)	0.0234	0.0425	0.0644	0.1490	0.1573	0.3986	0.2738	0.0598	0.1243

The computed diffusivities in the 0-5 cm layer are unusually low. For example, assuming heat capacity of 0.35 $cal/cm^3/°C$, a diffusivity of 0.0598 cm^2/min (depth 0 to 5 cm) means that the apparent thermal conductivity would have to be 3.49×10^{-4} cal/cm/sec/°C; this value is 60 times smaller than the thermal conductivity of quartz at 10°C given by de Vries (1963). Some of the discrepancy is probably due to the fact that Equation (19) assumes constant diffusivity with depth. Considering the dry soil vertical moisture distribution (from approximately 0.02 cm^3/cm^3 at 0 cm to 0.17 cm^3/cm^3 at 5 cm),

this assumption was clearly violated. Nevertheless, the rapid decrease in the temperature wave amplitudes with depth indicates that heat penetration into deeper layers was strongly attenuated. If heat transfer is assumed to have occurred by conduction only (as described by Equation (18)), then the above observations imply that the computed thermal diffusivities must be reduced in order to achieve satisfactory correspondence between computed and measured temperature values. Consequently, the thermal conductivities computed from de Vries' (1963) model were multiplied by 0.3 in the dry soil case, while no correction was applied to wet soil computations. Figure 34 shows that the reduction was adequate for the period of low heat load only. This suggests that other processes may not have been sufficiently accounted for, e.g. latent heat loss.

In spite of these discrepancies, the prediction of the soil temperatures was reasonably satisfactory, the computed values for most time/depth/moisture combinations being within 1.5°C of the measured values. In the following sections, these discrepancies will be of minor importance because relative changes in soil temperature will be of primary interest.

3.2 DIURNAL SOIL TEMPERATURE CHANGES

The soil temperature simulation model described and tested in the previous section can now be used to estimate the effect of important environmental variables on soil temperature. Since changes in soil temperatures ranging from very small to very large can be caused by numerous parameters, some restrictions must be imposed to make the analysis manageable. Consequently, the problem here is limited to estimating probable "average maximum" variations of bare soil temperatures for mid-latitudes.

From the many parameters related to diurnal soil temperature variations, the following are of major importance: moisture content, time of day, zenith angle at solar noon, and depth. Clear sky is assumed because then extreme temperatures can be reached. To render results of this analysis more representative, hypothetical experimental conditions were defined as follows:

(i) The hypothetical bare field was located near Topeka, Kansas. The site had three surface configurations:

slope 0°;
slope 30°; aspect $+90^{\circ}$, i.e. facing West;
slope 30°; aspect -90°, i.e. facing East.

Roughness length was taken as 0.5 cm, a value intermediate between 0.03 cm given by Pasquill (1962) for level desert and 2.1 cm for fallow field (van Wijk and Borghorst, 1963). As will become apparent later, choice of another roughness length would result in somewhat different temperatures.

(ii) The experiment took place around July 20 when solar declination was 20.85°N.

(iii) Hourly values of screen height air temperature, wind speed, and relative humidity were obtained by averaging observations taken at 3-hour intervals during four clear sky days in July, 1973, at the Topeka Weather Station (latitude $39^{\circ}04'$N, longitude $95^{\circ}38'$W, altitude 267 m). Solar radiation was calculated (Appendix A) assuming the coefficient of atmospheric transparency in Kastrow's equation TC = 0.314 for the optical mass OM = 1.0. Under these conditions, total solar radiation was equal to 1.414 cal/cm^2/min for a horizontal surface at the solar noon. The same meteorological conditions were assumed for both wet and dry soil.

(iv) Bulk density was assumed to be 1.25 g/cm^3 throughout the soil profile. The soil mineral fraction was assumed to consist of 30% quartz and 70% other minerals. Thermal conductivity computed by the method of de Vries (1963) was not reduced for the dry soil case, primarily because the computations yielded thermal diffusivities comparable to those of Hanks et al. (1971) and Wierenga et al. (1969) for equivalent conditions. Field capacity was assumed equal to 0.300 cm^3/cm^3 except for the top 2 cm where it was reduced by a factor of 0.9 (see section 2.2.1). For the high moisture

content profile (HMP), soil was considered to initially contain 0.300 cm^3/cm^3 throughout the profile. The dry profile (LMP) was derived by applying the layered water balance model to the soil initially at field capacity; the LMP was taken as the moisture profile after 20 days of drying without precipitation during which potential evaporation was a constant of 0.575 cm/day.

(v) Initial soil profile temperatures were derived by means of the soil temperature simulation model, separately for HMP and LMP. Using the above conditions and an initially constant soil temperature, iterrations were computed until temperatures at 2400 hours changed less than 0.1°C for depths 0 cm and 70 cm between successive iterrations. The adequacy of this procedure was verified on the 9/20/73 data set (see Table 10).

Diurnal soil temperatures discussed below were computed during six different runs. The results are identified by three parameters, namely moisture condition (H = high, L = low), slope (in degrees), and aspect (in degrees); for example, H/30/-90 refers to temperatures of soil with high moisture content, surface slope 30°, and surface facing East.

Figure 36 shows diurnal changes in surface soil temperature for the two moisture contents (H/0/0 and L/0/0) and roughness length 0.5 cm. Before dawn, surface temperature of the wet soil was slightly higher, apparently due to higher heat conduction from deeper layers (Figure 39, 40). Following sunrise, dry soil surface temperature increased much faster than that of the wet soil as a result of lower latent heat expenditure. Maximum surface temperatures were reached approximately 80 minutes after solar noon in both cases which agrees with the observations of Idso et al. (1975). The surface temperature wave amplitude was doubled for dry soil compared to wet soil. Soil moisture thus exerted a major effect on the daytime surface temperature. However, Figure 36 suggests that this amplitude is also a function of surface roughness. The pairs of curves were computed for identical conditions except for the roughness length which was 0.50 cm and 0.01 cm, respectively. As a consequence of smaller roughness, the surface temperature amplitudes increased by a factor of 1.5 for both wet and dry soil. This difference was caused by lower turbulent transfer coefficient D in the smooth case which decreased latent heat transfer. For example, for the wet soil, latent heat decreased from 516.6 ly/day (rough) to 376.0 ly/day (smooth). Surface temperature thus increased, in spite of an increase in sensible heat exchange

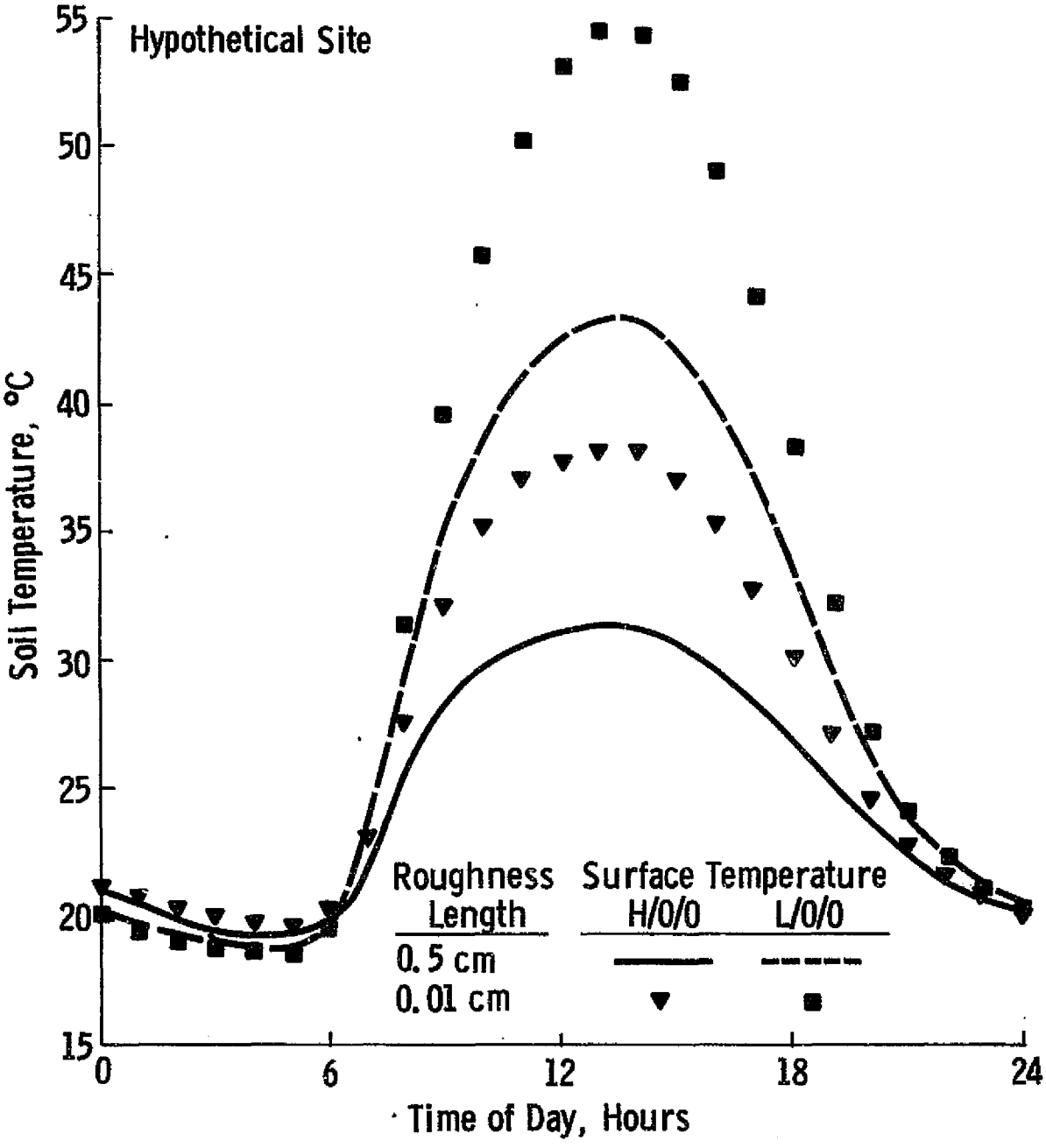

Figure 36. Effect of soil moisture and surface roughness on the surface temperature of a bare soil.

(from -48.0 ly/day for rough surface to 26.9 ly/day for smooth surface). It should be noted that the surface temperature computed by the model represents an "average" value over the surface soil elements. Soil moisture content also affected soil temperatures at greater depths; this is evident from Figure 37b and 38b which show temperatures at 10 cm. With increasing surface temperature amplitude, the amplitudes at greater depths also increased. This occurred because the thermal diffusivity was not appreciably reduced for the LMP (both thermal conductivity and thermal capacity decreased, resulting in a small diffusivity change).

The effect of slope and aspect of soil surface is shown in Figure 37 for the dry soil. As expected, surface temperature was highest for L/30/-90during morning hours and for L/30/90 in the afternoon; this was determined by the actual solar zenith angles for individual surfaces. The daily maximum surface temperature increased somewhat as the aspect changed from east to west, but the increase was small for LMP (Figure 37) and negligible for HMP (Figure 38). These data suggest that the surface temperature may vary considerably; for example, surface tempetatures L/30/90 and L/30/-90 differed by 13.3 ^{o}C at 0900 hours. The differences were somewhat lower in the afternoon. The slope/aspect effect was smaller for the HMP (Figure 38) because of the lower surface temperature amplitude but the trends were similar. In both cases, the differences in surface tempetatures were propagated to greater depths (Figure 37,38).

The changing depth/time pattern is illustrated in Figure 39 (L/0/0) and Figure 40 (H/0/0). Between midnight and dawn, soil temperature increased almost linearly to 20-30 cm and remained approximately constant at greater depths. Following sunrise, surface temperature increased first and the heat wave began to penetrate to deeper layers. After surface temperature started to decrease, the temperature profile had both concave and convex portions, causing heat transfer to proceed in two directions. This condition was well developed by 1800 hours, and from then on soil temperature decreased. The time/depth patterns for dry (Figure 39) and wet (Figure 40) soil were similar, the main difference being temperature amplitudes at different depths. The amplitudes shown in Figure 41 permit two observations: (i) on the diurnal basis, soil tempetature changed relatively little at depths below 30 cm; and (ii) the amplitudes were doubled in the case of dry soil.

Data for the above soil temperature simulation were chosen so as to represent "average maximum" changes in bare soil temperature to be expected at mid-latitudes. The good performance of the model in matching measured data suggests that the simulated results are representative for the chosen environment. Considering all factors that affect

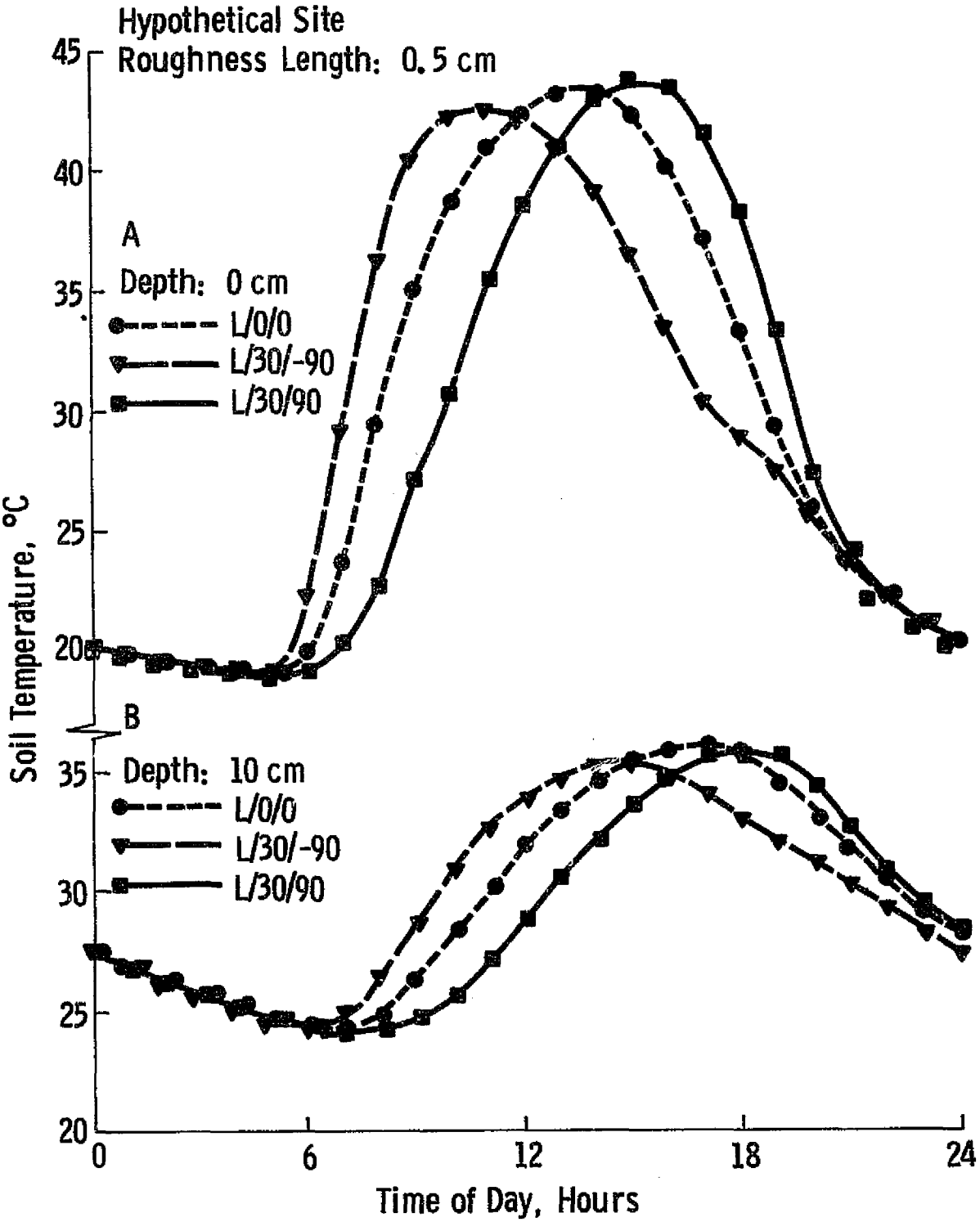

Figure 37. Temperature of a dry soil at the surface (A) and at 10 cm depth (B) as affected by the surface configuration.

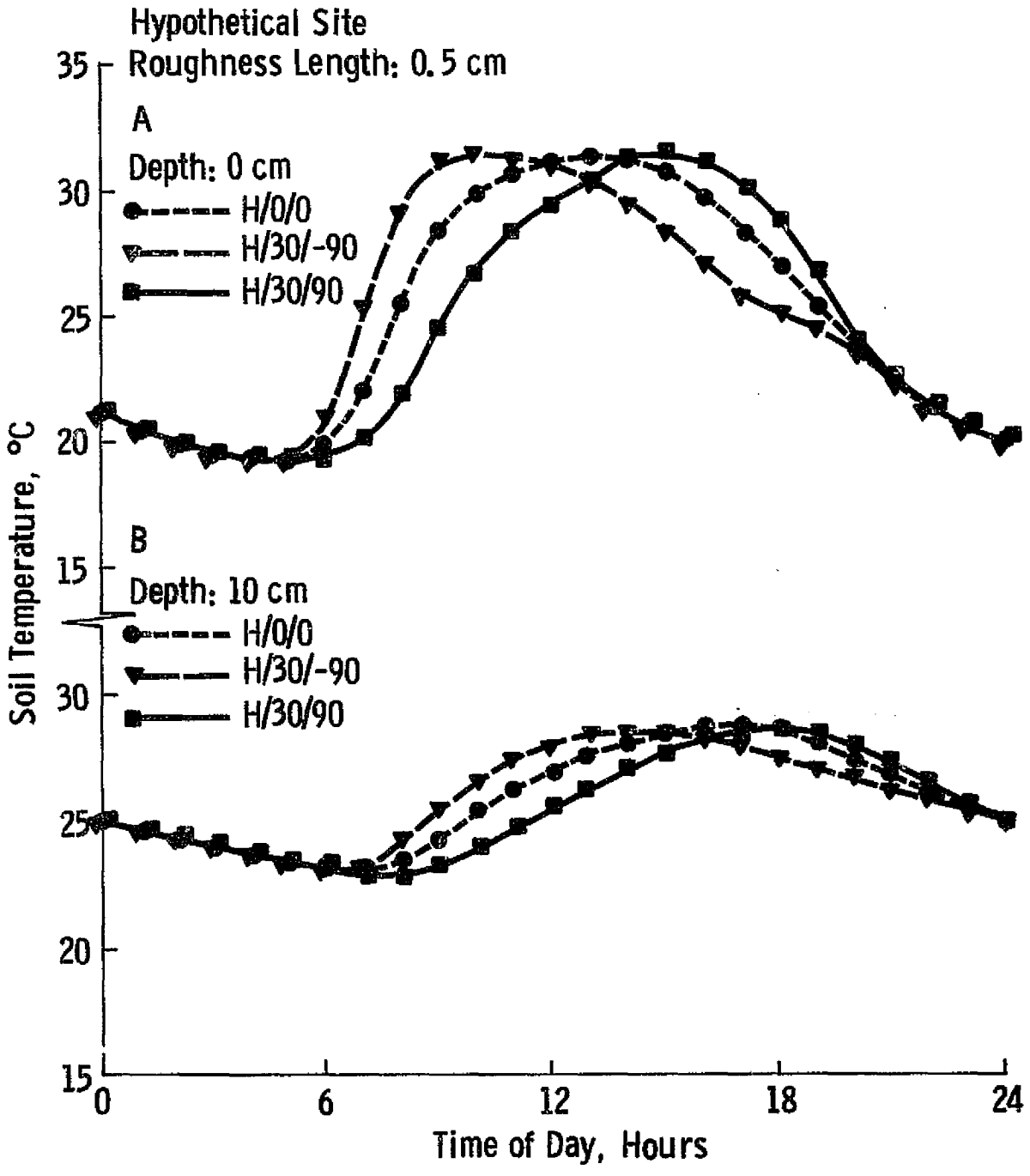

Figure 38. Temperature of a wet soil at the surface (A) and at 10 cm depth (B) as affected by the surface configuration.

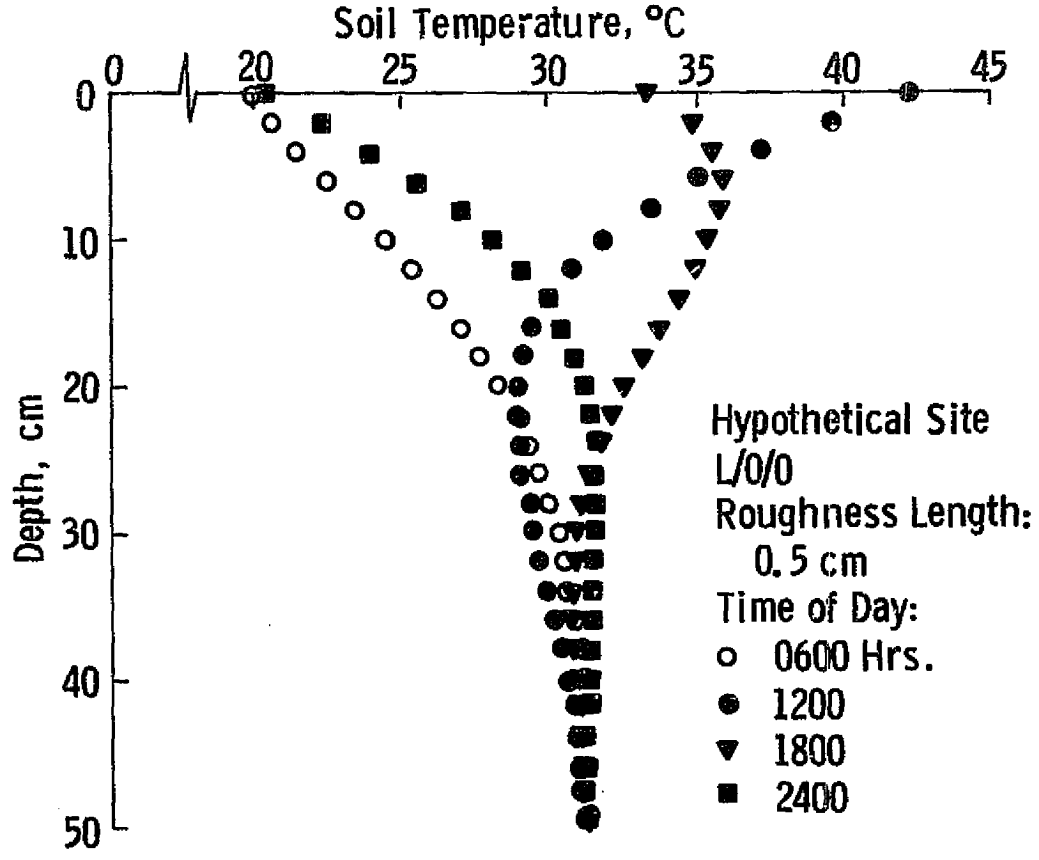

Figure 39. Temperature of a dry soil as a function of depth and time of day.

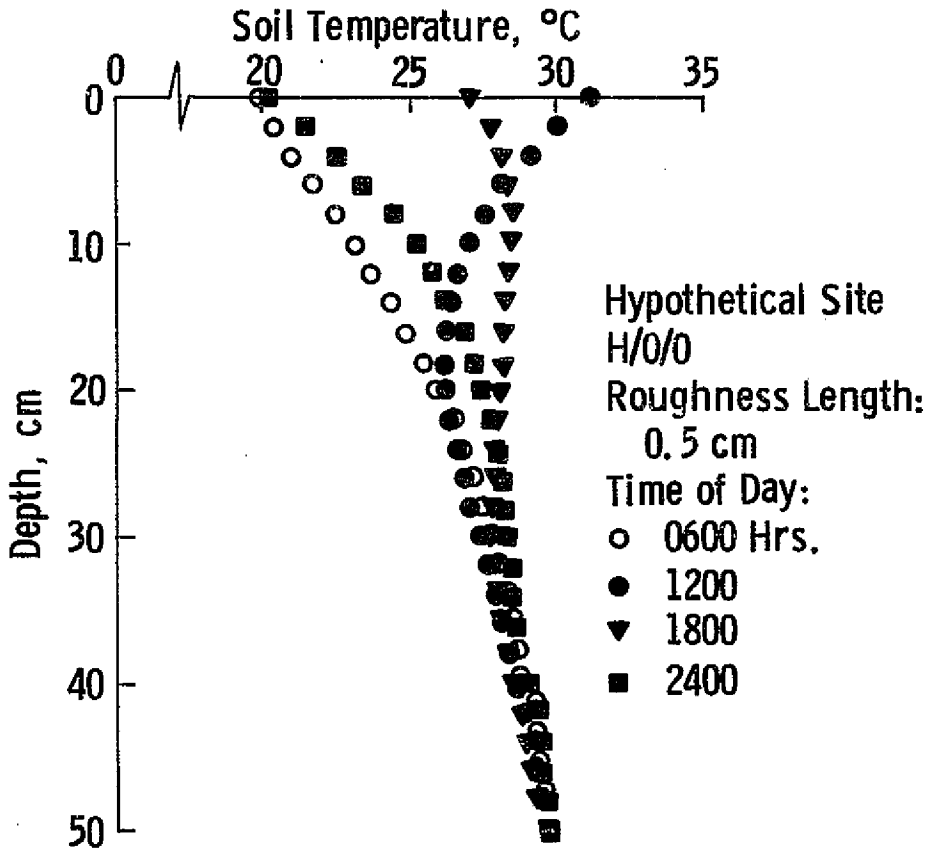

Figure 40. Temperature of a wet soil as a function of depth and time of day.

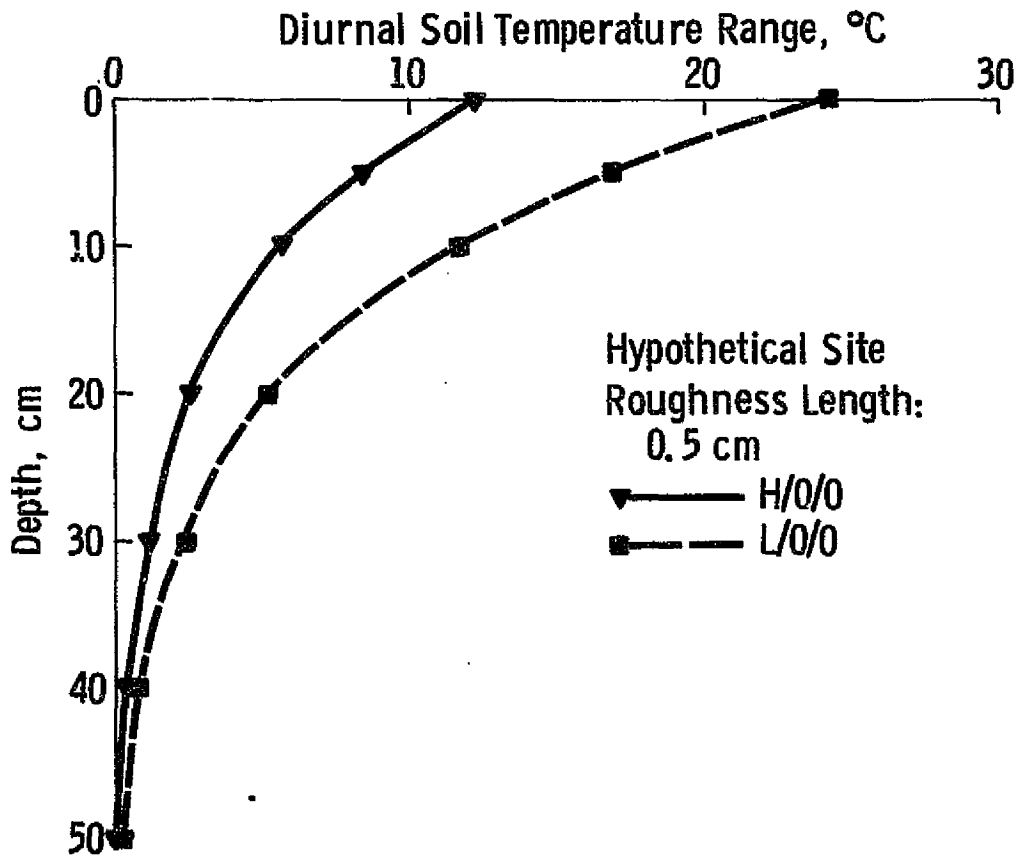

Figure 41. Diurnal range of soil temperature as a function of depth and soil water content.

surface temperature and magnitudes of the changes, it is apparent that it would be quite difficult and impractical to predict bare soil temperature for small parts of an extensive area. Such a prediction would be further complicated by variable cloud cover. However, the accuracy to which soil temperature should be known for microwave remote sensing of soil moisture is not obvious at this point; therefore, this question will be addressed again after the soil temperature data are analyzed in terms of the microwave signal in Chapter 4.

CHAPTER 4.

SOIL MOISTURE AND TEMPERATURE REGIMES AS A FACTOR IN MICROWAVE REMOTE SENSING OF SOIL WATER CONTENT

In the previous sections, the attention was focused on soil temperature and moisture regimes per se, without studying their implications regarding microwave remote sensing of soil moisture. Mathematical models were employed to illustrate major features of these regimes as well as to generate hypothetical sets of data. These models allowed examination of some features of the moisture and temperature regimes under relatively extreme conditions. In addition, actual measurements collected during various field moisture experiments were analyzed to examine particular aspects of the moisture regime. Results arrived at in the previous chapters can now be evaluated from the viewpoint of the microwave method of remote sensing of soil moisture. A microwave sensor designed for remote sensing of soil moisture would operate in active (radar) or passive (radiometer) mode and at specified frequency, incidence angle, and polarization. To render the analysis manageable, primary attention is given here to three frequencies (1.4 GHz, 4.0 GHz, 10.0 GHz; 1 GHz = 10^9 cycles/second), normal incidence (incidence angle 0°),and a passive system. The frequencies were chosen for two reasons. First, dielectric constant measurements were available at 1.3 GHz, 4.0 GHz, and 10.0 GHz (Cihlar and Ulaby, 1974). Secondly, the 1.4 to 10.0 GHz range encompasses most of the recent experimental studies (Ulaby, 1974; Ulaby et al., 1974; Batlivala and Cihlar, 1975; and Newton et al., 1974) and thus a microwave sensor for soil moisture sensing would likely cover one or more of the intermediate frequencies. The discussion is limited to normal incidence in order to simplify the analysis of polarization and angular effects. As shown in Chapter 1, the passive (radiometric) signal is directly influenced by both temperature and moisture of the soil; therefore, the passive mode was chosen here to illustrate the combined effects of the previously discussed soil moisture and temperature regimes. In addition, a limited comparison is made between power reflection coefficient (active case) and emissivity (passive case) values computed independently for identical soil moisture profiles, and the effect of soil temperatures on soil dielectric constant (and therefore directly on power reflection coefficient and emissivity) is illustrated for relatively extreme conditions. More extensive analysis

of the active case was limited by financial constraints as the power reflection coefficient computations were rather costly. It should be emphasized that although the above choice of mode or system parameters was made with the objective of accurately portraying the effects of soil moisture and temperature regimes on the microwave signal, the choice was arbitrary and not intended to imply optimum sensor design criteria.

The second problem addressed in this chapter was the possibility of estimating moisture content within the soil profile and over large geographical areas. The algorithm proposed in section 4.2 is based on the assumption that a microwave remote sensor is available which yields near-surface soil moisture information on a periodical basis. Again, the optimum sensor characteristics have not been dealt with here, as an entirely different approach to the latter problem would be required.

4.1 EFFECT OF SOIL MOISTURE AND TEMPERATURE REGIMES ON THE BRIGHTNESS TEMPERATURE

According to Equation (2), the radiometric temperature T_{ap} is a function of soil emissivity ϵ at a given frequency, physical soil temperature T_p, and of the radiation T_s emitted by the upper hemisphere; T_s consists of contributions by the galaxy (T_{gal}) and of the atmosphere (T_{atm}), respectively. Since the microwave energy measured by the radiometer is emitted at various depths in the soil prior to emerging above the surface, T_p and (Equation (2)) may be considered "effective" quantities describing the total soil effect on the microwave radiation. If T_p and ϵ are constant with depth, then they will be equal to these effective quantities and the brightness temperature T_{ap} can be readily determined. However, both moisture (and therefore emissivity) and temperature vary with depth. Therefore, in order to determine the effective T_p and ϵ values in this case, some kind of weighting as a function of depth must be employed.

Burke and Paris (1974) described a model based on radiation transfer theory which predicts brightness temperature over a bare soil. This model assumes that:

(i) soil consists of a number of layers with smooth parallel interfaces between adjacent layers;

(ii) radiation is incoherent;

(iii) there is no attenuation or emission between the surface and the sensor;

(iv) the sky brightness is isotropic; and

(v) dielectric properties are constant across any given layer of the soil.

If the soil consists of N layers (N^{th} layer has an infinite thickness), then brightness temperature immediately above the surface measured at a given frequency, polarization q and look angle θ is equal to

$$T_{bq}(\theta) = \sum_{i=1}^{N} T_{pi}\left(1 - \exp\left(-\gamma_i(\theta)\Delta z_i\right)\right)\left(1 + R_{q,i+1}(\theta)\exp\left(-\gamma_i(\theta)\Delta z_i\right)\right)$$

$$\cdot \prod_{j=1}^{i}\left(1 - R_{qj}(\theta)\right)\exp\left(-\sum_{\ell=2}^{i}\gamma_{\ell-1}(\theta)\Delta z_{\ell-1}\right), \qquad (20)$$

$$\gamma_i(\theta) = \frac{2\omega\alpha_{zi}(\theta)}{c},$$

$$\alpha_{zi} = \frac{k''}{2\beta_{zi}},$$

$$\beta_{zi} = \sqrt{\frac{\left(k_i' - \sin^2(\theta)\right)}{2}\left[1 + \sqrt{1 + \left\{\frac{k_i''}{k_i' - \sin^2(\theta)}\right\}^2}\right]},$$

where

Δz_i = thickness of the i^{th} layer, in cm;

$R_{qj}(\theta)$ = power reflection coefficient for a given polarization q, layer j, and look angle θ, dimensionless;

c = velocity of light, in cm/sec;

ω = angular frequency, Hz;

k' = real part of the relative dielectric constant, dimensionless;

k'' = imaginary part of the relative dielectric constant, dimensionless.

A computer program written to compute Equation (20) was provided for the present study.* The program was modified to fit data generated in Chapter 3 and expanded so that the following parameters could be calculated for each moisture/temperature profile combination:

$$\Delta T_{bqj}(\theta) = \frac{T_{bqj}(\theta)}{T_{bq}(\theta)} , \tag{21}$$

$$\Delta \epsilon_{qj}(\theta) = \frac{T_{bqj}(\theta)}{T_{pj}} , \tag{22}$$

$$\epsilon_q(\theta) = \sum_{j=1}^{N} \Delta \epsilon_{qj}(\theta) , \tag{23}$$

$$m_{eb} = \sum_{j=1}^{N} \frac{m_j T_{bqj}(0)}{T_{bq}(0)} , \tag{24}$$

$$m_{ea} = \sum_{j=1}^{N} \frac{m_j \Delta \epsilon_{qj}(0)}{\epsilon_q(0)} , \tag{25}$$

*Courtesy of Dr. W. J. Burke, National Research Council, Johnson Space Center, Houston, Texas.

where

T_{bq} = brightness temperature for polarization q immediately above the surface, in ^{o}K;

T_{bqj} = brightness temperature contribution of the j^{th} layer for polarization q when it emerges above the soil surface;

$\Delta\epsilon_{qj}$ = j^{th} layer contribution to the total emissivity ϵ_{qj}, dimensionless;

ϵ_q = total (i.e. "effective") emissivity of the soil, dimensionless;

m_{eb} = sum of moisture contents of individual layers weighted by the contribution of individual layers to the total brightness temperature, in cm^3/cm^3;

m_{ea} = sum of moisture contents of individual layers weighted by the contribution of each layer to the total emissivity, in cm^3/cm^3;

m_j = volumetric water content of the j^{th} layer, in cm^3/cm^3.

Reasons for defining two different measures of equivalent moisture will become obvious later. For the present, note that in the case of constant temperature and moisture profiles with depth, $m_{eb} = m_{ea}$.

Equations (20) through (25) were applied to soil moisture and temperature profiles computed in Chapter 3 for the following combinations:

time: 0000, 0600, 1200, 1800, 2400 hours;

moisture: high (H), low (L) water content;

surface configuration (slope/aspect): 0/0, 30/90, 30/-90;

frequency: 1.4 GHz, 4.0 GHz, 10.0 GHz.

Throughout section 4.1, it should be kept in mind that the moisture/temperature profile pairs were generated assuming a clear-sky day, around July 20, and for mid-latitudes. The above combinations therefore illustrate the diurnal (0000 to 2400 hrs) changes in moisture and temperature to be expected under these conditions for initially moist and initially dry soils, respectively. Tables 13 and 14 contain moisture and temperature profiles for H/0/0 and L/0/0 as the representative combinations. Dielectric constant values k' and k" were computed from polynomials (Table 12) based on data for loam provided by Cihlar and Ulaby (1974). The 1.3 GHz data given by Cihlar and Ulaby (1974) were considered representative of 1.4 GHz.

Table 12. Polynomial coefficients for computing the real and imaginary parts of the relative dielectric constant of a moist soil.*

Frequency (GHz)	Part	Coefficient			
		a_0	a_1	a_2	a_3
1.3	Real (k')	3.611374	7.45875	137.3191	-66.51187
	Imaginary (k")	-0.010487	7.11036	-12.07477	30.45856
4.0	Real	3.18690	-1.03203	163.3028	-89.56088
	Imaginary	0.112123	6.34419	18.2682	-18.18166
10.0	Real	2.38487	16.3802	83.2034	-94.9502
	Imaginary	0.23435	2.9045	63.4922	-68.01396

*the general equation is

$$k' \text{ or } k'' = a_0 + a_1 m + a_2 m^2 + a_3 m^3$$

where m = volumetric soil water content in cm^3/cm^3.

Temperature dependence of k' and k" was not taken into account since most of the experimental k' and k" data were obtained at 20°C. Values of $\Delta z_i = 2.0$ cm were used for 1.4 GHz and 4.0 GHz while computations at 10.0 GHz were made with $\Delta z_i = 1.0$ cm to achieve better depth resolution. Although calculations were made for look angles between 0° and 90°, only 0° results are discussed because here the effect of soil temperature and moisture on brightness temperature is most explicit. At this angle, brightness temperatures for horizontal (T_{bh}) and vertical (T_{bv}) polarizations are equal and will be subsequently referred to as $T_b(0)$. Furthermore, $\epsilon_q(0) = \epsilon(0) = \epsilon$, and $\Delta\epsilon_{qj}(0) = \Delta\epsilon_j$ in the following discussion.

Figure 42 shows diurnal $T_b(0)$ changes for H/0/0 and L/0/0 at three frequencies. The soil initially at field capacity (Figure 42A) exhibited rapid rise in the brightness temperature throughout the daytime but changes during the night were small. Since soil temperatures at 0000 and 2400 hrs. were very similar at all depths (Table 14), the rise in $T_b(0)$ must be attributed to moisture loss due to evaporation. The loss was small during nighttime (Table 13) which explains the low brightness temperature change. This statement is further supported by the L/0/0 data (Figure 42B) where the evaporation was lower and therefore $T_b(0)$ values at 0000 and 2400 were much closer. The brightness temperature dependence on moisture content implies that between 1800 and 2400, $T_b(0)$ should decrease more than Figure 42A indicates. This is because the layered evaporation model used for computing soil evaporation losses (Section 3.1) did not account for near-surface recharge due to capillary action during late afternoon and evening hours. According to data in Figure 15, near-surface moisture content at 2400 equalled approximately that at 1400. Consequently, if the recharge were accounted for, maximum $T_b(0)$ values for wet soil (Figure 42A) would be somewhat lower and $T_b(0)$ would probably decrease to about 215°K at 2400. This is also supported by Figure 42B which shows that when moisture content changed little during the 24 hr. period, the difference between brightness temperatures was also small. The three surface configurations (0/0,30/90,30/-90) affected brightness temperatures mainly during daytime. The maximum differences occurred at 1200 and were equal to 10.4°C (1.4 GHz), 11.1 °C (4.0 GHz) and 9.3°C (10.0 GHz), respectively. It should be noted that the maximum diurnal range of brightness temperatures (e.g., 38.9°K at 4.0 GHz, Figure 42A) was mainly due to high evaporation loss which in turn was affected by the roughness length used during temperature regime simulations

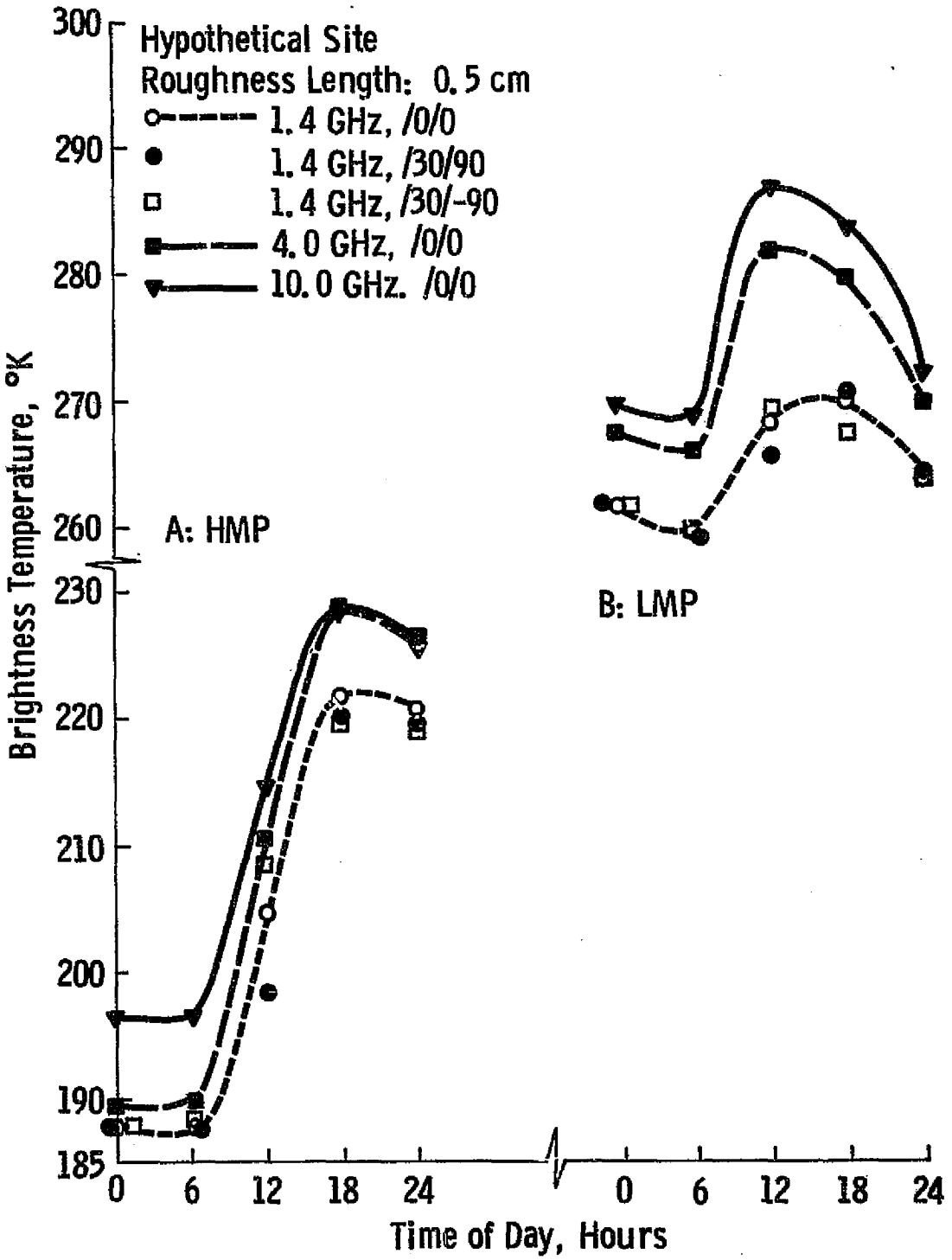

Figure 42. Diurnal changes of a bare soil brightness temperature for a wet (A) and a dry (B) soil at three frequencies and three surface configurations.

Table 13. Moisture contents for the hypothetical profiles at various depths and times of day.

Depth in cm	MOISTURE PROFILE									
	H/0/0					L/0/0				
	Moisture Content at Time (hours), in cm^3/cm^3									
	00	06	12	18	24	00	06	12	18	24
1	0.300	0.296	0.249	0.188	0.181	0.042	0.042	0.040	0.035	0.035
3	0.300	0.298	0.267	0.231	0.226	0.107	0.107	0.103	0.095	0.094
5	0.300	0.298	0.280	0.257	0.254	0.156	0.156	0.152	0.147	0.146
7	0.300	0.299	0.284	0.264	0.261	0.172	0.172	0.169	0.164	0.163
9	0.300	0.299	0.286	0.268	0.265	0.181	0.181	0.179	0.174	0.173
11	0.300	0.299	0.287	0.270	0.268	0.188	0.188	0.186	0.181	0.181
13	0.300	0.299	0.289	0.272	0.270	0.191	0.191	0.189	0.185	0.184
15	0.300	0.299	0.290	0.275	0.273	0.195	0.195	0.193	0.189	0.188
17	0.300	0.299	0.291	0.277	0.275	0.203	0.202	0.200	0.196	0.195
19	0.300	0.299	0.292	0.280	0.278	0.211	0.210	0.208	0.204	0.203
21	0.300	0.299	0.293	0.283	0.281	0.215	0.215	0.213	0.209	0.209
23	0.300	0.300	0.295	0.286	0.284	0.222	0.221	0.219	0.216	0.215
25	0.300	0.300	0.296	0.289	0.288	0.230	0.230	0.228	0.224	0.224
27	0.300	0.300	0.297	0.292	0.291	0.240	0.241	0.239	0.235	0.235
29	0.300	0.300	0.298	0.295	0.295	0.257	0.257	0.255	0.252	0.252
31+	0.300	0.300	0.299	0.299	0.298	0.278	0.277	0.277	0.276	0.275

(0.5 cm, section 3.2). Whether or not such a $T_b(0)$ range would occur under field conditions would to a considerable extent depend upon the evaporation loss.

The diurnal fluctuation of $T_b(0)$ for a dry soil (Figure 42B) was caused primarily by soil temperature changes. As a result, the maximum range $\Delta T_b(0)$ was higher at 10.0 GHz (20°K) than at 1.4 GHz (12°K); this reflects smaller soil temperature fluctuation at greater depths (Figure 41). As mentioned before, the 0000 hours and 2400 hours brightness temperatures were almost identical due to small moisture loss (and consequently small emissivity change) during that period. Surface configuration had less effect on $T_b(0)$ of dry soil.

The effect of soil moisture changes on the brightness temperature has been isolated in Figure 43 which shows total emissivity computed using Equations (22) and (23). Emissivity varied considerably during periods of large evaporation loss but remained approximately constant if soil moisture changed little; the latter condition existed when either atmospheric evaporative demand was low (nighttime, Figure 43A) or soil was dry (Figure 43B). As previously mentioned, the emissivity should decrease somewhat during evening hours; such a trend is not shown in Figure 43A. The difference between emissivities at individual frequencies for 0000 hours (Figure 43A) was caused by the frequency dependence of the dielectric properties of moist soil because soil moisture profiles were identical (Table 14). The same explanation may be used to account for the time trend of emissivity at 4.0 GHz (Figure 43A) which increased more during the 24-hour period than those at both 1.4 GHz and 10.0 GHz; as a consequence of this trend, brightness temperature at 4.0 GHz behaved the same way (Figure 42A).

If all other parameters in Equation (20) remained unchanged, the brightness temperature contribution from the j^{th} layer, ΔT_{bj} (0) (Equation (21)), would decrease with increasing frequency because the term $\exp(-\ _j(0)\ z_j)$ would decrease. This relationship is illustrated in Figure 44 for the 0-2 cm layer; contributions from 0-1 cm and 1-2 cm at 10.0 GHz were added. While for H/0/0 (Figure 44A) only 0.23 of $\Delta T_{bj}(0)$ was contributed from the 0-2 cm depth, the fraction was 0.75 at 4.0 GHz and 0.99 at 10.0 GHz (at 10.0 GHz, 0.947 was contributed by the 0-1 cm layer alone). As the soil dried out, contributions from 0-2 cm layers dropped at all three frequencies, but the maximum decrease occurred at 4.0 GHz. In contrast, although the dry soil $\Delta T_{bj}(0)$ contribution at 1.4 GHz decreased to one third of its value for wet soil (Figure 44A,B) the absolute change was much smaller (0.23 to 0.08). Consequently,

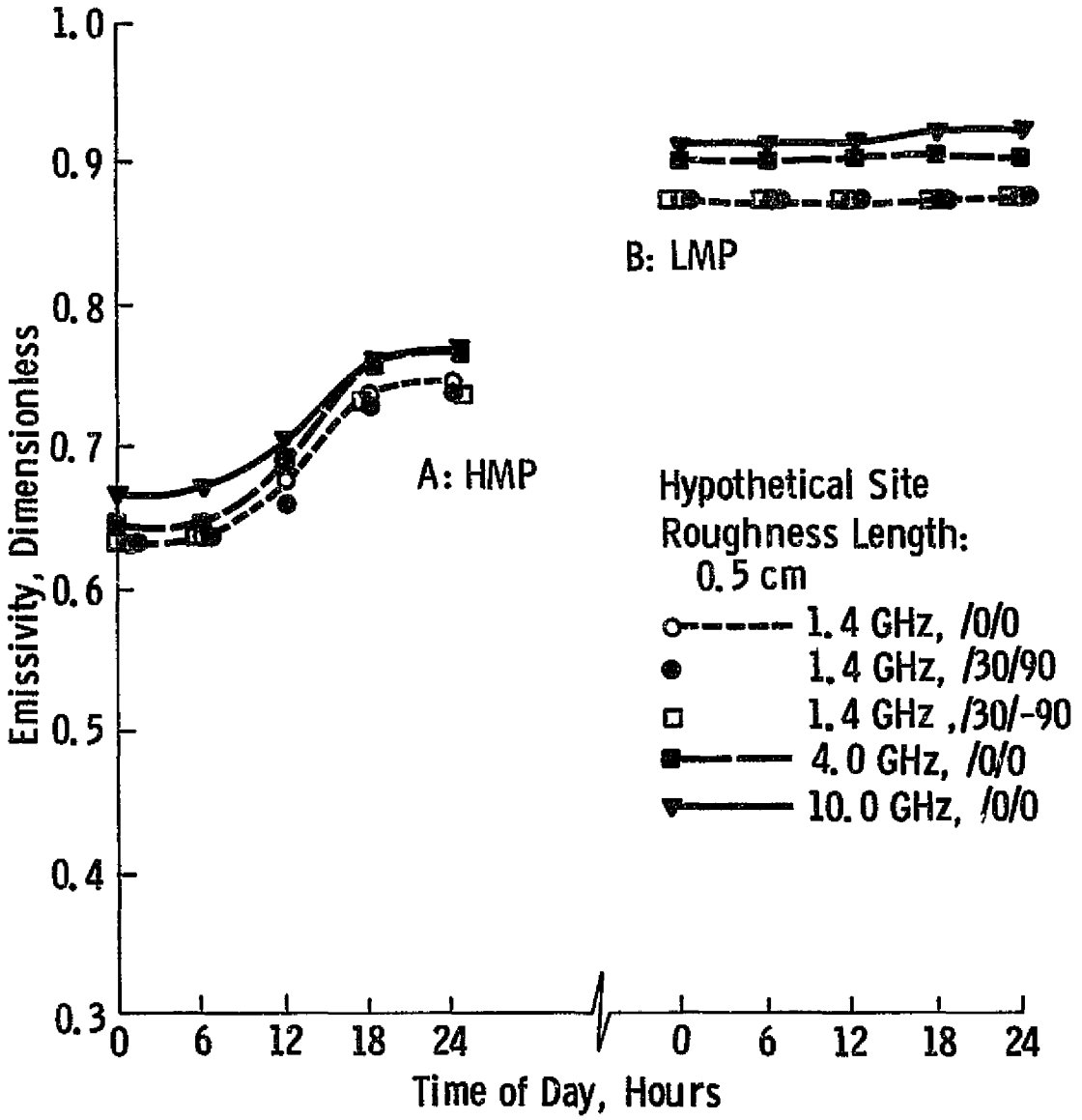

Figure 43. Diurnal changes of a bare soil emissivity for a wet (A) and a dry (B) soil at three frequencies and three surface configurations.

Table 14. Soil temperatures for the hypothetical profiles at various depths and times of day.

Depth in cm	Moisture Profile									
	H/0/0					L/0/0				
	Temperature at time (hours), in °C									
	00	06	12	18	24	00	06	12	18	24
0	20.5	19.9	31.1	27.0	20.2	20.0	19.9	42.3	33.5	20.2
1	21.0	20.1	30.6	27.3	20.8	20.9	20.2	40.9	34.1	21.2
3	22.0	20.7	29.5	27.9	21.9	22.7	21.0	38.4	35.2	23.1
5	23.8	21.4	28.7	28.2	22.9	24.4	21.9	36.1	35.7	24.7
7	24.5	22.1	27.9	28.4	23.9	25.9	22.9	34.2	35.7	26.2
9	25.2	22.7	27.3	28.5	24.7	27.2	23.9	32.6	35.5	27.4
11	25.9	23.4	26.9	28.4	25.4	28.3	24.8	31.4	35.1	28.5
13	26.3	24.1	26.5	28.4	25.9	29.4	25.7	30.4	34.6	29.4
15	26.8	24.6	26.3	28.2	26.4	30.0	26.5	29.7	34.0	30.1
17	27.1	25.2	26.2	28.1	26.9	30.5	27.3	29.2	33.4	30.6
19	27.4	25.7	26.2	28.0	27.2	31.0	27.9	29.0	32.9	31.0
21	27.7	26.1	26.3	28.0	27.5	31.2	28.5	28.8	32.9	31.3
23	27.9	26.6	26.5	27.9	27.7	31.4	29.0	28.8	31.9	31.4
25	28.1	26.9	26.7	27.9	27.9	31.5	29.5	28.9	31.6	31.5
27	28.3	27.3	26.9	27.9	28.1	31.6	29.8	29.1	31.2	31.6
29	28.4	27.6	27.2	28.0	28.3	31.6	30.2	29.3	31.0	31.6
31+	28.5	27.9	27.4	28.1	28.4	31.6	30.4	29.5	30.8	31.5

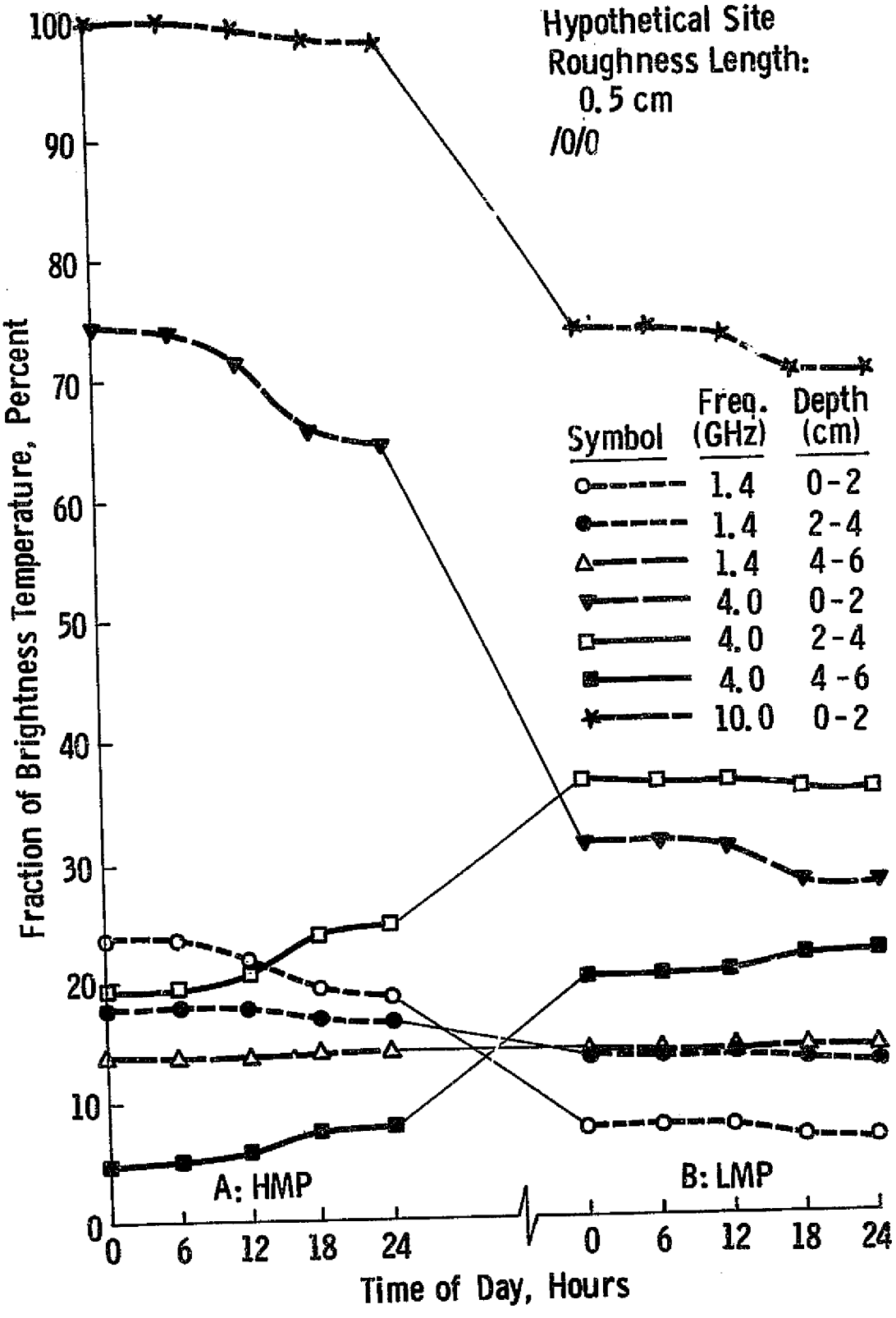

Figure 44. Fraction of brightness temperature contributed for a wet (A) and a dry (B) soil for various depths and frequencies as a function of time.

large moisture changes in the 0-2 cm layer would best be observed at 4.0 GHz (note that at 10.0 GHz, the 0-2 cm layer still contributed more than 0.7 of $T_b(0)$ when the soil was dry). In addition to the depth distribution of the contributions, this conclusion is supported by the brightness temperature change at 4.0 GHz. For wet soil (Figure 42A, 0000 hours), the $T_b(0)$ equalled that at the lower frequency, while in the case of dry soil (Figure 42B), $T_b(0)$ at 4.0 GHz was similar to that at 10.0 GHz. For deeper layers, trends became reversed as the soil dried out. This is illustrated in Figure 44 for 4-6 cm and 10-12 cm layers at 1.4 GHz. It is apparent that the $T_{bj}(0)$ trend for these layers was opposite to that for 0-2 cm, both diurnally and for a longer period: as the 0-2 cm contribution (and more generally that from shallower layers) decreased, that from the deeper layers increased.

The magnitude of $\Delta T_{bj}(0)$ as a function of depth is shown in Figure 45A for H/0/0. While the bulk of microwave energy was contributed by the 0-1 cm layer at 10.0 GHz and 0-4 cm layer at 4.0 GHz, contributions at 1.4 GHz diminished only gradually with depth, and some radiation traveled from depth(s) even below 32 cm. At all three frequencies, the contributions decreased asymptotically with depth. For a dry soil, however, the asymptotical decrease occurred at 10.0 GHz only, while at the lower frequencies the layer of maximum brightness temperature contribution shifted downward. This resulted in extending the "effective" depth of penetration at all frequencies.

It is interesting to note that the changes of $\Delta T_{bj}(0)$ due to soil drying depended on frequency. That is, the $\Delta T_{bj}(0)$ decrease for near-surface layers and consequent $\Delta T_{bj}(0)$ increase for the deeper layers were confined to a smaller total thickness of the soil at the higher frequencies; this resulted in smaller $\Delta T_{bj}(0)$ gradients with depth at the lower frequencies. For example, between H/0/0 and L/0/0, $\Delta T_{bj}(0)$ decreased for the 0-6 cm layers at 1.4 GHz, but only for 0-2 cm at 4.0 GHz, and for 0-1 cm at 10.0 GHz; beneath these layers, $\Delta T_{bj}(0)$ increased for depths 6-32+ cm (1.4 GHz), 2-14 cm (4.0 GHz), and 1-7 cm (10.0 GHz). However, the $\Delta T_{bj}(0)$ increases at greater depths were quite small (less than 0.02 at all depths for 1.4 GHz) and possibly negligible. This is shown in Table 15 using $T_{bj}(0)$ values for H/0/0 and L/0/0 at 1200 hours. Although the total brightness temperature changed by 65.1°K, only contributions from the top 4 cm shifted by more than 2%. Such a small change is apparently insufficient to appreciably affect the measured brightness temperature; consequently, only the moisture changes closer to the surface can be expected to have a marked effect on the measured $T_b(0)$.

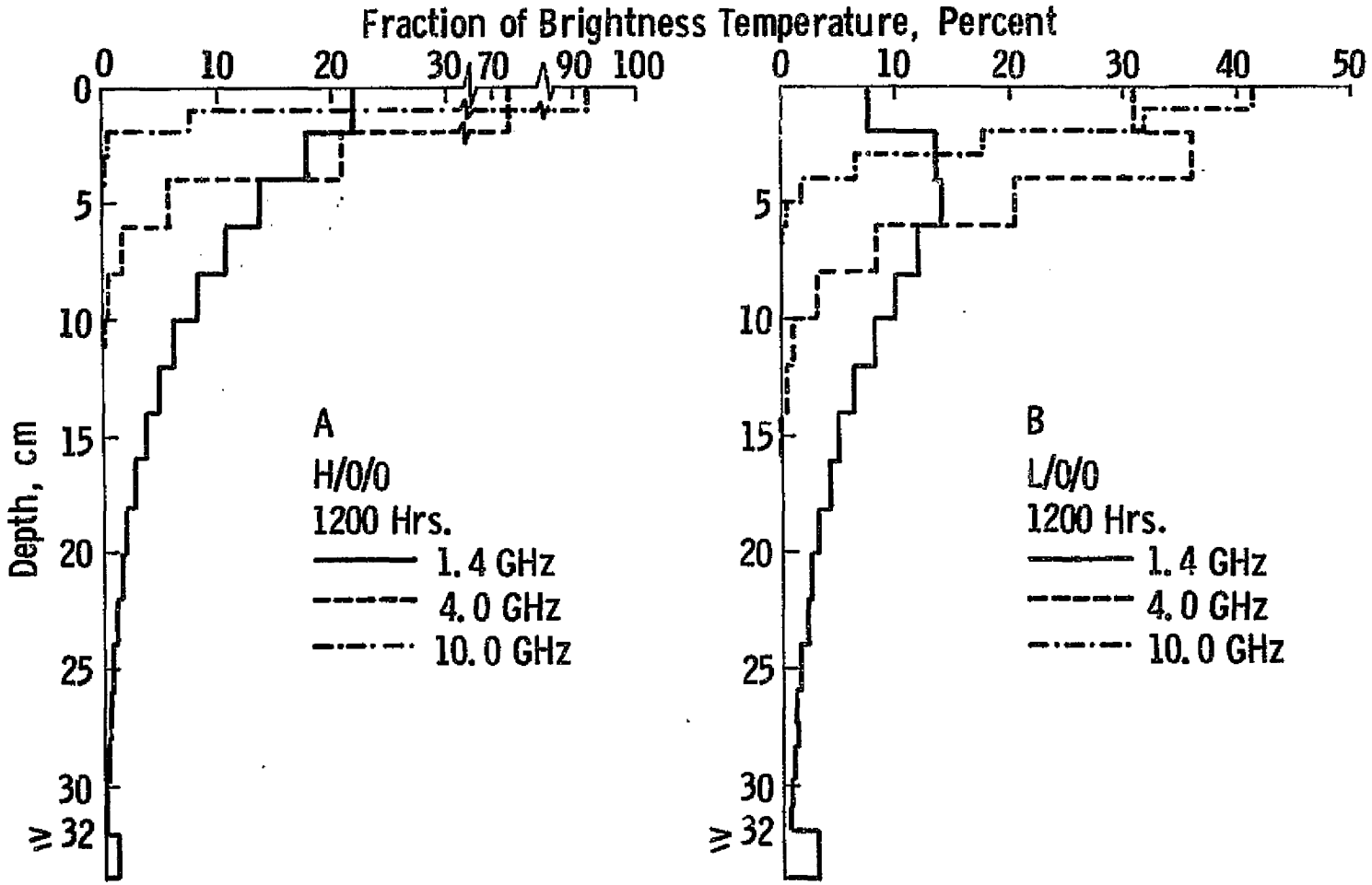

Figure 45. Fraction of brightness temperature contributed for a wet (A) and a dry (B) soil at three frequencies as a function of depth.

Table 15. Brightness temperature contributions for a wet and a dry moisture profile as a function of depth at 1.4 GHz, 1200 hrs.

Depth in cm	Brightness Temperature Contribution				
	$T_{bj}(0)$ (°K)		$T_{bj}(0)$ (dimensionless)		
	H/0/0	L/0/0	H/0/0	L/0/0	Difference H - L
(1)	(2)	(3)	(4)	(5)	(4-5)
0-2	44.7	20.2	0.219	0.075	0.144
2-4	36.0	36.6	0.176	0.136	0.040
4-6	28.6	37.6	0.140	0.140	0.000
6-8	22.1	32.2	0.108	0.120	-0.012
8-10	17.0	26.8	0.083	0.100	-0.017
10-12	13.1	22.0	0.064	0.082	-0.018
12-14	10.1	17.9	0.049	0.067	-0.018
14-16	7.7	14.5	0.038	0.054	-0.016
16-18	5.9	11.9	0.029	0.044	-0.015
18-20	4.5	9.7	0.022	0.036	-0.014
20-22	3.5	7.8	0.017	0.029	-0.012
22-24	2.7	6.3	0.013	0.024	-0.011
24-26	2.0	5.1	0.010	0.019	-0.009
26-28	1.6	4.1	0.008	0.015	-0.007
28-30	1.2	3.3	0.006	0.013	-0.007
30-32	0.9	2.8	0.004	0.010	-0.006
32+	2.9	9.2	0.014	0.036	-0.022
SUM	204.5	268.0	1.000	1.000	0.000

While soil moisture contents generally vary with depth, a radiometrically measured brightness temperature is an integrated, weighted expression of contributions from various depths (Equation (20)). There should exist, then, some single moisture value which could be considered representative of that part of the soil profile involved in generating the measured microwave radiation. From Equation (20) it would appear that for a given measured brightness temperature, the closest effective moisture estimate is one in which the moisture content of each layer m_j is weighted by the contribution of the j^{th} layer $T_{bj}(0)$ to the total brightness temperature, $T_b(0)$. Such a parameter was defined by Equation (24) and designated m_{eb}. Column 4 of Table 16 contains m_{eb} values for H/0/0 and L/0/0 at the three frequencies for 6-hour intervals during the diurnal cycle. As expected, these values (i) changed less than and (ii) were higher than near-surface moistures in all cases because of increasing moisture contents with depth (Table 13). Since m_{eb} values are affected by the current physical temperature of the soil, it is of interest to determine the extent of soil temperature influence on the effective soil moisture. This has been done by defining m_{ea} (Equation (25)) on the basis of emissivity contribution of the j^{th} layer $\Delta\epsilon_j$ to the total emissivity ϵ. The results, presented in column 5 of Table 16, indicate that there was little difference between m_j values calculated by the two methods; in fact, they differed in all cases by less than 0.40 % of the m_{ea} value (Table 16, column 7). The worst case was L/0/0, 4.0 GHz, and 1200 hours with a difference of 0.39%. In other words, the various soil temperature profiles had a negligible influence on the effective soil moisture computed for various conditions.

While useful in evaluating the effect of vertical temperature distribution on the weighting of contributions from individual layers, m_{ea} and m_{eb} do not seem to be the moisture contents which are most closely correlated to the computed brightness temperatures in the cases studied. Supporting evidence for this statement can be found in Figure 46 in which m_{ea} (Table 16, column 5) is plotted against ϵ (Table 16, column 6) for the three frequencies. At 1.4 GHz for example, the L/0/0 profile had emissivity of approximately 0.89 although its m_{ea} was equal to 0.17 cm^3/cm^3. Note that for a completely dry soil, $\epsilon = 0.91$ at this frequency. This means that while some water was present within the soil that contributed to the total computed brightness temperature, the moisture did not substantially affect the value of ϵ. Results for the remaining frequencies were similar, except the curves were shifted toward lower moisture contents (Figure 46). In other words, the profiles behaved radiometrically almost as if no water were present, although some water always was within the contributing depth.

Table 16. Equivalent moisture contents, emissivity, and the "brightness temperature" just below the surface for two profiles as a function of frequency and time of day.

Soil Profile	Frequency (GHz)	Time (hrs.)	Moisture (cm^3/cm^3)		Emissivity (dimensionless)	(4)-(5) (5) (%)	$T_b(0,1-)$ (^oK)	T_{p1} (^oK)
			$m_{eb}(0)$	$m_{ea}(0)$				
1	2	3	4	5	6	7	8	9
H/0/0	1.4	00	0.3000	0.3000	0.633	0.00	296.8	294.0
		06	0.2980	0.2980	0.637	0.00	295.1	293.1
		12	0.2749	0.2750	0.678	- 0.04	301.3	303.6
		18	0.2474	0.2474	0.737	0.00	300.2	300.3
		24	0.2442	0.2440	0.744	0.08	295.8	293.8
	4.0	00	0.3000	0.3000	0.644	0.00	294.4	294.0
		06	0.2965	0.2965	0.648	0.00	293.3	293.1
		12	0.2553	0.2554	0.694	- 0.04	303.2	303.6
		18	0.2057	0.2057	0.760	0.00	300.4	300.3
		24	0.2002	0.2001	0.768	0.05	294.2	293.8
	10.0	00	0.3000	0.3000	0.669	0.00	294.0	294.0.
		06	0.2961	0.2961	0.671	0.00	293.1	293.1
		12	0.2498	0.2498	0.707	0.00	303.6	303.6
		18	0.1916	0.1916	0.762	0.00	300.3	300.3
		24	0.1851	0.1851	0.768	0.00	293.9	293.8
L/0/0	1.4	00	0.1693	0.1687	0.872	0.36	296.6	293.9
		06	0.1691	0.1686	0.873	0.30	294.1	293.2
		12	0.1663	0.1669	0.875	- 0.36	303.3	313.9
		18	0.1638	0.1640	0.878	- 0.12	304.3	307.1
		24	0.1639	0.1634	0.878	0.31	297.2	294.2
	4.0	00	0.1052	0.1055	0.905	- 0.28	294.5	293.9
		06	0.1054	0.1052	0.905	0.19	292.7	293.2
		12	0.1029	0.1033	0.906	- 0.39	309.5	313.9
		18	0.1003	0.1002	0.908	0.10	306.6	307.1
		24	0.0999	0.0996	0.908	0.30	295.1	294.2

CONTINUED--

Table 16. Equivalent moisture contents, emissivity, and the "brightness temperature" just below the surface for two profiles as a function of frequency and time of day.

Soil Profile	Frequency (GHz)	Time (hrs.)	Moisture, in (cm^3/cm^3)		Emissivity (dimensionless)	$\frac{(4)-(5)}{(5)}$ (%)	$T_b(0,1-)$ (^oK)	T_{pl} (^oK)
			$m_{eb}(0)$	$m_{ea}(0)$				
1	2	3	4	5	6	7	8	9
L/0/0	10.0	00	0.0721	0.0720	0.915	0.14	294.3	293.9
		06	0.0720	0.0720	0.915	0.00	293.1	293.2
		12	0.0700	0.0700	0.917	0.00	312.2	313.9
		18	0.0660	0.0659	0.922	0.15	307.1	307.1
		24	0.0657	0.0656	0.922	0.15	294.7	294.2

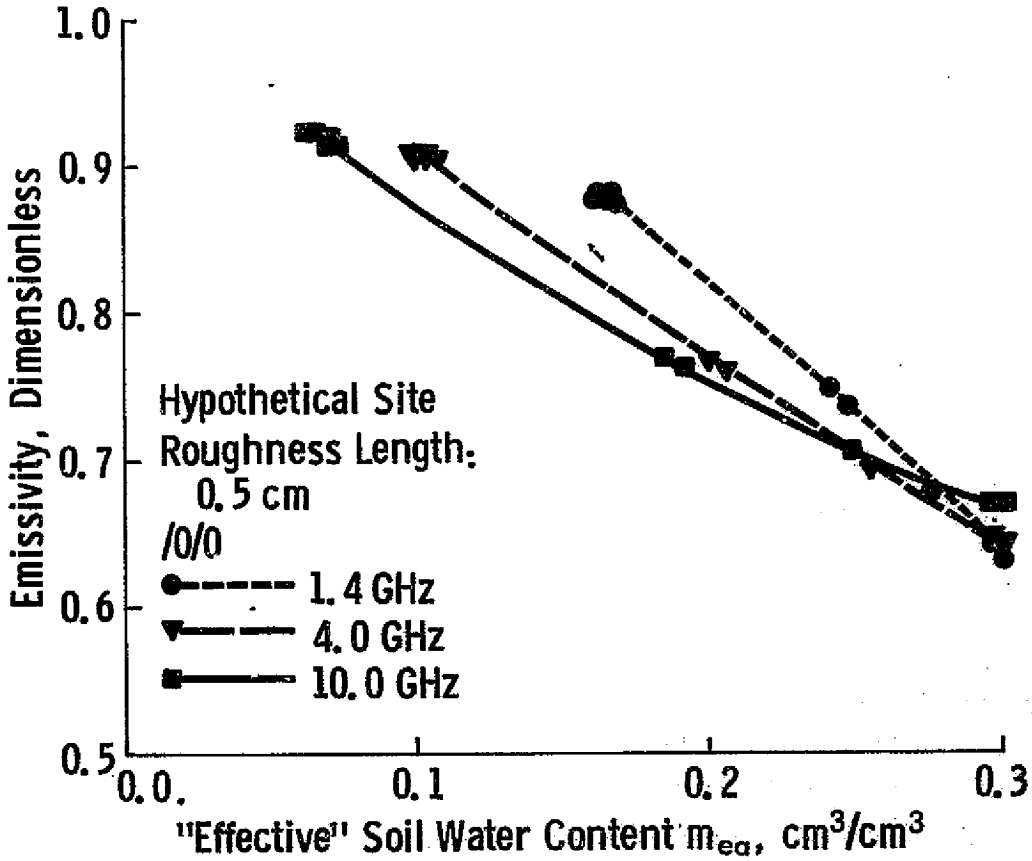

Figure 46. Bare soil emissivity as a function of an "effective" water content m_{ea}.

To help understand the above results, one can write Equation (20) assuming that the reflections at the interfaces between individual layers are negligible. In this case, the radiometric temperature which would be measured immediately below the air-soil interface at the normal incidence $T_b(0,1-)$ is equal to

$$T_b(0,1-) = \sum_{i=1}^{N} T_{pi}\left(1 - \exp\left(-\gamma_i(0)\Delta z_i\right)\right) \cdot \prod_{j=2}^{i} \exp\left(-\sum_{\ell=2}^{i} \gamma_{\ell-1}(0)\Delta z_{\ell-1}\right). \quad (26)$$

For the first three layers, (26) becomes

$$T_b(0,1-) = T_{p1} + (T_{p2} - T_{p1})\exp\left(-\gamma_1(0)\Delta z_1\right) + (T_{p3} - T_{p2}) \cdot \exp\left(-\gamma_1(0)\Delta z_1 - \gamma_2(0)\Delta z_2\right) \cdot T_{p3}\exp\left(-\gamma_1(0)\Delta z_1 - \gamma_2(0)\Delta z_2 - \gamma_3(0)\Delta z_3\right). \quad (27)$$

From (27) it is obvious that if soil temperature is constant with depth and if reflections between individual layers are negligible, the radiometric temperature which would be measured immediately below the soil-air interface is equal to the physical temperature of the first layer, T_{p1}. Secondly, if the reflections are negligible but soil temperature varies appreciably from layer to layer, $T_b(0,1-)$ will also be affected somewhat by T_p values and the moisture contents (due to the latter's influence on $\gamma(0)$) of the respective layers. Finally, if the interface reflections are not negligible, contributions from individual layers will be further modified by these reflections.

Values of radiometric temperature immediately below the air-soil interface $T_b(0,1-)$ were calculated at the three frequencies for H/0/0 and L/0/0. The results, given in Table 16 (column 8) show that especially for H/0/0, $T_b(0,1-)$ was indeed very close to T_{p1} (column 9 of Table 16). That is, internal soil reflections and temperature gradients were not important in this case. For the dry soil, larger differences

between $T_b(0, 1-)$ and T_{p1} occurred which can be attributed to the diurnal heat wave penetration into the soil. Nevertheless, an inspection of $T_b(0, 1-)$ and T_{p1} results in Table 16 reveals that the maximum difference between the two was about 4.4°K which represents only 0.02 of the commonly observed soil temperatures.

In terms of microwave remote sensing, $T_b(0, 1-)$ is not the value that is measured, however. As expressed by Equation (20), the measured value is $T_b(0)$ which is related to $T_b(0, 1-)$ as follows:

$$T_b(0) = T_b(0, 1-)(1 - R), \tag{28}$$

where R is the power reflection coefficient at the air-soil interface. For a plane smooth soil surface, the value of R is a function of dielectric properties of the soil which in turn depend primarily on soil moisture content (Chapter 1). The above results thus imply that under conditions where the brightness temperature model of Burke and Paris (1975) is valid and where soil moisture and temperature profiles are similar to those used here, it is only the soil moisture content at and near the soil surface which determines the brightness temperature measured by microwave radiometers. This also explains why the L/0/0 profile exhibited high emissivity although it contained an appreciable amount of water within the contributing soil profile section; the reason suggested by the above analysis was the low water content in the first soil layer (Table 13). It is noteworthy that in an experimental study of the relationship between soil moisture and radiometric temperatures measured by Skylab S194 radiometer (frequency 1.4 GHz), Eagleman and Ulaby (1974) also found that moisture in 0-2.5 cm (4 data sets) or 0-5.0 cm (1 data set) was most closely correlated to the microwave measurements. The above conclusion does not contradict the previous discussion of contributions from various subsurface layers (Figure 44, 45) because in the case of small temperature differences and small reflections between individual layers, the radiative energy transfer proceeds similarly as in a homogeneous medium.

In extrapolating the brightness temperature model predictions to natural conditions, it should be kept in mind that the model neglected surface and volume scattering. Since scattering is a form of reflection, the microwave energy can be scattered only if a change in dielectric properties exists between the media on the opposite sides of the scattering surface. To get an idea of the magnitude of scattering, consider inter-

faces between three media, namely air, dielectrically uniform soil with 0.05 cm^3/cm^3 moisture, and dielectrically uniform soil with 0.25 cm^3/cm^3 moisture content. Using coefficients in Table 12 to estimate k' and computing power reflection coefficient between media 1 and 2, R_{12}, from

$$R_{12} = \left\{ \frac{\sqrt{k_1'} - \sqrt{k_2'}}{\sqrt{k_1'} + \sqrt{k_2'}} \right\}^2$$

the following results can be obtained at 1.4 GHz:

Medium 1	Medium 2	R_{12}
air (assumed dry)	soil, 0.05 cm^3/cm^3	0.09
soil, 0.05 cm^3/cm^3	soil, 0.25 cm^3/cm^3	0.06
air (assumed dry)	soil, 0.25 cm^3/cm^3	0.31

Thus if soil is relatively dry (0.05 cm^3/cm^3) near the surface and below this layer moisture suddenly increases to 0.25 cm^3/cm^3, the second reflection (0.06) and therefore the higher moisture would have less impact on the microwave signal than the first one (0.09). An air-moist soil (0.25 cm^3/cm^3) interface would have a higher effect, however ($R_{12} = 0.31$). These considerations seem to suggest that subsurface scattering (and therefore the effect of subsurface moisture on microwave signal) will be higher for a soil consisting of more or less homogeneous clods separated by air voids; these clods should be larger than approximately one tenth of the wavelength measured in order for scattering to take place. On the other hand, in a relatively homogeneous soil (in terms of air-soil material distribution), even sudden large moisture changes do not seem to have a major effect on the microwave radiation ($R_{12} = 0.06$) and therefore their impact on the measured signal will be smaller.

It should also be noted that the assumed soil moisture change from 0.05 cm^3/cm^3 to 0.25 cm^3/cm^3 is unrealistically large compared to cases which might be encountered under field conditions. For example, the maximum moisture change with depth reported by Jackson (1973) for the July, 1970 experiment (average daily potential evaporation of 1.077 cm) was from 0.079 (depth 0-1 cm) to 0.168 cm^3/cm^3 (1-2 cm), or a change of approximately 0.09 cm^3/cm^3 compared to 0.20 cm^3/cm^3 used here. Furthermore, the radiation transfer in the soil proceeds continuously and not in discrete steps, and soil moisture also changes in a more or less continuous fashion with increasing depth; therefore, the chance of encountering a sudden moisture change appears relatively small.

If only the surface and near-surface moisture contents are of major importance in determining the microwave brightness temperature, then it follows that the soil surface temperature may be used as the representative soil temperature without generating appreciable errors. The passive microwave sensors could thus be supplemented with infrared radiometers to yield soil emissivities (computed from Equation (2)). This sensor combination was proposed by Poe et al. (1971). Consequently, predictions of soil temperature would not be necessary provided that physical soil temperature values can be isolated from the infrared measurements for areas corresponding to the microwave resolution cells.

Brightness temperature calculations discussed so far in section 4.1 were made with the assumption that dielectric properties of a moist soil depend on water content only. This is because the temperature dependence of the soil dielectric constant has not been studied experimentally, most laboratory measurements having been made at approximately 20°C. On the other hand, the dependence of the dielectric constant of water on temperature has been well established (Paris, 1969). To determine the order of magnitude for temperature effect on dielectric properties of a moist soil, the following procedure was used:

(i) Calculation of the ratio between dielectric constant of water at 5°C and 35°C and that at 20°C. This was done separately for k' and k'', at each frequency, and for salinities 0 °/oo, 10 °/oo, and 20 °/oo. To obtain the ratios for k' and k'' as a function of frequency and temperature, values for the different salinities were averaged.

(ii) Using these ratios and dielectric constant values of a moist loam (Cihlar and Ulaby, 1974), k' and k" for a given temperature (5°C or 50°C) were calculated by multiplying the measured values by the above ratio and the volumetric water content. In other words, the assumption was made that the change of the dielectric constant of a moist soil with temperature is solely due to the temperature dependence of the dielectric constant of the water portion. Except for possible ionic complex interactions, such an assumption appears justified since the dielectric properties of dry soil are practically constant with temperature (Cihlar and Ulaby, 1974).

(iii) Power reflection coefficient and emissivity were computed for soil profiles in which moisture was constant with depth (profiles between 0.00 cm^3/cm^3 and 0.35 cm^3/cm^3) and temperature was also constant (either 5°C or 50°C).

Figure 47 shows the results at three frequencies; all 5°C data are joined by curves. Apart from the frequency dependence, these data also show a systematic effect of temperature on power reflection coefficient and emissivity: at all three frequencies, the power reflection coefficient decreased with increasing frequency, particularly at higher moisture content. The maximum difference (0.007) corresponds to a moisture content difference of approximately 0.010 cm^3/cm^3. Considering the relatively extreme soil temperatures which this moisture differential represents, it would appear that the temperature effect on the soil dielectric properties could be neglected in an algorithm designed to extract soil moisture information from microwave measurements without introducing appreciable errors.

As stated in section 4.1, calculations of brightness temperatures $T_b(0)$ (and therefore effective emissivities $\epsilon(0)$) were made for incoherent radiation. Active sensors transmit a coherent beam, however, and the question thus arises whether the same relation between power reflection coefficient R and emissivity ϵ, $\epsilon = 1 - R$, is valid for both coherent and incoherent radiation. To answer this question, power reflection coefficients were calculated for 11 soil moisture profiles in two ways:

(i) $R = 1 - \epsilon$

where $\epsilon = \epsilon(0)$ from the brightness temperature model (Equation (23)).

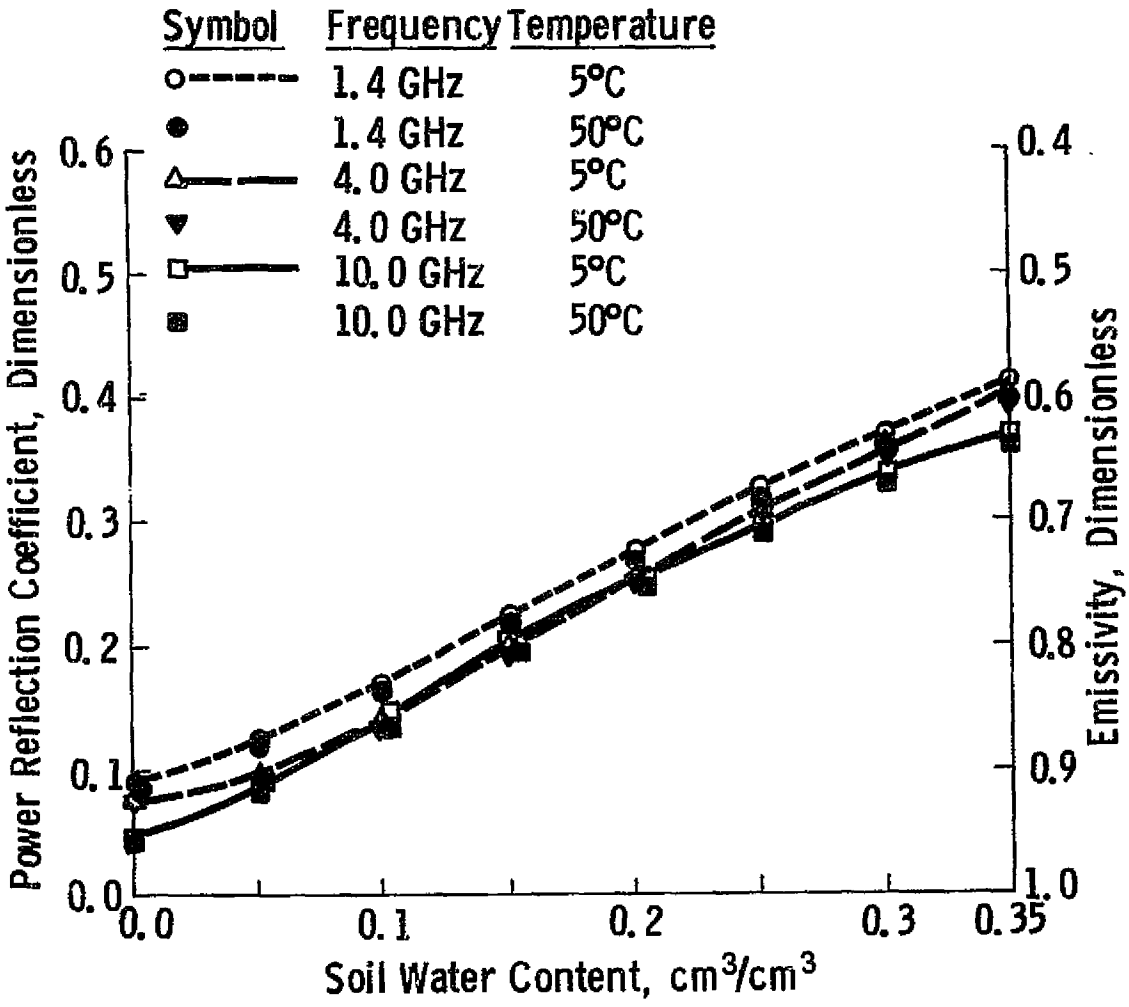

Figure 47. Power reflection coefficient and emissivity as a function of soil water content and soil temperature.

(ii) $R = \rho^2$

Values of ρ were calculated* by a method outlined by Casey (1973) in which the second-order linear differential equations describing the electromagnetic field behavior in the vertical direction within the soil are solved in terms of Hill's functions.

A comparison of results obtained by the two methods is given in Table 17. The two power reflection coefficients are almost identical at higher frequencies and high moisture contents, but the agreement is also very close at 1.4 GHz if the moisture content is high. Greatest discrepancies occurred at 1.4 GHz when moisture content was low. The discrepancy between power reflection coefficients computed for coherent and incoherent radiation thus appeared to increase with increasing depth of penetration or vertical nonuniformity of soil moisture contents (see Table 13) or both. This agreement also suggests that under conditions when the assumptions of the plane interface, multi-layer, nonscattering soil material are valid, the return of coherent active microwave signal will be determined by the surface and near surface moisture content, similarly as was the case with brightness temperature. In addition, the discussion of diurnal variation of emissivity may be directly extrapolated to power reflection coefficient.

4.2 SOIL MOISTURE CONTENT DETERMINATION OVER LARGE AREAS

The following discussion is based on two premises. First, soil water content should be specified in volumetric units in order to provide usable information, be it equivalent depth (in cm), amount of water per unit soil volume (in cm^3/cm^3), or some other parameter. Secondly, the soil moisture results should be location-specific to be of maximum benefit to the user. While the first premise rests on the fact that water is involved in various processes and environments as quantities, the second assumption appears justified by the growing environmental concern about conditions at specific locations (Holtan and Lopez, 1970), as well as economics of land use of particular areas (such as fields).

Results of the previous section and consideration of the effect of moisture on the electromagnetic radiation propagation suggest that microwave remote sensors may

*Calculations were made by Dr.K.F. Casey, Department of Electrical Engineering, Kansas State University, Manhattan, Kansas.

Figure 17. Comparison of power reflection coefficients calculated for coherent and incoherent radiation.

Moisture Profile	Time	Frequency (GHz)					
		1.4		4.0		10.0	
		C*	I*	C	I	C	I
H/0/0	06	0.364	0.363	0.349	0.352	0.327	0.329
H/0/0	12	0.306	0.322	0.299	0.306	0.290	0.293
H/0/0	18	0.250	0.262	0.230	0.240	0.233	0.238
H/0/0	24	0.246	0.256	0.223	0.232	0.226	0.232
H/30/0	18	0.251	0.264	0.232	0.241	0.234	0.242
H/30/90	18	0.256	0.269	0.239	0.249	0.241	0.248
H/30/-90	18	0.255	0.267	0.237	0.246	0.239	0.246
L/30/-90	06	0.073	0.118	0.053	0.082	0.047	0.069
L/30/-90	12	0.072	0.113	0.050	0.078	N.A.	0.069
L/30/-90	18	0.072	0.109	0.047	0.074	N.A.	0.060
L/30/-90	24	0.072	0.109	0.048	0.074	N.A.	0.060

*Note C = coherent case I = incoherent case

provide soil moisture information about the soil surface and near subsurface layers unless the soil material appears geometrically or dielectrically rough relative to the wavelength measured. Since various types of land use and management are concerned with deeper layers as well(e.g. profile thickness of 100 to 200 cm), it follows that a microwave remote sensing technique of soil moisture estimation would have to become a part of a larger system involving other inputs. Following is a discussion of a possible algorithm of which the objective is providing site-specific profile soil moisture content information during frost-free periods over areas with agriculture as the main land use category.

The total area of interest is divided into a number of small cells i of equal size, thus forming an equal area grid system (Tomlinson, 1972). The maximum cell size must be smaller than the smallest area element the soil water content of which is needed and larger than the minimum resolution cell size of the microwave sensor. The algorithm is based on the soil water balance equation (Equation (4),(7)) which, in the absence of irrigation and after $(F_i - F_o)$ is replaced by $-(R+D)$, may be written as

$$S(t+\Delta t) = S(t) + P(\Delta t) - R(\Delta t) - AE(\Delta t) - D(\Delta t), \qquad (29)$$

where R = surface runoff. To implement Equation (29) in a site-specific algorithm, the following information is needed for each area element i and time increment Δt: precipitation, runoff, actual evaporation or actual evapotranspiration, and drainage below the terminal depth of the profile. If the remote sensing mission takes place every other day, $\Delta t = 2$, and the remaining necessary parameters may be obtained for the period of Δt as follows.

Precipitation

Precipitation amounts P (Δt)and duration PD can be acquired from meteorological stations as values representative of the cells in which they are located. Point-rainfall extrapolation methods (Hutchinson and Walley, 1972; Chidley and Keys, 1970; Unwinn, 1969) can then be used to obtain areal rainfall. As mentioned in Chapter 2, however, precipitation patterns vary considerably even at short distances, and areal rainfall may be far from representative for specific locations. To solve this problem, microwave sensors can be used for determining the actual precipitation patterns over the entire area. Thus, the actual precipitation for the cell i can be considered a) equal to the areal rainfall computed above if the microwave remote sensing data show that cell i received precipitation, b) equal to zero otherwise.

Runoff

Runoff can be computed as the difference between precipitation intensity and infiltration capacity. If the infiltration capacity is calculated by Holtan's (1970) formula, runoff R(Δt) for cell i and precipitation (P(Δt)), is equal to

$$R(\Delta t) = P(\Delta t) - PD\left(f_c + a S_a^{1.4} \right), \qquad (30)$$

where

a = infiltration capacity in inches/hour/(inch) $^{1.4}$ of available storage;

S_a = available storage in the surface layer ("A" horizon in agricultural soils) in inches of equivalent water layer;

f_c = constant rate of infiltration after prolonged wetting in inches/hour.

Values of a were given by Holtan et al. (1974) for various crop types and those of f_c by Musgrave (1955) for different soil hydrologic classes. Considering possible multiple precipitation events as one will not result in large errors because of $\Delta t = 2$ (Richards and Strahl, 1969). The runoff R(Δt) can be either routed to the channel (Holtan et al., 1974) or simply ignored; the former strategy would help to account for that

part of R(Δt) which enters the soil prior to its reaching the channel. At this point, the actual amount that entered the soil, $P_{eff}(\Delta t)$, can be calculated for each cell i as

$$P_{eff}(\Delta t) = P(\Delta t) - R(\Delta t) . \tag{31}$$

Actual Evaporation or Evapotranspiration

Various methods can be used to compute actual evaporation (section 2.1). Holtan et al. (1974) described a technique for evapotranspiration estimation which is based on pan-evaporation data, growth index, and soil moisture status.

Drainage

The drainage component D(Δt) can be estimated with the assumption that only a certain maximum amount of water, S_p, can be retained for extended periods of time (section 2.3). Results in section 2.3 also suggest that D(Δt) may be considered negligible if the soil storage capacity S_p is not exceeded. Consequently, drainage can be determined as

$$\begin{aligned} D(\Delta t) &= 0 \quad \text{if} \quad P_{eff}(\Delta t) \leq S_p - S(t) \\ &= P_{eff}(\Delta t) + S(t) - S_p \quad \text{otherwise.} \end{aligned} \tag{32}$$

A more refined approach to computing D(Δt) would consist of combining Equations (32) and (30).

The values of P, R, AE, and D must be determined for each cell i and period Δt. Then, given the initial soil moisture storage S(t), the amount of water stored at time $(t + \Delta t)$ can be computed from Equation (29). Figure 48 is a flowchart of the sequence of computations for one Δt period.

The procedure described above would yield one moisture storage value for the entire soil profile. As pointed out in Chapter 2, however, it is preferrable to subdivide

N = Number of cells
M = Number of cells with meteorological data available
P = Precipitation amount
PD = Precipitation duration
MET = Meteorological variables
R = Runoff
PRS = Precipitation pattern from microwave sensors
AE = Actual evaporation (evapotranspiration)
D = Drainage below the terminal depth of the soil profile

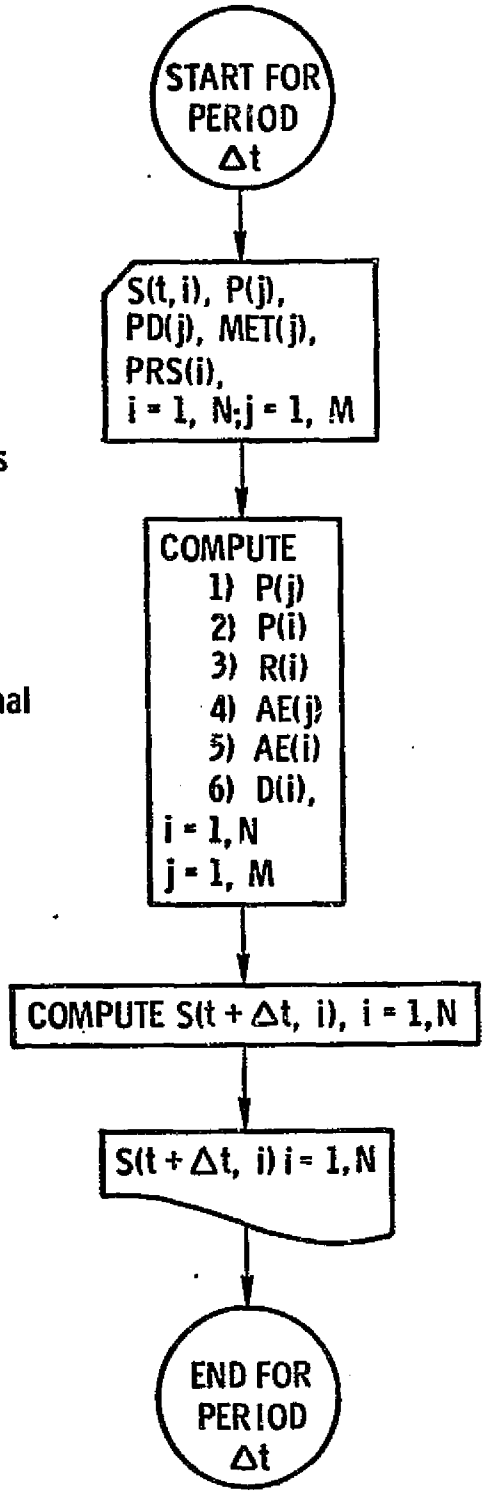

Figure 48. Flowchart of an algorithm for large area monitoring of soil water content.

the profile into zones and monitor moisture changes for each zone separately. For a bare soil, the two zones model used in Chapter 2 can be used with the upper zone divided into layers as thin as 1 cm if such resolution is warranted; the lower zone would comprise the remainder of the profile (section 2.4). In the case of vegetated areas, the layered model of Baier et al. (1972) would be more appropriate because it allows for changing root structure of the plants. In the multi-layer case, drainage from one layer can be regarded as input into the layer immediately below.

To implement the above algorithm for monitoring soil water content, the following data would be needed:

a) Time - invariant parameters:
   - Hydrological soil group to determine f_c (Equation (30)).
   - Storage capacities of individual zones within the soil profile; these could be obtained from soil survey reports.

b) Time - varying parameters:
   - Land use (crop type), to be specified for longer periods (e.g., a season).
   - Precipitation amounts, durations, and meteorological variables needed for AE (t) calculations.

The above described algorithm would allow combining advantages of various methods of soil moisture estimation useful for large areas (section 1.1) while avoiding their drawbacks. Furthermore, it would employ data readily available in many areas. It should be noted that various hydrological models (Knapp, 1973; Staff, Hydrological Research Laboratory, 1972; Holtan et al., 1974) approach soil moisture accounting in a way similar to that used here. The difference is that soil moisture was the only output parameter required which allowed simultaneous simplification and expansion compared to the other models.

CHAPTER 5.

MICROWAVE RESPONSE TO SOIL MOISTURE: A REVIEW OF EXPERIMENTAL MEASUREMENTS

As stated in Chapter 1, the concept of soil moisture estimation from remote microwave sensor measurements is based on the microwave signal response to the presence of water in the soil. This phenomenon has been demonstrated in Chapter 1 (Figure 2) and Chapter 4 by applying simplified theoretical solutions to vertical soil temperature and/or moisture profiles which were either constant with depth or computed from empirical models. In order to investigate the role of moisture and temperature regimes in microwave remote sensing of soil moisture, only the intrinsic relationships between microwave reflection (and emission) and soil moisture content were considered. Under natural conditions, however, other target parameters also affect the scattering and emission properties of the surface; namely, roughness and vegetation cover.

The difficulty involved in relating some of the statistical parameters used in theoretical scattering and emission models to easily specifiable target parameters has led investigators to construct empirical models based on experimental data. One of the major objectives of microwave remote sensing of soil moisture programs is to establish sensor parameters (frequency, polarization and angle of incidence range) for which the effects of target characteristics other than soil moisture are at a minimum. The objective of this chapter is to present a summary of active and passive microwave measurement programs in remote sensing of soil moisture. The presentation is divided into sections according to platform (ground, airborne, spaceborne) and each section is divided into active and passive observations.

5.1 GROUND BASED PLATFORMS

5.1.1 Active Microwave Observations

Backscatter data acquired by a truck mounted Active Microwave Spectrometer over the 4-8 GHz frequency region were reported by Ulaby (1974) for a bare field.

The soil type was Pawnee clay loam and the surface was slightly rough (2.5 cm rms height). With soil moisture represented by the average gravimetric moisture content in the top 5 cm of the soil, $m_w(0,5)$*, the backscattering coefficient σ^o showed a linear increase with soil moisture after the latter quantity had exceeded 15%; no change in σ^o was observed for moisture contents below 15%.

In an attempt to provide a more representative value for soil moisture, Ulaby et al. (1974) computed an "effective" moisture content, $m_v(0,\delta)$ in grams per cm^3, where $m_v(0,\delta)$ was defined as the average moisture content within the skin depth δ. Plots of σ^o as a function of $m_w(0,5)$ and $m_v(0,\delta)$ are shown in Figures 49 and 50, respectively. With this new approach for defining moisture content, σ^o indicates a linear response over the entire range of $m_v(0,\delta)$. The radar signal change with soil moisture was highest at low incidence angles (Figure 50) and the highest frequency (7.1 GHz) and decreased as the incidence angle increased from 0° to 70° and as frequency decreased from 7.1 GHz to 4.7 GHz. These trends were quantified in terms of sensitivity, defined as the change in scattering coefficient resulting from a change in $m_v(0,\delta)$ of 0.01 g/cm^3 (Figure 51). The various frequency/polarization combinations exhibited an approximately equal sensitivity at 20° incidence angle for the Pawnee clay loam data.

Because of the range of roughness characteristics that exist under field conditions, the most reliable method for determining the effect of roughness on the sensitivity of microwave sensors to soil moisture variations is by analysis of experimental data. During the summer of 1974, σ^o data were acquired for each of three bare fields having identical soil type but different scales of surface roughness (Batlivala and Ulaby, 1975). The three fields, which for identification purposes will be referred to as smooth, medium rough and rough, had rms surface heights of 0.88 cm, 2.6 cm and 4.3 cm respectively. Simultaneous with the radar measurements, passive radiometric measurements were also acquired by Texas A&M University. Analysis of the passive data, however, has not yet been completed. The active microwave measurements were conducted at 8 frequencies between 2 and 8 GHz, for all linear polarization configurations at angles of incidence between nadir and 40° (in 10° increments).

---

* In Chapter 5, the parameter used to describe soil water content is $m_a(b,c)$, where a is w (moisture in % by weight) or v (moisture in g/cm^3), and b and c represent upper and lower depths of the layer represented (in cm).

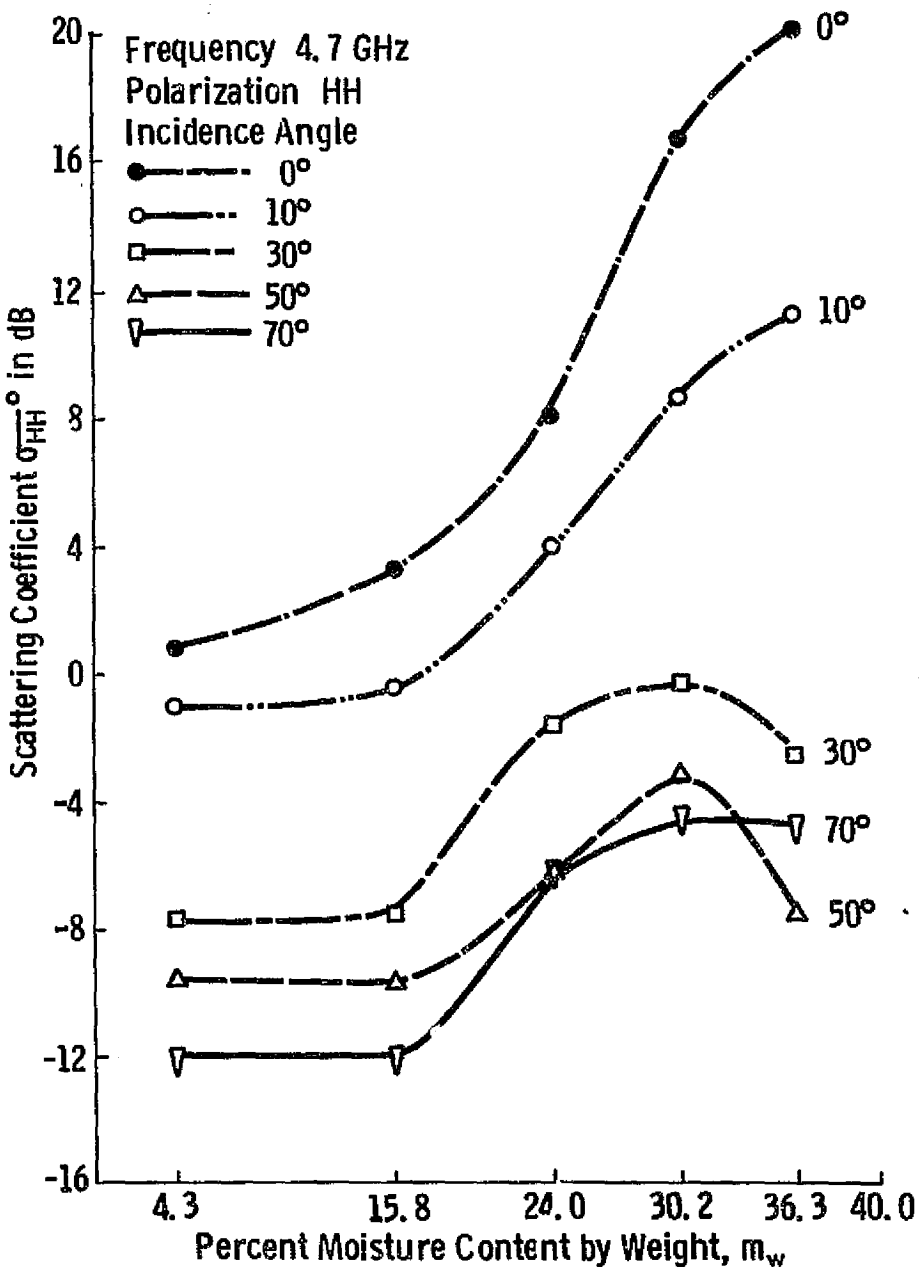

Figure 49. Scattering coefficient as a function of moisture content in the top 5 cm. Frequency is 4.7 GHz.

From Ulaby, Cihlar and Moore (1974)

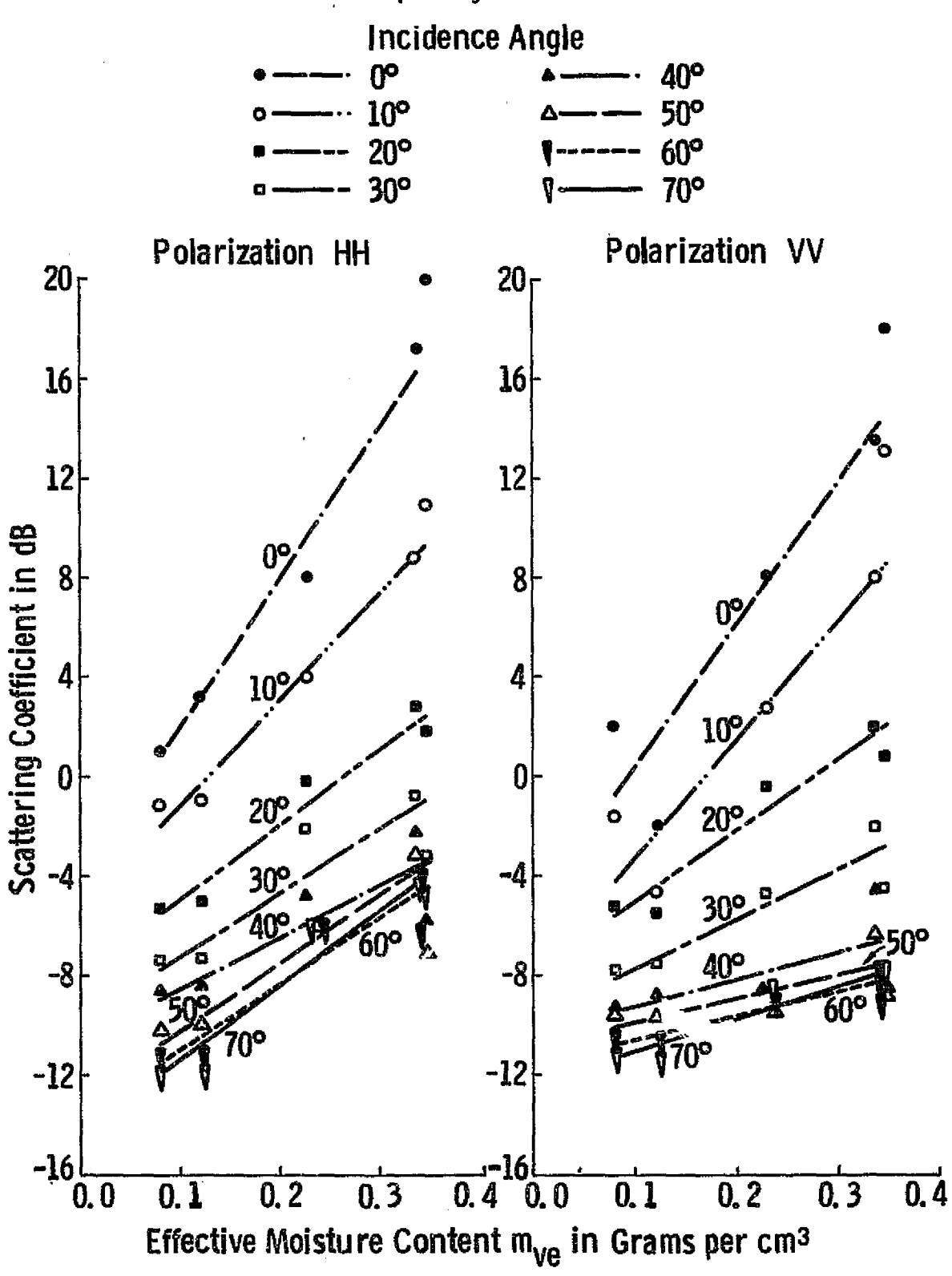

Figure 50. Scattering coefficient as a function of effective moisture content. Frequency is 4.7 GHz.

From Ulaby, Cihlar and Moore (1974).

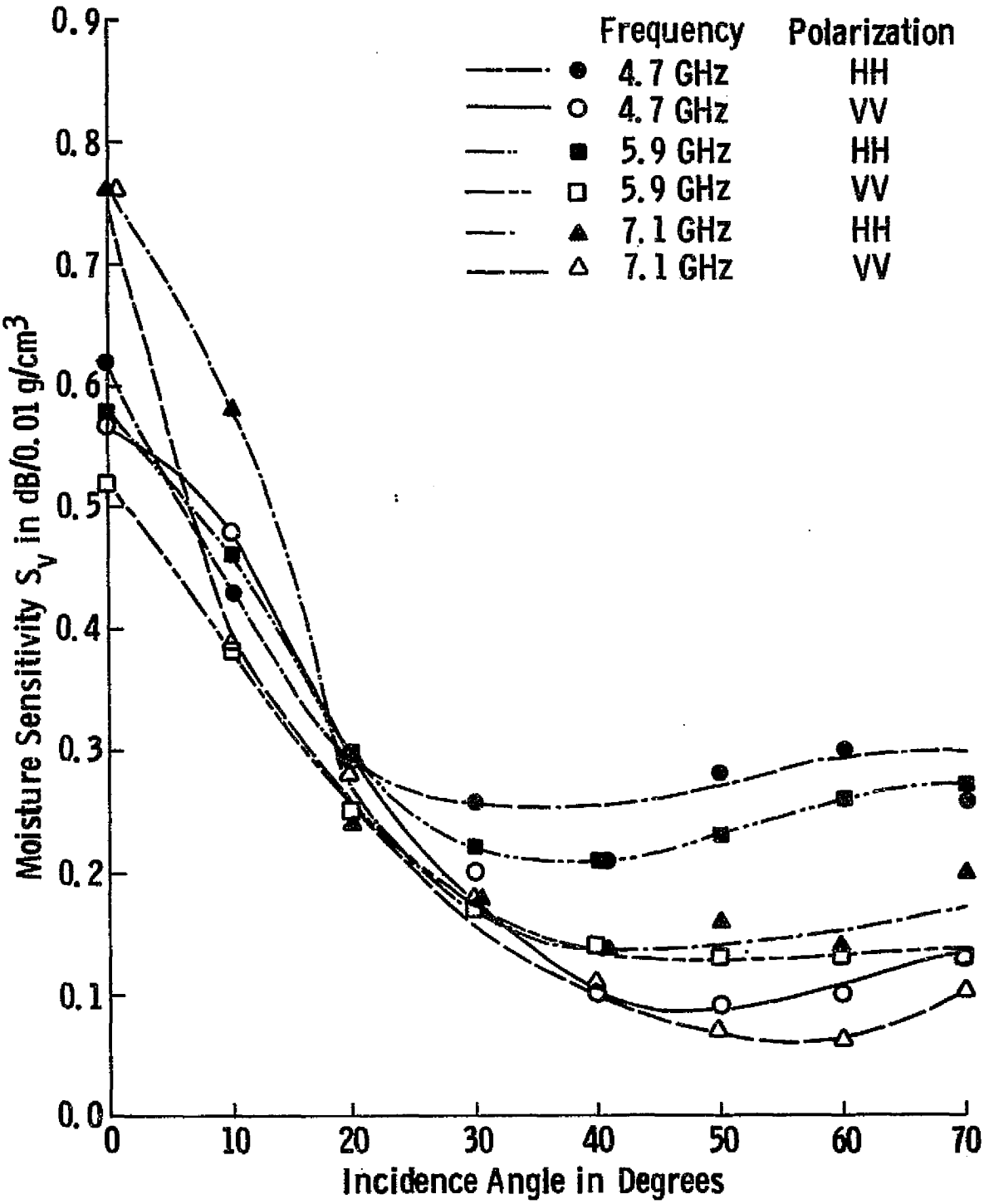

Figure 51. Moisture sensitivity S_V as a function of incidence angle.

From Ulaby, Cihlar and Moore (1974).

After acquiring radar data with the fields dry, the three fields were sprinkled with water until saturation. Each of the fields was then periodically monitored with active microwave measurements and ground truth equipment as the soil dried up.

Figure 52 is a time plot of moisture content and σ^o at nadir, 10^o and 20^o for VV polarization at 2.75 GHz. The data are for the medium rough field. Based on moisture samples acquired at 8 sampling sites on the field, the mean and standard deviation of the moisture content were calculated; the moisture interval shown in Figure 52 represents the mean $\pm$ standard deviation. The large uncertainty in soil moisture content, represented by the width of this interval, illustrates the difficulty in correlating σ^o with moisture content. The uncertainty in $m_v(0, \delta)$ is attributed in part to the difficulty in sampling thin layers of soil and in part to the spatial variation of moisture content across a field.

Comparison of σ^o to $m_v(0, \delta)$ shows good correlation at all angles. Similar results are obtained at other frequencies and polarizations for each of the three fields individually. To demonstrate the effect of surface roughness, Figure 53 shows the angular response of σ^o for the three fields at approximately the same moisture content. Whereas the smooth field at 2.75 GHz shows a drop of about 23 dB between nadir and 10^o, the rough field, on the other extreme, shows less than 1 dB change. The interesting observation in Figure 53 is that at each of the three frequencies shown, a narrow range in angle of incidence exists for which the effect of roughness is at a minimum; at 5.25 GHz 10^o appears as a crossover point and at 7.25 GHz, 20^o is the crossover point. Application of this phenomenon is shown in Figure 54 where σ^o is plotted as a function of $m_v(0, \delta)$ for all three fields combined. The frequency is 4.75 GHz, the angle of incidence is 10^o and the polarization is VV. Even with the uncertainty associated with the values of $m_v(0, \delta)$, the correlation coefficient is 0.69.

Vegetation cover hinders the microwave remote sensing of soil moisture. In addition to attenuating the backscattered or emitted soil radiation, the vegetation canopy adds its own contribution to the radiation measured by the radar or radiometer. The degree to which vegetation affects the capabilities of microwave sensors in soil moisture content determination is a function of plant geometry and the dielectric properties of the canopy volume, both of which are related to plant type, stage of growth, standing biomass, and other soil and plant variables. Given the complexity of interactions

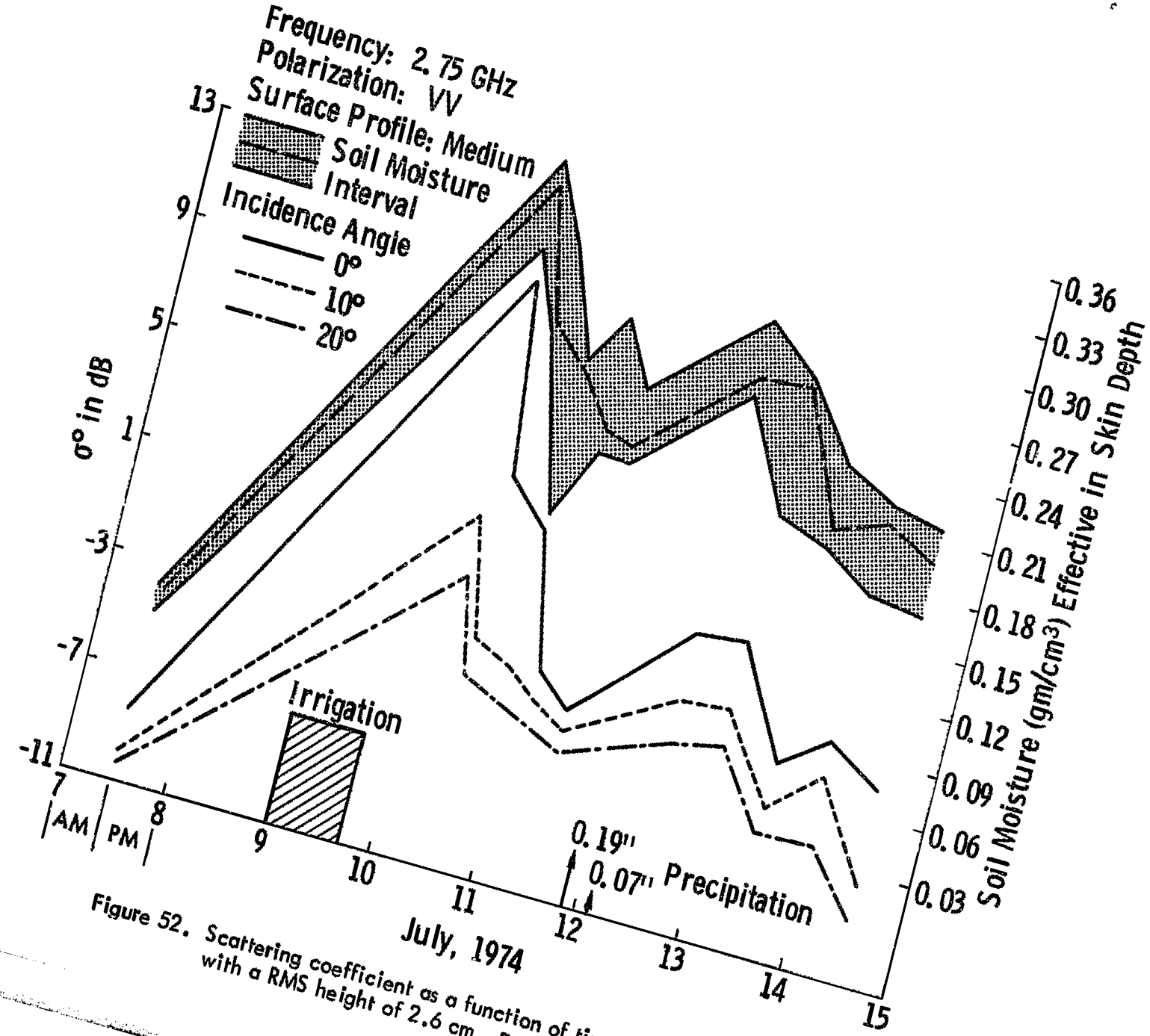

Figure 52. Scattering coefficient as a function of time for a bare field with a RMS height of 2.6 cm. From Batlivala and Ulaby (1976)

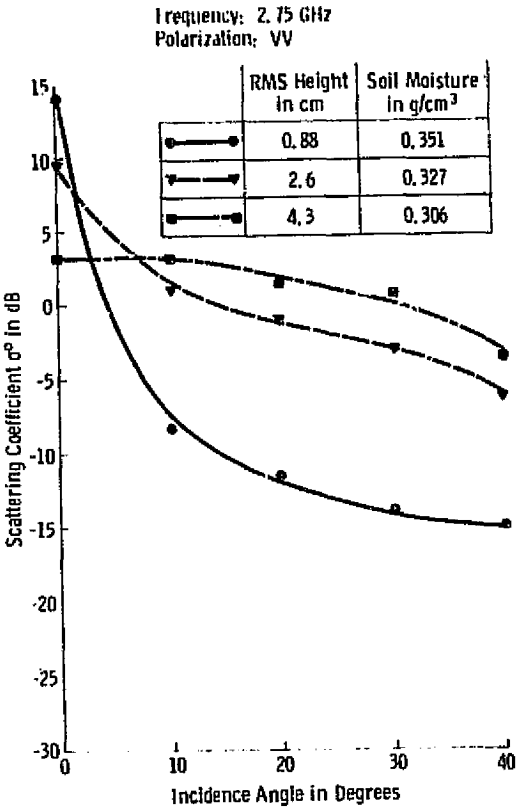

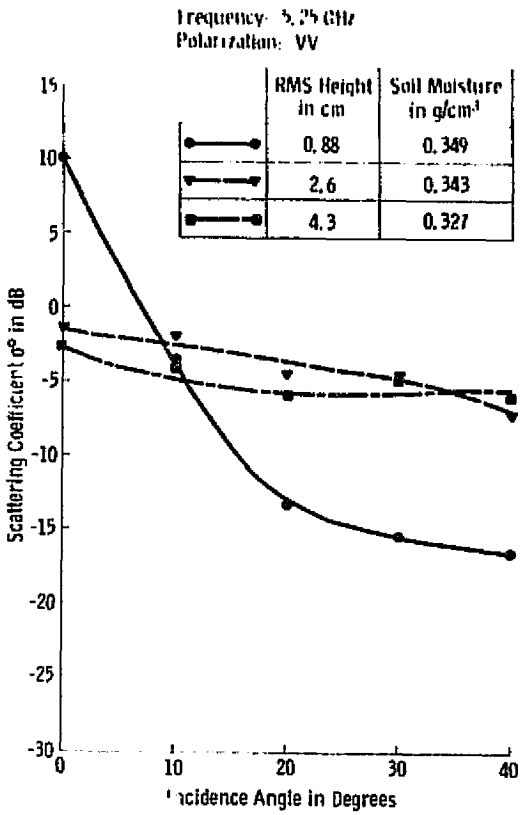

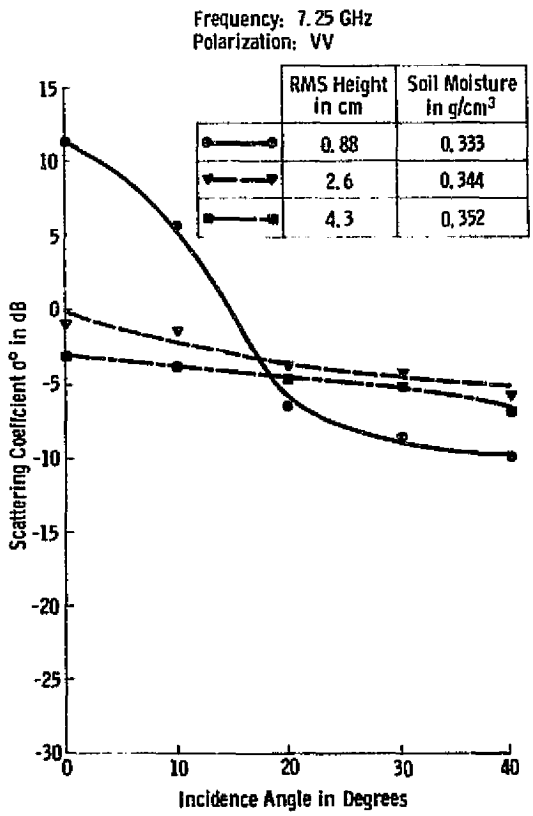

Figure 53. Angular response for three bare fields with similar soil moisture conditions but considerably different surface roughnesses.

From Batlivala and Ulaby (1975).

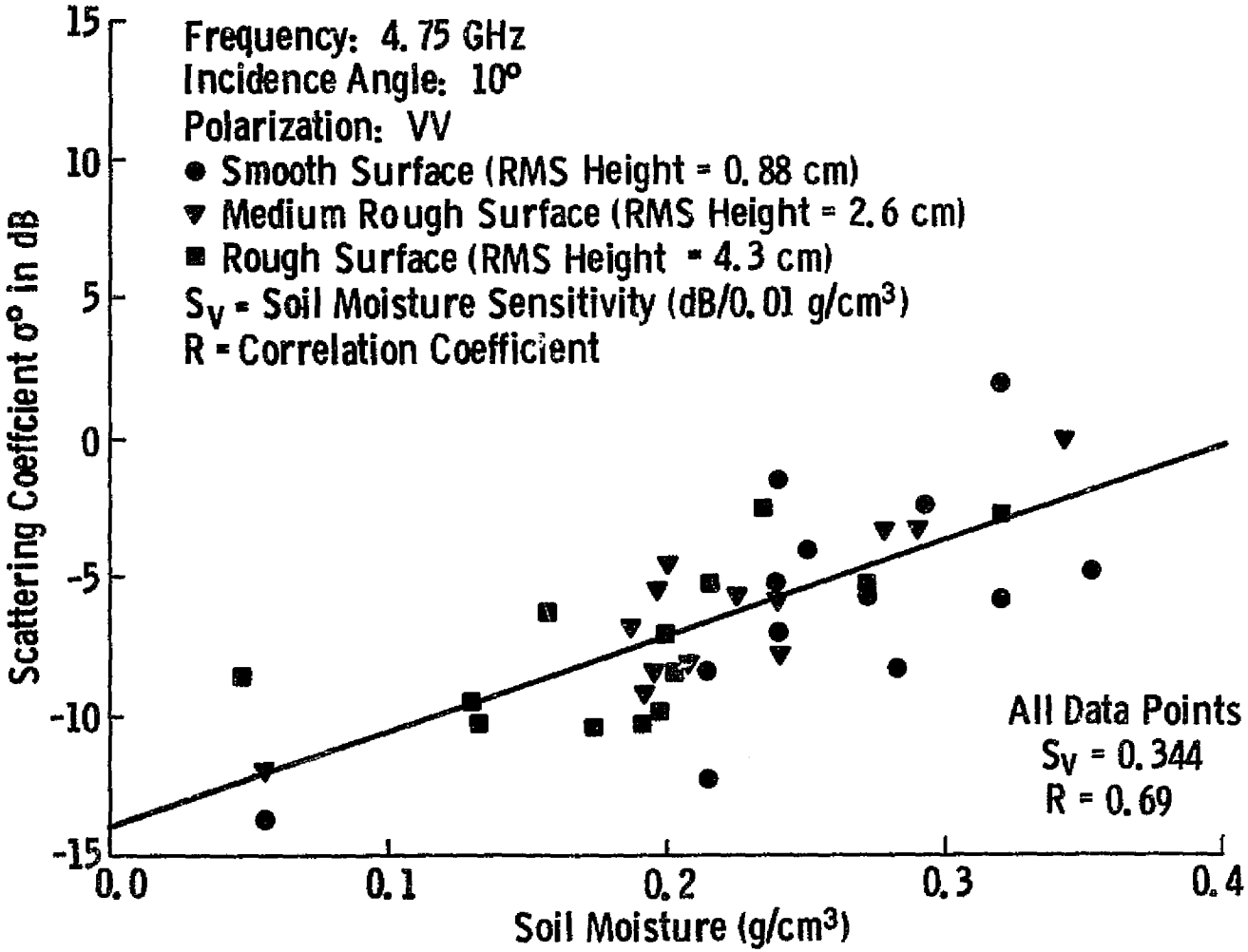

Figure 54. Scattering coefficient response as a function of soil moisture for three surface roughness profiles combined. From Ulaby, et al. (1975).

among these factors and the lack of understanding of how they relate to one another and to the microwave response of vegetation, experimental measurements of the soil/canopy system under a variety of conditions are the most efficient method for determining the effects of plant canopy on microwave measurement of soil moisture. So far, the attention has been focused primarily on agricultural crops.

Figure 55 (Ulaby, 1975) illustrates the effect of frequency on the radar sensitivity to soil moisture differences for a field of mature milo. At nadir, a large separation is observed between the frequency responses of dry (8.2%) and wet (26.8%) soils. This separation, however, decreases by about 7 dB between 4 and 8 GHz. In contrast, a much smaller difference is observed at 30°, particularly at the higher frequencies.

Backscatter data from 43 fields of mature corn, milo, soybeans and alfalfa are shown in Figure 56 where σ° data at 10° and 30° are plotted as a function of gravimetric moisture content in the top 5 cm (Ulaby, 1975). The frequency and polarization are 4.7 GHz and HH, respectively. The calculated sensitivity (slope) at 10° is 0.3 dB/1% moisture. Similar calculations were performed at other frequencies and angles of incidence and are summarized in Figure 57.

An optimum active sensor for microwave remote sensing of soil moisture should operate at the frequency, incidence angle, and polarization for which (i) the correlation between σ° and soil moisture is very high, thus implying low interference by other variables, and (ii) the σ° change with changing moisture content is also very high, thereby enabling accurate moisture estimates. Figure 57b indicates that practically at all incidence angles, the correlation between σ° and moisture was higher at the low frequency, and the difference between polarizations was small. Furthermore, the sensitivity S_w, was highest at 0° and 10° but decreased quite rapidly for higher incidence angles, particularly at 7.1 GHz (Figure 57a). Consequently, Ulaby's (1975) study suggested that the low frequency and an incidence angle around 10° would exhibit highest moisture sensitivity for the ranges of sensor parameters and experimental conditions investigated.

5.1.2 Passive Microwave Observations

The passive microwave response to soil moisture has been demonstrated by several investigators (Poe, 1971; Edgerton, 1968; Edgerton et al., 1968; Blinn and Quade, 1973; Lee, 1974; Newton et al., 1974). An example is shown in Figure 58 (Blinn and Quade, 1973) where the measured emissivity is plotted as a function of moisture

Crop Type : Milo
Crop Height : 1.0 Meters
Polarization : VV

Incidence Angle	0°	0°	30°	30°
Average Soil Moisture	8.2%	26.8%	8.2%	26.8%
Designation	▲— — —	○- - - -	△— — —	●———

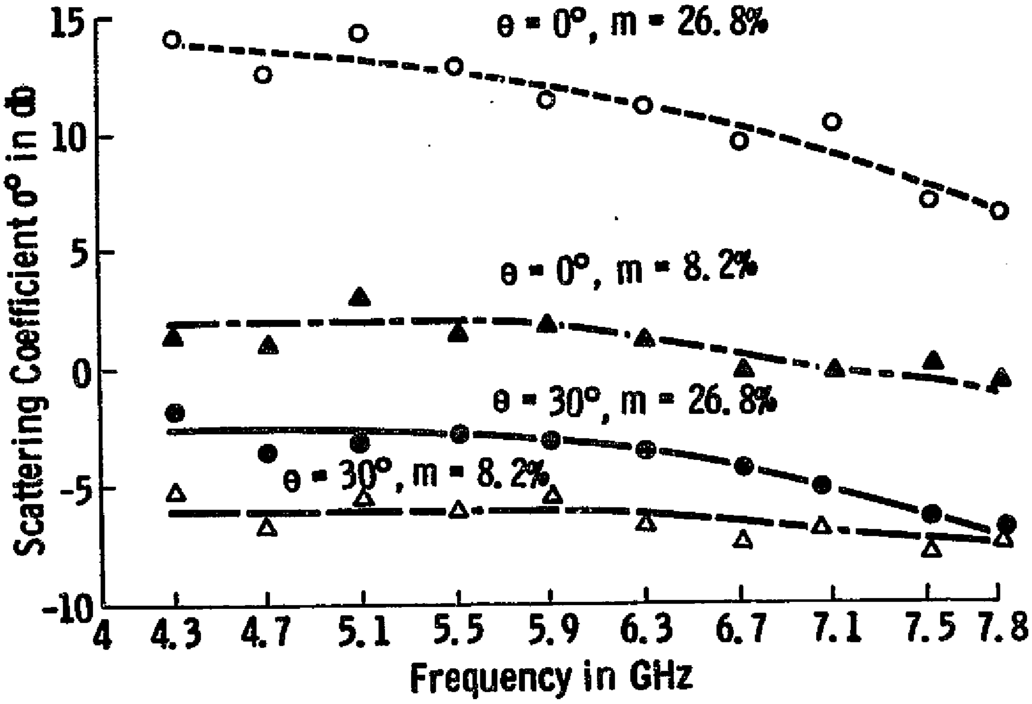

Figure 55. 4-8 GHz SPECTRAL RESPONSE OF MILO AT θ = 0° AND 30° FOR LOW AND HIGH SOIL MOISTURE CONDITIONS.

From Ulaby (1975).

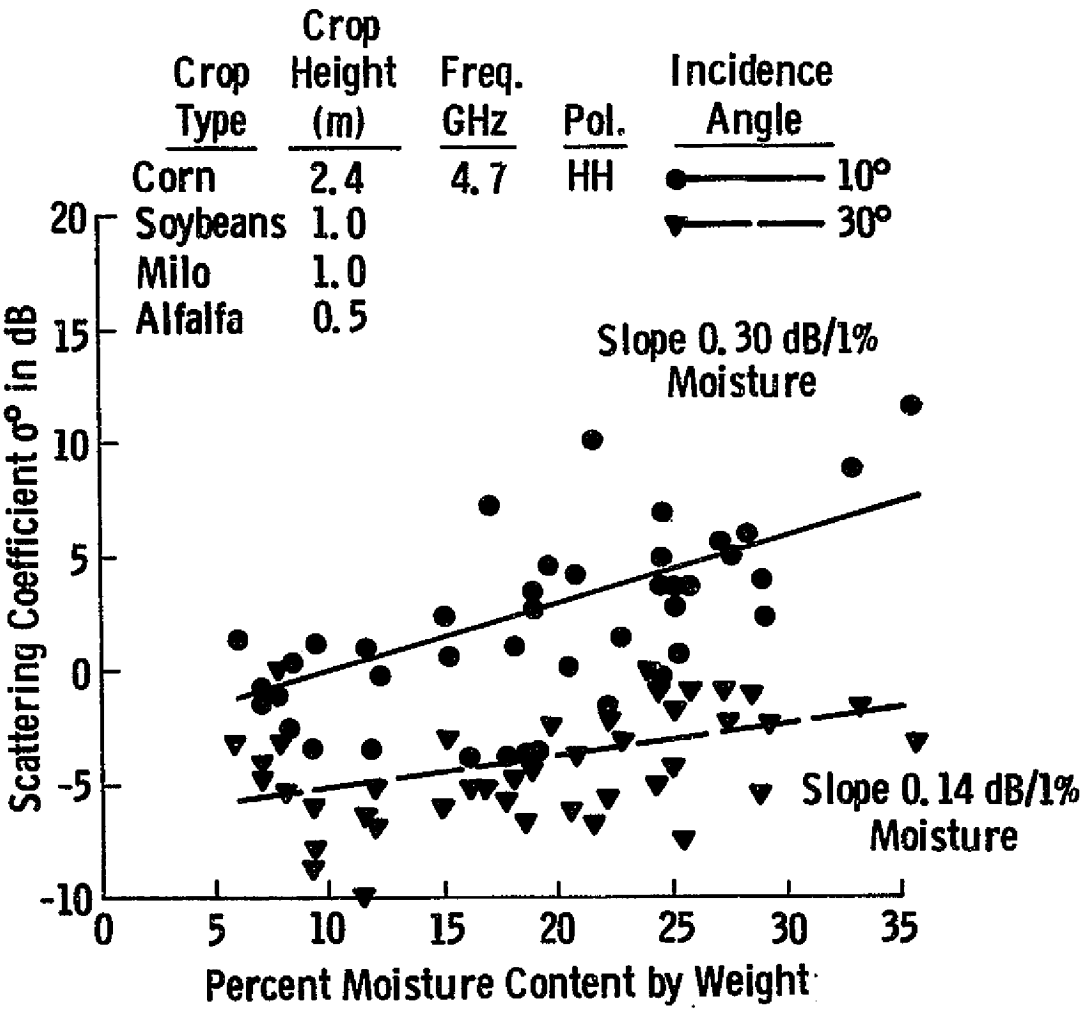

Figure 56. Scattering coefficient response as a function of soil moisture for entire data set regardless of crop type. From Ulaby (1975).

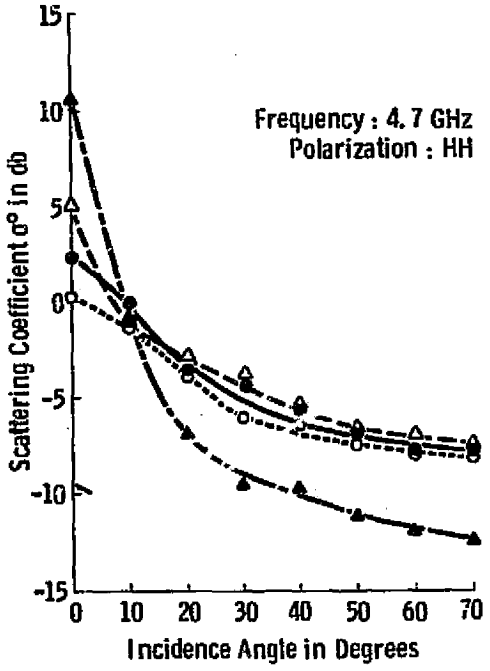

Figure 10a. HH Polarization

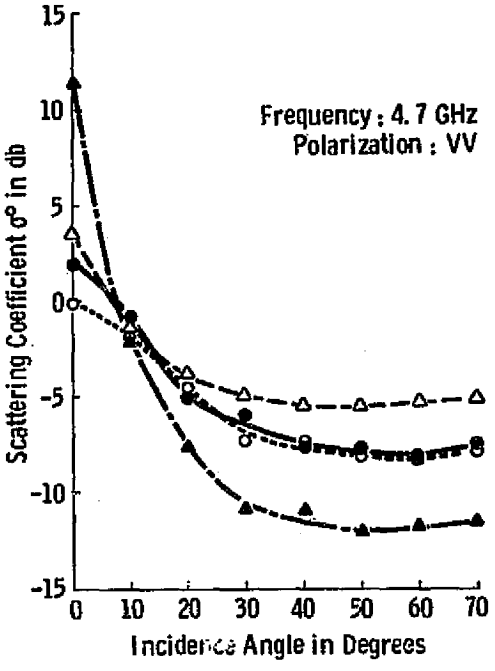

Figure 10b. VV Polarization

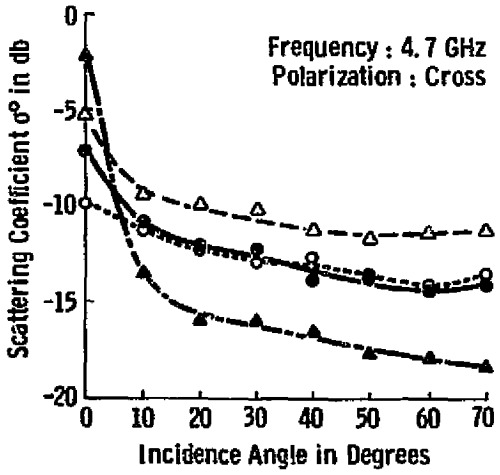

Figure 10c. Cross Polarization

Crop Type	Corn	Milo	Soybeans	Alfalfa
Crop Height in Meters	2.4	1.0	1.0	0.5
Average Soil Moisture	10.6%	8.2%	8.1%	10.5%
Designation	------ ○	—●—	— — △	—▲—

Figure 57. SCATTERING COEFFICIENT RESPONSE AT 4.7 GHz FOR FOUR CROP TYPES. SOIL MOISTURE CONDITION IS LOW.

From Ulaby (1975).

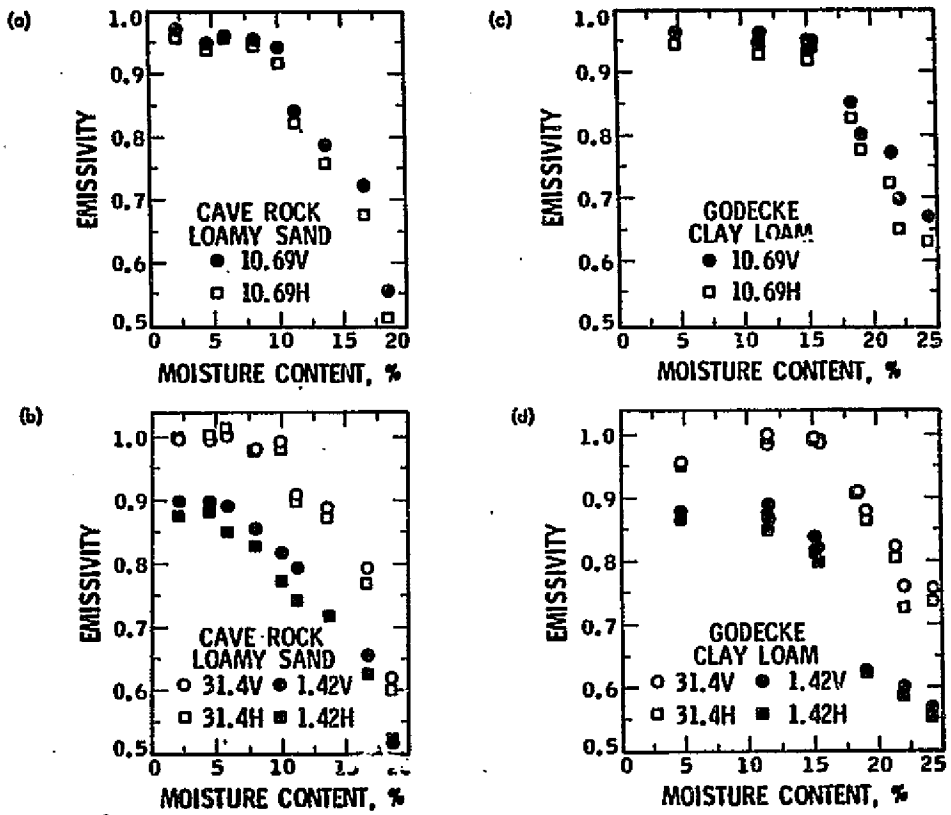

Figure 58. Moisture effects for loamy sand and clay loam. From Blinn and Quade (1973).

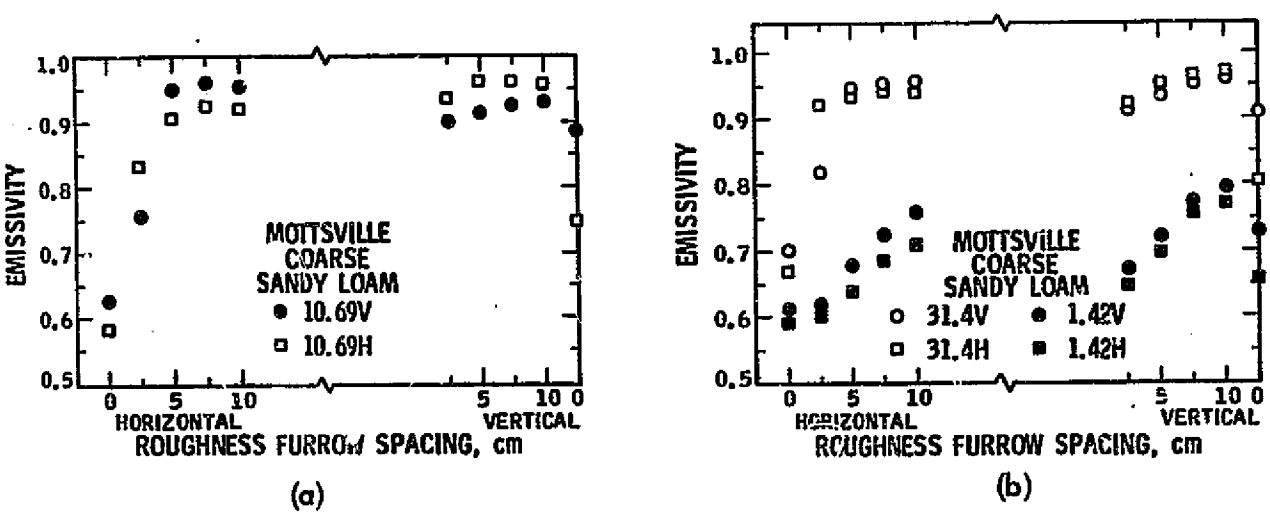

Figure 59. Moisture and roughness effects for sandy loam. From Blinn and Quade (1973).

content at 1.42, 10.69 and 31.4 GHz. The angle of incidence is 25° from nadir. Blinn and Quade (1973) reported that the emissivity remainded constant for moisture contents below a "breakpoint" ranging between 1.5% and 15%. The breakpoint increased with frequency and with the soil clay content. The moisture content is presumably the average moisture content over a 15 cm layer. The existance of such a breakpoint is similar to the radar response shown earlier in Figure 49. Moreover, the explanation for the change in the value of the breakpoint between 1.5% and 15% as a function of frequency and clay content is in agreement with the change in linearity observed for the active microwave data when moisture content was expressed in terms of an effective value over the skin depth. The effective layer contributing to the emission is closer to 15 cm at 1.42 GHz than at 31.4 GHz.

In addition to measuring the emissivity as a function of moisture content, Blinn and Quade (1973) investigated the effect of surface roughness on the emissivity. Regular roughness patterns were prepared by pulling a triangular toothed template over the surface of the soil. Tooth spacings of 2.5, 5, 7.5 and 10 cm were used. The grooves were oriented first in the direction of horizontal polarization and then in the direction of vertical polarization. Their results, shown in Figure 59, indicate that increasing roughness (furrow spacing) can have a substantial effect on the emissivity, particularly at the higher frequencies.

The effects of surface roughness and vegetation cover were investigated by Texas A&M University (Lee, 1974; Newton et al., 1974). Radiometric measurements were acquired at L-band (1.42 GHz) and X-band (10.69 GHz) with horizontal and vertical polarizations. Three fields with surface roughnesses comparable to those shown in Figure 53 were used. With regard to surface roughness, Lee's (1974) results confirm the findings of Blinn and Quade (1973) as indicated by Figure 60. The effect of vegetation is illustrated in Figures 61a-c where brightness temperature values of oatgrass can be compared to the response observed with the fields bare. All the data shown in Figure 61 is at 30° angle of incidence, L-band. The vegetation appears to produce lower brightness temperature values than those obtained for the bare soil, particularly for the medium rough and rough fields. Similar results were also evident in data at other angles of incidence and for different definitions of moisture content (0-18 cm depth and equivalent soil moisture). At X-band, the vegetation appeared to completely mask the radiometric sensitivity to soil moisture.

5.2 AIRBORNE PLATFORMS

5.2.1 Active Microwave Observations

Using airborne scatterometer measurements, Dickey et al. (1974) analyzed radar return from dry and irrigated portions of the same fields. The crops grown included corn, alfalfa, grain sorghum, sugar beets and hay. They found that at 13.3 GHz and for incidence angles below approximately 45°, σ^o values measured from irrigated sections were 5 to 7 dB higher than σ^o values from the dry sections; an example for a corn field (48 cm tall, coverage 40%) is shown in Figure 62. The difference in angular responses varied with crop type, however. For example, in one alfalfa field, σ^o for the wet section was only 2 dB higher at angles above 20°. The response to moisture was also observed when all dry section (4239 resolution cells) and wet section measurements (85 cells) were combined (Figure 63). Dickey et al. (1974) concluded that similar effects occurred at 0.4 GHz but they were obscured because of the large resolution element size. Ulaby et al. (1975) utilized some data from the same mission to illustrate the relationship between $m_w(0, 15)$ and σ^o at 13.3 GHz for seven fields with various covers (Figure 64). In spite of the variety of crops, σ^o increased nearly linearly with increasing moisture at 10°. The response at 20° was weaker except for one moist field; this anomaly could be related to row configuration. At 50°, σ^o did not change with moisture content in a monotonous fashion; this is consistent with the data discussed in section 5.1.1.

5.2.2 Passive Microwave Observations

Several airborne experiments have been conducted to determine the effects of soil moisture on the microwave emission (Poe and Edgerton, 1971; Jean, 1971; Schmugge et al., 1974). In most cases, an aggregate soil moisture sample from the top 15 cm layer was used for defining moisture content.

Brightness temperature data acquired at 19.35 GHz over an agricultural test site in the vicinity of Phoenix, Arizona, was reported by Schmugge et al. (1974) as a function of moisture content in the top 15 cm. A breakpoint of about 15% moisture followed by a linear decrease of brightness temperature with moisture was observed, in agreement with Blinn and Quade's (1973) findings (Figure 59). Data acquired at 1.4 GHz for the same fields, however, showed a similar linear decrease but no clearly discernible breakpoint was apparent. Schmugge et al. (1974) attributed the breakpoint effect in part to the behavior of the dielectric properties of soil as a function of

moisture content, and in part to the inappropriate representation of moisture content by the 15 cm layer. Whereas the average moisture in a 15 cm layer may not vary much between different fields, the moistures in the top surface layer may be considerably different. Differences in skin depth between the 19.35 GHz (λ = 1.55 cm) and 1.4 GHz (λ = 21 cm) frequencies may partially explain the absence of a breakpoint in the 1.4 GHz brightness temperature response to moisture.

In a more recent analysis of the data by Schmugge (in: Ulaby et al., 1975), the effect of soil type was accounted for by plotting the data for heavy soils (clay loam) and light soils (sandy loam and loam) separately as shown in Figure 65. Also, the moisture content is that of the top 1 cm. The differences in response to soil moisture (slope) was then eliminated by plotting the combined data as a function of field capacity (Figure 66). The result is an improvement in the correlation coefficient over either of the plots shown in Figure 65. Similar results were also obtained for the 21 cm data as shown in Figure 67.

5.3 SATELLITE PLATFORMS

Microwave observations of the earth have been conducted by both Nimbus 5 and Skylab sensors. Aboard Nimbus 5 was flown the 19.35 GHz Electrically Scanning Microwave Radiometer (ESMR) and Skylab carried a 13.9 GHz Radiometer-Scatterometer (S-193) and a 1.4 GHz nadir-looking radiometer (S-194).

During Skylab's June 5, 1973 pass over a test site in Texas, soil samples were collected by ground crews and later analyzed for their moisture contents (Eagleman, 1974). The test site was about 300 km in length, which for the S-194 footprint of approximately 120 km in diameter, corresponds to only 3 independent data points. Successive data points contain about 94% overlap of the area seen on the ground. Brightness temperature plots against soil moisture (Eagleman, 1974) produce a correlation coefficient of -0.97 with all the data included. Since inherent in the data is at least 94% correlation due to the overlaps, it is not possible to determine the correlation with moisture content alone. Hence, S-194 data will not be reproduced in this report.

At 13.9 GHz, S-193 footprints were about 10 times smaller than S-194, thereby making it possible to investigate the sensitivities of the radiometer and the radar to soil moisture content. Figures 68 and 69 are plots of the emissivity and the

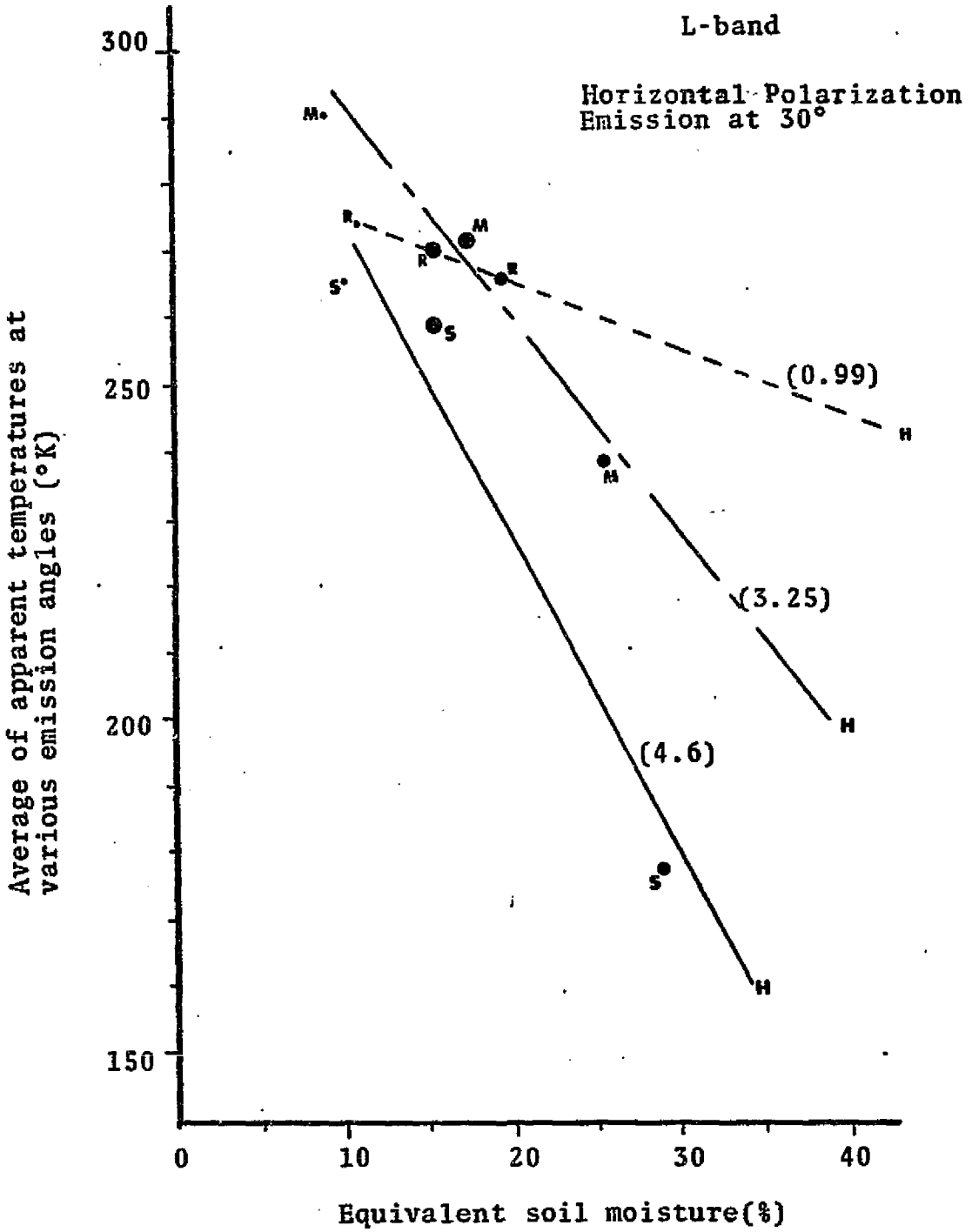

Figure 60. Apparent temperature versus soil moisture content, bare condition. From Lee (1974).

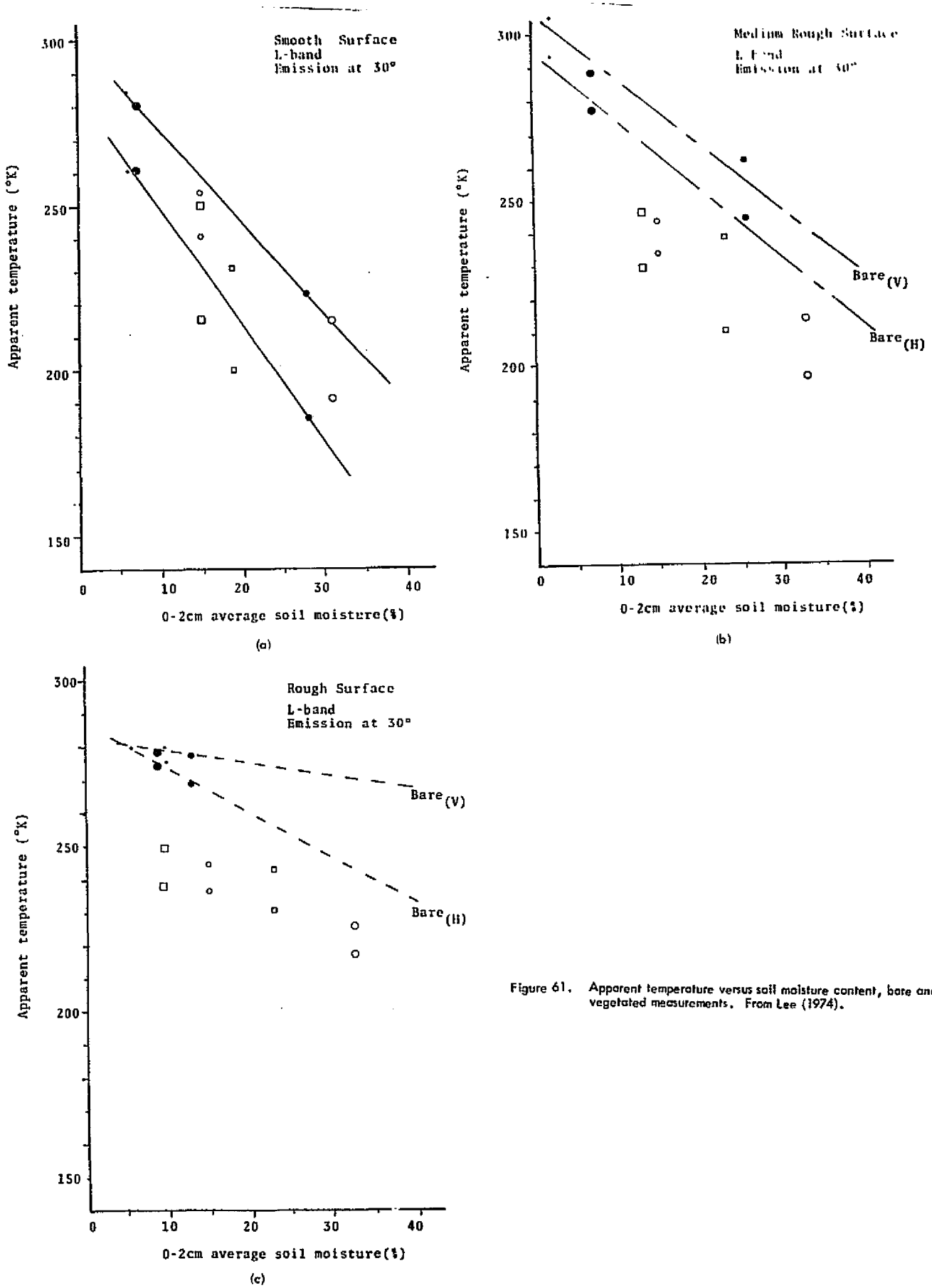

Figure 61. Apparent temperature versus soil moisture content, bare and vegetated measurements. From Lee (1974).

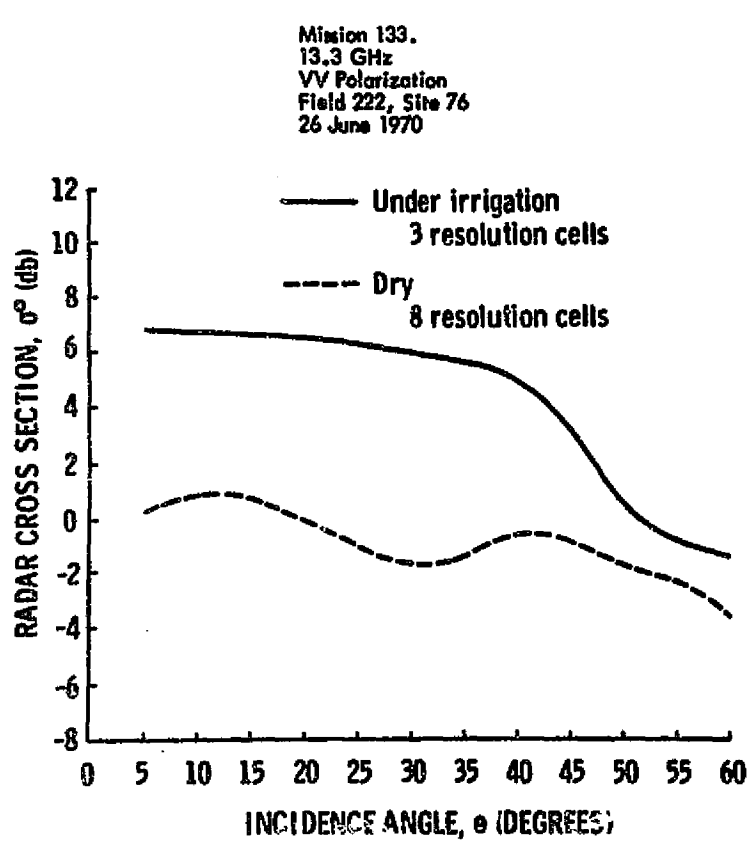

Figure 62. Scattering coefficient as a function of incidence angle for irrigated and non-irrigated sections of a corn field. From Ulaby, et al. (1975).

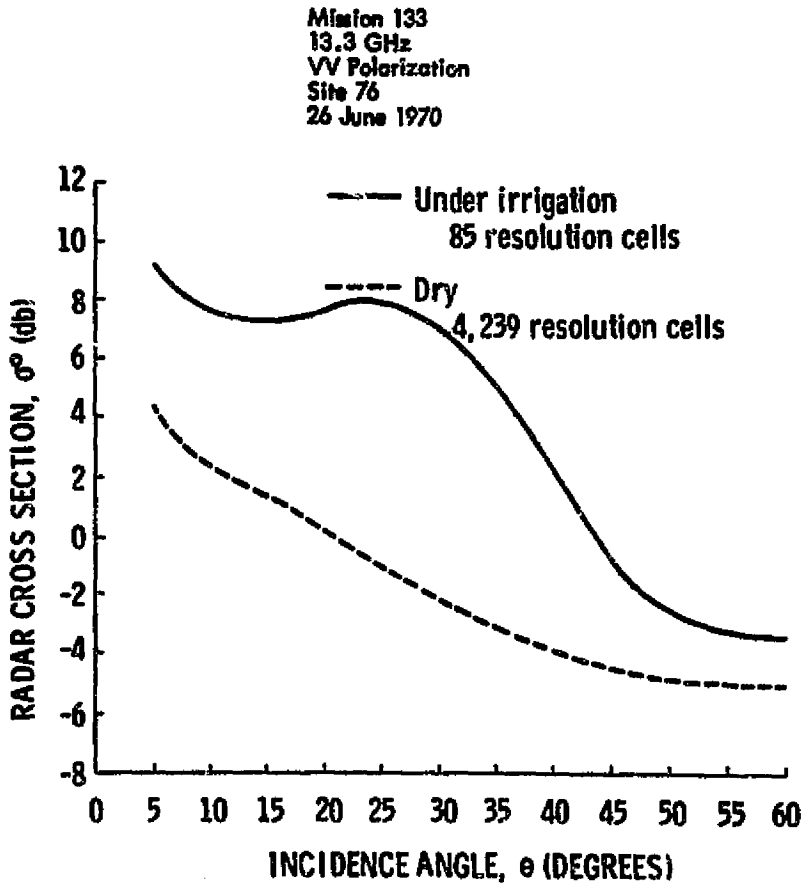

Figure 63. Average scattering coefficient as a function of incidence angle for irrigated and dry terrain. From Ulaby, et al. (1975).

Field	Soil Moisture
#30: Wheat: Stubble, Just Cut	15.7%
#37: Wheat: Ripe, 24" Tall	19.5%
#122: Bare: Cultivated	21.8%
#31: Bare: Cultivated; 10 % Stubble	23.9%
#14: Corn: 16" Tall	29.3%
#18B: Alfalfa 10" Tall, Mixed Wheat	31.0%
#125: Sorghum: 4" Tall, 5% Emerged	37.5%

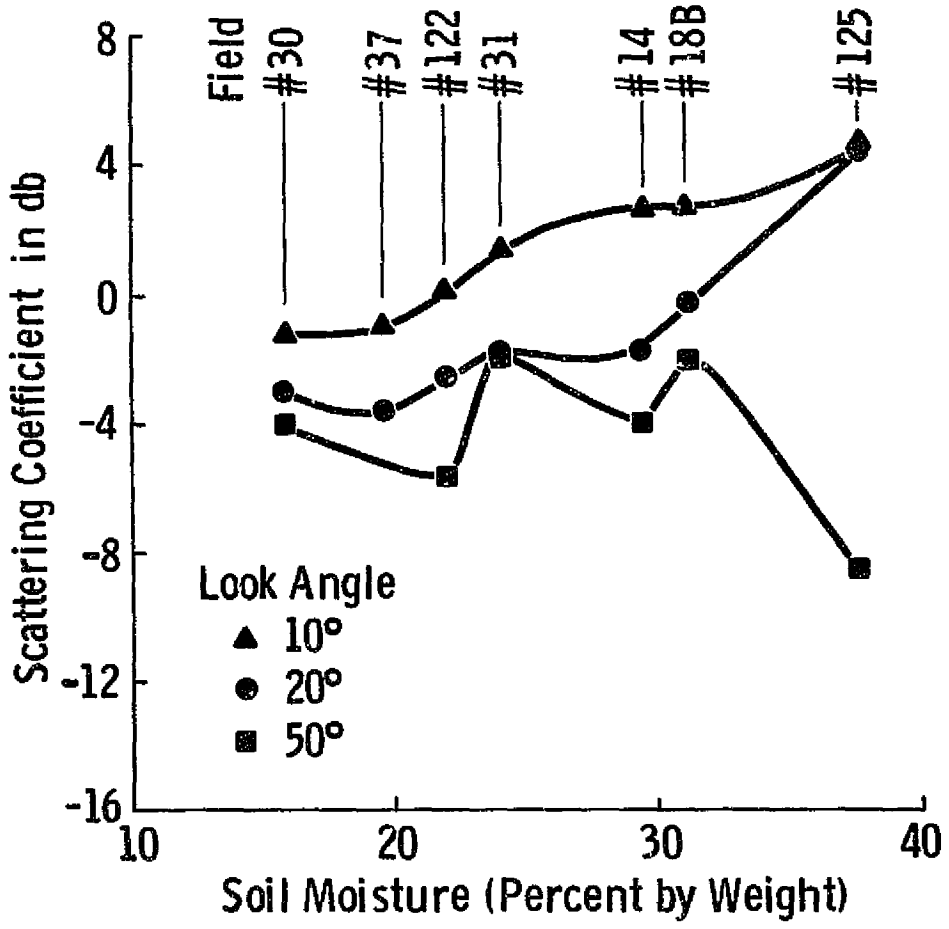

Figure 64. Scattering coefficient as a function of soil moisture content at 13.3 GHz, VV polarization. Garden City, Kansas.

From Ulaby et al. (1975).

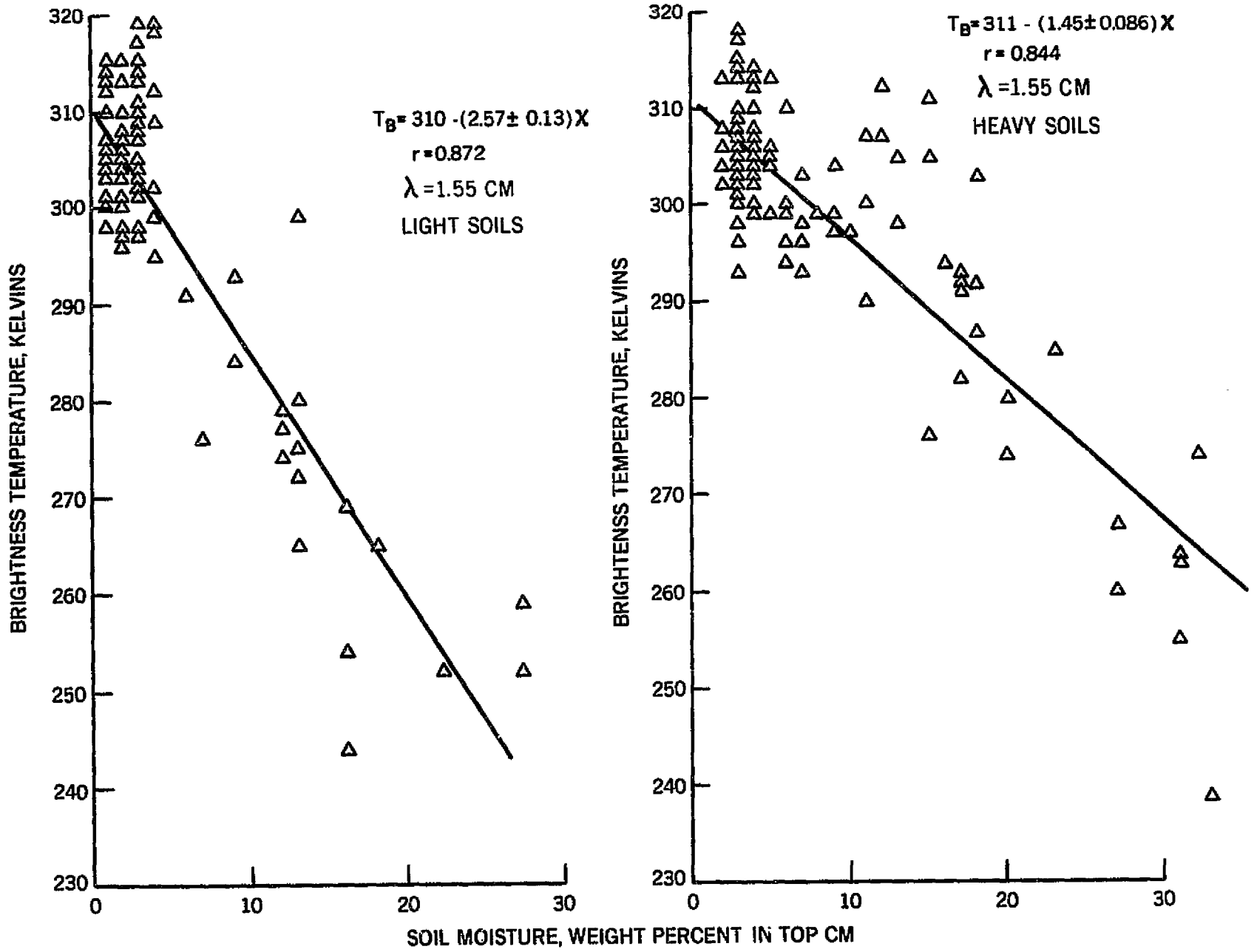

Figure 65. Plot of 1.55 cm brightness temperatures versus soil moisture for light soils (sandy loam and loam) and heavy soils (clay loam). From Ulaby, et al. (1975).

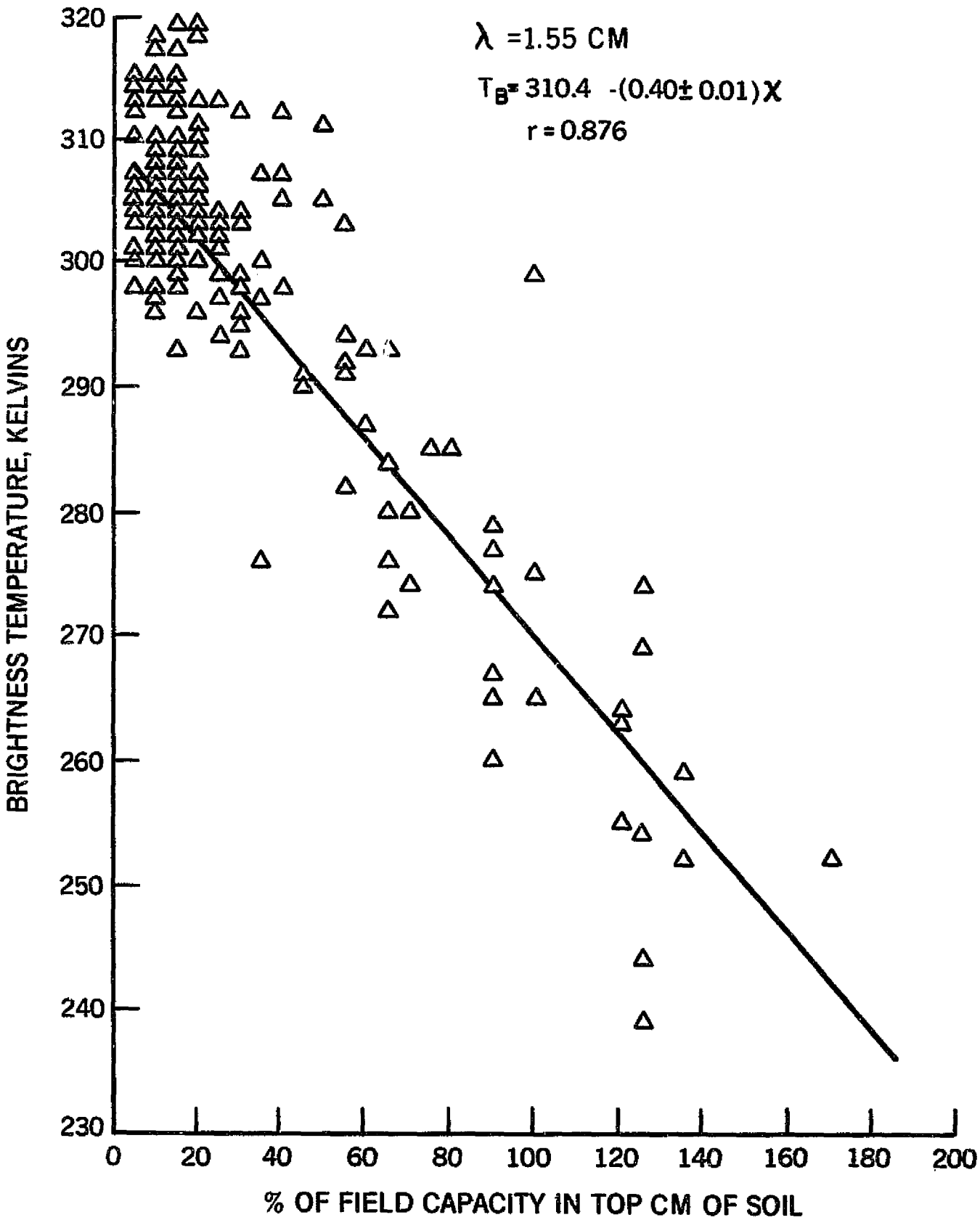

Figure 66. Plot of 1.55 cm brightness temperature versus soil moisture in top 1 cm expressed as a percent of field capacity. From Ulaby, et al. (1975).

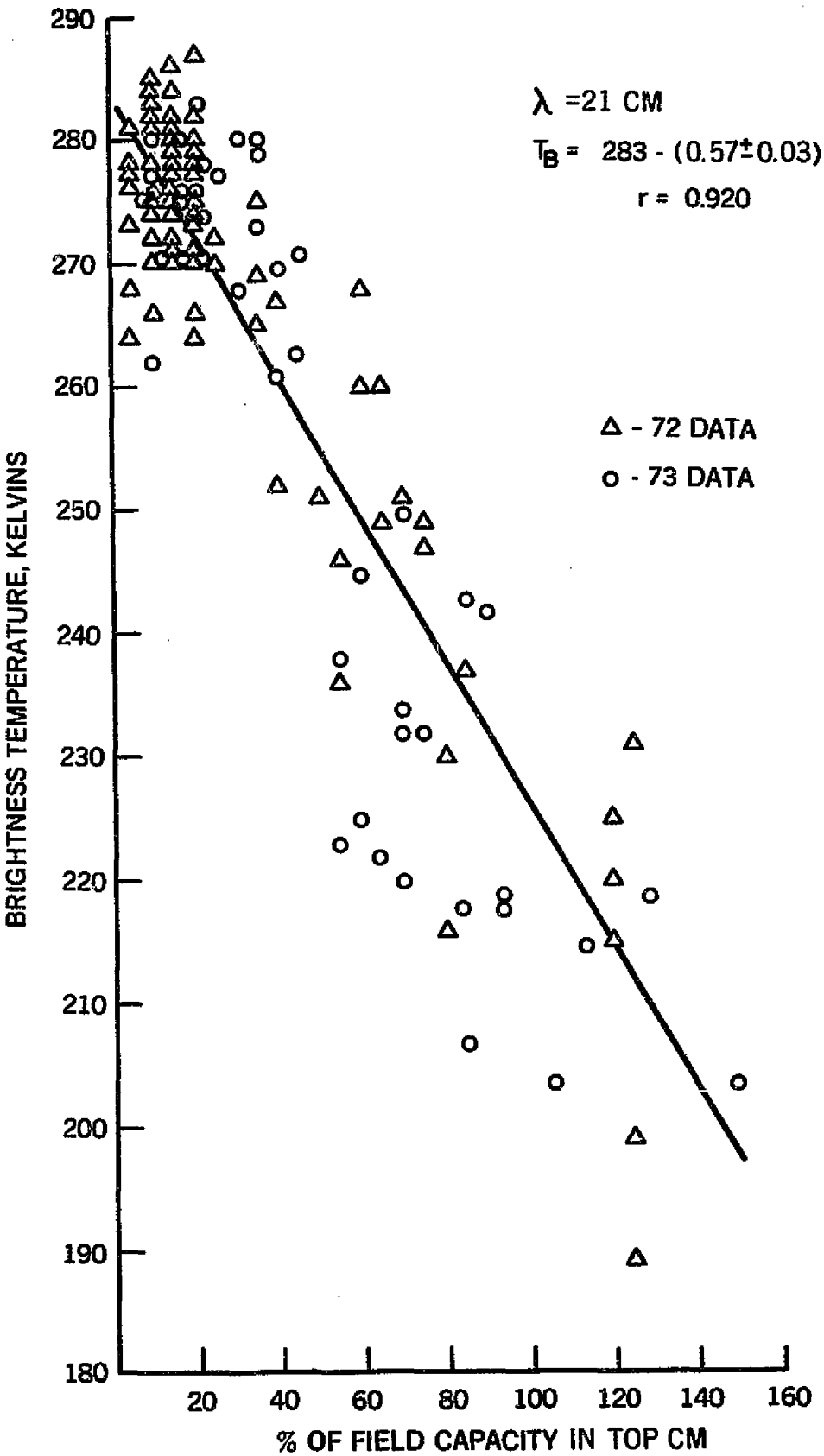

Figure 67. Plot of 21 cm brightness temperature versus soil moisture in top 1 cm expressed as a percent of field capacity. From Ulaby, et al. (1975).

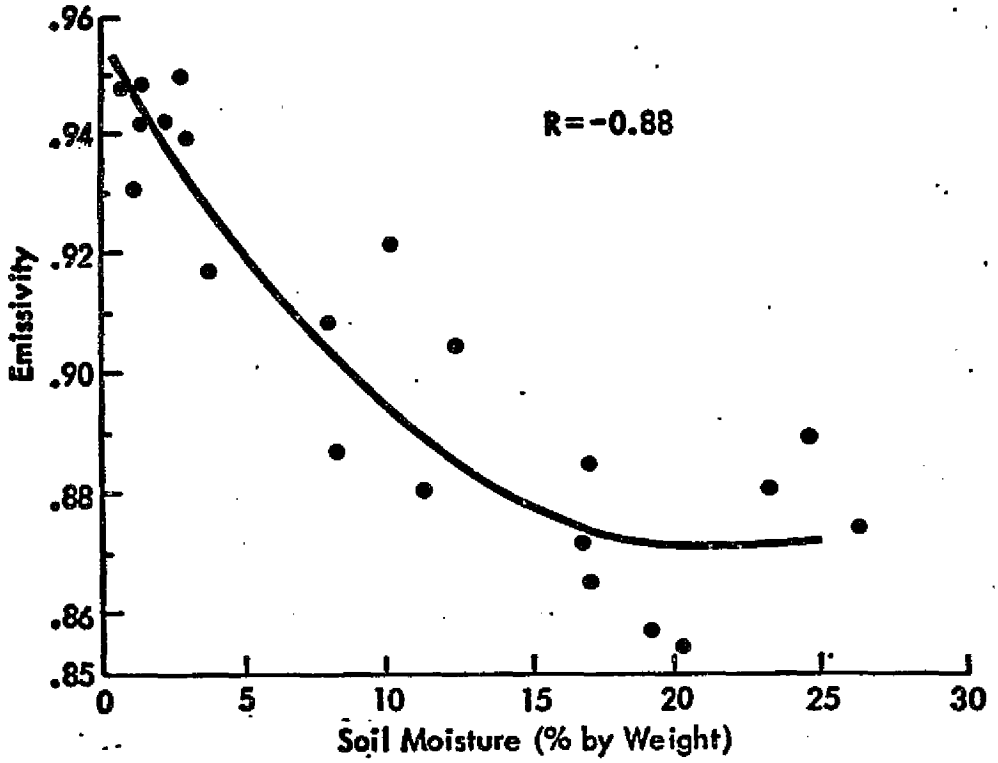

Figure 68. The emissivity as a function of soil moisture content determined from Skylab S193 data (2.1 cm wavelength). From Eagleman and Ulaby (1974).

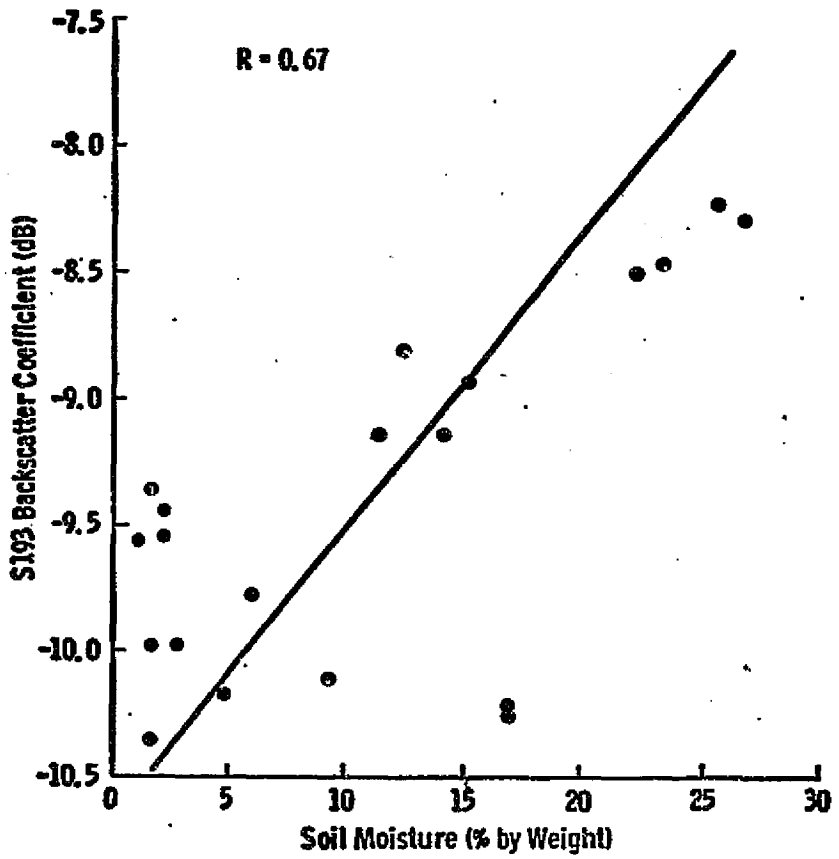

Figure 69. The S193 backscatter coefficient as a function of soil moisture for the June 5, 1973 EREP pass. From Eagleman and Ulaby (1974).

scattering coefficient derived from S-193 measurements over the Texas site (Eagleman and Ulaby, 1974). The moisture content value of each of the points shown in the plots is an average of 2 to 3 soil samples gathered within the approximately 100 km^2 footprint. Hence, some of the points may not necessarily be good representatives of the moisture content ofthe entire footprint. Under these circumstances, the correlations shown in Figures 68 and 69 are indeed very encouraging.

CHAPTER 6.

SUMMARY AND CONCLUSIONS

This study was approached on the premise that an understanding of problems inherent in the microwave approach to soil water content determination as well as the development of an operationally efficient algorithm for an extraction of moisture information from the microwave data will not be completely successful unless consideration is also given to the major parameters of the soil involved, namely its moisture and temperature regimes. This necessitated a rather broad-based research encompassing problems traditionally approached in several scientific disciplines. To render the work manageable, mathematical models were employed wherever possible. Furthermore, the scope was limited to several specific problems (section 1.2) and a set of environmental conditions, the major of which were bare soil in an agricultural area, cloudless sky, high radiation regime, deep ground water level, and absence of scattering at the microwave frequencies of interest. However, care was taken to ensure that the mathematical models reproduced reality reasonably well so that data generated by the models could be considered representative of the actual conditions. Soil moisture and temperature profiles generated by the models for various conditions were analyzed at three frequencies (1.4 GHz, 4.0 GHz, 10.0 GHz) using a brightness temperature model and, for a portion of the data, using a coherent radiation model which computed an effective power reflection coefficient. It should be stressed that the choice of frequencies and incidence angle (0°) and the emphasis on passive mode represent an attempt to accurately reflect the effect of moisture and temperature regimes on the microwave signal, and consequently are not intended to imply optimum sensor design criteria. The major results of this study can be summarized as follows.

(i) A layered water balance model was developed which could be used to predict daily soil water contents for 1-cm increments in the 0-30 cm depth soil zone within approximately 0.02 cm^3/cm^3. The model was successfully tested on four data sets. Additional testing appears warranted, however, primarily to determine whether the storage capacity values (estimated here to correspond to a soil tension of 0.09 bars) apply in conditions different from those under which the four data sets were collected.

(ii) Diurnal soil water content changes appear quite large near the soil surface (0.125 cm^3/cm^3 in 0-0.5 cm layer if moisture content is about 0.175 cm^3/cm^3) but decrease rapidly with depth so that at the depth of 2-3 cm, the diurnal range of moistures becomes less than 0.03 cm^3/cm^3. It should be remembered that these values were based on measurements of only one soil in four different months (March, April, September, October). Although the exact values may differ from case to case, it is apparent that considerable near-surface diurnal soil moisture variation can occur. This should be taken into account when estimating soil moisture by real-time methods, particularly those which respond primarily to surface and near-surface soil moisture.

(iii) In the case of bare soil, large soil moisture changes were found to be confined largely to the top 30 cm of the soil, based on data collected in Eudora silt loam. This was primarily because the water lost by evaporation originated near the surface, and the precipitation amounts were on the average not sufficiently large (in spite of an abnormally wet season) to penetrate into the deeper layers. Thus it is concluded that under conditions of frequent precipitation, the error in computed vertical moisture distribution in a bare soil caused by assuming zero evaporation from depths greater than 30 cm would be sufficiently small or negligible under conditions similar to those of the experiment.

(iv) If the effective precipitation P_{eff} during a certain period exceeds the storage capacity of the lower zone of the soil profile (depths greater than 30 cm in this study), it may be assumed that the lower zone contains only the amount equal to the storage capacity at the end of the period. The length of time needed for the excessive water to drain out will vary, however, depending on the hydraulic properties of the soil (and on ground water level if present).

(v) Moisture content near the surface, surface configuration, and surface roughness all affected surface and profile temperature of a bare soil in addition to the time of day. The variations were largest at the surface. Although all the temperature fluctuations

observed at the surface were propagated to greater depths, the differences encountered there were smaller than those at the surface; data generated by the soil temperature simulation model indicated that at depths greater than 30 cm, diurnal soil temperature variations can be expected to be around 5°C or less.

(vi) Microwave brightness temperature of a bare soil varied diurnally in response to changing moisture and temperature profiles. Large soil moisture changes, such as rapid evaporation loss following precipitation, can cause greater diurnal brightness temperature changes than relatively large soil temperature fluctuations.

(vii) A detailed analysis of the microwave brightness temperatures and associated moisture and temperature profiles revealed that even at the lowest frequency (1.4 GHz), the brightness temperature was affected primarily by the air/soil discontinuity and much less so by the subsurface soil properties. That is, the vertical soil moisture and temperature profile variations, although generated so as to represent relatively extreme conditions (for an agricultural area), were not large enough to substantially influence the brightness temperatures. For all frequency/moisture/temperature profile combinations investigated, the major dielectric discontinuity existed between air and the first soil layer which rendered the surface and near-surface moisture content to have a major effect on the brightness temperatures. Furthermore, a consideration of dielectric properties suggests that subsurface soil moisture gradients would have to be in excess of those commonly found in a cultivated soil in order to produce reflections comparable to those at the soil surface. Similar results were arrived at when effective power reflection coefficients were computed for coherent radiation, such as transmitted by radar.

It is important to remember that the "surface layer domination" was established using a model which neglected scattering. A cursory examination of the factors involved suggested that the most effective scatterers in the soil would be dielectrically homogeneous soil clods separated by air spaces; the optimum clod size would depend on the wavelength. Since it is not known to which extent such clods occur under field conditions, the conclusions derived on the basis of the brightness temperature model should not be considered final.

(viii) By combining water balance, hydrological, and microwave remote sensing concepts, an algorithm was developed to monitor soil water storage in the profile as a function of time and location. Suitable primarily for an agricultural area, the algorithm could be used for the entire soil profile or for individual zones within the profile. It would require the following input: hydrological soil group, storage capacity of the profile or of individual zones, crop type, precipitation amounts and durations, meteorological variables needed for computing actual evaporation (evapotranspiration), and a rainfall pattern as determined by the remote sensors.

(xi) Although active and passive microwave sensors have demonstrated their sensitivities to soil moisture variations for bare and vegetated fields, additional experimental work is needed before an optimum set os sensor(s) parameters can be defined such that the effects of soil surface roughness and vegetation cover are minimized.

REFERENCES

Baier, W. 1967. Relationships between soil moisture, actual and potential evapotranspiration. Proceedings of Hydrology Symposium No. 6, National Research Council of Canada: 155-204.

Baier, W. 1969. Concepts of soil moisture availability and their effect on soil moisture estimates from a meteorological budget. Agricultural Meteorology 6: 165-178.

Baier, W., and G. W. Robertson. 1965. Estimation of latent evaporation from simple weather observations. Canadian Journal of Plant Sciences 45: 276-284.

Baier, W., and G. W. Robertson. 1966. A new versatile soil moisture budget. Canadian Journal of Plant Sciences 46: 299-315.

Baier, W., D. Z. Chaput, D. A. Russello, and W. R. Sharp. 1972. Soil moisture estimation program system. Technical Bulletin 78, Plant Research Institute, Research Branch, Canada Department of Agriculture, Ottawa, Ontario.

Batlivala, P. P. and J. Cihlar. 1975. Joint Soil Moisture Experiment (Texas): Documentation of radar backscatter and ground truth data. RSL Technical Report 264-1, The University of Kansas Center for Research, Inc., Lawrence, Kansas. 25p. + appendix.

Batlivala, P. P. and F. T. Ulaby. 1975. Effects of roughness on the radar response to soil moisture of bare ground. RSL Technical Report 264-5, University of Kansas Center for Research, Inc., Lawrence, Kansas.

Baver, L. D. 1956. Soil Physics. John Wiley & Sons, Inc., New York. 489p.

Baver, L. D., W. H. Gardner, and W. R. Gardner. 1972. Soil Physics. John Wiley & Sons, Inc., New York. 498p.

Bell, J. P. 1973. Neutron probe practice. Report No. 19, Institute of Hydrology, Crowmarsh Grifford, Wallingford, Berks, England, 63p.

Benoit, G. R., and D. Kirkham. 1963. The effect of soil surface conditions on evaporation of soil water. Soil Science Society of America Proceedings 27: 495-498.

Black, T. A., W. R. Gardner, and G. W. Thurtell. 1969. The prediction of evaporation, drainage, and soil water storage from a bare soil. Soil Science Society of America Proceedings 33: 655-660.

Blanchard, M. B., R. Greenley, and R. Goettelman. 1974. Use of visible, near-infrared, and thermal infrared remote sensing to study soil moisture. NASA Technical Memorandum X-62, 343. 4p.

Blinn, J. C., III. and J. G. Quade. 1973. Dependence of microwave emission on moisture content for three soils. G-AP International Symposium: 372-375. University of Colorado. Boulder, Colorado.

Burke, W. J., and J. F. Paris. 1975. Remote detection of soil moisture by the Passive Microwave Imaging System. To be published in Transactions of the American Geophysical Union.

Carter, D. B., T. H. Schmudde, and D. M. Sharpe. 1972. The interface as a working environment; a purpose for physical geography. Commission on College Geography, Technical Paper No. 7, Association of American Geographers, Washington, D. C. 52p.

Casey, K. F. 1973. Radiation from a line source near an inhomogeneous layer. IEEE Transactions on Antennas and Propagation AP-21: 640-648.

Chidley, T. R. E., and K. M. Keys. 1970. A rapid method of computing areal rainfall. Journal of Hydrology 12: 15-24.

Christiansen, J. E. 1968. Pan evaporation and evapotranspiration from climatic data. Journal of the Irrigation and Drainage Division, Proceedings of the American Society of Civil Engineers, IR2: 243-264.

Cihlar, J. 1973. Ground data acquisition for 1973 microwave (MAPS) measurements: results. CRES Technical Memorandum 177-44, University of Kansas Center for Research, Inc., Lawrence, Ks. 47p.

Cihlar, J., and F. T. Ulaby. 1974. Dielectric properties of soils as a function of moisture content. CRES Technical Report 177-47, University of Kansas Center for Research, Inc., Lawrence, Kansas.

Cooper, C. F. , and F. M. Smith. 1966. Color aerial photography: toy or tool? Journal of Forestry 64: 373-378.

de Vries, D. A. 1963. Thermal properties of soils. Chapter 7 in: Van Wijk, W. R. (Ed.), Physics of plant environment, North Holland Publishing Co., Amsterdam: 210-235.

Dickey, F. M., C. King., J. C. Holtzman and R. K. Moore. 1974. Moisture dependency of radar backscatter from irrigated and non-irrigated fields at 400 MHz and 13.3 GHz. IEEE Transactions on Geoscience Electronics GE-12: 19-22.

Dyer, J. A. 1974. Simulation of the daytime bare soil surface temperature. M. Sc. Thesis, University of Guelph.

Eagleman, J. R. 1967. Pan evaporation, potential and actual evapotranspiration. Journal of Applied Meteorology 6: 482-488.

Eagleman, J. R. 1971. An experimentally derived model for actual evapotranspiration. Agricultural Meteorology 8: 385-394.

Eagleman, J. R. 1974. Moisture detection from skylab. Proceedings of the Ninth International Symposium on Remote Sensing of Environment 1: 701-705.

Eagleman, J. R.,and F. T. Ulaby. 1974. Remote sensing of soil moisture by Skylab radiometer and scatterometer sensors. Proceedings of American Aeronautical Society, The Skylab Results, August 20-22, Los Angeles, California.

Edgerton, A. T. 1968. Engineering applications of microwave radiometry. Proceedings of the Fifth International Symposium on Remote Sensing of Environment: 711-724.

Edgerton, A. T., R. M. Mandl, G. A. Poe, J. E. Jenkins, F. Soltis and S. Sakamoto. 1968. Passive microwave measurements of snow, soils, and snow-ice-water systems. Technical Report no. 4, Aerojet General Corporation, El Monte, California.

Eftimova, N. A.,and G. V. Tsitsenko. 1963. Comparison of experimental and computational methods for determining the temperature of the surface of the body. Trudy Glavnoy Geofizikalnoy Obzervatorii 139: 115-121.

Foster, K. E. 1972. Mathematical analysis of soil temperatures in an arid region. Ph. D. Dissertation, The University of Arizona.

Foster, K. E., and R. E. Fye. 1973. Soil temperature simulation. Arizona Academy of Science 9: 51-55.

Fritton, D. D., D. Kirkham, and R. H. Shaw. 1970. Soil water evaporation, isothermal diffusion, and heat and water transfer. Soil Science Society of America Proceedings 34: 183-189.

Gardner, H. R. 1973. Prediction of evaporation from homogeneous soil based on the flow equation. Soil Science Society of America Proceedings 37: 513-516.

Gardner, H. R. 1974. Prediction of water loss from a fallow field soil based on soil water flow theory. Soil Science Society of America Proceedings 38: 379-382.

Gardner, H. R., and W. R. Gardner. 1969. Relation of water application to evaporation and storage of soil water. Soil Science Society of America Proceedings 33: 192-196.

Gardner, W. H. and C. Calissenforff. 1967. Gamma-ray and neutron attenuation in measurement of soil bulk density and water content. In: Isotope and radiation techniques in soil physics and irrigation studies, International Atomic Energy Agency, Vienna: 101-113.

Hanks, R. J., and H. R. Gardner. 1965. Influence of different diffusivity water content relations on evaporation of water from soils. Soil Science Society of America Proceedings 29: 495-498.

Hanks, R. J., D. D. Austin, and W. T. Ondrechen. 1971. Soil temperature estimation by a numerical method. Soil Science Society of America Proceedings 35: 665-667.

Hershfield, D. M. 1969. A note on areal rainfall definition. Water Resources Bulletin 5: 49-55.

Hillel, D. 1971. Soil and water. Academic Press, New York and London. 288p.

Holmes, R. M., and G. W. Robertson. 1960. The relationship between actual and potential evapotranspiration and its application to a problem in arid zone agriculture. Proceedings of the American Society of Agricultural Engineers No. 16-200.

Holtan, H. N. 1970. An infiltration model adapted to agricultural watersheds. Proceedings of Hydrology Conference, Clemson University, South Carolina. 12p.

Holtan, H. N., and N. C. Lopez. 1970. USDAHL-70 model of watershed hydrology. Technical Bulletin No. 1435, Agricultural Research Service, United States Department of Agriculture. 84p.

Holtan, H. N., G. J. Stiltner, W. H. Henson, and N. C. Lopez. 1974. USDAHL-74 revised model of watershed hydrology. Plant Physiology Institute Report No. 4, Agricultural Research Service, United States Department of Agriculture. 110p.

Hunter, G. T. 1969. Infrared scanning for terrain data acquisition. M. Sc. Thesis, Department of Civil Engineering, University of Toronto.

Hutchinson, P., and W. J. Walley. 1972. Calculation of areal rainfall using finite element techniques with altitudinal corrections. Bulletin of the International Association of Hydrological Sciences 17: 259-272.

Idso, S. B., R. J. Reginato, R. D. Jackson, B. A. Kimball, and F. S. Nakayama. 1974. The three stages of drying of a field soil. Soil Science Society of America Proceedings 38: 831-837.

Idso, S. B., T. J. Schmugge, R. D. Jackson, and R. J. Reginato. 1975. The utility of surface temperature measurements for the remote sensing of soil water status. Journal of Geophysical Research. In Press.

Jackson, R. D. 1973. Diurnal changes in soil water content during drying. In: Bruce, R. R., Field soil water regime, Soil Science Society of America: 37-55.

Jackson, R. D., B. A. Kimball, R. J. Reginato, and F. S. Nakayama. 1973. Diurnal soil-water evaporation: time-depth-flux patterns. Soil Science Society of America Proceedings 37: 505-509.

Jackson, R. D., R. J. Reginato, B. A. Kimball, and F. S. Nakayama. 1974. Diurnal soil-water evaporation: comparison of measured and calculated soil water fluxes. Soil Science Society of America Proceedings 38: 861-866.

Jean, B. R. 1971. Selected applications of microwave radiometric techniques. Technical Report RSC-30, Remote Sensing Center, Texas A&M University, College Station, Texas. 135p.

Keen, B. A. 1927. The limited role of capillarity in supplying water to plant roots. Proceedings of the First International Congress of Soil Science I: 504-511.

Knapp, R. M. 1973. The development and field testing of a basin hydrology simulator. Ph. D. Dissertation, University of Kansas. 149p.

Kondratyev, K. Ya. 1969. Radiation in the atmosphere. Academic Press, New York. 912p.

Lee, Siu Lim. 1974. Dual frequency microwave radiometer measurements of soil moisture for bare and vegetated rough surfaces. Technical Report RSC-56, Remote Sensing Center, Texas A&M University, College Station, Texas. 211p.

Lemon, E. R. 1956. The potentialities for decreasing soil moisture evaporation loss. Soil Science Society of America Proceedings 20: 120-125.

List, R. J. 1951. Smithsonian meteorological tables. Smithsonian Miscellaneous Collections, Vol. 114.

Mather, J. R. (Ed.). 1964. Average climatic water balance data of the continents. Part VII. United States. Publications in Climatology 17: 419-615.

McGuinness, J. L., and E. F. Bordne. 1972. A comparison of lysimeter-derived potential evapotranspiration with computed values. Technical Bulletin No. 1452, Agricultural Research Service, United States Department of Agriculture. 71p.

Myers, V. I., and M. D. Heilman . 1969. Thermal infrared for soil temperature studies. Photogrammetric Engineering 35: 1024-1032.

Myrup, L. O. 1969. A numerical model of the urban heat island. Journal of Applied Meteorology 8: 908-918.

Musgrave, G. W. 1955. How much of the rain enters the soil? In: USDA Yearbook of Agriculture, Water: 151-159.

Newton, R. W., S. L. Lee, J. W. Rouse, Jr. and J. F. Paris. 1974. On the feasibility of remote monitoring of soil moisture with microwave sensors. Proceedings of the Ninth International Symposium on Remote Sensing of Environment 1: 725-738.

Nielsen, D. R., J. W. Biggar, and R. J. Miller. 1967. Field observations of infiltration and soil water redistribution. Transactions of the America Society of Agricultural Engineering: 382-387,410.

Nielsen, D. R., J. W. Biggar, and K. T. Erh. 1973. The spatial variability of field-measured soil-water properties. Department of Water Science and Engineering, University of California, Davis.

Nunn, J. R., L. J. Bledsoe, and R. D. Burman. 1970. Models for inferring evaporation from meteorological measurements. Technical Report No. 47, Grassland Biome U. S. International Biological Program. 20p.

Ogata, G., and L. A. Richards. 1957. Water content changes following irrigation of bare-field soil that is protected from evaporation. Soil Science Society of America Proceedings 21: 355-356.

Outcalt, S. I. 1972. The development and application of a simple digital surface-climate simulator. Journal of Applied Meteorology 11: 629-636.

Paris, J. F. 1969. Microwave radiometry and its application to marine meteorology and oceanography. Texas A&M University, College Station, Texas. 210p.

Pasquill, F. 1962. Atmospheric diffusion. D. Van Nostrand Company Ltd., New York.

Peake, W. H. 1959. Interaction of electromagnetic waves with some natural surfaces. IRE Transactions on Antennas and Propagation: 5324-5329.

Penman, H. L. 1941. Laboratory experiments on evaporation from fallow soil. Journal of Agricultural Science 31: 454-465.

Penman, H. L. 1948. Natural evaporation from open water, bare soil and grass. Proceedings of the Royal Society of London, Ser. A 193: 120-145.

Philip, J. R. 1957. Evaporation, and moisture and heat fields in the soil. Journal of Meteorology 14: 354-366.

Philip, J. R. 1967. The second stage of drying of soil. Journal of Applied Meteorlogy 6: 581-582.

Planet, W. G. 1970. Some comments on reflectance measurements of soils. Remote Sensing of Environment 1: 127-129.

Poe, G. A. 1971. Remote sensing of the near-surface moisture profile of specular soils with multi-frequency microwave radiometry. Proc. SPIE. V. 27.

Poe, G. A. and A. T. Edgerton. 1971. Determination of soil moisture content with airborne microwave radiometry. Aerojet General Corporation, Summary Report 4006R-2.

Poe, G., A. Stogryn, and A. T. Edgerton. 1971. Determination of Soil moisture content using microwave radiometry. Final Technical Report 1684R-1, Aerojet General Corporation, El Monte, California.

Priestley, C. H. B., and R. J. Taylor. 1972. On the assessment of surface heat flux and evaporation using large-scale parameters. Monthly Weather Review 100: 81-92.

Quashu, H. K. 1969. Infiltration and water depletion in lysimeters. Soil Science Society of America Proceedings 33: 775-778.

Rawlins, S. L., and F. N. Dalton. 1967. Psychrometric measurement of soil water potential without precise temperature control. Soil Science Society of America Proceedings 31: 297-301.

Reginato, R. J., and R. D. Jackson. 1971. Field measurements of soil-water content and soil-water pressure. In: Hydrology and Water Resources in Arizona and the Southwest 1, University of Arizona Press: 143-151.

Richards, M. M., and J. A. Strahl. 1969. Elements of river forecasting. ESSA Technical Memorandum WBTMHYDRO 9, Office of Hydrology, U. S. Department of Commerce. 57p.

Richards, L. A., W. R. Gardner, and G. Ogata. 1956. Physical processes determining water loss from soil. Soil Science Society of America Proceedings 20: 310-314.

Richtmyer, R. D., and K. W. Morton. 1967. Difference methods for initial value problems. Interscience Publishers, New York. 405p.

Rose, C. W. 1968a. Water transport in soil with a daily temperature wave. 1. Theory and experiment. Australian Journal of Soil Research 6: 31-44.

Rose, C. W. 1968b. Water transport in soil with a daily temperature wave. 2. Analysis. Australian Journal of Soil Research 6: 45-57.

Ryhiner, A. H., and J. Pankow. 1969. Soil moisture measurement by the gamma transmission method. Technical Bulletin 66, Institute for Land and Water Management Research, Wageningen, The Netherlands: 194-205.

Salter, P. J., and J. B. Williams. 1965. The influence of texture on the moisture characteristics of soils. II. Available-water capacity and moisture release characteristics. Journal of Soil Science 16: 310-317.

Schmugge, T., P. Gloersen, T. Wilheit and F. Geiger. 1974. Remote sensing of soil moisture with microwave radiometers. Journal of Geophysical Research 27: 317-323.

Selirio, I. S. 1969. Climatological estimation of planting days. M. Sc. Thesis, University of Guelph. 64p.

Selirio, I. S., and D. M. Brown. 1971. Moisture budgeting technique for a fallow soil in spring. Canadian Journal of Soil Science 51: 516-518.

Sellers, W. D. 1965. Physical climatology. The University of Chicago Press, Chicago. 272p.

Sivkov, S. I. 1971. Computation of solar radiation characteristics. Israel program for Scientific Translations, Jerusalem. 185p.

Skaggs, R. W., and E. M. Smith. 1967. Apparent thermal conductivity of soil as related to soil porosity. Paper No. 67-114, presented at the Annual Meeting of the American Society of Agricultural Engineers, Saskatoon, Saskechewan.

Smith, R. L., and A. M. Lumb. 1967. Derivation of basin hydrographs. Contribution No. 19, Kansas Water Resources Research Institute, Lawrence, Kansas.

Staff, Hydrologic Research Laboratory. 1972. National Weather Service River Forecast System Forecast Procedures. NOAA Technical Memorandum NWS-HYDRO-14, U. S. Department of Commerce.

Stone, L. R., T. C. Olson, and M. L. Horton. 1973. Water loss estimates from a fallow soil. Journal of Soil and Water Conservation 28: 122-124.

Taylor, S. A., and G. L. Ashcroft. 1972. Physical edaphology. W. H. Freeman & Co., San Francisco. 533p.

Thornthwaite, C. W. 1948. An approach toward a rational classification of climate. Geographical Review 38: 55-94.

Thornthwaite, C. W., and J. R. Mather. 1957. Instructions and tables for computing potential evapotranspiration and the water balance. Publications in climatology 10: 185-311.

Tomlinson, R. F., 1972. Geographical data handling, Volume I, II. International Geographical Union Commission on Geographical Data Sensing and Processing, Ottawa, Canada.

Trouse, A. C., Jr., and L. D. Baver. 1965. Tillage problems in the Hawaiian sugar industry. III. Vehicular traffic and soil compaction. Technical supplement to soil report No. 12, Experimental Station, Hawaiian Sugar Planter's Association.

Ulaby, F. T. 1974. Radar measurement of soil moisture content. IEEE Transactions on Antennas and Propagation AP22: 257-265.

Ulaby, F. T., J. Cihlar,and R. K. Moore. 1974. Active microwave measurement of soil water content. Remote Sensing of Environment 3: 185-203.

Ulaby, F. T. 1975. Radar response to vegetation. IEEE Transactions on Antennas and Propagation 23: 36-45.

Ulaby, F. T., P. P. Batlivala, J. Cihlar and T. Schmugge. 1975. Microwave remote sensing of soil moisture. Proc. Earth Resources Survey Symposium. Houston, Texas, 8-13 June.

United States Department of Commerce. 1958. Rainfall intensity-frequency regime. Part 2. Southeastern United States. Technical Paper No. 29. 51p.

Unwinn, D. J. 1969. The areal extension of rainfall records: an alternative model. Journal of Hydrology 7: 404-414.

Vanderlip, R. L., and M. J. Brown. 1974. Estimation of daily soil moisture for winter wheat in Kansas. Contribution No. 139, Kansas Water Resources Research Institute , Manhattan, Kansas. 30p.

van Wijk, W. R. 1963. General temperature variations in a homogeneous soil. Chapter 5 in: van Wijk, W. R. (Ed.), Physics of Plant Environment, North Holland Publishing Co., Amsterdam: 144-170.

van Wijk, W. R., and A. J. W. Borghorst. 1963. Turbulent transfer in the air. Chapter 8 in: van Wijk, W. R. (Ed.), Physics of Plant Environment, North Holland Publishing Co., Amsterdam: 236-276.

van Wijk, W. R., and W. J. Derksen. 1963. Sinusoidal temperature variation in a layered soil. Chapter 6 in: van Wijk, W. R. (Ed.), Physics of Plant Environment, North Holland Publishing Co., Amsterdam: 102-143.

Westcot, D. W., and P. J. Wierenga. 1974. Transfer of heat by conduction and vapor movement in a closed soil system. Soil Science Society of America Proceedings 38: 9-14.

Wierenga, P. J., and C. T. de Wit. 1970. Simulation of heat transfer in soils. Soil Science Society of America Proceedings 34: 845-848.

Wierenga, P. J., D. R. Nielsen, and R. M. Hagan. 1969. Thermal properties of a soil based upon field and laboratory measurements. Soil Science Society of America Proceedings 33: 354-360.

Wilcox, J. C. 1959. Rate of soil drainage following an irrigation. I. Nature of soil drainage curves. Canadian Journal of Soil Science 39: 107-119.

Willis, W. O. 1964. Bibliography on soil temperature (through 1963). ARS 41-94, Agricultural Research Service, United States Department of Agriculture. 82p.

Willis, W. O., and J. J. Bond. 1971. Soil water evaporation: reduction by simulated tillage. Soil Science Society of America Proceedings 35: 526-529.

Winkler, E. M. 1966. Moisture measurements in glacial soils from airphotos. Ecology 47: 156-158.

APPENDIX A.

SOIL TEMPERATURE SIMULATION MODEL

The purpose of the soil temperature model is to predict diurnal variations of surface as well as subsurface temperatures of a bare soil. As stated in Chapter 3, the prediction is accomplished by (i) computing the surface soil temperature as a function of time, and (ii) using the surface temperature as a boundary condition to solve the one-dimensional heat diffusion equation. These two steps are described in the following sections.

A.1 DETERMINATION OF SURFACE TEMPERATURE

The magnitude of surface soil temperature at any time is governed by the energy exchange at and near the soil surface. It is therefore possible to estimate the surface temperature by determining magnitudes of individual terms in the energy balance equation which, neglecting horizontal radiation terms, can be written as

$$R_N = H + LE + G,$$

where

$$R_N = S_a - L_o ,$$
$$S_a = (1 - \alpha) S_i ,$$
$$L_o = L_e - L_i .$$

Therefore

$$S_a - L_o = H + LE + G . \qquad (33)$$

(Individual symbols are defined at the end of this section).

The longwave radiation contribution to net radiation L_o consists of two parts, L_e and L_i. If energy emitted by the surface L_e is considered a function of air temperature, then according to the Stefan-Boltzman law,

$$L_e = \epsilon \sigma T_a^4 .$$

The energy emitted by a cloudless atmosphere L_i has been determined to follow the relationship (Sellers, 1965)

$$L_i = \epsilon \, (0.165 - 0.000769RH) .$$

For a cloudy sky a factor $(1 - k_1 n)$ approximates the reduction of outgoing radiation L_e (Sellers, 1965). Furthermore, Sellers (1965) derived a correction factor to account for the difference between surface and air (screen height) temperatures in computing L_e. Combining the above formulas, L_o can be computed as follows:

$$L_o = 4 \epsilon \sigma T_a^3 \, (T_s - T_a) + \epsilon \, (1 - k_1 n) \, (0.165 - 0.000769RH). \qquad (34)$$

Sensible heat H can be computed from the aerodynamic equation:

$$H = \frac{\rho C_p k^2 u \, (T_s - T_a)}{(\ln \frac{z}{z_o})^2} .$$

If

$$D = \frac{k^2 u}{(\ln \frac{z}{z_o})^2}$$

and

$$\rho = \frac{p}{R T_a} ,$$

then $$H = \frac{p C_p D (T_s - T_a)}{R T_a} . \quad (35)$$

The basic equation for latent heat flux LE calculation is given by

$$LE = \frac{0.622 \rho L D (e_s - e_z) a}{p} . \quad (36)$$

As explained by Foster (1972), surface vapor pressure e_s can be eliminated from Equation (36) by employing a finite difference form of the Clausius-Clapeyron equation

$$e_s - e_{sa} = \frac{0.622 L e_{sa} (T_s - T_a)}{R T_a^2} . \quad (37)$$

If e_z is added to and subtracted from the left side of Equation (37) and the equation is written in terms of $(e_s - e_z)$, the result can be substituted in Equation (36) to yield

$$LE = \frac{0.622 L D a}{R T_a} \left\{ \frac{0.622 L e_{sa} (T_s - T_a)}{R T_a^2} + e_{sa} - e_z \right\} . \quad (38)$$

Parameter a in Equation (38) accounts for the reduction of potential evaporation of the soil after moisture content decreases below a certain level. It was assumed that actual evaporation AE equals potential evaporation PE if moisture content is above soil storage capacity, and that the ratio AE/PE decreases when moisture conient is below the storage capacity. Therefore

$$a = 1 \text{ if } m_{02} \geq 0.95SC_{02}$$

$$= \frac{m_{02}}{SC_{02}} \quad \text{otherwise.} \tag{39}$$

For a homogeneous semi-infinite soil, the soil heat flux at the surface G(0,t) can be expressed in the form (Sellers, 1965)

$$G(0,t) = \Delta T_o (\lambda C \omega)^{1/2} \sin(\omega t + \frac{\pi}{4}) \tag{40}$$

provided that the soil is heated in a periodic manner so that surface temperature follows Equation (41):

$$T_s(t) = \bar{T}_s + \Delta T_o \sin \omega t. \tag{41}$$

The amplitude term ΔT_o can be removed from Equation (40) by using Equation (41). Furthermore, Equation (40) can be manipulated to express G in terms of $(T_s - T_a)$. The resulting equation will be

$$G(0,t) = 0.7071 (\lambda C \omega)^{1/2} \left\{ (1 + \frac{1}{\omega})(T_s - \bar{T}_a) + T_a - \bar{T}_s + \frac{1}{\omega}(T_a - T_{s1}) \right\}. \tag{42}$$

Before the individual terms of the energy balance equation are combined to yield a formula for T_s computation, Equation (34), (35), (38), and (42) will be replaced by simpler expressions:

$$L_o = C_1 (T_s - T_a) + C_2$$
$$H = C_3 (T_s - T_a)$$
$$LE = C_4 (T_s - T_a) + C_5$$
$$G = C_6 (T_s - T_a) + C_7.$$

Then the surface temperature can be determined from Equation (43):

$$T_s = T_a + \frac{S_a - C_2 - C_5 - C_7}{C_1 + C_3 + C_4 + C_6}, \qquad (43)$$

where:

$$C_1 = 4 \epsilon \sigma T_a^3,$$
$$C_2 = \epsilon (1 - k_1 n) (0.165 - 0.000769 RH),$$
$$C_3 = \frac{p C_p D}{R T_a},$$
$$C_4 = \frac{0.38688 L^2 D a e_{sa}}{R^2 T_a^3},$$
$$C_5 = \frac{0.622 L D a (e_{sa} - e_z)}{R T_a},$$
$$C_6 = 0.7071 (\lambda C \omega)^{1/2} \left(\frac{\omega + 1}{\omega}\right),$$
$$C_7 = 0.7071 (\lambda C \omega)^{1/2} \left(T_a - \bar{T}_s + \frac{T_a - T_{s1}}{\omega}\right).$$

(Individual symbols used in this section indicate the following variables:

a = ratio of actual and potential evaporation, dimensionless;
C = soil heat capacity, cal/cm^3/°C;
C_p = specific heat of air, cal/g/°C;
D = transfer coefficient, cm/min;
e_s = soil surface water vapor pressure, mb;
e_{sa} = saturated water vapor pressure of the air, mb;
e_z = actual air vapor pressure at the height z, mb;
G = soil heat flux, ly/min;
H = sensible heat flux, ly/min,
k = von Karman constant, dimensionless;
k_1 = cloud type coefficient, dimensionless;
L = latent heat of vaporization, cal/g;
L_e = longwave radiation emitted by the soil, ly/min;
LE = latent heat flux, ly/min;
L_i = counter longwave atmospheric radiation, ly/min;
L_o = outgoing longwave radiation, ly/min;
m_{02} = average moisture content in the 0-2 cm layer, cm^3/cm^3;
n = cloud cover in tenths, dimensionless;
p = atmospheric pressure, mb;
R = gas constant, R = 2870.4 mb cm^3/g/°K;
RH = relative humidity, percent;
R_N = net radiation, ly/min;
S_a = absorbed shortwave solar radiation, ly/min;
SC_{02} = average storage capacity in the 0-2 cm layer, cm^3/cm^3;
S_i = incoming shortwave solar radiation, ly/min;
T_a = air temperature, °K;
T_s = surface soil temperature, °K;
u = wind speed, cm/min;
z = height of meteorological measurements, cm;
z_o = roughness length, cm;
α = soil albedo, dimensionless;
ϵ = infrared soil emissivity, dimensionless;

ΔT_o = surface temperature amplitude, °C;
λ = apparent soil thermal conductivity, cal/cm/min/°C;
ρ = air density, g/cm^3;
σ = Stefan-Boltzman constant, $\sigma = 8.17$ ly/min/°K^4;
ω = angular frequency, radians/time increment.)

A.2 DETERMINATION OF SUBSURFACE TEMPERATURES

Assuming horizontal uniformity and heat transfer by conduction only, the change in soil temperature is described by (Sellers, 1965)

$$\frac{\delta T(z,t)}{\delta t} = \frac{d}{dz}\left(D'(z) \frac{\delta T(z,t)}{\delta z} \right) . \tag{44}$$

If $D'(z)$ is not constant with depth, Equation (44) cannot be solved analytically. A numerical solution is available, however. Equation (44) can be written in a finite difference form as follows (Richmeyer and Morton, 1967)

$$\frac{T_i^{j+1} - T_i^j}{\Delta t} = \frac{D'(z)\left(T_{i+1}^j - 2T_i^j + T_{i-1}^j \right)}{(\Delta z)^2} , \tag{45}$$

where

$D'(z)$= soil thermal diffusivity, cm^2/min;
i = depth increment sequential number;
j = time increment sequential number;
T = soil temperature, °C;
Δt = time increment, min;
Δz = depth increment in the soil, cm.

Equation (45) can be solved provided both the initial temperature as a function of depth and the temperatures at the upper (soil surface) and lower boundaries are known as a function of time. If the last Δz increment is located sufficiently deep

below the surface, the lower boundary condition is constant. The upper boundary can be computed as stated in the previous section. The initial temperature profile can be measured or arrived at by simulation; the latter procedure was described in section 3.2.

A.3 THE COMPUTER PROGRAM

Figure 70 is a generalized flow chart of the computer program for soil temperature computations. The governing time parameters are PERL (= length of the period between measurements of meteorological parameters) and DT(=Δt). The number of intervals NHA for which soil surface temperature T_s will be calculated is given by

$$NHA = 1440/PERL.$$

For the calculations described in this report, the values used were: PERL=10, DT=2.5, NHA=144.

The soil variables needed are soil texture and moisture content, bulk density, field capacity, and initial temperature profile as a function of depth. The depth-dependent parameters are specified for NL layers; the layers were assumed to be 2 cm thick in this study.

The site is described by latitude, declination slope and aspect. Besides air temperature, relative humidity and wind speed at PERL increments, magnitudes of air pressure, surface roughness length, surface temperature for 0^{th} time increment, and of the average daily surface temperature are required.

The computation for a given time increment proceeds as follows:

- hour angle;
- incoming solar radiation (see below);
- albedo (from data given by Idso et al. (1975b));
- soil thermal conductivity and capacity (see below);
- surface temperature from Equation (43);
- profile temperatures in NTINC iterations using Equation (45); NTINC=PERL/DT;
- evaporation from individual layers in the 0 to 30 cm zone, based on the method described in section 2.2.1.1 and latent heat computation from Equation (38).

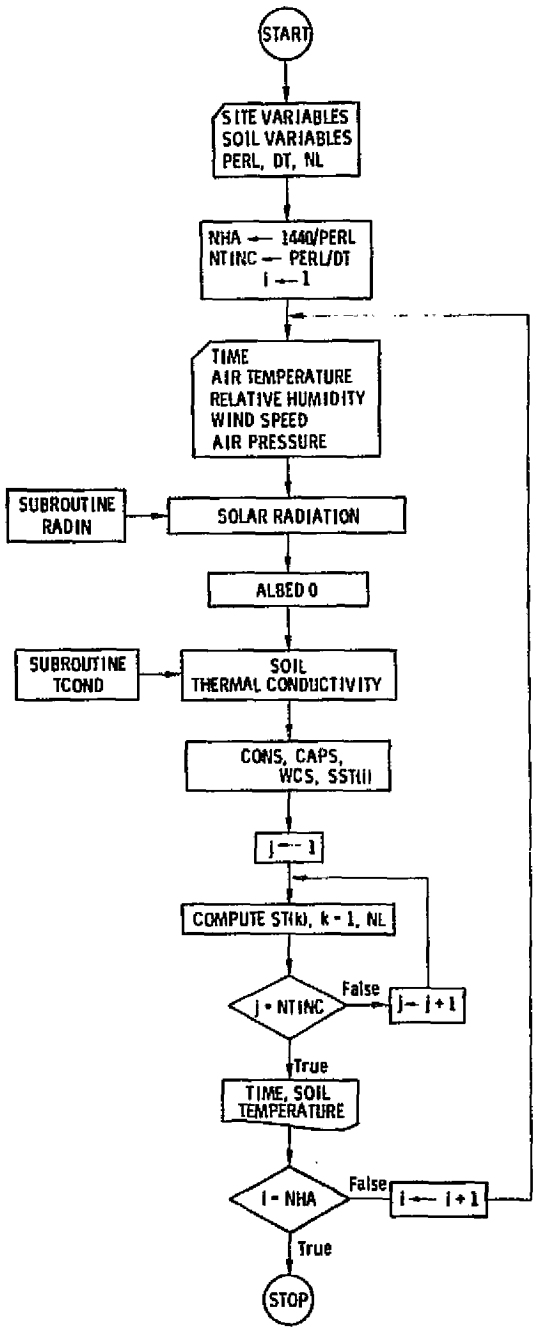

Figure 70. Flowchart for the soil temperature simulation model.

The computation of surface temperature requires knowledge of soil thermal conductivity CONS, thermal capacity CAPS, and water content near the surface WCS (Equation 42, 43). These quantities were calculated as an average of values at the surface (computed by assuming constant gradient for the 0 to 4 cm depth) and at the depth of 2 cm.

Solar radiation incident on a generally sloping surface was computed as

$$Q = QDR + QDF ,$$

where

$$QDR = \frac{SMT\ (\cos\ (ZEN)\ \cos(SL) + \sin(ZEN)\ \sin(SL)\ \cos(AZS - ASP))}{DIS^2\ (\ 1 + (TC)\ (OM))} ,$$

and

$$QDF = \frac{0.38\ TC\ (\cos\ (0.5SL))^2\ (SMT)}{DIS^2\ (1 + (\ TC)\ (OM))}$$

where

SMT	=	solar meteorological constant, ly/min;
DIS	=	radius vector of the sum, dimensionless;
TC	=	transparency coefficient for Kastrow's equation (Sivkov, 1971), dimensionless;
OM	=	actual optical mass of the atmosphere, dimensionless;
ZEN	=	zenith angle (0° = solar noon), degrees;
SL	=	slope of the surface, degrees;
AZS	=	azimuth angle of the sun, degrees;
ASP	=	aspect of the surface (0° = south-facing), degrees.

Derivations of the formulas and values of the various coefficients used in the solar radiation computations can be found in Sivkov (1971), Sellers (1965), List (1951), and Kondratyev (1969).

Thermal conductivity was calculated separately for each layer using the procedure described by de Vries (1963; see also Wierenga et al., 1969). The basic formula is

$$\lambda = \frac{\sum_{i=0}^{n} k_i X_i \quad i}{\sum_{i=0}^{n} k_i X_i} , \tag{46}$$

where

n = the number of different types of particles;

X_i = volumetric fraction of the i^{th} particles;

λ_i = thermal conductivity of the i^{th} particles.

The subscript i = 0 refers to the continuous phase. Following de Vries (1963), the continuous phase was water if moisture content was above 0.03 * IT cm^3/cm^3 (IT = 1 for sand, 2 for loam, 3 for clay) and air if moisture content of the layer was below this value. Besides air and water, two other kinds of particles were considered, namely quartz, and other mineral constituents; the reason for separating soil mineral fraction into two groups was the difference in λ_i between them. Values of λ_i for all components were taken from de Vries (1963) for the temperature of 20°C; temperature dependence of λ_i was not accounted for in the computations since it is generally small. The thermal conductivity of air-filled pores was equal to the sum of thermal conductivity of dry air, λ_a, and of λ_v which accounts for the heat movement by vapor phase across the gas-filled pores (de Vries, 1963). The value of λ_a was constant, while λ_v was constant only above the field capacity; below field capacity, λ_v decreased linearly to λ_a for a dry soil. The values of k_i were computed as follows:

$$k_i = \frac{1}{3} \sum_{j=1}^{3} \frac{\lambda_o}{\lambda_o + (\lambda_i - \lambda_o) g_j} , \tag{47}$$

where g_j is a factor that depends on the shape of the i^{th} particles, with $g_1 + g_2 + g_3 = 1$. For solid particles, the values used were $g_1 = g_2 = 0.125$, $g_3 = 0.750$ (Wierenga et al., 1969). Values of g_1 and g_2 for air particles were assumed to decrease linearly

from 0.333 for water-saturated soil to some value at field capacity and then linearly to 0.013 for a dry soil; the value at field capacity depended on both porosity and field capacity in the given soil layer. For moisture contents below 0.03 * IT, the soil thermal conductivity was determined by interpolation between the λ value at 0.03 * IT and λ for a dry soil; in accordance with the data by Skaggs and Smith (1967), the λ of a dry soil was first multiplied by a factor of 1.65.

Thermal capacity C was computed for each layer from the formula

$$C = 0.2\,\rho_s + m, \tag{48}$$

where

ρ_s = soil bulk density;
m = moisture content.

APPENDIX B.

EXPERIMENTAL PROCEDURES

Data from three different experiments were used in various parts of this study. Procedures employed to obtain these data are summarized in this Appendix.

B.1 EUDORA SOIL MOISTURE REGIME STUDY

This experiment was carried out on an agricultural field*(latitude 38°57.8'N, longitude 95°08.1'W; NWNENE36-12S-20E) approximately 4 miles east from Lawrence, Kansas. The experiment was initiated following wheat harvest and plowing and progressed until tensiometric measurements had to be discontinued due to freezing temperatures.

The experimental site was located on the floodplain of the Kansas River; consequently, the soils exhibit considerable spatial variability. Two soil mapping units were identified at the site, namely Eudora silt loam and Kimo silty clay loam (Dickey and Zimmerman, in press). The first soil occupied a somewhat elevated ridge, while the second one was located in a depression; no sharp boundary existed between them. Typical profiles of these soils have been described as follows (Dickey and Zimmerman, in press).

B.1.1 Eudora Silt Loam

In a representative profile the surface layer is very dark grayish brown silt loam about 12 inches thick. The upper part of the substratum is dark grayish brown coarse silt loam about 36 inches thick. The lower part of the substratum is grayish brown coarse silt loam thinly stratified with a few sandy and clayey layers less than 1 inch thick.

*The cooperation of Mr. A. Wichman is gratefully acknowledged.

Eudora soils are very friable and easily worked. They have high natural fertility and available water capacity. Permeability is moderate.

Nearly all the acreage of these soils is cultivated. Eudora soils are well suited to all crops commonly grown in the county. Also vegetable crops produce well on these soils.

Representative profile of Eudora silt loam, 125 feet south and 50 feet west of the northeast corner of Sec. 15, T. 12 S., R. 19 E., in a cultivated field:

Ap — 0 to 7 inches, very dark grayish brown (10YR 3/2) silt loam; moderate medium granular structure; very friable; mildly alkaline; gradual smooth boundary.

A1 — 7 to 12 inches, very dark grayish brown (10YR 3/2) silt loam; moderate medium granular structure; very friable; many worm casts; mildly alkaline; gradual smooth boundary.

C1 — 12 to 23 inches, dark grayish brown (10YR 4/2); coarse silt loam; massive; very friable; many worm casts; mildly alkaline; gradual smooth boundary.

C2 — 23 to 40 inches, dark grayish brown (10YR 4/2); coarse silt loam; massive; very friable; few worm casts; at 33 to 34 inches a layer of silty clay loam; mildly alkaline; gradual smooth boundary.

C3 — 40 to 43 inches, dark grayish brown (10YR 4/2); silt loam; massive; very friable; mildly alkaline; clear smooth boundary.

C4 — 48 to 72 inches, grayish brown (10YR 5/2); coarse silt loam; massive; very friable; some thin, less than 1 inch thick of sandy and clayey layers; mildly alkaline; strong effervescence.

The A horizon ranges from 10 to 20 inches in thickness. The A horizon may be dark grayish brown in areas where 6 inches or more of silty sediments were deposited by the flood in 1951. The A horizon can be coarse silt loam, loam or medium silt loam. The C horizon is usually a coarse silt loam with some layers more sandy or clayey textures. Below 36 inches the texture can be coarse silt loam, loam, very fine sandy loam, fine sandy loam or loamy very fine sand that is usually calcareous.

B.1.2 Kimo Silty Clay Loam

Representative profile of Kimo silty clay loam, 250 feet north and 60 feet west of southeast corner of sec. 7, T. 12 S., R. 20 E., in a cultivated field:

Ap 0 to 6 inches, very dark gray (10 YR 3/1) heavy silty clay loam; weak fine granular structure; firm; mildly alkaline; slight effervescence; gradual smooth boundary.

A1 6 to 14 inches, black (10 YR 2/1) silty clay; weak fine and medium subangular blocky structure; very firm; mildly alkaline; gradual smooth boundary.

A12 14 to 24 inches, very dark gray (10 YR 3/1) silty clay; few fine strong brown mottles in lower part; weak, fine, subangular blocky structure; very firm; mildly alkaline; clear smooth boundary.

AC 24 to 28 inches, dary gray (10 YR 4/1) light silty clay loam with some streaks and fingers of darker color; few, fine, strong-brown mottles; some weak fine granular structure and massive; friable; mildly alkaline; strong effervescence; gradual smooth boundary.

IIC 28 to 60 inches, grayish brown (10 YR 5/2) coarse silt loam; massive; very friable; mildly alkaline; strong effervescence.

To monitor changes in soil moisture and meteorological parameters related to these changes, the following instrumentation was used:

(i) Tensiometers were built using polyvinyl chloride (PVC) pipe (Schedule 80, 1.27 cm I.D.), porous ceramic cups (manufactured by R&J Ceramics, 2552 Cottage Way, Sacramento, California), acrylic tubing (1.59 cm O.D.), and translucent nylon tubing (0.107 cm I.D.). The porous cup and acrylic tubing were glued with contact cement to opposite ends of the PVC pipe cut to the required length. The nylon tubing was fit into a hole drilled through the PVC pipe wall and glued. During the measurements, the upper end of the tensiometer was closed with a neoprene stopper. All tensiometers were tested for air leaks prior to installation.

(ii) Rainfall gauge (diameter 10 cm).

(iii) Hygrothermograph with a weekly recording cycle.

(iv) Anemometers at three heights (10 cm; 30 cm, 300 cm).

(v) Pyranometer for solar radiation measurements; however, the recording equipment broke down permanently after two weeks of operation.

The experiment was designed so as to encompass main sources of soil moisture variability, namely depth, time, distance, and soil type. Depth was taken into account by installing the tensiometers 10 cm, 25 cm, 40 cm, 55 cm, 70 cm, 85 cm, 100 cm, 115 cm, 130 cm, and 145 cm ("complete" set) or 115 cm, 130 cm, and 145 cm ("partial" set) below the soil surface. In either case, the nylon tubings from all tensiometers of one set were fastened to a single meter stick and drew mercury from one container. One complete and one partial set were installed 2 m apart on the Kimo silty clay loam (="Site 3"). On Eudora silt loam, two complete sets were installed 2 m apart ("Site 1") and an additional partial set was placed approximately 100 m away from the complete sets ("Site 2"). A dike (5 cm high above the soil surface) was installed around all sets to prevent runoff. A neutron probe access tube was inserted at a 50 cm distance from each set; unfortunately, the neutron counts were found to give moisture contents incompatible with both tensiometric and gravimetric measurements as well as the precipitation history, and therefore had to be discarded.

All tensiometers were installed 30 and 31 July, 1973. Subsequently, mercury level reading and precipitation were taken at approximately 0730 every day (period 8/2/73 to 9/6/73) or at intervals 1 to 3 days (9/6/73 to 11/3/73).

Six (on Site 1) and three (on Site 3) undisturbed core samples 4 cm in diameter and 10 cm high were taken for moisture characteristics (i.e., tension vs. moisture content relationship) determination. Due to unavailability of suction plates, a Soil Moisture Equipment Corporation pressure membrane extractor was adjusted for measurements at low tensions by adding a water column manometer and an air pressure manometer (pressure range 0 to 60 p.s.i.); water manometer was used for tensions up to 100 cm. Each set of samples was placed on a pressure plate (maximum pressure 3 bars) into a larger basin; after slowly raising the water level within the basin so that the samples were almost submerged, the basin was covered to prevent evaporation from the samples, and the samples saturated for approximately 16 hours. Following this period, the pressure plate with the samples were transferred into a pressure cooker, closed tightly, and the pressure was set at 0.01 atmosphere. Subsequently,

air pressure was increased to 0.02, 0.05, 0.1, 0.2, 0.5, 1.0 and 2.0 atmospheres; when an equilibrium was established following every pressure increase, the outflow from the cooker was measured and recorded. At the end, samples were taken out weighed individually, dried at 105°C, and weighed again. Moisture characteristics were then calculated from the final moisture content, measured outflows, and from the pressures applied. Difficulties were experienced in processing samples from Site 3, due mainly to their lower number and finer texture. Consequently, only moisture data from Site 1 are presented here.

Tensiometric readings T (in cm) were converted into values of suction S (in cm) using Equation 49*:

$$S = 12.6\,T - 13.6\,H - D + 14\,, \tag{49}$$

where H = height of the mercury level in the container above soil surface in cm;

D = depth of the porous cup below the surface in cm.

Constant of 14 accounts for friction loss inside the nylon tubing.

Using the moisture characteristic for a given depth, moisture contents corresponding to measured S values were determined for all measurements on Site 1 and 2.

B.2 PHOENIX EXPERIMENTS

Some data used in various parts of this study were generated during experiments carried out in 1970, 1971, and 1973 in Phoenix, Arizona. The experimental conditions were quite similar, however, and may therefore be summarized collectively. The following information was provided by Jackson (1973) and Idso et al. (1974).

The experiments were carried out on a 72 by 90 m field at the U. S. Water Conservation Laboratory in Phoenix, within which three lysimeters are installed. The soil, Adelanto loam (fine-loamy, mixed, hyperthermic, Torrifluventic Haplustoll), is fairly uniform to about 100 cm and has been cultivated numerous times

*Courtesy of Dr. W. Powers, Department of Agronomy, Kansas State University, Manhattan, Kansas.

during the past years. At the start of each experiment, the lysimeters and surrounding area were irrigated with approximately 10 cm of water.

During the drying period, soil samples for gravimetric moisture content determination were taken at frequent intervals for depths of 0-0.5 cm, 0.5-1 cm, 1-2 cm, 2-3 cm, 3-4 cm, 4-5 cm, 5-7 cm, and 7-9 cm; the sampling was not begun until some drying had occurred, thus allowing access to the field. The July, 1970, experiment was conducted between 10 July and 17 July, and sampling was done at 0.5 hour intervals. In the March, 1971, experiment (March 3 to April 8) measurements were taken from 5-18 March, 25 March, and 8 April, also at 0.5 hour intervals. In the 1973 experiments, samples were collected at 20 minute intervals. Jackson et al. (1973) estimated that the total error in resulting moisture content values was about $\pm$ 0.001 cm^3/cm^3. Evaporation loss was measured by lysimeters at the same time as soil water content.

Soil temperatures were measured by thermocouples at the soil surface and at several depths below the surface. For example, in the September, 1973 experiment, the interval between adjacent sensors was 0.5 cm (at depths less than 10 cm), 2 cm (10 to 35 cm), 15 cm (35 to 65 cm), and 35 cm (above 65 cm).

In addition to soil temperature and moisture, several meteorological variables were measured: incoming and reflected solar radiation, net radiation, air temperature, atmospheric vapor pressure, and wind speed.